# Investigation of *Arabidopsis* HDC1-mediated histone deacetylation and its role in phosphate deficiency response

**Dissertation**

zur Erlangung des

Doktorgrades der Naturwissenschaften (Dr. rer. nat.)

der

Naturwissenschaftlichen Fakultät I-Biowissenschaften

Martin-Luther-Universität Halle-Wittenberg


vorgelegt

von Pinelopi Moutesidi, M.Sc.

# Table of Contents

# Abbreviations

| | |
|---|---|
| ANOVA | Analysis of variance |
| ATP | Adenosine triphosphate |
| BGC(s) | Biosynthetic gene cluster(s) |
| bp | Base pairs |
| cDNA | Complementary deoxyribonucleic acid |
| ChIP | Chromatin immunoprecipitation |
| Da | Dalton |
| DEG(s) | Differentially expressed gene(s) |
| DNA | Deoxyribonucleic acid |
| dNTPs | Deoxyribonucleotide triphosphates |
| DTT | Dithiothreitol |
| e.g. | *Exempli gratia*-for example |
| EDTA | Ethylenediaminetetraacetic acid |
| EGTA | Ethylene glycol tetraacetic acid |
| et al. | *Et alia*-and others |
| FDR | False discovery rate |
| Fe | Iron |
| FPKM | Fragments per kilobase of exon per million mapped fragments |
| GFP | Green fluorescent protein |
| GSL(s) | Glucosinolate(s) |
| h | Hour(s) |
| I3M | Indolyl-3-methyl glucosinolate |
| kb | Kilo bases |
| kDa | Kilodalton |
| mg | Milligram |
| min | Minute(s) |
| ml | Milliliter |
| mM | Millimolar |
| mm | Millimeter |
| mRNA | Messenger ribonucleic acid |
| ng | Nanogram |
| padj | Adjusted probability value |
| p value | Probability value |
| PCR | Polymerase chain reaction |
| Pi | Phosphate |
| pmol | Picomolar |
| PMSF | Phenylmethylsulfonyl fluoride |
| PSR(s) | Phosphate starvation response(s)/responsive |
| RNA | Ribonucleic acid |
| RNA-seq | Ribonucleic acid sequencing |
| ROS | Reactive oxygen species |
| rpm | Rotations per minute |
| RT-qPCR | Real-time quantitative polymerase chain reaction |

| | |
|---|---|
| RSA | Root system architecture |
| SCN | Stem Cell Niche |
| SDS | Sodium dodecyl sulfate |
| SDS-PAGE | Sodium dodecyl sulfate-polyacrylamide gel electrophoresis |
| sec(s) | Second(s) |
| T-DNA | Transfer deoxyribonucleic acid |
| v/v | Volume per volume |
| w/v | Weight per volume |
| WT | Wild type |
| µg | Microgram |
| µl | Microliter |
| µM | Micromolar |
| 1MOI3M | 1-hydroxy-indolyl-3-methyl glucosinolate |
| 3MSOP | 3-methylsulfinylpropyl glucosinolate |
| 3MTP | 3-methylthiopentyl glucosinolate |
| 4MOI3M | 4-hydroxy-indolyl-3-methyl glucosinolate |
| 4MSOB | 4-methylsulfinylbutyl glucosinolate |
| 4MTB | 4-methylthiobutyl glucosinolate |
| 5MTP | 5-methylthiopentyl glucosinolate |
| 6MSOH | 6-methylsulfinylhexyl glucosinolate |
| 6MTH | 6-methylthiohexyl glucosinolate |
| 7MSOH | 7-methylsulfinylheptyl glucosinolate |
| 7MTH | 7-methylthioheptyl glucosinolate |
| 8MSOO | 8-methylsulfinyloctyl glucosinolate |
| 8MTO | 8-methylthiooctyl glucosinolate |

# List of Figures

# List of Tables

# List of Supplementary Figures

# List of Supplementary Tables

## List of supplementary data files (see compact disc)

Suppl. File 1    Differentially expressed genes between *pdr3* and WT shoots at Pi replete conditions.

Suppl. File 2    Differentially expressed genes between *pdr3* and WT roots at Pi replete conditions.

Suppl. File 3    Phosphate starvation responsive genes in WT root tips.

Suppl. File 4    Phosphate starvation responsive genes in *pdr3* root tips.

Suppl. File 5    Differentially expressed genes between *pdr3* and WT root tips at Pi replete conditions.

Suppl. File 6    Differentially expressed genes between *pdr3* and WT root tips at Pi deficient conditions.

Suppl. File 7    Basal transcriptional differences between *pdr3* and WT root tips.

Suppl. File 8    Hierarchical clustering of common phosphate starvation responsive genes between *pdr3* and WT root tips.

# 1 Introduction

## 1.1 HDC1 and its role in chromatin dynamics

### 1.1.1 Chromatin structure modulates gene expression

DNA is packed in the nucleus in the form of chromatin, the basic unit of which is the nucleosome, consisting of 147 bp of DNA wrapped around an octamer of the core histones (H2A, H2B, H3 and H4) (Ma et al., 2013). Additional to the canonical histones, variants of H2A and H2B have been identified, which are replacing their canonical equivalent under certain conditions (Jiang and Berger, 2017). Chromatin does not only serve a structural role for DNA organization, but also a functional one, as its three-dimensional architecture heavily affects gene expression and thus downstream developmental processes. Chromatin at a highly condensed state (closed) is less accessible to the transcriptional machinery and typically transcriptionally inactive, which however may be altered upon chemical or conformational changes that affect chromatin structure (Jenuwein and Allis, 2001). Alterations in chromatin structure can have a stable, long-term transcriptional effect and may be even mitotically or meiotically heritable, known as "epigenetic" changes (NIH "Roadmap Epigenomics Project 2013" , reviewed in Sudan et al., 2018). From the mechanisms that govern chromatin dynamics, the most well-studied are ATP-dependent chromatin remodeling, DNA methylation and histone modifications.

One of the most characterized mechanisms that regulate plant chromatin is post-translational modifications (PTMs) of histone tails. These modifications usually occur at the C- or N-terminal end that protrude from the nucleosomes and they include acetylation, methylation, phosphorylation, ubiquitylation, propionylation, butyrylation, sumoylation, ADP ribosylation, glycosylation, biotinylation, and carbonylation (Hildmann et al., 2007). Distinct combinations and distribution patterns of these marks are characterizing different chromatin states; for example, trimethylation of lysine 4 on histone 3 (H3K4me3) and H3 and H4 acetylation are typical to promoters of transcriptionally active genes (Barrera et al., 2008; Deckert and Struhl, 2001), while H3K27me3 is considered a repressive mark (Sequeira-Mendes et al., 2014). The epigenetic code, comprised of the entirety of these marks, is established and dynamically regulated by the action of enzymatic writers and erasers, while it is functionally translated by its readers (reviewed in Tianyi et al., 2015).

### 1.1.2 Histone deacetylases and their functions in plant development

*1.1.2.1 Histone deacetylation is catalyzed by members of three HDAC families in Arabidopsis*

Histone acetylation and deacetylation are two of the most well studied PTMs and have been correlated with gene activation and repression respectively. Histone acetylases act as the writer of histone acetylation by adding acetyl groups ($CH_3COO-$) to lysine residues on the N-terminal tails of the core histones (Pandey et al., 2002; Sterner and Berger, 2000). In plants, H3 has been reported to be acetylated at lysine positions 9, 14, 18 and 23 and H4 at positions 5, 8, 12, 16 and 20 (Fuchs et al., 2006). This modification has been correlated with expressive (open) chromatin; it is characteristic that transcriptional starting sites of active genes have been found to be enriched in histone acetylation (Kim et al., 2020). To explain this effect, it has been proposed that histone acetylation neutralizes the positive charge of the histones, reducing their electrostatic affinity for DNA and thus, resulting in an open chromatin state (Bauer et al., 1994; reviewed in Kumar et al., 2021). Another theory suggests that acetylated residues on histone tails provide binding

platform on the nucleosome, recognized by proteins bearing a bromodomain, an acetyl-lysine-specific protein interaction module (Dyson, 2001; Shogren-Knaak et al., 2006).

The reverse process is catalyzed by histone deacetylases (HDACs), which increase the interaction between DNA and histones by removing acetyl groups from histone tails, thus switching chromatin state to a more condensed status (Ma et al., 2013). *Arabidopsis thaliana* encodes 18 HDACs distributed across three families, namely HD2 (HD-tuins), SIR2-like (sirtuins) and RPD3-like. The latter family is homologous to RPD3 (REDUCED POTASSIUM DEFICIENCY 3) in yeast and consists of 12 members, all of which contain a histone deacetylase domain (Interpro: IPR003084) (Pandey et al., 2002). The proteins in this superfamily are further subcategorized into three classes; class I typically includes HDA19, HDA6, HDA7 and HDA9, while additionally HDA10 and HDA17, which only have partially HDAC domains but high similarity to HDA9, have often been proposed to belong to this class (Chen et al., 2020; Pandey et al., 2002). The rest of the RPD3-like HDACs are distributed across class II (HDA5, HDA15, and HDA18), class III (HDA2), while HDA8 and HDA14 remain unclassified (Hollender and Liu, 2008; Pandey et al., 2002). The members of this class have a curved-tubular shaped, $Zn^{2+}$-dependent active site, where the catalytic $Zn^{2+}$ ion is located at the bottom of the pocket adjacent to conserved histidine, aspartic and tyrosine residues (Porter and Christianson, 2019; Ruijter et al., 2003). The catalytic activity of the $Zn^{2+}$-dependent HDACs can be impaired pharmacologically with trichostatin A (TSA) or sodium butyrate application, which interfere with $Zn^{2+}$ binding (Hollender and Liu, 2008).


*1.1.2.2    HDACs transcriptionally regulate a diverse array of physiological and developmental pathways*
Numerous studies have demonstrated the diverse functions of HDACs in the transcriptional regulation of a broad range of biological pathways, from developmental processes, including germination, flowering and hormone signal transduction, to abiotic and biotic stress responses (reviewed in Chen et al., 2020; Hollender and Liu, 2008). In *Arabidopsis*, HDA19 is one of the earliest identified and most well understood HDACs (Chen et al., 2020; Feng et al., 2021; Wu et al., 2000). Localized in the nucleus, HDA19 is expressed ubiquitously throughout all plant tissues and developmental stages (Fong et al., 2006). HDA19 seem to be having a global function, as the loss-of-function mutant *hda19* shows deregulation of 7% of all genes (Tian et al., 2005). Additionally, genome-wide transcriptional analysis showed the upregulation of many stress response-related genes in *hda19*, suggesting a central role for HDA19 in transcriptional regulation of stress responses (Feng et al., 2021). Indeed, previous reports demonstrated HDA19-mediated tuning of certain phosphate (Pi) deficiency responses (Chen et al., 2015), while it has been proposed that HDA19 is positively affecting basal resistance to bacterial pathogens (Kim et al., 2008). The function of HDA19 seem to be shifted to specific pathways upon association with specific cofactors; SCARECROW has been shown to recruit HDA19 to specific loci participating in the cell fate determination of root cortical cells (Chen et al., 2019), while interaction with MSI1 (MULTICOPY SUPRESSOR OF IRA1) seem to lead to repression of ABA-responsive genes (Mehdi et al., 2016). Moreover, association of HDA19 with HDC1 (HISTONE DEACETYLASE COMPLEX 1) has a pivotal role in promoting plant growth (Perrella et al., 2013) as well as in flowering time determination (Ning et al., 2019). The interplay between HDA19 and HDC1 will be further discussed in section 1.1.3.1.

Other members of the HDAC superfamily in *Arabidopsis* have been functionally allocated to several pathways. Both HDA6 and HDA9 have been implicated in flowering time regulation, through controlling the expression of the floral integrator FT (FLOWERING LOCUS T) (Kang et al., 2015; Yu et al., 2011). Additionally, HDA6 is a regulator of the circadian clock,  forming a repressive complex with a H3K4 lysine

specific histone demethylase (LDL1) to repress core components of this pathway (Hung et al., 2019, 2018). In parallel, HDA15 is responsible for the repression of light-responsive chlorophyll and photosynthesis related genes in dark conditions, via protein-protein interaction with PIF3 (PHYTOCHROME INTERACTING FACTOR3) (Liu et al., 2013).

### 1.1.3    HDC1 and its role in transcriptional regulation

*1.1.3.1    HDC1 is a subunit of HDA19 and HDA6 Sin3-type HDAC complexes*

As described in section 1.1.2.2, association of HDACs with certain cofactors leads to specialized regulation of certain developmental and physiological pathways; such a cofactor with emerging significance in transcriptional regulation is HDC1 (HISTONE DEACETYLASE COMPLEX 1). Localized in the nucleus, HDC1 is encoded by a single-copy gene in *Arabidopsis* (AT5G08450), which has three splice variants that differ only at the 5' prime end untranslated region. Homologs have been found in all sequenced plant species (Perrella et al., 2013). *HDC1* has ubiquitous expression during all developmental stages and in all vegetative tissues, except anthers and stigmas, probably during reproduction-triggered silencing (Perrella et al., 2013).

HDC1 has a length of 918 amino acids and can be structurally divided in the N-terminal part, which has no homologous sequences in organisms outside the plant kingdom, and a ~300-amino-acid-long, C-terminal end. Between amino acids 603-645, this region shows high similarity with Rxt3 proteins, which are present in algae, protozoa and fungi, and specifically with the protein family domain "Histone deacetylation protein Rxt3" (InterPro ID: IPR013951) (Perrella et al., 2013). In yeast, Rxt3 is subunit of the large, Sin3-type RPD3 complex (RPD3L) and is involved in histone deacetylation, acting as a transcriptional regulator (Carrozza et al., 2005; Ruiz-Roig et al., 2010). Although there is no sequence similarity with the catalytic domains of other HDACs, based on its homology with Rxt3 it has been proposed that HDC1 is implicated in histone deacetylation.  Indeed, protein extracts of HDC1 knockout (*hdc1)* plants show elevated acetylated H3 levels (H3K49K14), supporting the notion that HDC1 has a role in histone deacetylation (Ning et al., 2019; Perrella et al., 2013). Moreover, the importance of the C-terminal, Rxt3-like part of HDC1 is highlighted by the fact that, its expression as a truncated version of HDC1 in the *hdc1* background partially rescues the growth and developmental defects of the mutants (Perrella et al., 2016). Additionally, a LCCL superfamily domain (InterPro ID: IPR036609) is predicted in the C-terminal end of HDC1, spanning between amino acids 587-597. The LCCL module has been mainly described in mammalian proteins and it has been suggested to participate in lipopolysaccharide binding (Liepinsh et al., 2001; Robertson et al., 1998; Trexler et al., 2000).

As mentioned above, the yeast Rxt3 is a component of the RPD3L complex, associated with the yeast HDAC RPD3 and the transcriptional repressor Sin3 (Carrozza et al., 2005). In *Arabidopsis,* HDC1 is interacting with two members of the RPD3-like HDAC family, HDA6 and HDA19, as part of their respective Sin3-type complexes as well as with the SIN3-LIKE protein SLN3 (Feng et al., 2021; Ning et al., 2019; Perrella et al., 2016, 2013). The functional significance of these interactions is supported by the fact that the transcriptome of *hdc1* mutants is highly correlating with HDA19 mutants (*hda19*) and to a lesser extent, with HDA6 mutants (*hda6*) (Feng et al., 2021). However, HDC1 is not necessarily always present in the HDA6/HDA19 complexes, as recent reports showed that the latter have the capacity to form SANT-/ESANT-/ARID-type complexes, each with distinct subunit composition (Feng et al., 2021; Ning et al., 2019). This fact may explain why *hdc1* mutants do not share all physiological phenotypes of *hda19* and *hda6* mutants. Additional interactions of HDC1 have been identified with the histone readers SHL1 (SHORT LIFE 1), ING2

(INHIBITOR OF GROWTH 2), MSI1 (MULTICOPY SUPRESSOR OF IRA 1) as well as with the transcriptional repressor SAP18 (SIN3 ASSOCIATED POLYPEPTIDE P18) (Perrella et al., 2016). Interestingly, Bimolecular Fluorescence Complementation (BiFC) assays indicated that HDC1 is associated with the linker histone H1 and not with the core histones H3 and H4, which are the ones usually subjected to deacetylation (Perrella et al., 2016). Based on these data and the lack of a catalytic domain in its protein sequence, it has been proposed that HDC1 may act as a scaffold protein in the HDAC complexes, stabilizing the assembly of these multiprotein complexes and/or their association with chromatin (Perrella et al., 2013).
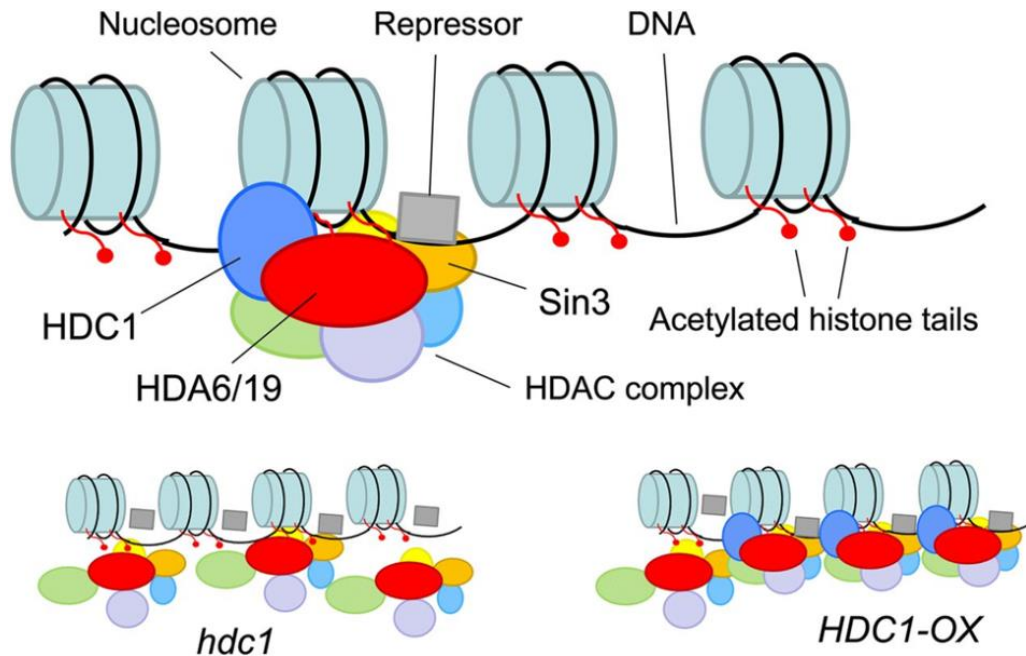


**Fig. 1 Proposed model for HDC1 function.**
*HDC1 is proposed to aid histone deacetylation by stabilizing the HDAC complex and/or its association with chromatin. In absence of HDC1, the function of the respective HDC1 complex is impaired, resulting in differential histone deacetylation and gene expression. The opposite effect takes place during HDC1 overexpression, possibly due to increased binding of the HDAC complex on its target loci. From Perrella et al., 2013.*

### 1.1.3.2 Loss of HDC1 transcriptionally affects flowering determination, ABA sensitivity, plant growth and stress responses

As described above, HDC1 seems to be an important component of at least two RPD3-like histone deacetylation complexes in *Arabidopsis*, with its absence severely deregulating transcriptional processes. The physiological importance of HDC1-mediated deacetylation has firstly been described from Perrella et al., who showed that *hdc1* mutants produce less biomass than WT, while the opposite effect was observed in transgenic overexpression lines. In the same publication, it was also demonstrated that ABA treatment and less intensely salt stress are interfering with the germination of *hdc1* mutants, a phenotype that can be attributed to higher expression of certain salt- or ABA-responsive genes in the mutant. The same team also reported the late flowering phenotype of the *hdc1* mutants, which was later mechanistically explained by Ning et al., 2019. This group showed the transcriptional upregulation of the floral suppressors GASA5 (GIBBERELLIC ACID-STIMULATED 5) and GA2OX6 (GIBBERELLIN 2-OXIDASE 6) in *hdc1* and *hda19* in long day conditions, which leads to repression of the core floral integrator FT, suggesting a role for HDC1 in photoperiodic determination of flowering. This effect is reversed at short day conditions, when *hdc1*

mutants exhibit an earlier than WT transition from vegetative to reproductive stage, possibly due to the de-repression of an unidentified positive floral regulator (Ning et al., 2019).

The role of HDC1 in transcriptional regulation of stress responses is further supported by the hypersensitive phenotype of *hdc1* mutants during Pi deficiency, exhibited by exaggerated WT-like responses and specifically, uncontrolled root growth inhibition and Fe deposition (Xu et al., 2020). To explain this, it was suggested that Pi-deficiency is promoting post-translational degradation of HDC1, leading to abnormal induction of *LPR1* (*LOW PHOSPHATE RESPONSE 1*) and *ALMT1* (*ALUMINUM-ACTIVATED MALATE TRANSPORTER 1*), two key genes in root tip-initiated low Pi responses. However, other studies are supporting that LPR1 is not transcriptionally regulated by Pi status, but rather by substrate availability or from the function of the P5A-type ATPase PDR2 (PHOSPHATE DEFICIENCY RESPONSE 2) by an unknown mechanism (Müller et al., 2015; Naumann et al., 2022). Nevertheless, the abovementioned phenotypes and the observation that, *hdc1* transcriptome is enriched in genes involved in stress processes (Feng et al., 2021), emphasize the pivotal role of HDC1 in development and plant adaptation to changing environmental conditions.


## 1.2    Mechanisms of plant adaptation to Pi starvation

### 1.2.1    The importance of phosphorus for plant development

Life greatly depends on the abundance and efficient acquisition of several macronutrients, like carbon (C), sulfur (S), nitrogen (N) and phosphorus (P). The latter and its bioavailable form, inorganic phosphate (Pi), has a dominant role in biological processes, like photosynthesis, energy storage and signal transduction, as well as acting as a building component of nucleic acids, biological membranes and other important molecules (Bowler et al., 2010). For normal growth, plants require approximately 2000 ppm Pi per dry weight, which is acquired from soil by the root system in the form of $H_2PO_4^-$ and $HPO_4^{2-}$ (Vance et al., 2003). However, Pi chemistry often restricts its bioavailability, due to the low diffusion rate and its retention by insoluble Fe/Al or Ca oxides at acidic or alkaline soil pH respectively (Hinsinger, 2001). Additionally, unlike N that continuously enters ecosystems through biological $N_2$ fixation, soil Pi content depends also on its original P composition of the parental rock, rendering it a finite resource (Abel, 2017).

The high biological demand for Pi in contrast with its low soil availability often force plants to initiate a set of physiological and developmental responses in order to avoid the repercussions of Pi deficiency. These phosphate starvation responses (PSRs) can be distinguished to systemic, aiming internal Pi recycling and conservation, or local, increasing Pi scavenging by the root system (Abel, 2017; Chien et al., 2018), and will be discussed in sections 1.2.3 and 1.2.4 respectively.


### 1.2.2    Signaling of Pi deficiency responses

Apart from its biological role, Pi has been proposed to be a signal, differentially regulating PSRs including the remodeling of root system architecture (RSA). External Pi supply defines RSA-related, local responses, driven by the sensing of Pi status from the root tip, while low internal Pi content triggers systemic responses, including Pi recycling and lipid metabolism (Svistoonoff et al., 2007; Thibaud et al., 2010). The notion that Pi can act as a signal is further supported by the non-metabolized Pi analog, phosphite (Phi), which suppresses PSRs, e.g., anthocyanin and starch accumulation, membrane lipid replacement and induction of several PSI (phosphate starvation induced) genes (Varadarajan et al., 2002; Kobayashi et al.

2006; Jost et al., 2015). Recent studies demonstrated that $InsP_8$, a inositol pyrophosphate, is a messenger molecule for intracellular Pi status, acting as a ligand between SPX (SYG1/Pho81/XPR1) domain-containing proteins SPX1 and SPX2 and PHR1 (PHOSPHATE STARVATION RESPONSE 1), a key positive regulator of PSRs (Dong et al., 2019; Ried et al., 2021). At Pi replete conditions, high intracellular Pi content promotes $InsP_8$ formation and accumulation, which binds to SPX1 and promotes physical association with PHR1, inhibiting its transcriptional activity (Dong et al., 2019). At limiting Pi concentration, reduced ATP levels lead to insufficient $InsP_8$ pools, causing dissociation of the SPX1-PHR1 complex and subsequently, PHR1-mediated activation of PSI genes (Dong et al., 2019; Zhu et al., 2019).

### 1.2.3 Systemic responses to Pi starvation enhance Pi recycling and conservation

Upon Pi deficiency, plants trigger a set of metabolic adjustments to ensure conservation of internal Pi (Plaxton and Tran, 2011). Low Pi availability results in reduction of cytosolic Pi and adenylate pools, which are co-substrates of the enzymes participating in classical glycolysis. To ensure respiratory C flux and energy production during Pi stress, a metabolic shift occurs, to alternative reactions that do not require Pi or adenylates (Duff et al., 1989; Plaxton and Podestá, 2006). Additionally, photosynthesis efficiency drops, as an attempt to conserve the Pi pool, resulting in accumulation of non-$P_i$ sugar, such as sucrose and starch (Giersch and Robinson, 1987; Rao et al., 1990). In parallel, increased anthocyanin content in shoots of plants grown at low Pi conditions is a typical PSR and is thought to prevent photoinhibitory damage in the chloroplasts (Takahashi et al., 1991; Zeng et al., 2010).

Another mechanism of internal Pi conservation is the adaptation of membrane composition to low cellular Pi levels, by replacing phospholipids with sulfolipids and galactolipids, like sulfoquinovosyldiacylglycerol and digalactosyldiacylglycerol, respectively (Essigmann et al., 1998; Frentzen, 2004; Yu et al., 2002). Specifically, sulfolipids are synthesized by the action of SQD1/2 (SULFOQUINOVOSYLDIACYLGLYCEROL 1/2), which are phosphate starvation induced, while *sqd2* mutants have impaired growth during Pi scarcity (Benning, 1998; Yu et al., 2002).

Among PSRs aiming more efficient Pi use is the mobilization of Pi from external and internal resources (Plaxton and Tran, 2011; Ticconi and Abel, 2004). One such external source could be the decaying organic matter in soil, where Pi is bound in the form of nucleic acids. Notably, *Arabidopsis* plants can normally grow in Pi deficient agar medium supplemented with DNA or RNA (Chen et al., 2000). This is possible because *Arabidopsis* root secrete an array of enzymes, including ribonucleases, nucleases, phosphodiesterases and acid phosphatases into the rhizosphere, that will degrade these compounds and release Pi for high-affinity uptake (Plaxton and Tran, 2011; Ticconi and Abel, 2004). Such enzymes have PSI expression, as was demonstrated by the induction of RNS1 and cyclic nucleotide phosphodiesterases upon Pi stress (Bariola et al., 1994; Abel et al., 2000). Similarly, Pi is recycled from intracellular sources, like expendable Pi monoesters and anhydrides or nucleic acid molecules (Vance et al., 2003).

### 1.2.4 Pi limitation-triggered reorganization of root architecture

Around 70-80% of all terrestrial plant species have the capacity to form symbiotic relationships with arbuscular mycorrhiza (AM), a heterogenous group of fungi (Barea et al., 2008). These interactions are beneficial for plants during Pi limitation as AM hyphal network scavenge Pi further into the soil and translocate it to the colonized roots (Schnepf et al., 2011; Smith et al., 2011). *Arabidopsis* lacks the genetic symbiotic toolkit that would allow association with AM and is considered a non-host species (Delaux et al.,

2014). Nevertheless, *Arabidopsis* enhances Pi uptake by extending the barrier between soil and root surface through remodeling of RSA (Abel, 2017; Sato and Miura, 2011). Specifically, Pi deficiency leads to a shallow root system, by attenuating primary root growth, while simultaneously promoting lateral root and root hair development; these adaptations result in extending the absorbing surface of the root system as well as better Pi scavenging from the topsoil, which is richer in this macronutrient (Abel, 2017; Giehl and von Wirén, 2014; Péret et al., 2014; Salazar-Henao et al., 2016).

The mechanisms that govern primary root growth inhibition upon Pi deficiency have been extensively studied over the last years (Balzergue et al., 2017; Müller et al., 2015; Naumann et al., 2022). Short Pi stress (<2 h) inhibits cell elongation in the differentiation zone while prolonged Pi limitation (<2 days) negatively affects cell division in the root meristem (Balzergue et al., 2017; Müller et al., 2015). Continuous Pi absence effectively leads to stem cell niche (SCN) exhaustion, finally leading to primary root growth attenuation (Ticconi et al., 2009). Interestingly, local Pi sensing and inhibition of primary root elongation depend on external Fe availability, as it has been shown by the continuous growth of Pi-starved roots in absence of external Fe (Müller et al., 2015; Ward et al., 2008). Additionally, Pi starved root tips hyperaccumulate Fe localized at the root meristem (Müller et al., 2015; Svistoonoff et al., 2007). These phenotypic responses are related to the function of two modules, the ALMT1-STOP1 module (ALUMINUM-ACTIVATED MALATE TRANSPORTER 1-SENSITIVE TO PROTON RHIZOTOXICITY 1) and the LPR1-PDR2 module (LOW PHOSPHATE ROOT 1-PHOSPHATE DEFICIENCY RESPONSE 2) (Abel, 2017). ALMT1 is a malate efflux transporter, controlled by the transcriptional factor STOP1 (Liu et al., 2009; Tokizawa et al., 2015) LPR1 is a cell-wall resident, multicopper ferroxidase with $Fe^{2+}$ oxidizing activity, the action of which is restricted by an unknown mechanism by the function of the ER-based P5-ATPase PDR2 (Müller et al., 2015; Naumann et al., 2022). According to the current model, upon Pi deficiency leads to STOP1 stabilization and induction of *ALMT1*, leading to malate exudation in the rhizosphere and mobilization of Pi from Fe–Pi complexes by $Fe^{3+}$-chelation (Balzergue et al., 2017; Naumann et al., 2022). Ascorbate-mediated reduction of $Fe^{3+}$-malate triggers reactive oxygen species production (ROS), stimulating callose deposition in the stem cell niche (Naumann et al., 2022). This cell wall modification interferes with symplastic communication and results in rapid reduction in cell division in the SCN, thus impairing root growth (Müller et al., 2015). In parallel, Fe redox cycling is promoted by LPR1-dependent $Fe^{2+}$ oxidation, exhibited as $Fe^{3+}$ accumulation in the apoplast of SCN, alleviating ROS formation (Naumann et al., 2022). Overall, it is proposed that local Pi responses are governed by Fe-dependent cues, translated by LPR1-dependent processes in the root tip (Naumann et al., 2022).
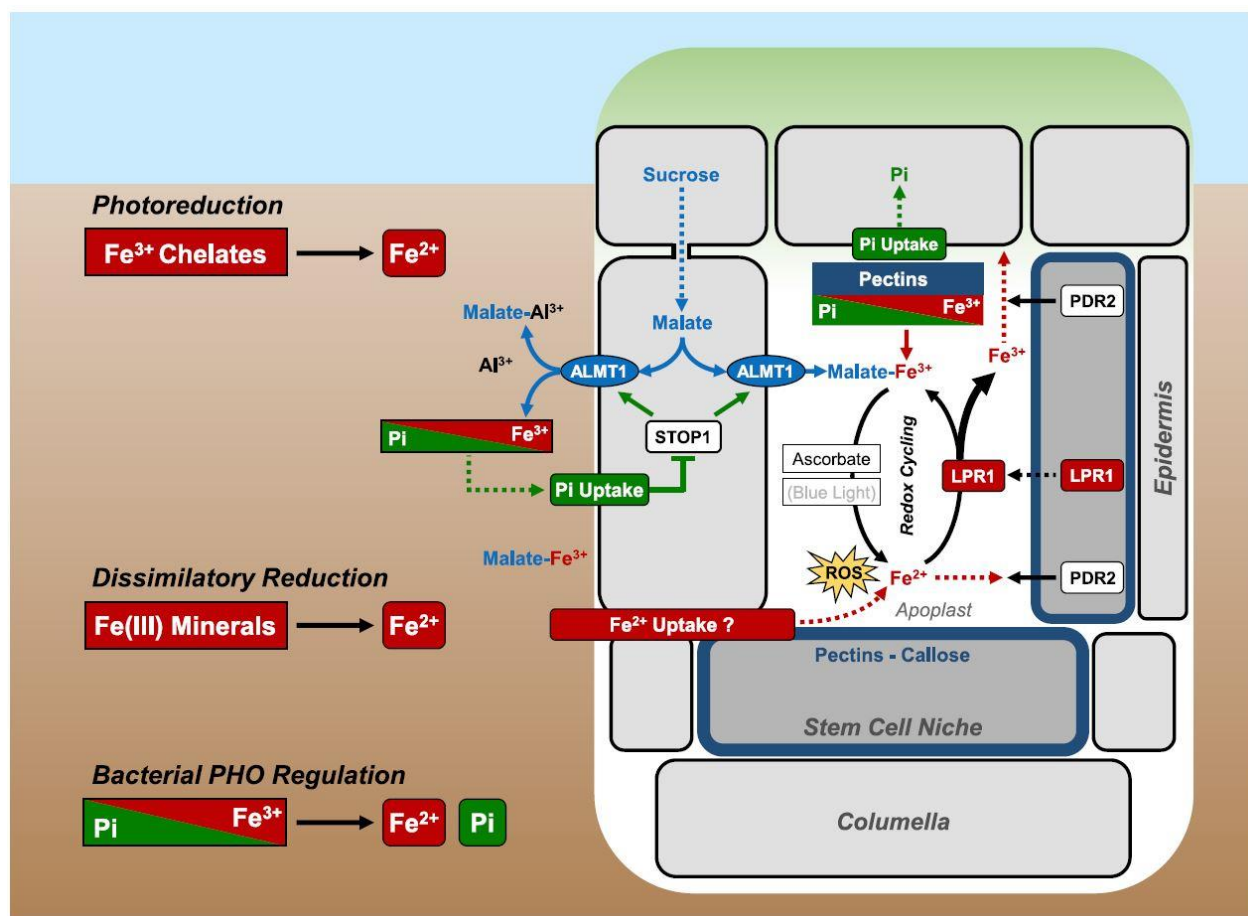
**Fig. 2 Important players of local phosphate deficiency responses. From Naumann et al. (2022).**
*ALMT1 release malate into the rhizosphere as well as root apoplast, resulting in mobilization of Pi from Fe-Pi complexes by $Fe^{3+}$-chelation. Subsequent reduction of $Fe^{3+}$-malate promotes ROS formation, while LPR1 dependent $Fe^{2+}$ oxidation relieves from ROS production and possibly mediates ROS signaling in SCN. PDR2 counteracts LPR1 function by maintaining Fe homeostasis in root tips.*
*Abbreviations: LPR1, LOW PHOSPHATE ROOT1; PDR2, PHOSPHATE DEFICIENCY RESPONSE2; ALMT1, ALUMINUM-ACTIVATED MALATE TRANSPORTER 1; STOP1, SENSITIVE TO PROTON RHIZOTOXICITY 1; PHO, PHOSPHATE REGULON; ROS, Reactive Oxygen Species.*

## 1.3    Glucosinolates biosynthesis and biological role

Glucosinolates (GSLs) are sulfur- and nitrogen- containing compounds, occurring naturally in members of the Brassicaceae family, including the agriculturally important species cabbage, broccoli, horseradish, mustard as well as the model plant *Arabidopsis thaliana* (Harun et al., 2020). Typically associated with plant defense responses, they give a characteristic flavor to these vegetables and are thought to have health promoting effects for humans (Hecht, 2000; Possenti et al., 2017).

Structurally, the basic core of all GSLs is comprised of a β-thioglucose residue, linked via a sulfur atom to a (Z)-*N*-hydroximinosulfate ester and variable side chain, deriving from a precursor amino acid (Fahey et al., 2001). Depending on the precursor, the biosynthetic pathways of GSLs are branched into aliphatic, deriving from methionine, aromatic from phenylalanine or tyrosine and indolic from tryptophan (reviewed in Harun et al., 2020; Blažević et al., 2020). This gives rise to a remarkable variety amongst the final compounds, with 137 suggested GSL structures, from which 88 are confirmed, while 36 have been

identified in *Arabidopsis* (Brown et al., 2003; Ivica Blažević et al., 2020). The biosynthetic pathway of aromatic GSLs is very similar to the one producing aliphatic GSLs, although  less comprehensively characterized (Harun et al., 2020); for that reason, only the pathways of aliphatic and indolic GSLs will be described, in sections 1.3.1.1 and 1.3.1.2 respectively.

## 1.3.1   Glucosinolate metabolism

### *1.3.1.1   Biosynthesis of aliphatic and aromatic glucosinolates*

The first stage in the biosynthetic pathway of aliphatic GSLs is the side-chain elongation of the precursor amino acid, in this case methionine; firstly, methionine is converted to 2-oxoacid by BCAT4-mediated deamination (Schuster et al., 2006), which is then transferred to the chloroplasts via bile acid transporter BAT5-mediated transportation (Gigolashvili et al., 2009). Next, 2-oxoacid is undergoing through a 3-step transformation, initiated by its conversion to a methylthioalkylmalate (MAM) intermediate via condensation with acetyl-CoA by MAM1-3 (Kroymann et al., 2001). Subsequent reactions are MAM isomerization by IIL1 and IPMI1/2 and oxidative decarboxylation by IMDH1-3 (Bones and Rossiter, 1996; He et al., 2011, 2009; Knill et al., 2009; Sawada et al., 2009); the resulting compound is a chain-elongated 2-oxo acid, that can either enter the next biosynthetic stage or undergo more elongation cycles. Depending on how many such cycles will follow, this process will finally produce homomethionine or various chain-elongated derivatives of methionine, corresponding to short or long final GSL compounds, with 3-5 or 6-8 carbons number on their side chain respectively (Harun et al., 2020). From the enzymes mentioned above, MAM1 is involved in biosynthesis of GSLs via two elongation cycles, while MAM3 participates in side elongation of 2-oxoacid via one, five or six cycles (Field et al., 2004; Kroymann et al., 2001; Textor et al., 2007).

The next stage is the core structure synthesis of aliphatic GSLs, beginning with conversion of side-chain elongated amino acids to aldoximes, by CYP79F1/2; CYP79F1 has universal activity while the substrates of CYP79F2 are limited to long-chained elongated amino acids (Chen et al., 2003; Hansen et al., 2001; Miao et al., 2013). Aldoximes are oxidized to *aci*-nitro compounds by CYP83A1 (Naur et al., 2003) and later conjugated with glutathione (GSH) by GSTF1/20 (Czerniawski and Bednarek, 2018; Wentzell et al., 2007). These GSH conjugates are converted into thiohydroximates by cleavage, first from GGP1 producing Cys-Gly conjugates (Geu-Flores et al., 2011) and then, by the C-S lyase SUR1 (Mikkelsen et al., 2004). Thiohydroximates are glycosylated into desulfo-GSLs by action of UGT74B1 and UGT74C1 (Gachon et al., 2005; Grubb et al., 2014, 2004) and finally sulphated into intact GSLs by SOT16/17/18 (Klein and Papenbrock, 2009; Piotrowski et al., 2004).

The last step in biosynthesis of aliphatic GSLs is the side-chain modification, which is essential for formulation the biological activities of the GSL hydrolysis products (isothiocyanates and nitriles) (Li et al., 2011). Firstly, methylthiolalkyl-GSLs are metabolized to methylsulfinylalkyl-GSLs via S-oxygenation catalysed by seven flavin monooxygenases, FMO-GS$_{OX1-7}$ (Hansen et al., 2007; Li et al., 2008, 2011). Side chain modification is continued by oxygenation mediated by 2-oxoglutarate-dependent dioxygenases AOP2 and AOP3, converting methylsulfinylalkyl-GSLs to alkenyl-GSLs and hydroxyalkyl-GSLs, respectively (Burow et al., 2015; Jensen et al., 2015). Lastly, alkenyl-GSLs are converted into hydroxylated alkenyl GSL by GSL-OH and hydroxyalkyl-GSLs into benzoylated GSLs or sinapoylated GSLs by carboxypeptidase-like acyltransferase SCPL17 (Kliebenstein et al., 2007; Lee et al., 2012).

### 1.3.1.2   Biosynthesis of indolic glucosinolates

Unlike the biosynthetic pathways of aliphatic and aromatic GSLs, indolic GSLs biosynthesis is initiated directly at the core synthesis stage, by conversion of tryptophan to indole-3-acetaldoxime by CYP79B2 and CYP79B3, omitting entirely the step of side chain elongation (Hull et al., 2012; Mikkelsen et al., 2003). Next, the acetaldoxime is metabolized to nitrile oxide compounds by CYP83B1 (Bak et al., 2001; Naur et al., 2003), followed by sulfur addition through the activities of GSTF9, GSTF10 and GSTU13 (Hirai et al., 2006; Piślewska-Bednarek et al., 2018; Wentzell et al., 2007). The GSH conjugate that is formed in the previous step is converted to Cys-Gly conjugate by the glutamyl peptidases GGP1 and GGP3 (Geu-Flores et al., 2011; Malka and Cheng, 2017), which is transformed thiohydroximate via SUR1-dependent C–S lyase reaction (Malka and Cheng, 2017; Mikkelsen et al., 2004; Nintemann et al., 2018). The core synthesis of indolic GSLs is concluded by UGT74B1-mediated glycosylation (Grubb et al., 2004) and generation of 3-indolmethyl GSL (I3M) via subsequent sulfonation by SOT16 and SOT17 (Klein and Papenbrock, 2009; Sønderby et al., 2010).

The first step of the ring modification is catalysed by members of the cytochrome P450 monooxygenase subfamily CYP81F; CYP81F1-4 metabolize I3M to 1-hydroxy-3-indolylmethyl GSL (1OH13M), while CYP81F1-3 to 4-hydroxy-3-indolyl-methyl GSL (4OHI3M) (Pfalz et al., 2011, 2009). The previous hydroxy-GSLs are converted to the methoxy-GSLs, via the action of the O-methyltraferases IGMT1/2/5 or IGMT/1/2 respectively (Pfalz et al., 2016, 2011, 2009). Methoxy-GSLs 1MOI3M and 4MOI3M are the final compounds of this pathway.

### 1.3.1.3   Glucosinolate transportation, storage and catabolism

In *Arabidopsis*, previous studies led to the identification of several GSL transporters. As mentioned above, one of them is BAT5, which is involved in the subcellular translocation of 2-oxoacids inside chloroplasts, during the side-chain elongation stage of aliphatic GSLs (Gigolashvili et al., 2009). Additionally, two other transporters, GTR1 and GTR2, have pivotal role in long-distance aliphatic GSL transportation to seeds and distribution of GSLs between shoots and roots (Andersen et al., 2013; Nour-Eldin et al., 2012). These high affinity transporters are expressed in cortex cells and vasculature and are involved in phloem-loading of GSLs, thus shaping the GSL distribution pattern (Andersen et al., 2013; Nour-Eldin et al., 2012). During the vegetative stage, rosettes are the main source and sink for short-chain aliphatic glucosinolates, while roots are the sink tissues for long-chained aliphatic GSLs; both rosettes and roots have the capacity for *de novo* biosynthesis of long aliphatic and indolic GSLs (Andersen et al., 2013). Transportation of long-chained GSLs can be directional between above- and below- ground tissues, however their retention in the roots and upward movement is GTR1/2-dependent (Andersen et al., 2013).

Upon translocation to their sink tissue, GSLs are stored in the vacuoles of sulfur-rich, specialized cells, called S-cells, which are located in proximity to the vasculature (Koroleva et al., 2000; McCully et al., 2008). Additionally, in *Arabidopsis* leaves, GSLs are also found in long, longitudinal cells across the leaf margin, thus acting as a defense perimeter in the leaf periphery (Shroff et al., 2008). The biological relevance of nonuniformal GSL distribution is also underlined by the fact that there is higher GSL accumulation at the more vulnerable abaxial side of the leaf (Shroff et al., 2015).

In the event of herbivory attack, GSLs are released and then hydrolyzed by thioglucoside glucohydrolases (TGG), also known as myrosinases (Bones and Rossiter, 1996; Thangstad Op et al., 2004); the *Arabidopsis* genome encodes 6 TGGs, while TGG1 and TGG2 were found to be involved in GSL degradation upon insect attack (Barth and Jander, 2006). Myrosinases are localized in different cells or cellular compartments than

GSLs and are in contact with GSLs only upon tissue disruption, e.g., through chewing (Halkier and Gershenzon, 2006; Thangstad et al., 2004). Depending on the plant species, pH and GSL side-chain, the hydrolysis products include a variety of isothiocyanates and nitriles, which have toxic effects (Wittstock and Burow, 2010); isothiocyanates and nitriles are degradation products of all types of GSLs, while epithionitriles are deriving only from aliphatic GSLs (Blažević et al., 2020).
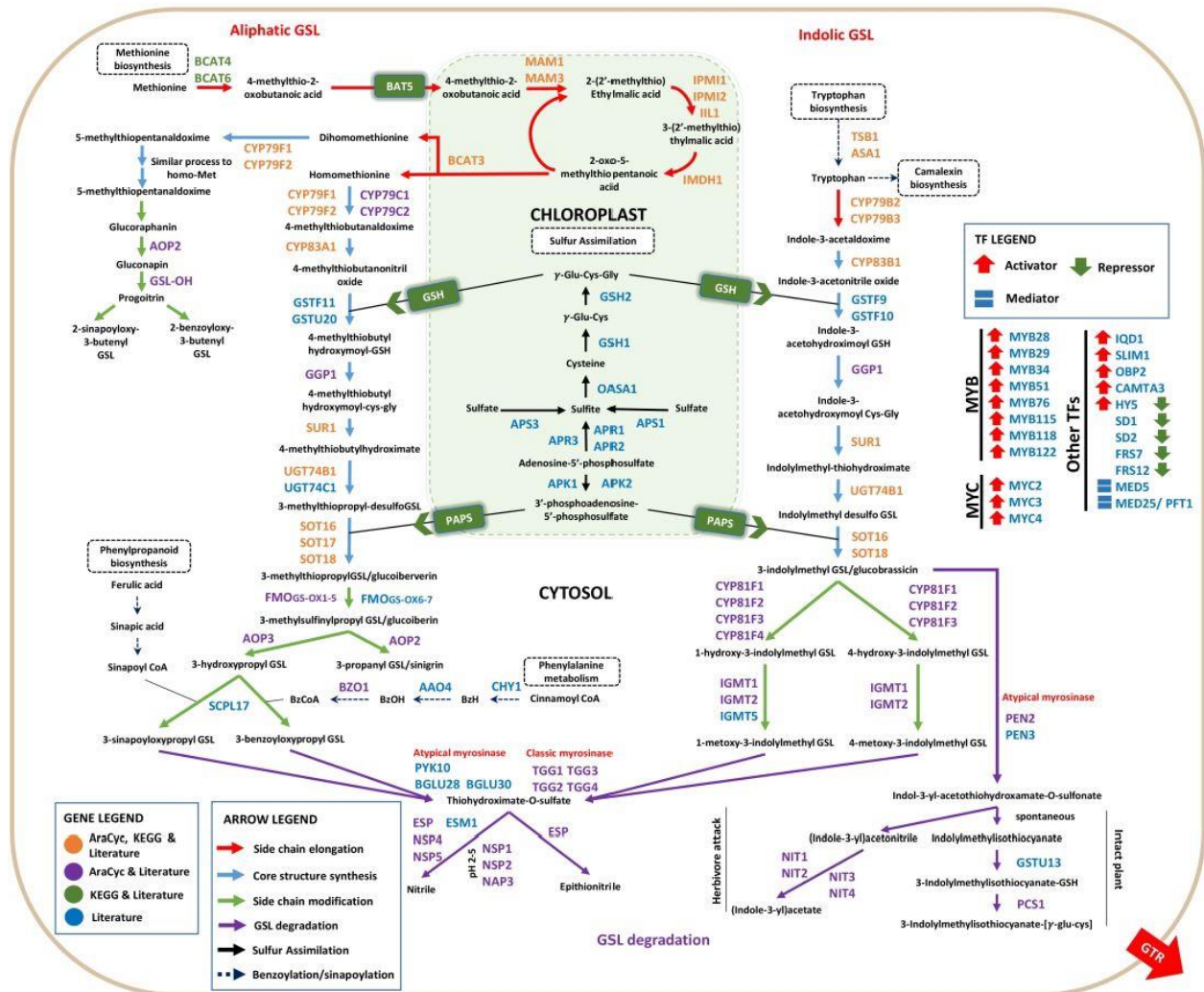


*Fig. 3* **Aliphatic and indolic GSL metabolic pathways and transcriptional regulation in Arabidopsis. From Harun et al., 2020.**
*Biosynthesis and degradation pathways of methionine-derived, aliphatic GSLs (left) and tryptophan-derived indolic GSL (right) are depicted in this scheme. Main transcriptional players regulating the pathways are also shown to the far right.*
*Abbreviations: AAO4, aldehyde oxidase 4; AOP2, 2-oxoglutarate-dependent dioxygenase; APK, adenylyl-sulfate kinase; APR, 5'-adenylylsulfate reductase; ATPS, ATP sulfurylase; BAT5, probable sodium/metabolite cotransporter BASS5; BCAT, branched-chain amino acid aminotransferase; BZO1, benzoyloxy GSL 1; BzH, benzaldehyde; BzOH, benzoic acid; BzCoA, benzoyl-coenzyme A; CHY1, 3-hydroxyisobutyryl-CoA hydrolase 1; CYP79A, phenylalanine N-monooxygenase; CYP79B, tryptophan N-monooxygenase; CYP79F, cytochrome P450 79F1; CYP83B, CYP83B monooxygenase; FMOGS-OX, flavincontaining monooxygenase; GGP1, γ-glutamyl peptidase 1; GSH, glutathione; GSH1, glutamate–cysteine ligase; GSTF, glutathione S-transferase F; GTR, GSL transporter; IGMT, indole GSL O-methyltransferase; IIL1, isopropylmalate isomerase large subunit 1; IPMI, isopropylmalate isomerase small subunit 1; MAM, methylthioalkylmalate synthase; PAPS, 3'-phosphoadenosine-5'-phosphosulfate; SOT, sulfotransferase; SCPL17, serine carboxypeptidase-like 17.*

## 1.3.2 Regulation of glucosinolate biosynthesis

Expression of GSL core pathway genes is controlled by transcription factors of the myeloblastosis (MYB) and myelocytomatosis (MYC) families. Aliphatic GSLs are mainly regulated by MYB28, MYB29 and MYB76 (Gigolashvili et al., 2007b, 2008; Hirai et al., 2006), while MYB115 and MYB118 were found to negatively control biosynthesis of benzoyloxy GSLs, Arabidopsis-specific methionine-derived GSLs (Zhang et al., 2015). MYB28 is considered the master regulator of aliphatic GSLs metabolism, contributing to the biosynthesis of both long and short side-chain aliphatic GSLs, (Gigolashvili et al., 2007b; Sønderby et al., 2010). *Myb28* mutants show a strong reduction in transcripts of genes involved in the side-chain elongation stage of aliphatic GSLs (*BCAT4*, *MAM1*, *MAM3*, the *IPMIs,* and *BAT5*), as well as genes at the later stages (*FMO-GS$_{OX1}$* and *FMO-GS$_{OX3}$*)(Sønderby et al., 2010); interestingly, chemotype of *myb28* is almost devoid of long side-chain aliphatic GSLs, while two-thirds of the wild-type levels of short-chained aliphatic GLS are still present. MYB29/MYB76 are mostly involved in the biosynthesis of short GSLs, while an interdependency network of the three aliphatic GSL-related MYB genes has been proposed, where MYB76 is positively regulation MYB29, which is negatively regulating MYB28 (Sønderby et al., 2010). In parallel, the tryptophan-deriving indolic GSLs are under the control of MYB51, MYB34 and MYB122 (Gigolashvili et al., 2007a; Malitsky et al., 2008). MYC2, MYC3 and MYC4 constitute additional components of the GSL biosynthesis regulatory machinery, physically interacting with GSL-regulating MYB factors to promote both aliphatic and indolic GSL biosynthesis (Schweizer et al., 2013).

Several cues have been shown to be involved in the transcriptional regulation of the GSL biosynthetic pathways. One such internal cue is the phytohormone abscisic acid (ABA); previous studies demonstrated that the glucose-induced ABA signaling  positively regulates *MYB28* and *FMO$_{GS-OX2/4}$* expression, through ABI5 and ABI1/2 regulation respectively (Li et al., 2021; Miao et al., 2013). A better studied case is the regulation of GSL metabolism through jasmonate (JA), which has been shown to be a major player in plant defenses against herbivory and a potent elicitor of glucosinolate biosynthesis (Mikkelsen et al., 2003; Wasternack and Hause, 2013). Upon JA treatment, indolic GSL accumulation is observed, coinciding with upregulation of several genes involved in their biosynthesis (Mikkelsen et al., 2003). In parallel, methyl JA is an elicitor of *MYB29* expression, which promotes aliphatic GSL biosynthesis (Gigolashvili et al., 2008). Moreover, the GSL biosynthesis-inducing factors MYC2/3/4 factors are involved in JA signaling, promoting JA-mediated insect herbivory-induced defense responses (Fernández-Calvo et al., 2011; Schweizer et al., 2013). In line with these findings, Ca$^{2+}$/calmodulin (CaM)-dependent signaling in response to insect herbivory is involved in GSL metabolism, via IQD1 (IQ DOMAIN 1)/CAMTA3 (CALMODULIN-BINDING TRANSCRIPTION ACTIVATOR 3)-mediated regulation (Laluk et al., 2012). Another interesting module of GSL biosynthesis regulation is the light dependent tuning of the gene expression in this pathway. Huseby et al. proposed the diurnal regulation of GLS biosynthesis, by HY5 (LONG HYPOCOTYL5)-mediated induction of MYB34 and MYB122 and repression of MYB28/MYB29/76, which control the indolic and aliphatic GSL abundance respectively (Huseby et al., 2013). Moreover, overexpression of CIRCADIAN CLOCK-ASSOCIATED1 (CCA1), a well-studied central circadian clock regulator, increased the defense capacity of the transgenic plants against aphid infestation, due to enhanced indolic GSLs accumulation (Lei et al., 2019). Additional proof for the circadian control of GSL metabolism were provided by the work of Fernández-Calvo et al., 2020; the authors demonstrated the repression of the GSL pathway during short days by the circadian integrators FRS7/12 (FAR1 RELATED SEQUENCE 7/12), through physical interaction with the corepressor Novel Interactor of JAZ (NINJA). Given the fact that NINJA is a corepressor of the JA signaling pathway and that there is a growing body of evidence that plant defenses might be synchronized

with circadian clock (Fernández-Calvo et al., 2020; Goodspeed et al., 2012; Greenham and McClung, 2015), regulation of GSL biosynthesis might be an example of the interplay of these processes.

### 1.3.3  Biological function of glucosinolates

Typically, the biological role of GSLs is thought to be revolving around defense responses. As described above, the mechanical wounding of the tissue, e.g. through chewing, initiates their degradation through myrosinase-mediated enzymatic hydrolysis, hence rendering them an important weapon in plants' arsenal against herbivores, like mammals, insects, birds and nematodes (Giamoustaris and Mithen, 1995; Halkier and Gershenzon, 2006). Their mode of action includes toxic effects, growth inhibition or general deterrence of the attacker (Agrawal and Kurashige, 2003; Burow et al., 2006; Kos et al., 2012; Newman et al., 1992), while it is interesting that herbivores have differential tolerance to different GSL species (Müller et al., 2010). For example, indolic GSLs have a stronger toxicity effect on aphids due to their potent post-ingestive breakdown products, an attribute lacking from aliphatic GSLs (Kim et al., 2008; Kim and Jander, 2007). Additionally, the antimicrobial properties of GSLs have been extensively studied; aliphatic glucosinolates have been shown to be involved in non-host resistance against bacteria (Fan et al., 2011), while several studies demonstrated the antifungal activity of indolic GSLs (Bednarek et al., 2009; Clay et al., 2009; Sanchez-Vallet et al., 2010).

GSL metabolism has also been implicated with several development and physiological processes. A number of GSL mutants have growth defects, which can be attributed to impaired cross-talk between GSL biosynthesis and hormone signaling, including auxin or jasmonate (JA) (Burow et al., 2015; Mikkelsen et al., 2004). Specifically for auxin, an intersection of IAA biosynthesis with indolic GSL metabolism has been described by Fu et al., 2016;  they suggested that degradation of indolic GSLs by the root tip-specific myrosinases TGG4 and TGG5 leads to unstable aglycones, which are forming indole-3-acetonitrile (IAN), that can finally be converted to indole-3-acetic acid (IAA). Additionally, different types and severity of abiotic stresses seem to differentially affect GSL metabolism (Martínez-Ballesta et al., 2013). For instance, different *Brassica* species show increase or decrease of GSL abundance upon drought stress, depending on the severity of the stress (Martínez-Ballesta et al., 2013). Furthermore, potassium deficiency leads to GSL accumulation in *Arabidopsis*, probably through JA-signalling (Troufflard et al., 2010).

A metabolic relationship between GSL and Pi starvation responses (PSRs) was demonstrated by metabolite profiling of Pi-starved roots and shoots of *Arabidopsis* seedlings, showing low Pi-induced accumulation of mainly aliphatic GSL compounds and upregulation of the expression of their respective biosynthetic genes (Pant et al., 2015). Another functional link between GSL biosynthesis and PSRs was provided by Hiruma et al.; their work indicated that Pi deficiency triggers colonization of *Arabidopsis* roots by the fungal endophyte *Colletotrichum tofieldiae (Ct)*, enhancing plant growth via direct, *Ct*-mediated Pi transfer into the host. (Hiruma et al., 2016). However, this interaction was beneficial for the plant only if the indolic GSL biosynthetic pathway was intact, demonstrated by the deleterious effect of *Ct* colonization of *cyp79B2cyp79B3* double mutant plants, depleted in indolic GSL and camalexin. Additionally, the growth promoting effect of low Pi-triggered *Ct* colonization was significantly reduced in mutants of PSR regulators PHR1 and PHL1. Moreover, another study proposed the co-ordination of plant PSRs with immune responses by PHR1, via negative regulation of salicylic acid (SA)-responsive defense response-related genes and positive regulation of PSI genes participating in GSL biosynthesis (Castrillo et al., 2017). The notion that GSL biosynthesis is responsive to Pi status via PHR1-mediated regulation is also corroborated by the fact that *phr1* mutants fail to show enhanced GSL abundance during Pi deficiency (Pant et al., 2015).

## 1.4    Chlorophyll metabolism and regulation

### 1.4.1    The biosynthetic pathway of chlorophyll

Chlorophylls (Chls) are the most abundant tetrapyrroles in plants and they are best known for their pivotal role in photosynthesis, as pigments of light energy harvesting and transfer to the reaction centers (Masuda and Fujita, 2008). Tetrapyrroles are macrocyclic molecules, composed of four pyrrole rings, linked by unsaturated methine groups; the different properties these molecules are defined by their molecular structure of conjugated double bonds, the variation of substituted side chains and the chelation of their bound metal ions, such as Fe (e.g., in hemes) or Mg (in Chl) (Brzezowski et al., 2015). Chl shares the same biosynthetic pathway as other tetrapyrroles and metabolic flux towards them can affect its biosynthesis (Kobayashi and Masuda, 2016).

The biosynthetic pathway of Chl has been extensively studied; in this section, it will be summarized according to Kobayashi and Masuda, 2016. In plants, algae and many bacteria, the first step of heme and Chl biosynthesis is the generation of 5-aminolevulinic acid (ALA), the common precursor of all tetrapyrroles (Oborník and Green, 2005). This processes requires three enzymatic steps, starting from Glu-tRNA$^{Glu}$ formation from Glu and tRNA$^{Glu}$ within plastids and subsequent reduction to Glu 1-semialdehyde (GSA) by Glu-tRNA reductase (GluTR); the latter reaction is the first rate-limiting step in tetrapyrrole biosynthesis, as the rate of ALA synthesis is crucial for metabolic flow through the pathway (Klein and Papenbrock, 2009). ALA is formed by a transfer of an amino group to GSA by GSA aminotransferase (GSAT) and finally two ALA molecules are condensed to form the monopyrrole porphobilinogen (PBG). Four PBG molecules are then sequentially polymerized and form the unstable linear tetrapyrrole hydroxymethylbilane (HMB). This will be metabolized to a series of macrocyclic intermediates, a process that will result in the generation of protoporphyrin (Proto) IX, which is the common precursors in the following biosynthetic pathways for Chl (Mg-branch) and the heme pathway (Fe-branch).

The first step in the Mg-branch is the incorporation of an Mg$^{2+}$ ion into the Proto IX macrocycle, to form Mg-Proto IX. This reaction is catalyzed by the Mg-chelatase, comprised of the three subunits CHLD, CHIH, and CHLI in plants, while GUN4 has a regulatory role in the complex stability and substrate and/or product channeling (Adhikari et al., 2011; Kopečná et al., 2015). Mg-Proto IX is converted to 3,8-divinyl-protochlorophyllide (DV-Pchlide) by two consecutive reactions and then reduced by Pchlide oxidoreductase (POR) to form 3,8-divinyl-chlorophyllide (DV-Chlide), a step that is light-dependent in Angiosperms. Then, DV-Chlide is converted to 3-vinyl Chlide *a* (MV-Chlide *a*) by the function of DV-Chlide reductase (DVR), which is then esterified with geranylgeraniol or phytol by Chl synthase to form Chl *a*. A portion of Chlide *a* or Chl *a* is metabolized to Chlide *b* or Chl *b*, by Chlide *a* oxygenase (CAO)-mediated catalysis. Mature Chl *a/b* is then incorporated into chlorophyll binding proteins, including the members of the nuclear-encoded superfamily of light-harvesting complexes (LHC), the LHC-like proteins and the plastid-encoded structural components of PSII and PSI, D1, D2, CP43, CP47, PsaA, and PsaB (Wang and Grimm, 2021).

### 1.4.2    Regulatory mechanisms of chlorophyll biosynthesis

Cells have developed multi-leveled mechanisms for control of Chl biosynthesis, ranging from transcriptional tuning of biosynthetic genes to metabolic regulation. These mechanisms ensure the synchronization of chloroplast biogenesis with Chl biosynthesis, which is crucial for avoiding cell damage from reactive oxygen species generation from Chl intermediates (Triantaphylidès and Havaux, 2009). Key

metabolic checkpoints are located at the rate of ALA synthesis, at the branch point for proto IX which controls the distribution of this intermediate to heme or Chl or at the light dependent formation of Chlide (Papenbrock and Grimm, 2001). Below, the key transcriptional components and the external/internal cues governing Chl biosynthesis will be summarized.

### 1.4.2.1   Dark-regulated expression of PORA/B is crucial for Chl biosynthesis upon illumination

Light is one of the most important cues controlling Chl metabolism. As described in section 1.4.1, the formation of chlorophyllide from Pchlide is catalyzed by the POR enzymes. This step is of particular interest as in some organisms, including algae, cyanobacteria and some plant taxa, can take place in the dark, by the action of light-independent (dark-operative) DPORs (Kobayashi and Masuda, 2016). Angiosperms possess only light-dependent PORs (LPORs) and for that reason, Chl biosynthesis requires light for its catalysis, otherwise leading to Pchlide accumulation. *Arabidopsis* encodes three *POR* genes (*PORA,PORB, PORC*), from which *PORA* and *PORB* are expressed during skotomorphogenesis (Matsumoto et al., 2004), while the proteins are accumulating in etioplasts, promoting the formation of prolamellar bodies (Franck et al., 2000; Paddock et al., 2010). This process is dependent on COP1 (CONSTITUTIVE PHOTOMORPHOGENIC 1) and also involves the ethylene-inducible transcription factors EIN3/EIL1 (ETHYLENE INSENSITIVE3/EIN3-LIKE1) for the upregulation of *PORA/B*, thus integrating ethylene signaling in regulation of Chl biosynthesis (Sperling et al., 1998; Zhong et al., 2009). Additionally, DELLA proteins can enhance *PORA/B* expression in the dark, through gibberellin signaling (Cheminant et al., 2011; Feng et al., 2008), while ABI4 (ABA INSENSITIVE 4) positively regulates *PORA*, probably through COP1 induction (Xu et al., 2016). The tight regulation of dark-maintained expression of PORs ensures that upon de-etiolation, Pchlide will be efficiently metabolized, thus avoiding the photo-oxidative damage of free Pchlide (not bound to POR) (Cheminant et al., 2011; Sperling et al., 1998). In parallel with these processes, the expression of most Chl biosynthetic genes is repressed in the dark by the action of PIFs or COP1, in order to prevent photodamage upon exposure to light (Kobayashi and Masuda, 2016; Matsumoto et al., 2004).

### 1.4.2.2   Light signaling promotes Chl biosynthesis

Light signaling is the driving force for initiation of Chl biosynthesis and photomorphogenesis. Light quality and quantity is monitored by photoreceptors, including phytochrome and cryptochrome families of photoreceptors, which translate the light cues into a signaling cascade in the nucleus (Chen et al., 2004; Leivar and Quail, 2011; Quail, 2002). Two groups of transcriptional factors are responsible for the transduction of the light signal, the PHYTOCHROME-INTERACTING FACTORS (PIFs) and ELONGATED HYPOCOTYL 5(HY5)  (Bae and Choi, 2008; Leivar and Quail, 2011; von Arnim and Deng, 2003). PIFs are negative regulators of Chl, biosynthesis by directly repression their expression in dark-grown seedlings (Huq et al., 2004; Moon et al., 2008; Stephenson et al., 2009). Targets of PIF-mediated regulation are key genes in Chl biosynthetic, like *PORC*, *HEMA1*, *GUN4* and *CHLH,* controlling rate-limiting steps of the pathway (Moon et al., 2008; Stephenson et al., 2009). HY5 mediates far-red, red, blue, and UV-B light signaling and is a positive regulator of seedling photomorphogenesis and chloroplast development (Bae and Choi, 2008). HY5 promotes the expression of light-responsive genes by direct binding to their promoters of via recognition of the G-box *cis*-element (CACGTG), which is found in approximately 24% of the total genes in this category (Lee et al., 2007); *CHLH, GUN4, PORC, CAO*, *CHL27* as well as *HEMA1* have been suggested to be targets of HY5-mediated regulation (Lee et al., 2007; McCormac and Terry, 2002). In absence of light, HY5 is destabilized via the COP1/DET1-mediated ubiquitination degradation pathway (Lau

and Deng, 2012; Osterlund et al., 2000; Saijo et al., 2003). Another important group influencing chloroplast biogenesis and Chl biosynthesis are the GOLDEN2-LIKE (GLK) transcription factors (Fitter et al., 2002; Wang et al., 1997). In *Arabidopsis*, the GLK1/2 pair has been suggested to coregulate and synchronize the expression of a subset of nuclear photosynthetic genes, after direct binding on a putative GLK-recognition *cis*-element (CCAATC) (Waters et al., 2009). Interestingly, GLK gain-of-function can cause greening and ectopic chloroplast development in non-photosynthetic organs like roots or fruits (Kobayashi et al., 2012; Nakamura et al., 2009; Powell et al., 2012).

Upon illumination, POR-dependent conversion of Pchlide to chlorophyllide takes place, while *PORA* and *PORB* expression drops, possibly to promote *de novo* Chl biosynthesis and plastid differentiation (Kobayashi and Masuda, 2016; Zhong et al., 2009). The rest of the Chl biosynthetic genes are derepressed, as phytochrome photoreceptors induce post-translational modifications of PIFs, resulting to their degradation via the ubiquitin–proteasome system (Chen et al., 2004; Leivar and Quail, 2011). Additionally, light-dependent inactivation of COP1 leads to HY5 accumulation and subsequent induction of *GLKs* and other Chl. biosynthesis-promoting transcriptional factors (Kobayashi and Masuda, 2016). The expression of the enzymes catalyzing Chl biosynthesis as well as the photosynthetic machinery is also undergoing circadian regulation, thus coordinating photosynthesis with the day–night cycle (Matsumoto et al., 2004; Papenbrock et al., 1999).

## 1.5    Previous work of the group on HDC1 loss-of-function mutants

As an attempt to identify new components of the local Pi sensing pathway adjusting root meristem activity, a simplified genetic screen was performed, aiming to isolate mutant lines with the characteristic low Pi-hypersensitive root phenotype, similar to *pdr2* mutants. Towards that, 50,000 M2 seedlings from a population of ethyl methanesulfonate (EMS) mutagenized M1 plants of the Columbia (Col-0) accession were screened on medium without Pi supplementation for the characteristic short-root phenotype that can be rescued upon transfer to +Pi condition. From this screen, the mutant line *pdr3* was isolated; *pdr3* mutants showed strong primary root growth inhibition upon transfer to low Pi conditions (Fig. 4A), an effect that was specific to Pi starvation and not upon deficiency of other elements like S, N or Fe (Fig. 4B). In line with the hypersensitive root phenotype, *pdr3* mutants also exhibit exaggerated systemic responses to Pi scarcity, displaying 2.5-fold higher than WT, low Pi-induced accumulation of anthocyanins (Fig. 4E) and intense starch staining (data not shown). Additionally, Pi-starved *pdr3* roots have higher free Pi concentrations than WT, although free Pi and total P content of roots and shoots are similar to WT at +Pi conditions (Fig. 4. F-G).

Genetic analysis of the *pdr3* mutant revealed that it is a novel allele of *HDC1* (*HISTONE DEACETYLASE COMPLEX 1,* AT5G08450), showing a transition from CAA to TAA, resulting in a premature stop codon (Gln263*, Suppl. Fig. 1A). Additional analysis of total histone acetylation levels in *pdr3* demonstrated elevated AcH3 content in root and shoot tissue as well as cell cultures, confirming that the *pdr3* mutation disrupts the normal function of HDC1 (Fig. 4C). Furthermore, loss of HDC1 in *pdr3* mutants causes physiological defects irrespectively of Pi nutrition. Specifically, root tips of the mutants emit autofluorescence, which can be attributed to ectopic chlorophyll accumulation (Fig. 4D). Analysis of *pdr3* root extracts with high-performance liquid chromatography (HPLC) revealed higher accumulation of Chlorophyll A in comparison to WT (data not shown). Moreover, in accordance with previous reports, *pdr3* mutants show photoperiod-dependent alteration of flowering time, delaying the transition to the

reproductive stage when the plants are grown in long day conditions. Another distinctive phenotype is the partial loss of apical dominance, exhibited as development of multiple stems ("bushy" phenotype).
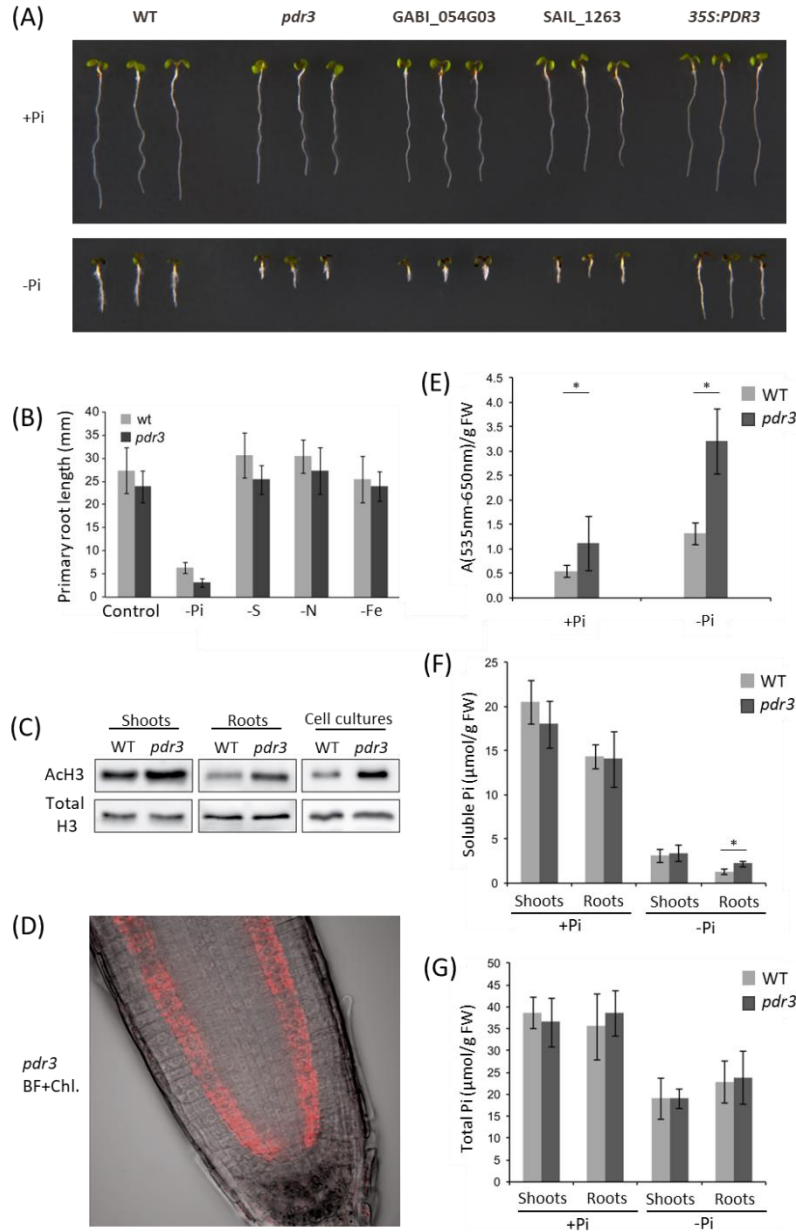


*Fig. 4 Pdr3 mutants demonstrate hypersensitive responses to Pi deficiency, as well as Pi status-independent physiological defects.*

*(A) Representative photos of 8-day-old seedlings of WT (Col-0), pdr3, GABI_054G03, SAIL_1263 and pdr3 complemented with 35S:PDR3, grown on +Pi and -Pi media.*

*(B) Root length measurements of 8-day-old seedlings of WT and pdr3, grown on standard growth medium and on medium without supplementation of Pi, S, N or Fe.*

*(C) Western blot for the detection of acetylated histone H3 with a-acetyl. H3-IgG (Abcam) in total protein extracts of leaves, roots and cell cultures of WT and pdr3 background (upper panel). As control, total H3 levels were detected with a-H3-IgG (lower panel).*

*(D) Confocal microscopy-based detection of chlorophyll-derived autofluorescence in root tips of pdr3 seedlings, grown at standard conditions. BF:brightfield channel; Chl.: Autofluorescence channel.*

*(E-G) Quantification of anthocyanin (E), free Pi (F) and total Pi (G) content in 8-day-old WT and pdr3 seedlings, grown on medium with or without Pi supplementation. Bar plots represent mean contents (±SD) (n = 3 independent extractions of 100-150 plants). Asterisks denote statistically significant differences between the means of the groups (p < 0.05).*

*The data presented in this figure were generated by Dr. Silke Richter.*

25

## 1.6  Aim of the present work

Evidence from the literature and previous work from our group support the hypothesis that HDC1 has a role in regulation of phosphate deficiency responses, probably at the transcriptional level. Root tips have a central role in perceiving external cues of Pi availability and translating this signal to a set of adaptive responses. Therefore, it is of high interest to identify changes in the root tip transcriptome that lead to root-specific adaptations to low external Pi supply and their connection with HDC1-mediated regulation. Additionally, the plethora of developmental and physiological phenotypes in loss-of-functions mutants of HDC1 indicate that the function of this protein extends beyond phosphate starvation responses, to other regulatory pathways e.g., chlorophyll biosynthesis. Based on these facts, the present study has the following objectives:

- Analyze which genes are transcriptionally responding to Pi scarcity in the root apex and how their function might be related to the local Pi deficiency adaptations.
- Identify low Pi responsive genes that are potentially subjected to HDC1-dependent regulation.
- Understand how the function of HDC1 is implicated in regulation of chlorophyll biosynthesis.
- Investigate how loss of HDC1 affects global transcriptome in a tissue-specific manner.
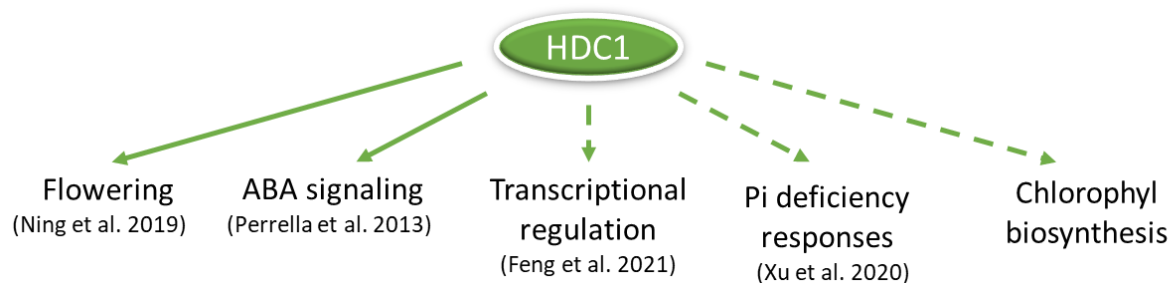


**Fig. 5 Overview of biological processes that have been shown to be affected by loss-of-function of HDC1.**
*Available studies demonstrating the role of HDC1 in the indicated processes are shown in parentheses. The pathways that will be the focus of this work are highlighted with dashed lines.*

# 2 Results

## 2.1 Phenotypic assessment of *pdr3* mutants under different Pi regimes

As described above, loss of HDC1 interferes with normal plant development, in terms of biomass, flowering time and root physiology. To further investigate the mechanisms underlying these phenotypes, two mutant lines were used, the *pdr3* mutant, which carries a nonsense mutation in the first exon, established in our group (section 1.5) and secondarily, the T-DNA insertion line *hdc1* (GABI_054G03). *Hdc1* line has been characterized by Perrella et al. as a knockout mutant of HDC1 (Perrella et al., 2013), which was also validated by RT-qPCR (Suppl. Fig. 1). Similar to other mutant alleles of *HDC1*, adult *pdr3* plants exhibited stunted growth compared to WT, showing smaller rosettes and delayed flowering (Suppl. Fig. 2); *hdc1* plants also displayed smaller rosettes and later flowering onset, but these phenotypes were less pronounced than for *pdr3* mutants. Additionally, adult plants overexpressing *HDC1* under control of the *35S Cauliflower Mosaic Virus* promoter in the *pdr3* background (*pdr3/35Sp::HDC1* or abbreviated OxP3) did not show obvious phenotypic differences compared to WT. The same was observed for lines expressing GFP-tagged HDC1 under the control of the endogenous *HDC1* promoter in the *pdr3* genetic background (*pdr3/HDC1p::HDC1-GFP* or abbreviated HDC1-GFP). Next, root development under Pi replete conditions was assessed in *hdc1* mutant plants and compared to WT. Young (9-days-old) *pdr3* and *hdc1* seedlings exhibited constitutively shorter primary roots than WT, showing 25-30% reduction in primary root length (Fig. 6A). Additionally, seedlings from both lines showed root skewing, deviating from the vertical (gravity) vector, approximately 12 degrees right wise for *pdr3* and 7 degrees for *hdc1*, in contrast to WT, which is slightly slanted to the left (Fig. 6C). On the contrary, no significant difference in root angle or length was observed in OxP3 or HDC1-GFP seedlings. Overall, these observations indicate that loss of function of HDC1 is affecting normal root growth in terms of size and gravitropic development, while its overexpression does not have a visible phenotypic output.

As described in section 1.5, *pdr3* plants show a hypersensitive response in comparison to WT when germinated on media without Pi supplementation, which manifests as rapid root growth inhibition and anthocyanin accumulation. To test whether low Pi supply can also trigger an exaggerated root growth phenotype in HDC1 loss-of-function mutants after germination at Pi replete conditions, 5-days-old seedlings were transferred from Pi sufficient to Pi deficient growth medium and their root growth was assessed 4 days after transfer (Fig. 6B). Although *pdr3* and *hdc1* mutants had shorter primary roots than WT already at standard +Pi growth conditions, this difference was more pronounced when seedlings were exposed to low Pi availability, exhibiting approximately 75% and 68% reduction of their initial primary root length respectively, in contrast to approximately 48% reduction in WT seedlings. Moreover, OxP3 seedlings demonstrated 41% reduction of their root length upon Pi deficiency, which was comparable to WT, indicating that overexpression of HDC1 rescues the *hdc1* phenotype and does not seem to additionally influence the low Pi-induced root growth inhibition. Seedlings from the HDC1-GFP line showed reduced sensitivity when exposed to -Pi conditions, demonstrating only 27% root growth reduction. Furthermore, we tested whether the exaggerated root phenotype of *pdr3* upon Pi deficiency is related to deregulation of callose deposition in the root tip. Preliminary results (one biological experiment) from aniline blue staining of WT and *pdr3* root tips revealed low Pi-specific callose deposition around the SCN in both genotypes, although with higher intensity in the *pdr3* background (Fig. 6D). Moreover, low-Pi triggered callose accumulation was also observed in the stele of *pdr3* root tips. These findings indicate that *hdc1* mutants respond differentially to Pi limitation in terms of root growth, showing pronounced inhibition of root development, a phenotype that coincides with uncontrolled callose depositions.
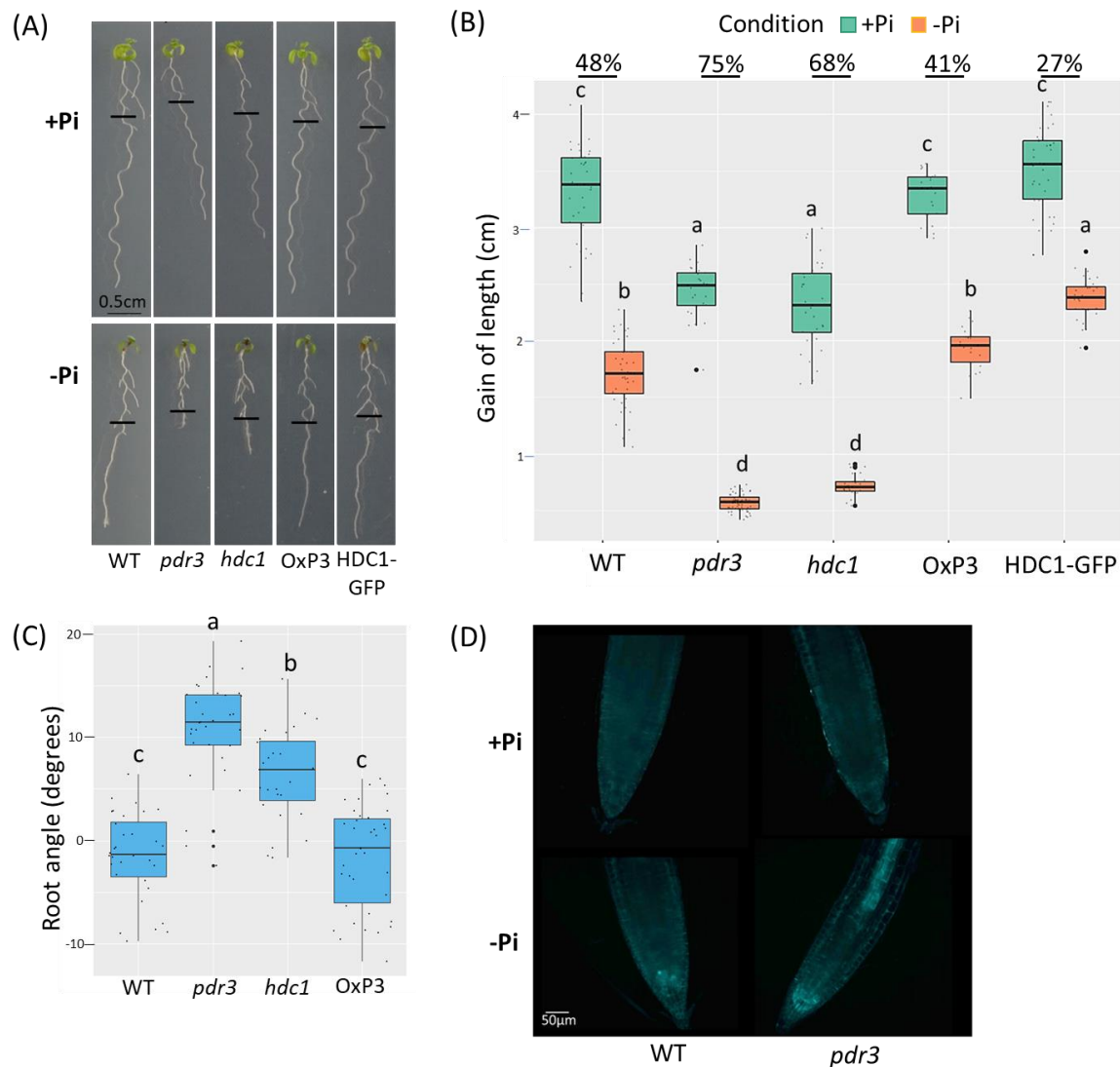
**Fig. 6 Loss of HDC1 interferes with normal root root growth depending on Pi supply.**

*(A-B) Primary root growth inhibition of indicated genotypes. 5-days-old seedlings germinated on +Pi agar plates were transferred to +Pi or -Pi conditions; 4 days after transfer (4 DAT) photographs were taken (A) and primary root length was quantified (B). The boxplot shows medians, depicted as solid line inside the box, and interquartile ranges, representing data from 1 out of 3 biological experiments (n=25-30). Outliers (> 1.5x interquartile range) are shown as a black dot. Single data points are depicted with small grey dots. Letters denote statistically significant differences among samples (two-way ANOVA, followed by Tukey's HSD test, p < 0.05). Horizontal black lines mark the root length after 5 days post germination and the onset of the elongation measurement. Percentages (B) indicate the low Pi-induced primary root growth reduction ratio of each genotype.*

*(C) Boxplot depicting the skewing angle of the primary roots of the indicated genotypes. 5-days-old seedlings germinated on +Pi agar plates were transferred to +Pi and the root angle was quantified 4 DAT. Roots of pdr3 and hdc1 seedlings were slanted to the right (positive values), as viewed from above the plates. Data represent 1 out of 3 biological experiments (n=25-30). Single data points are represented by black dots. Letters denote statistically significant differences among samples (one-way ANOVA, followed by Tukey's HSD test, p < 0.05).*

*(D) Representative images of callose deposition in root tips of seedlings grown in Pi replete of deficient conditions. 5-days-old seedlings germinated on +Pi agar plates were transferred to +Pi or -Pi conditions and low Pi-triggered callose accumulation was monitored 1 DAT by anniline blue staining (n=8-10). Scales: A, 0.5 cm; D, 50 μm.*

28

Several studies reported the interplay between external Fe availability and Pi starvation responses, during which the PDR2-LPR1 module regulates apoplastic $Fe^{3+}$ accumulation in a root cell type-specific manner, followed by a ROS burst and callose deposition, predominantly in the SCN (described in section 1.2.4). In parallel, previous work showed that mutants with impaired function of HDC1 hyperaccumulate $Fe^{3+}$ in the SCN area (Xu et al., 2020). To test how external Fe availability affects low Pi-triggered root growth inhibition, the root length of WT and *pdr3* seedlings was assessed after transfer to Pi-deficient media supplemented with increasing doses of Fe, ranging from 0 µM to 500 µM (Fig. 7). As reported previously, WT seedlings display a triphasic response to increasing Fe availability during Pi limitation, where low Fe supply (2.5–25 µM) gradually decreases root growth, with the response peaking at 25 µM, in which inhibition reaches approximately 54% (Naumann et al., 2022). Intermediate Fe doses (50–100 µM) have less inhibitory effect and higher Fe concentrations (>100 µM) leads to inhibition due to toxicity (Fig. 7, upper panel and Naumann et al., 2022). Like WT, low Pi-induced root growth inhibition of *pdr3* seedlings showed the same triphasic response to increasing Fe doses. However, the root growth inhibition phase is extended in the mutant, which shows a hypersensitive response in Fe concentrations ranging from 10-50 µM (Fig. 7, middle panel). Furthermore, overexpression of HDC1 does not seem to alter the triphasic response, as OxP3 showed the similar growth trend as WT for most Fe concentrations that were tested at both Pi regimes (Fig. 7, lower panel). Taken together, these results suggest that absence of a functional *HDC1* gene partially affects the dose dependent effect of Fe on root growth inhibition upon Pi scarcity, as an additional growth effect is present only at certain Fe ranges.
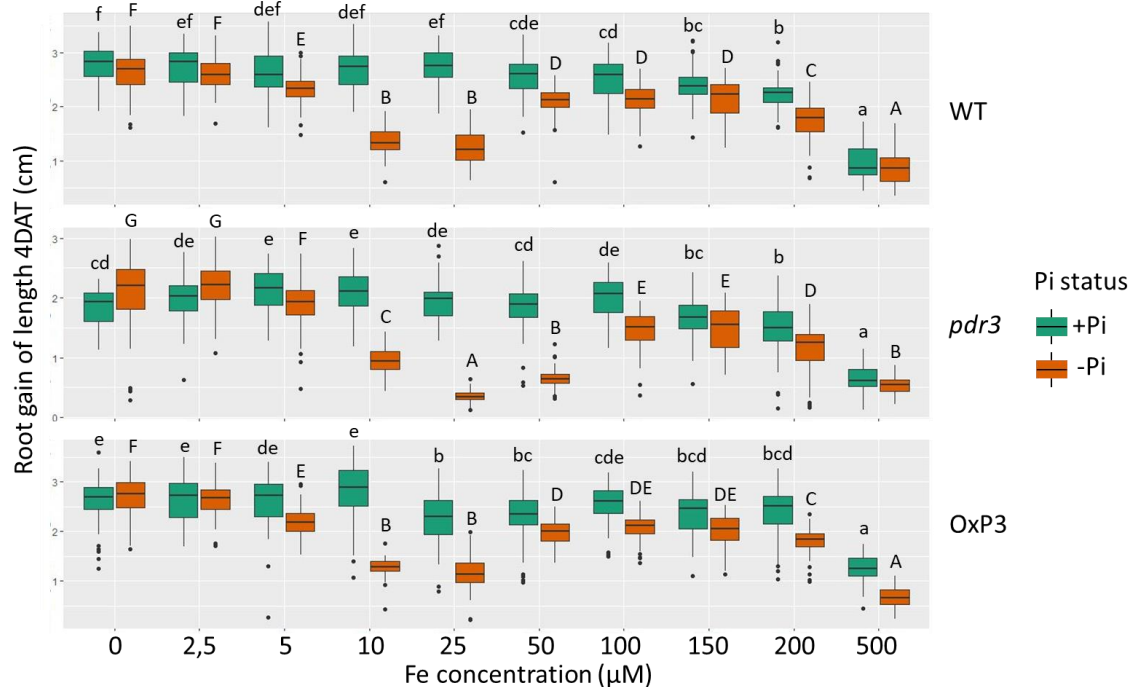


**Fig. 7 Loss of HDC1 selectively interferes with Fe-dependent root growth inhibition during Pi scarcity.**
*Primary root length of WT (upper panel), pdr3 (middle panel) and OxP3 (bottom panel) seedlings. 5-days-old seedlings germinated on +Pi agar plates were transferred to +Pi or -Pi agar plates, supplemented with increasing concetration of $Fe^{3+}$-EDTA and the primary root length was quantified 4 DAT. Boxplots show medians, depicted as solid line inside the box, and interquartile ranges, representing data from 1 out of 3 biological experiments for -Pi and 1 out of 2 experiments for +Pi and OxP3 at -Pi and +Pi (n=25-30). Outliers (> 1.5x interquartile range) are shown as a black dot. Letters denote statistically significant differences between Fe conditions, for each genotype and Pi regime separately (lowercase and uppercase letters correspond to +Pi and -Pi status respectively, one-way ANOVA, followed by Tukey's HSD post-hoc test, p < 0.05).*

## 2.2 Transcript profiling of *pdr3* tissues with RNA-sequencing

Given the fact that lack of a functional *HDC1* gene causes global transcriptional changes (Feng et al., 2021), an RNA-approach was implemented to compare the transcriptomes of *pdr3* and WT seedlings during Pi starvation. The experiment was carried out in a tissue specific manner, focusing on transcriptome analysis of the root tip, as it has been shown that this organ has a central role in detecting the external Pi status and orchestrating Pi starvation responses, leading to root architecture remodeling (Abel, 2017). Moreover, basal transcriptional differences between the two genotypes were also investigated in shoots and roots of seedlings, grown at standard, Pi replete conditions.

The experimental setup for the RNA-seq analysis is described in detail in section 6.4.3. Briefly, *pdr3* and WT seedlings were germinated for five days on Pi replete media (+Pi) and subsequently transferred to Pi deficient media (-Pi) or to fresh +Pi media (Fig. 8A). After one day from transfer, 150 root tips from seedlings grown in +Pi regime were excised and pooled into one sample, representing one biological replicate. Root tips were harvested after dissection approximately between the 10$^{th}$-20$^{th}$ root hair of the differentiation zone, thus ensuring that all cell types would be present across samples with different root area size (Fig. 8B). Three biological replicates were collected per genotype and condition and used for RNA extraction. Due to the small size of the root tips of Pi starved seedlings, -Pi samples from each genotype contained 150-200 root tips, ensuring sufficient amount of extracted RNA. Additionally, 25 shoots and 50 roots from seedlings grown only on Pi replete media were harvested and processed similarly. Depending on the transcriptional changes under investigation, the transcriptome of *pdr3* was compared to WT for each tissue separately (basal transcriptional changes), or the transcriptomes of both genotypes during Pi deficiency were normalized to the corresponding transcriptome under Pi replete conditions (Pi starvation-dependent changes). For each comparison, a dataset of differentially expressed genes (DEGs) was generated, applying the following thresholds: cutoff of logarithmic fold change (log$_2$FC) = 1 or -1, cutoff of p-value adjusted for multiple testing = 0.05, cutoff of FPKM value=0.5. A summary of the total DEGs is provided in Table 1 as well as in Suppl. Files 1-6 (see compact disc) and will be further analyzed below.
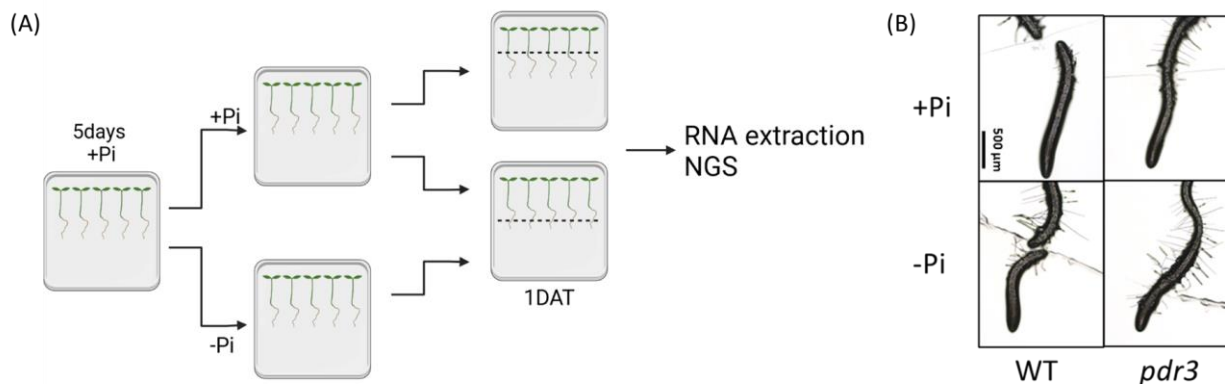


**Fig. 8 Overview of RNA-seq workflow.**
*(A) Schematic overview of the experimental setup for RNA-seq analysis. 5-days-old WT and pdr3 seedlings grown at +Pi medium were transferred to media with or without supplemented Pi. The root tips of seedlings grown in either Pi regime were excised approximately at the differentiation zone (B) and used for RNA extraction and next generation sequencing (NGS). Additionally, RNA samples from shoots and roots of seedlings grown at +Pi media were transferred to fresh +Pi media and treated similarly. Three biological replicates per genotype and condition were sequenced, each containing 150-200 root tips, 50 roots or 25 shoots. Figure designed with BioRender.*
*(B) Stereoscopic images of WT and pdr3 root tips, excised approximately between the 10$^{th}$-20$^{th}$ root hair of the differentiation zone. Root tips were collected and used for RNA-seq analysis as described in (A). Scale: 500µM.*

| Comparison | DEGs | |
|---|---|---|
| Shoots *pdr3* vs. WT | 708 | 527 ↑ 181 ↓ |
| Roots *pdr3* vs. WT | 843 | 362 ↑ 481 ↓ |
| Tips WT -Pi vs. +Pi | 373 | 288 ↑ 85 ↓ |
| Tips *pdr3* -Pi vs. +Pi | 1683 | 1271 ↑ 412 ↓ |
| Tips +Pi *pdr3* vs. WT | 674 | 440 ↑ 234 ↓ |
| Tips −Pi *pdr3* vs. WT | 2491 | 1776 ↑ 715 ↓ |

*Table 1 Overview of DEGs from RNA-seq analysis of WT and pdr3 seedlings, grown at different Pi regimes.*

*5-days-old WT and pdr3 seedlings grown at +Pi medium were transferred to media with or without supplemented Pi. The root tips of seedlings grown in either Pi regime were excised approximately at the differentiation zone and used for RNA extraction and next generation sequencing (NGS). Additionally, RNA samples from shoots and roots of seedlings grown at +Pi media were transferred to fresh +Pi media and treated similarly. Three biological replicates per genotype and condition were sequenced, each containing 150-200 root tips, 50 roots or 25 shoots. For each comparison under analysis, thresholds for differential expression analysis were set as follows: -1> log2-fold-change (log$_2$FC) >1, adjusted p value <0.05, FPKM value >0.5). Upregulated and downregulated DEGs within each comparison subset are indicated with red and blue arrows respectively. Each dataset can be found in Suppl. Files 1-6 (see compact disc), from top to bottom respectively.*

### 2.2.1 Transcriptional changes in *pdr3* during control conditions

#### 2.2.1.1 Transcriptional changes in root tips

The comparison of expressed genes in roots tips of *pdr3* and WT seedlings grown under Pi replete (control) conditions yielded 674 DEGs, from which 440 were upregulated and 234 were downregulated in the *pdr3* genotype (Suppl. File 5).  After transfer to Pi deficient conditions, 2491 genes were differentially expressed (1776 upregulated, 715 downregulated) in root tips of *pdr3* seedlings, compared to root tips of WT seedlings exposed at the same conditions (Suppl. File 6). The comparison of the two aforementioned gene sets revealed 431 transcripts that are differentially expressed between *pdr3* and WT root tips independently of the external Pi status and thus represent the basal transcriptional changes in *pdr3* root tips (Fig. 9A and Suppl. File 7).

In order to identify functional classes that are overrepresented in this dataset, a gene ontology (GO) enrichment analysis was performed using the online tool agriGO v2.0 (Tian et al., 2017).  From the 431 DEGs, 21 significantly enriched GO terms for biological processes were found and ranked based on their enrichment score (false discovery rate, FDR < 0.05, Fig. 9B and a full list in Suppl. Table 1). Among those, some of the most significantly enriched terms were related to photosynthetic processes, specifically "photosynthesis" and "photosynthesis, light reactions"; the significance of this finding will be discussed in detail in section 2.4. Moreover, metabolism-related GO terms, like "triterpenoid metabolic process", "isoprenoid metabolic process" and "isoprenoid metabolic process", were found to be enriched. These GO categories included genes belonging in biosynthetic gene clusters (BGC), which are characterized by the physical clustering and coordinated expression of genes encoding enzymes required for a specific metabolic pathway (Nützmann et al., 2018). Specifically, analysis of the genes showed that three out of four genes comprising the core BGC for the biosynthesis of the triterpenoid thalianol (*THAD1*, *THAH1*, *THAS1*) were downregulated in *pdr3* root tips in comparison to WT, in both Pi replete and deficient conditions (Fig. 9C). Similarly, two out of three genes of the BGC for marneral (*MRO*, *MR1*) had lower transcript levels in *pdr3* root tips than WT. Expanding the analysis to the entirety of the DEG dataset also showed that the remaining of the genes participating in these two biosynthetic pathways have lower expression in *pdr3* tips, however only during Pi replete conditions. Additionally, apart from the core

(physically clustered) genes, the thalianol BGC also includes three peripheral genes, which are not located in tandem with the core genes; however, their expression did not show any difference between *pdr3* and WT root tips.

Interestingly, another significantly enriched term in this group was "response to oxidative stress" and included 5 genes (*PER15*, *PER17*, *PER12*, *PER24* and *PRX47*) belonging in the secretory plant peroxidase superfamily (EC 1.11.17, class III peroxidase) as well as *CALASE1 (CAT1)*, encoding a hydrogen peroxide-degrading enzyme (Fig. 9C, lower panel). The deregulation of these genes could indicate unbalanced redox state in *pdr3* root tips. To test this, *pdr3* and WT seedlings were stained with nitroblue tetrazolium chloride (NBT), a dye that reacts with cellular superoxide ions to form formazan derivative and can be monitored macroscopically by the presence of purple-blue staining (Esfandiari et al., 2003; Stockert et al., 2018). The *pdr3* root tips exhibited enhanced accumulation of purple staining in the meristematic and elongation zone of the root apex in comparison to WT (Suppl. Fig. 7C) supporting the notion that knockdown of HDC1 affects redox balance in the root tip.
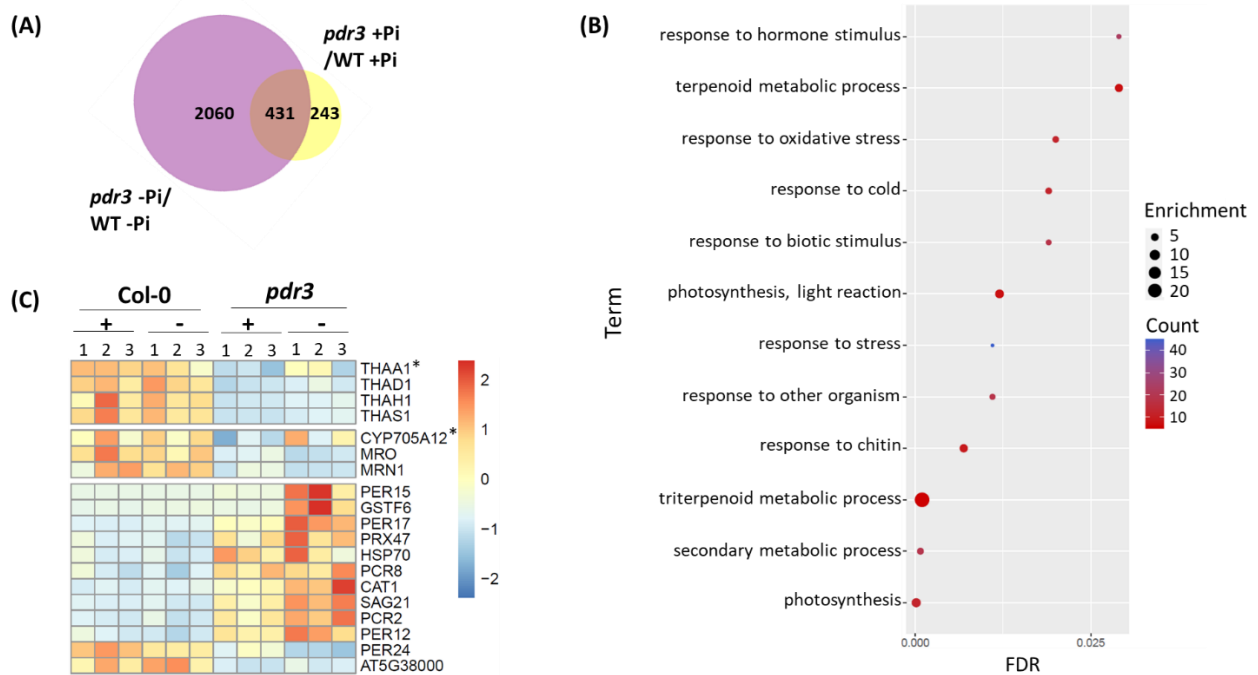


**Fig. 9 Loss of HDC1 causes basal transcriptional deregulation in root tips.**
*(A) Area-proportional Venn diagram, displaying the number of DEGs between pdr3 and WT in root tips during Pi replete (yellow) and Pi deficient conditions (purple). The genes in the overlapping region are representing the basal transcriptional changes in the mutants (basal DEGs), irrespectively of Pi presence in the growth media.*
*(B) Scatterplot of selected significantly enriched GO terms among the basal DEGs in pdr3 root tips. The vertical axis represents the functional annotation terms, and the horizontal axis represents the P value, adjusted for multiple testing using FDR. The color of the dots is representing the number of DEGs representing each term and the size of the dot corresponds to the enrichment score (% of number of DEGs annotated to this term divided by the total number of genes annotated to this term).*
*(C) Heat map showing the z-scores of the FPKM values of selected basal DEGs between WT and pdr3 biological replicates (1-3). The upper and middle block represents the DEGs that are belonging to the thalianol core gene cluster and to the marneral gene cluster respectively. The two genes marked with an asterisk are deregulated in pdr3 only at Pi replete conditions and therefore are not belonging to the basal DEGs. The bottom panel shows the DEGs that are annotated to the functional term "response to oxidative stress".*

Global transcriptional changes were compared between young (9-days-old) WT and *pdr3* shoots or roots, grown in Pi sufficient conditions. Analysis of differential gene expression demonstrated 708 DEGs in shoots and 844 in root of *pdr3* when compared to WT (Suppl Files 1 and 2, respectively). Among those, 527 and 362 genes showed upregulated expression in shoots and roots of the mutant, respectively.

GO enrichment analysis of the shoot-specific gene set revealed 20 GO terms of biological processes to be significantly represented (Fig. 10A and Suppl. Table 2). Four of them are related to cell wall loosening and organization, including five genes encoding expansin/expansin-like proteins (e.g*., EXPA17, EXPANSIN 17*), and five genes coding for enzymes regulating pectin metabolism (e.g., *PME46*, *PECTIN METHYLESTERASE46*). Additionally, the GO category "response to oxidative stress" contains, among other genes, 17 members of the peroxidase gene family. Peroxidases catalyze the reduction of $H_2O_2$ by transferring electrons from various donor molecules and thus participate in diverse processes, including cell wall elongation or defense (Cosio and Dunand, 2009; Shigeto and Tsutsumi, 2016).

In parallel, the GO analysis of the DEGs in *pdr3* roots clearly indicated the deregulation of genes participating in metabolic processes, specifically in the biosynthesis of the glucosinolate (GSL) defense metabolites. Of the 33 significantly enriched GO terms, the majority were related directly or indirectly to GSL metabolism (Fig. 10 B and Suppl. Table 3); the role of HDC1-mediated regulation of the GSL biosynthetic pathway is discussed extensively in section 2.3. Moreover, genes involved in the metabolism of the triterpenoids thalianol and marneral (*THAS1, THAD1, THAH1* and *MRN1* respectively) were also deregulated. As described in section 2.2.1.1, these genes participate in the biosynthetic gene cluster (BGC) of thalianol and marneral and had downregulated expression in *pdr3* roots, following a similar expression trend as in root tips. Seeking a more in-depth approach, all genes participating in the characterized BGCs of thalianol, marneral, tirucalladienol and arabidiol were mined from the literature (Field and Osbourn, 2008; Huang et al., 2019; Liu et al., 2020) and their transcript levels were compared between WT and *pdr3* roots (Suppl. Table 4). This analysis revealed that, similarly to root tips, all core genes in the thalianol BGC were downregulated in the mutant in comparison to WT. Additionally, two out of three peripheral genes, *AT1G66800* and *SDR4* (*SHORT-CHAIN DEHYDROGENASE REDUCTASE 4*), had also lower transcript abundance in *pdr3* roots, indicating that the expression of nearly the entirety of the thalianol BGC is affected in this tissue. The same was shown for the marneral BGC, where also all three genes were downregulated in *pdr3*. Moreover, the tirucalladienol BGC showed lower expression of three genes, out of 5 in total, compared to WT, specifically *PEN3* (*PUTATIVE PENTACYCLIC TRITERPENE SYNTHASE 3*), *CYP716A2* (*CYTOCHROME P450, FAMILY 716, SUBFAMILY A, POLYPEPTIDE 2*) and *AT5G36130*; these genes showed aberrant expression only in the whole root transcriptome and not in the root tips. The arabidiol BGC was the least affected in the mutant, where only two genes were downregulated, namely *BIA1* (*BRASSINOSTEROID INACTIVATOR1*) and *CYP705A3* (*CYTOCHROME P450, FAMILY 705, SUBFAMILY A, POLYPEPTIDE 3*).

Overall, these results indicate that although shoots and roots of *pdr3* mutants exhibit extensive changes in gene expression when compared to WT, different functional groups of genes are affected in each organ type. In *pdr3* shoots, genes related to cell wall modification or to the regulation of redox state were affected by the loss of HDC1, while in the roots, a remarkable number of DEGs was related to certain metabolic pathways.
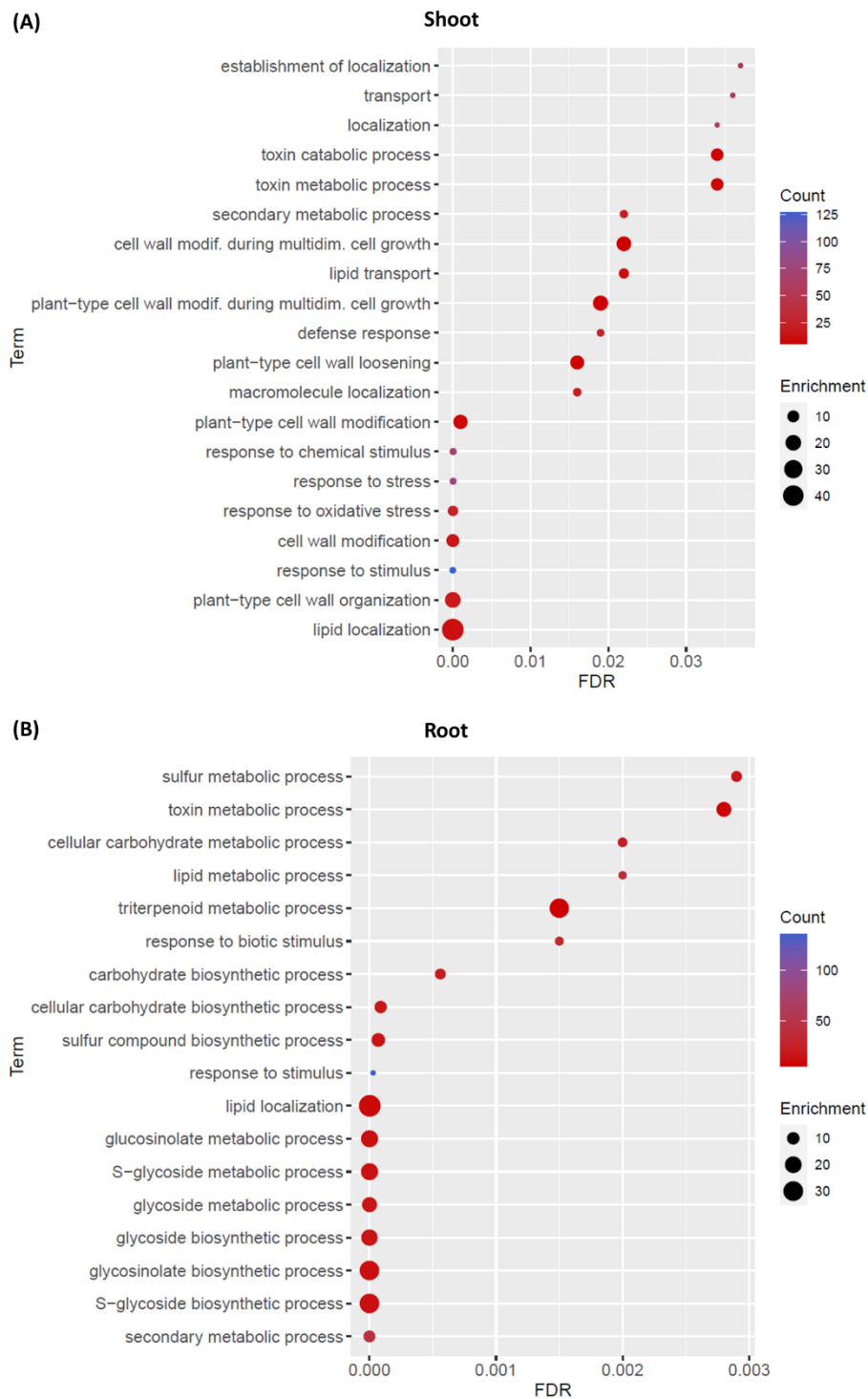
**Fig. 10 HDC1 differentially affects gene expression in shoots and roots, even at control conditions.**
(A and B) Scatterplots significantly enriched GO terms among the DEGs in shoots (A) or roots (B) of pdr3 seedlings grown at control conditions. The vertical axis represents the functional annotation terms, and the horizontal axis represents the P value, adjusted for multiple testing using FDR. The color of the dots is representing the number of DEGs representing each term and the size of the dot corresponds to the enrichment score (% of number of DEGs annotated to this term divided by the total number of genes annotated to this term).

## 2.2.2 Pi starvation-dependent transcriptional changes in *Arabidopsis* root tips

### *2.2.2.1 Root-tip specific transcriptional changes upon Pi deficiency in WT*

To study the role of HDC1 in the transcriptional regulation of Pi deficiency responses in root tips, we first analyzed the transcriptional responses of WT root tips upon Pi scarcity. Our RNA-seq approach showed that the expression of 373 transcripts is responsive to Pi starvation changes, corresponding to 288 upregulated and 85 downregulated DEGs (Fig. 11B and Suppl. File 3). GO enrichment analysis of these DEGs revealed 40 significantly enriched terms of biological processes (selected terms in Fig. 11A, full list in Suppl. Table 5). Among those, there was significant representation of functional terms related to Pi homeostasis ("phosphate ion homeostasis" and "cellular response to nutrient levels") (Fig. 11A and B, middle panel). These categories included Pi starvation responsive (PSR) marker genes, such as *SPX1* (*SPX-DOMAIN GENE 1*), *PAP17* (*PURPLE ACID PHOSPHATASE 17*) or *PHO2*, which encodes a ubiquitin-conjugating enzyme, indicating that the implemented experimental design successfully induced Pi stress to the seedlings under analysis.

Furthermore, functional categories related to carbohydrate metabolism stood out among the enriched GO terms in this dataset. Genes present in these categories showed mainly Pi-responsive upregulation, and their function was related to carbohydrate metabolism of cell wall constituents, such as *XYLOGLUCAN ENDOTRANSGLUCOSYLASE/HYDROLASE 22* (*XTH22*) or to sugar metabolism, including *DIN10* (*DARK INDUCIBLE 10*), *MIOX2* (*MYO-INOSITOL OXYGENASE 2*), *MIOX4* (*MYO-INOSITOL OXYGENASE 2*) and *RS2* (*RAFFINOSE SYNTHASE 2*) (Suppl. Table 6). *MIOX4* showed notably upregulated expression (nearly 31-fold increased transcript levels) in Pi-starved root tips. Additionally, among the most significantly enriched terms were functional categories related to the metabolism of the disaccharide trehalose and were represented by three trehalose synthase (TPS), three trehalose phosphatase (TPP) genes, and by one trehalase (*TREHALASE 1*) gene (Fig. 11B, upper panel and Suppl. Table 6).

In parallel, several reports have demonstrated that Pi deficiency responses include changes in the oxidative status, which also are exhibited as a localized ROS burst and iron (Fe) as well as callose deposition in the meristematic zone (Hoehenwarter et al., 2016; Müller et al., 2015; Naumann et al., 2022). Indeed, functional enrichment analysis of the DEGs in this dataset showed significant representation of genes with an annotated function in "response to oxidative stress" (Fig. 11A and B, bottom panel). This category included genes encoding the Pi responsive phosphatase PAP17, the iron storage protein FER1 (FERRITIN1), the vacuolar iron transporter VLT2 (VACUOLAR IRON TRANSPORTER-LIKE 2), two proteins in the peroxidase family (PER54 and PER21) and the chromatin localized OXS3 *(*OXIDATIVE STRESS 3*).* On the contrary, no category related to iron homeostasis or callose deposition and synthesis was significantly enriched among this dataset. Individual assessment of genes involved in these processes (GO:0055072, GO:0052543 and GO:0006075 respectively) revealed that no gene participating in callose synthesis or deposition had altered expression in Pi starved WT root tips (Suppl. Table 7). Related to Fe homeostasis, only three genes that have functions in Fe homeostasis or distribution showed differential expression, namely *FER1* and *VTL2*, which are also responsive to oxidative stress, as well as the functionally uncharacterized gene *AT3G61010* (Suppl. Table 7). Taken together, these results indicate that in addition to the typical Pi limitation-responsive changes, the root tip transcriptome of WT plants may reflect the upcoming metabolic adaptations during Pi deficiency.
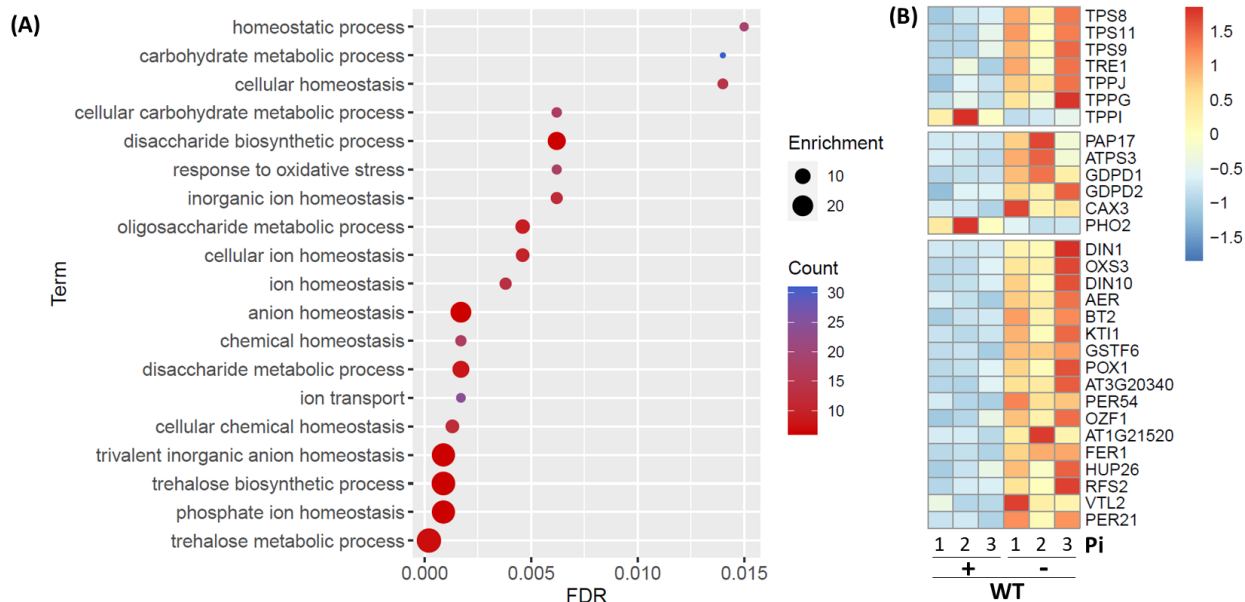
**Fig. 11 Pi limitation affects the expression of genes related to carbohydrate metabolism, cell wall plasticity and redox homeostasis in WT root tips.**

(A) Scatterplot of selected significantly enriched GO terms among PSR DEGs in WT root tips. The vertical axis represents the functional annotation terms, and the horizontal axis represents the P value, adjusted for multiple testing using FDR. The color of the dots is representing the number of DEGs representing each term and the size of the dot corresponds to the enrichment score (% of number of DEGs annotated to this term divided by the total number of genes annotated to this term).

(B) Heatmap showing the z-scores of the FPKM values of selected phosphate starvation responsive DEGs in WT root tips among biological replicates (1-3). Genes depicted are related to the GO term "trehalose metabolism" (upper panel), phosphate ion homeostasis" (middle panel) and "response to oxidative stress" (bottom panel).

*2.2.2.2    Shared root-tip specific transcriptional changes upon Pi deficiency in WT and pdr3 mutants*

RNA-seq analysis of Pi starved root tips of WT seedlings revealed a set of transcriptional responses upon low external Pi supply, which included changes in the expression of genes participating in carbohydrate metabolism as well as redox homeostasis. As a next step, we wondered whether absence of a functional HDC1 is affecting the ability of *pdr3* mutants to induce these changes in response to Pi limitation. Root tips of *pdr3* seedlings revealed differential expression of 1,683 transcripts in response to Pi starvation (Suppl. File 4). When this dataset was compared with the PSR DEG set of WT, an overlap of 263 DEGs was observed between the two genotypes, out of the total number of 373 PSR genes in WT (Fig. 12A and Suppl. File 8). Hierarchical clustering of the common PSR gene subset demonstrated that almost all genes showed the same expression trend between the two genotypes, in terms of up- or downregulation upon low Pi. However, a big portion of these genes exhibited more pronounced repression or induction in the mutant than in WT, corresponding to 13 and 120 genes respectively (Fig. 12B, 1st and 3rd cluster from top to bottom, Suppl. File 8). Additionally, another cluster containing 16 genes was representing mostly genes that showed higher induction in WT than in *pdr3* (Fig. 12B, 4th cluster from top to bottom); interestingly this cluster included two well-studied PSR genes, *SPX1* and *PAP17*.

To further investigate the shared Pi-starvation responses between WT and *pdr3*, the overlap of 263 PSR DEGs was subjected to GO enrichment analysis, yielding 24 significantly enriched GO terms (selected terms in Fig. 12C, full list in Suppl. Table 8). Similar to the results from the same analysis in WT PSR DEGs, an

36

overrepresentation of terms related to carbohydrate metabolism was observed. These GO categories included genes related to trehalose metabolism or to general carbohydrate metabolism (Fig. 12D), such as *MIOX4* or *DIN10*. Additionally, genes related to redox homeostasis were found in this subset, following the same expression trend in both genotypes. Taken together, this analysis shows that the standard low Pi-dependent transcriptional changes in WT root tips take also place in *pdr3* mutants, although at an amplified magnitude.
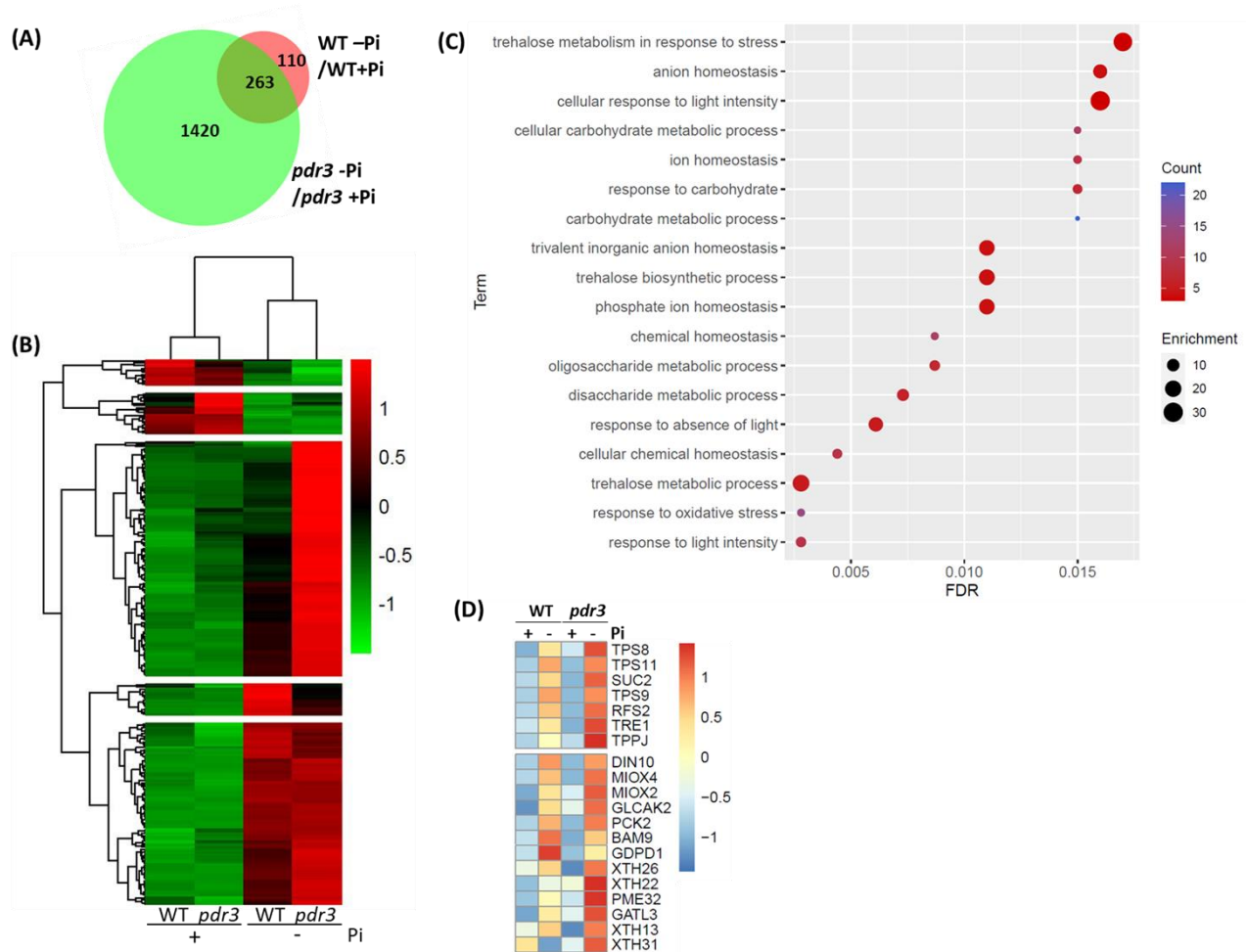


**Fig. 12 Pi deficiency is inducing similar transcriptional responses to both WT and pdr3 root tips.**
*(A) Area-proportional Venn diagram, displaying the number of phosphate starvation response (PSR) DEGs between pdr3 (green) and WT (pink) in root tips. The genes in the overlapping region are representing the common PSR DEGs between the two genotypes and were subsequently analyzed for GO enrichment*
*(B) Heat map showing the mean FPKM values of the 263 common PSR DEGs between WT and pdr3 root tips. The genes are divided into 5 classes according to hierarchical clustering analysis, depending on their expression trend across the different genotypes and conditions.*
*(C) Scatterplot of selected significantly enriched GO terms among common PSR DEGs in WT and pdr3 root tips. The vertical axis represents the functional annotation terms, and the horizontal axis represents the P value, adjusted for multiple testing using FDR. The color of the dots is representing the number of DEGs representing each term and the size of the dot corresponds to the enrichment score (% of number of DEGs annotated to this term divided by the total number of genes annotated to this term).*
*(D) Heatmap showing the z-scores of the mean FPKM values of selected PSR DEGs in WT and pdr3 root tips among 3 biological replicates. Genes depicted are related to the GO term "trehalose metabolism" (upper panel) and "response to oxidative stress" (bottom panel).*

*2.2.2.3    HDC1- dependent transcriptional changes upon Pi deficiency pdr3 mutants*

The transcriptomic analysis of Pi-starved *pdr3* root tips revealed that a large number of genes (1,420) are deregulated exclusively in the mutant, from which 1,042 were upregulated and 378 downregulated (Fig. 12A). The entirety of this subset was subsequently subjected to GO enrichment analysis, resulting to 77 significantly enriched functional categories (selected GO terms in Fig. 13A, full list in Suppl. Table 9). Interestingly, several GO terms were related to either defense processes or plant responses to other organisms such as fungus or bacterium. In this dataset, the GO term "defense responses" included 128 DEGs, of which 110 showed elevated expression in the mutant. Defense responses are governed by the action of several phytohormones, mainly jasmonic acid (JA), salicylic acid (SA) and ethylene (ET) (Vleesschauwer et al., 2014). To understand which hormonal signaling pathways might be over-represented in the gene subset, the DEGs from the GO term "defense responses" were categorized based on their annotation as responsive to JA, SA or ET (Fig. 13B, Suppl. Table 10). This analysis showed that, eight were responsive specifically to ET (e.g., *ERF1A*, *ETHYLENE RESPONSE FACTOR 1A*), three specifically to JA (e.g., *JAZ10*, *JASMONATE-ZIM-DOMAIN PROTEIN 10*) and five specifically to SA (e.g., *BIK1*, BOTRYTIS-INDUCED KINASE1). Moreover, several genes participated in combined signaling pathways of multiple hormones, specifically two genes both to JA and ethylene (e.g., *ERF2*, *ETHYLENE RESPONSE FACTOR 2*), four to JA and SA (e.g., *WRKY70*, *WRKY DNA-BINDING PROTEIN 70*) and two to all of the afore mentioned hormones (e.g., *PAD4*, *PHYTOALEXIN DEFICIENT 4*) (Suppl. Table 10). In parallel, the GO category "response to chitin" was significantly enriched, containing 31 DEGs (Suppl. Table 11). Chitin is a polymer of fungus cell wall and an elicitor of plant defense responses to fungi through several signaling pathways, including the mitogen-activated protein kinase (MAPK) pathway (Kawasaki et al., 2017). From the 31 DEGs present in this GO category, 30 genes were upregulated in Pi-starved tips of *pdr3* mutants and many were related to plant immunity (e.g., *MAPK3*, *WRKY70*, *WRKY46*). Two other immunity relevant categories, "response to bacterium" and "response to fungus", contained 47 and 48 DEGs respectively, from which the majority was upregulated in the mutant (Suppl. Table 11). Overall, these findings show that defense-related genes are rapidly induced in *pdr3* mutants upon Pi limitation, raising the question whether HDC1 is implicated in the crosstalk between immunity and Pi starvation responses.

Upon low external Pi supply, *Arabidopsis* is rapidly inhibiting primary root growth, an adaptive strategy that can be linked with cell wall dynamics (Balzergue et al., 2017; Müller et al., 2015); it has been shown that Pi starved root tips hyperaccumulate callose across the stem cell niche area, a phenotype that is further accentuated in the *pdr3* background (Müller et al., 2015, Fig. 6). Moreover, it has been suggested that low Pi-triggered pectin metabolism and modification at specific zones of the root tip might be connected to the inhibition of cell elongation that is typically observed in this area (Hoehenwarter et al., 2016). Interestingly, functional enrichment analysis of the Pi status responsive DEGs, unique in *pdr3* roots tips, revealed the differential expression of 52 genes, annotated to have a function in cell wall organization (GO:0071555). From these genes, 27 were upregulated while the rest 25 were downregulated in the tips of the mutant upon Pi deficiency. Among the genes in this dataset, two callose synthases (CALS1/7, CALLOSE SYNTHASES 1/7) were found to be upregulated, while additionally 5 genes involved in pectin catabolism (*PME2/22/44/53* and *PMEPCRF*, *PECTIN METHYLESTERASE2/22/44*/53 and *PECTIN METHYLESTERASE PCR FRAGMENT F*) were deregulated in the mutant (Fig. 13C). Moreover, 12 genes encoding enzymes of the xyloglucan endotransglycosylase/hydrolase family (XTH) exhibited deregulated expression in Pi depleted *pdr3* root tips. XTHs belong to a family of enzymes that cleave or reconnect xyloglucan molecules of the cell wall xyloglucan-cellulose network and their action is thought to affect the dynamics of cell wall extensibility (Eklöf and Brumer, 2010; Stratilová et al., 2020). Similarly, seven genes

from the expansin/expansin-like family of proteins showed deregulated expression in this dataset, five of which were upregulated in *pdr3* root tips upon low Pi availability. Collectively, these results show that loss of HDC1 is deregulating the expression of genes related to cell wall dynamics and plasticity, which might be linked to the exaggerated root growth phenotype that *pdr3* mutants are exhibiting during Pi limitation.



In parallel, the subset of 110 WT-specific PSR DEGs was analyzed for GO enrichment (Fig. 12A), but no significantly enriched GO categories were found. Individual assessment of the genes in this subset revealed the upregulation of the phosphate transporters PHT1;2/4 (PHOSPHATE TRANSPORTER 1;2/4) and of the phosphoenolpyruvate carboxylase kinase PPCK2 as well as the downregulation of PHO2 (PHOSPHATE2), an ubiquitin-conjugating enzyme that targets PHT1s and PHO1 for degradation (Aung et al., 2006; Liu et al., 2012). Although these genes are typically undergoing low Pi-triggered transcriptional regulation in WT, this effect was not observed in *pdr3* mutants; nevertheless, as described in section 2.2.2.2, the core Pi-deficiency transcriptional seem to be intact in *pdr3* mutants to the most extent. This fact suggests that possibly the Pi deficiency-related hypersensitive phenotype of these mutants might not be necessarily attributed to the part of the typical low Pi induced transcriptional response that is absent from the mutant (110 genes), but rather to the additionally deregulated genes on the *pdr3* background (1,420 genes), or to the hyper-induced PSR genes, as described above.

**Fig. 13 Pi-starved pdr3 root tips are showing differential expression of immunity related genes.**
*(A) Scatterplot of selected significantly enriched GO terms among phosphate starvation responsive DEGs exclusively in pdr3 root tips. The vertical axis represents the functional annotation terms, and the horizontal axis represents the P value, adjusted for multiple testing using FDR. The color of the dots is representing the number of DEGs representing each term and the size of the dot corresponds to the enrichment score (% of number of DEGs annotated to this term divided by the total number of genes annotated to this term).*
*(B-C) Heatmaps showing the z-scores of the FPKM values of selected phosphate starvation responsive DEGs in pdr3 root tips among biological replicates (1-3). Genes depicted are related to the GO term "defense response" (B) and have been categorized based on the hormonal signaling pathway in which they are involved, or to the term "cell wall organization" (C) and they have been distinguished to genes encoding for proteins in the family of callose synthases, pectin methylesterases, xyloglucan endotransglycosylases/hydrolases and expansisn/expansins-like (top to bottom).*

## 2.3 The role of HDC1 in GSL biosynthesis regulation

### 2.3.1 Loss of HDC1 impacts basal GSL biosynthesis in roots

As described in section 2.2.1.2., the functional annotation of DEGs in *pdr3* roots revealed that a set of genes participating in the metabolism of GSLs was significantly represented. To specify this analysis, the total set of genes involved in this biological process were acquired from TAIR (GO:0019760, glucosinolate metabolic process) and was compared with the dataset of DEGs in *pdr3* roots. This approach yielded 23 DEGs in *pdr3* that are related to GSL metabolism; 18 genes participate in GSL biosynthesis, 3 in GSL catabolism and 2 in transcriptional regulation of GSL biosynthesis (Fig. 14A, Suppl. Table 13). Interestingly, all genes but one were downregulated (the transcriptional factor MYB51 was upregulated). The expression of some selected GSL-related genes was validated by qPCR analysis (Fig. 14C). To gain a further insight into the role of the above-mentioned genes in GSL biosynthesis, each gene was characterized based on whether it participates in the biosynthesis of indolic or aliphatic GSL compounds. This type of characterization showed that out of the 22 previously characterized GSL-related DEGs in *pdr3 roots*, 18 were mapped on the pathway leading to aliphatic GSL synthesis and 4 to indolic GSL synthesis (Fig. 14A, B and Suppl. Table 13). Among those, the expression of two key regulators of the biosynthetic pathways of aliphatic and indolic GSLs, MYB28 and MYB51 respectively, was also deregulated in the *pdr3* mutant. These data indicate that HDC1 potentially participates in the basal transcriptional regulation of GSL biosynthesis, affecting mainly biosynthetic genes of aliphatic GSLs in the roots.

The transcriptional deregulation of GSL biosynthetic genes in *pdr3* roots indicated that the *pdr3* roots might show reduced GSL abundance. To validate that, the concentration of several GSL compounds was measured in roots and shoots of young *pdr3* seedlings and compared to WT (Fig. 14D). For the 11 GSL compounds that we detected in the root material, *pdr3* showed significantly lower concentration than WT for 6 long-chained aliphatic GSL compounds (6MTH, 7MTH, 8MTO, 6MSOH, 7MSOH, 8MSOO) and for one indolic GSL (1MOI3M), while higher abundance than WT was observed for two short-chained GSL (4MTB, 5MTP) and one indolic GSL (4MOI3M). However, since the metabolic GSL profile of roots is dominated by long aliphatic GSLs, the absolute content of aliphatic GSLs was overall lower than WT (Suppl. Table 14 and Suppl. Table 15). To further validate the impact of HDC1 loss-of-function on GSL biosynthesis, the chemical profile of *pdr3* roots was compared with *myb28*, a mutant allele of the central regulator of aliphatic GSL biosynthesis. Preliminary results from one biological experiment, consisting of four technical replicates of pooled root samples, showed that *pdr3* and *myb28* roots share a similar GSL chemotype, as both mutants exhibit low levels of long aliphatic GSLs (Suppl. Fig. 3), although *pdr3* roots still retain some capacity for biosynthesis of these compounds. Taken together, these results show that the suppressed expression of several GSL biosynthesis genes in *pdr3* roots results in a corresponding metabolic profile, where aliphatic GSL are profoundly affected and strengthen the hypothesis that HDC1 is a transcriptional co-regulator of long aliphatic GSL biosynthesis.
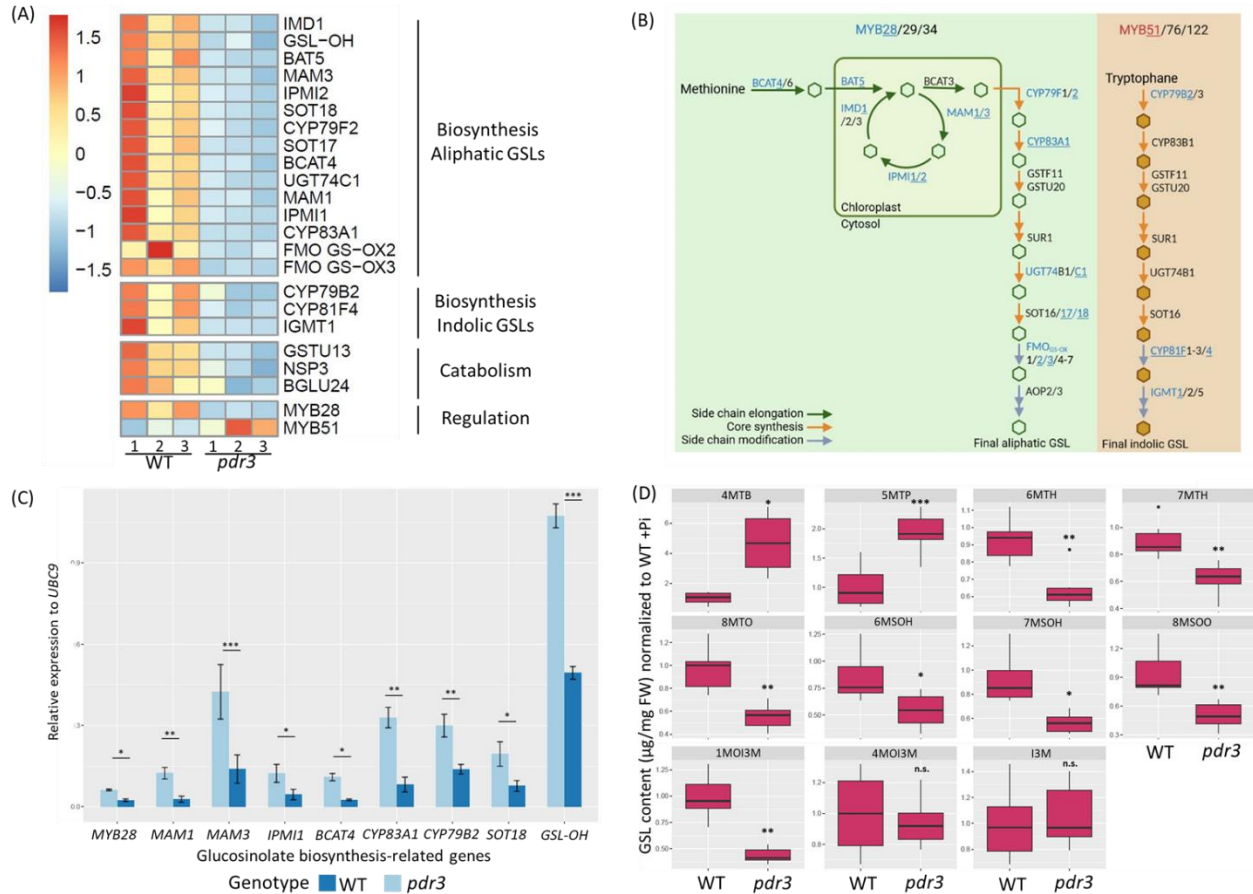
**Fig. 14 Pdr3 mutants exhibit impaired GSL biosynthesis, deriving from transcriptional downregulation of GSL metabolism genes.**
*(A) Heatmap showing the z-scores of FPKM values of GSL-related DEGs in pdr3 roots. Genes are categorized based on their function, as indicated.*
*(B) Simplified schematic representation of aliphatic (green box) and indolic (orange box) GSL biosynthetic pathways. DEGs in pdr3 roots are underlined and marked with blue (downregulated DEGs) or red (upregulated DEGs). Figure designed with BioRender.*
*(C) Gene expression of selected GSL biosynthesis genes in roots of 6-days-old WT and pdr3 seedlings. Seedlings were grown at +Pi for 5-days-old and transferred to +Pi; roots were harvested 1DAT. Bars represent the means of three biological replicates (±SD), each containing a pool of ~50 roots. Asterisks denote statistically significant differences between WT and pdr3 (Student's t-test, two-tailed, equal variances (\*p < 0.05, \*\*p < 0.01,\*\*\* p < 0.001).*
*(D) Normalized content of indicated GSL compounds in roots of of 6-days-old WT and pdr3 seedlings, grown at +Pi agar plates. The content of each analyte was normalized to fresh weight (FW) and then to the levels detected in WT. Boxplot shows medians, depicted as solid line inside the box, and interquartile ranges, from cummulative data of two biological experiments, each containing 7-8 roots per genotype. Outliers (> 1,5x interquartile range) are shown as a black dot. Asterisks denote statistically significant differences (depending on the distribution and homogeneity of variances in the data, Student's t-test, two-tailed, equal variances or Mann-Whitney-Wilcoxon Test (\*p < 0.05 , \*\*p < 0.01,\*\*\* p < 0.001).*

### 2.3.2 Pi limitation triggers accumulation of specific GSL in WT and *pdr3* roots

GSL metabolism has been shown to have a role in biotic as well as abiotic stress responses and specifically in phosphate deficiency responses. During a study of systemic metabolomic changes during Pi limitation, Pant et al. observed PHR-dependent accumulation of long aliphatic GSLs in *Arabidopsis* WT plants (Pant et al., 2015). Moreover, it has been proposed that indolic GSL are necessary for the establishment of a low Pi-triggered mutualistic relationship between *Arabidopsis* roots and *Colletotrichum tofieldiae*, a fungal root endophyte (Hiruma et al., 2016). HDC1 has been implicated to be a part of the regulatory transcriptional networks during Pi scarcity as well as of GSL metabolism. Since previous studies have demonstrated a link between Pi deficiency responses and GSL abundance, it was tempting to speculate that HDC1 can act as a regulator at the intersection between these two pathways.

Assuming that any Pi-dependent change in the GSL metabolism would take place at whole-root level and since most deregulated GSL-related changes were found in *pdr3* root tissue, the next step was the investigation of GSL biosynthetic gene expression in WT and *pdr3* roots during different Pi regimes. Therefore, seedlings of both genotypes were grown for five days on standard Pi replete media and then transferred at either Pi deficient media or to fresh Pi containing media as a control. The roots of each group of seedlings were excised at 1 DAT and used for subsequent gene expression analysis. Ten genes were selected to be tested (*MYB28, MYB51, MAM1, MAM3, IPMI1, BCAT4, CYP83A1, CYP79B2, SOT18* and *FMO-GS$_{OX3}$),* representing both biosynthetic pathways of aliphatic and indolic GSL as well as all stages of GSL biosynthesis, from regulation of the whole pathway until the side-chain modification of the final GSL compound. From the genes tested, only *MYB28*, the master regulator of aliphatic GSL biosynthesis and *CYP79B2*, encoding for a protein which catalyzes the first step in the core synthesis of indolic GSLs, showed Pi-responsive upregulation in roots of both WT and *pdr3* mutants (Fig. 15A, Suppl. Fig. 4). However, these changes in gene expression of pathway genes did not have the corresponding metabolic output; comparison of GSL abundance between roots of control and Pi-starved plants showed that long methylthiolalkyl GSLs (6MTH, 7MTH and 8MTO) are reduced upon Pi deficiency in both genotypes (Fig. 15B and detailed overview of absolute GSL content in Suppl. Table 14). Methylthiolalkyl GLSs are converted to methylsulfinylalkyl GSLs by the action of flavin-dependent monooxygenases (FMOs); however, no increase in the abundance of methylsulfinylalkyl GSLs was observed upon Pi deficiency, while the expression of one representative FMO that was tested was unchanged in Pi-starved roots of WT and *pdr3* seedlings (Suppl. Fig. 4). These results suggest that early responses to Pi deficiency in the roots include degradation of methylthioalkyl GSLs; however, it is possible that this reaction is not regulated at the transcriptional level, but maybe through the action of the existing enzymatic machinery of the cell or through other metabolic reactions.
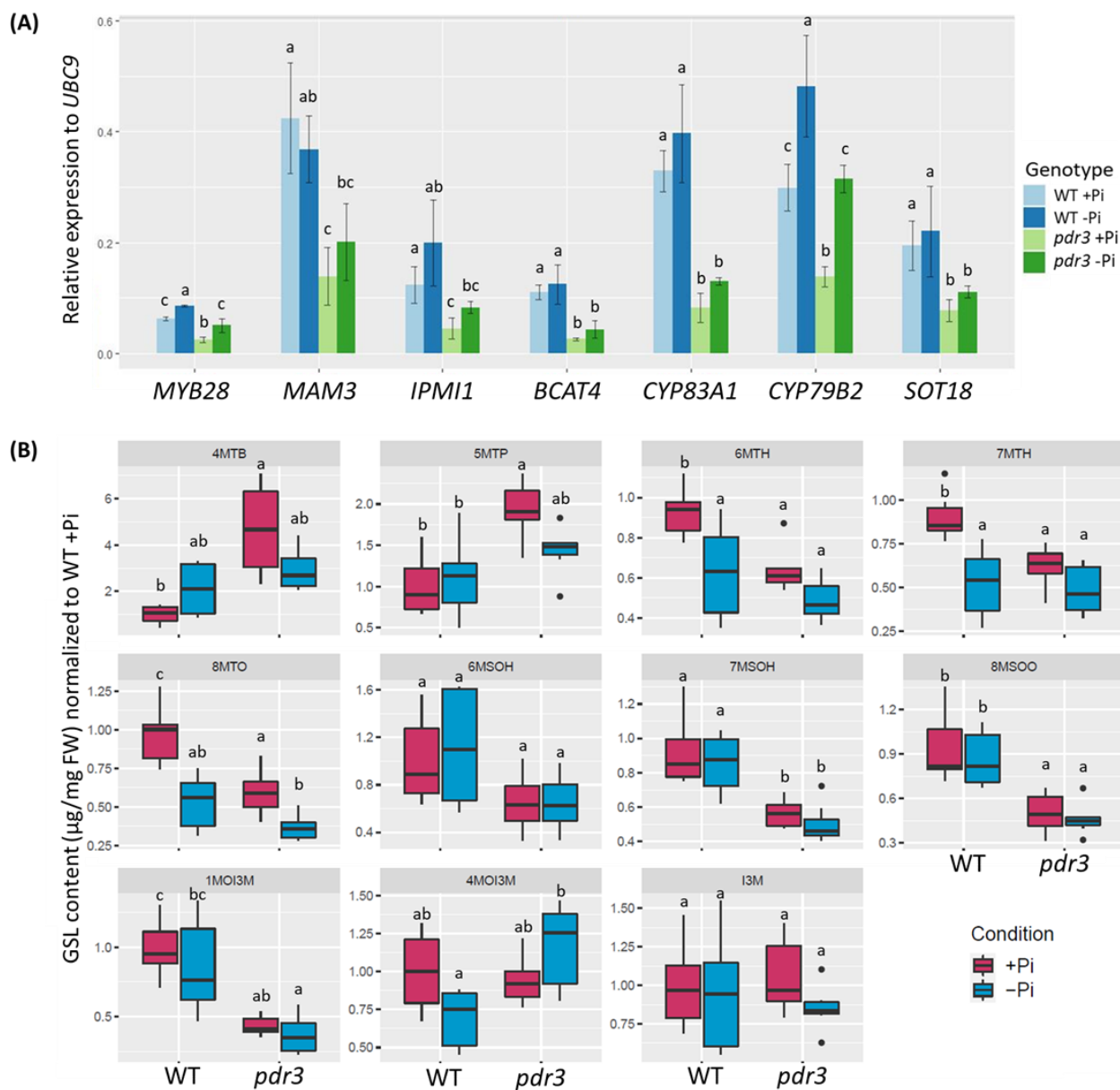
**Fig. 15 Early responses to Pi deficiency include reduction of long methylthiolalkyl GSL species in WT roots.**
*(A) and (B) Gene expression of selected GSL biosynthesis genes (A) and normalized GSL content of indicated compounds (B) in roots of 6-days-old WT and pdr3 seedlings. 5-days-old seedlings grown at +Pi agar plates were transferred to +Pi and -Pi conditions and the roots were harvested 1DAT. Bars (A) represent the means of three biological replicates (±SD), each containing a pool of ~50 roots. Boxplot (B) shows medians, depicted as solid line inside the box, and interquartile ranges, from cummulative data of two biological experiments, each consisting of 3-4 technical replicates, containing a pool of 7-8 roots per genotype and condition. The content of each analyte was normalized to fresh weight (FW) and then to the levels detected in WT. Outliers (> 1,5x interquartile range) are shown as a black dot. Letters (A and B) denote statistically significant differences across genotypes and conditions, for each gene or analyte separately (depending on the distribution and homogeneity of variances in the data, two-way ANOVA, followed by Tukey's HSD post-hoc test or Kruskal-Wallis, followed by Dunn's post-hoc test (p < 0.05).*

As described above, previous reports demonstrated that the GSL biosynthetic pathway is induced during Pi scarcity, both at the transcriptional and metabolic level. The fact that the same changes were not observed in the previously described experiment of this work could be attributed to differences in experimental design and specifically to the longer duration of the Pi starvation treatment that was implemented in these studies. To test that, GSL biosynthesis dynamics during Pi deficiency was assessed in WT and *pdr3* roots after 4 days of growth in Pi containing or depleted media. Firstly, the expression of genes encoding for proteins of the GSL biosynthesis pathway was compared between WT and *pdr3* seedlings grown at either Pi regime. From the 7 genes that were tested (*MYB28, MYB51, MAM3, IPMI1, BCAT4, SOT18* and *FMO-GS$_{OX3}$*), all but *MYB51* and *SOT18* showed upregulation in WT roots during Pi deficiency (Fig. 16A). Similarly, the expression of these genes followed the same trend in Pi-starved *pdr3* roots, with the exception of the aliphatic GSL regulator *MYB28* and the flavin monooxygenase *FMO-GS$_{OX3}$*, which surprisingly failed to show Pi-responsive upregulation in *pdr3*. Overall, this analysis showed that in terms of low Pi-triggered transcriptional activation of the GSL biosynthetic pathway, *pdr3* mutants partially show differential responses than WT when exposed to low Pi supply, although the activity of this pathway is also impaired in the mutant basal conditions.

In order to assess how the aforementioned transcriptional changes are reflected on the metabolic level, Pi-responsive changes in the abundance of GSL were investigated in roots of WT and *pdr3* seedlings, grown at different Pi regimes. As far as Pi deficiency-dependent changes are concerned, WT roots exhibited accumulation of the long aliphatic methylsulfinylalkyl GSLs 6MSOH, 7MSOH and 8MSOO as well as of the indolic GSL I3M (Fig. 16B and detailed overview of absolute GSL content in Suppl. Table 15). The short aliphatic GSL 5MTP also exhibited low-Pi induced abundance; however, the measurements of the short aliphatic GSLs 5MTP and 4MTB showed high intra-experimental variability (Suppl. Table 15), possibly due to the detection method's sensitivity and therefore cannot be reliably used to draw conclusions. Furthermore, 8MTO was the only GSL species that showed reduction in WT during Pi deficiency. Similarly, there was an increase in the abundance of long methylsulfinylalkyl GSLs as well as I3M in Pi starved *pdr3* roots. However, *pdr3* mutants failed to show the same Pi-dependent decrease of 8MTO as WT, while an increase in 1MOI3M levels was observed. Additionally, analysis of Pi-dependent GSL content was performed using the knockout T-DNA line *hdc1* and the overexpression line OxP3, as controls. At basal conditions, OxP3 has identical GSL profile as WT, while GSL abundance in *hdc1* was constitutively lower than WT, exhibiting a similar accumulation pattern as the *pdr3* mutant (Fig. 16B), further supporting the hypothesis that HDC1 participates in the regulation of GSL abundance. However, contrary to *pdr3*, *hdc1* roots did not show significantly reduced amount of 6MTH and 8MTO compared to WT at +Pi conditions. When seedlings were exposed to low Pi stress, OxP3 seedlings demonstrated an identical GSL accumulation trend as WT, while GSL content in *hdc1* roots was similar to *pdr3*.

Taken together, this study indicates that GSL biosynthesis is enhanced upon Pi limitation in WT roots; additionally, loss of HDC1 partially affects the mechanism of low Pi-dependent activation of GSL biosynthesis, indicating HDC1 as a potential basal regulator of GSL abundance, presumably at the transcriptional level.
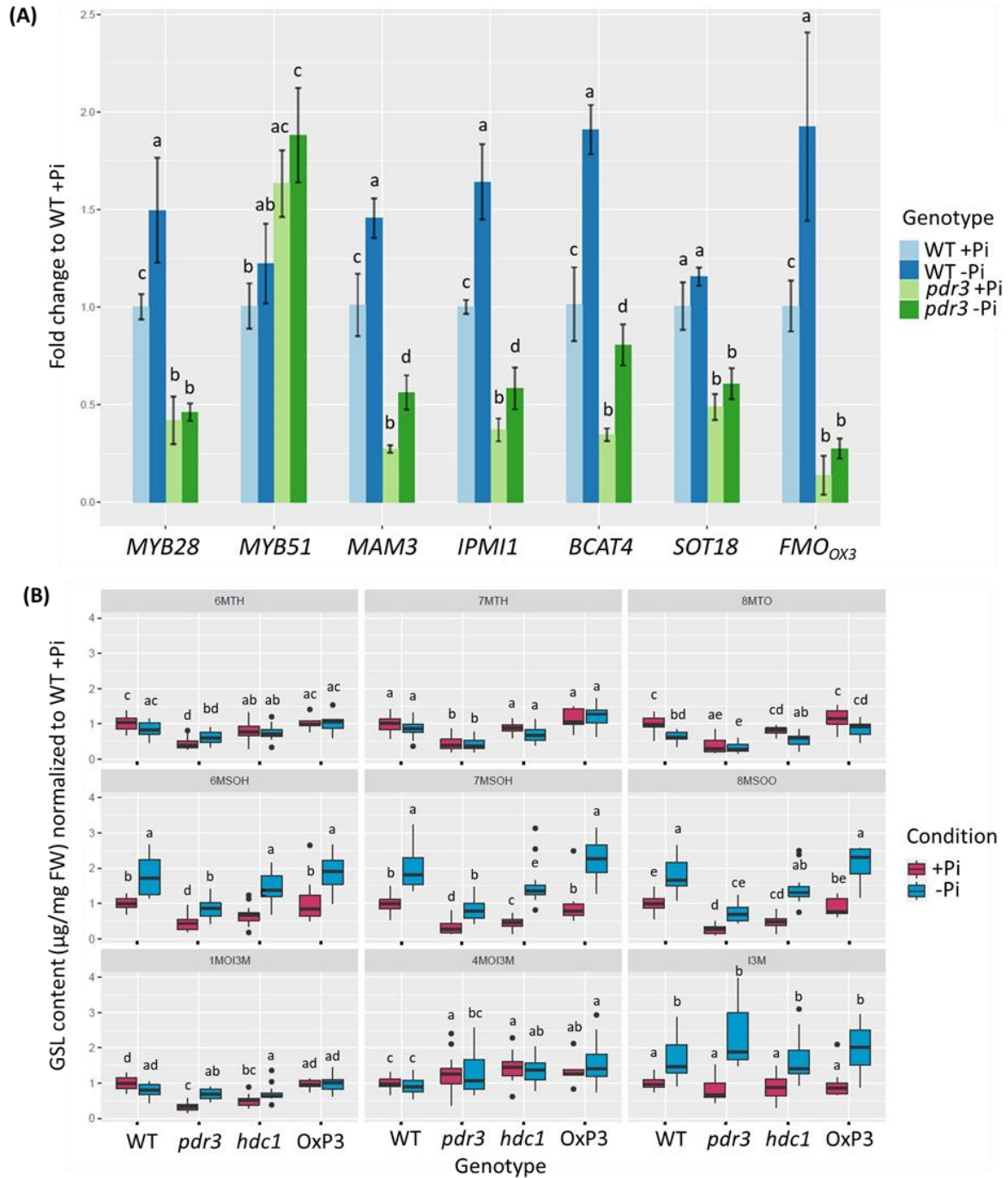
**Fig. 16 Pdr3 and WT roots respond similarly to prolonged Pi deficiency with transcriptional upregulation of GSL biosynthesis and accumulation of methylsulfinylalkyl GSL and I3M.**
*(A) and (B) Gene expression of selected GSL biosynthesis genes (A) and normalized GSL content (B) in roots of 9-days-old WT and pdr3 seedlings. 5-days-old seedlings grown at +Pi agar plates were transferred to +Pi and -Pi conditions and the roots were harvested 4 DAT. Bars (A) represent the means of three biological replicates (±SD), each containing a pool of ~50 roots. Boxplot (B) shows medians, depicted as solid line inside the box, and interquartile ranges, from cummulative data of six biological experiments, each containing 7-8 roots per genotype and condition. The content of each analyte was normalized to fresh weight (FW) and then to the levels detected in WT. Outliers (> 1,5x interquartile range) are shown black dots. Letters (A and B) denote statistically significant differences across genotypes and conditions, for each gene or analyte separately (depending on the distribution and homogeneity of variances in the data, two-way ANOVA, followed by Tukey's HSD post-hoc test or Kruskal-Wallis, followed by Dunn's post-hoc test ($p < 0.05$).*

### 2.3.3 Loss of HDC1 partially interferes with GSL accumulation in the shoots independently of Pi status

Based on the aforementioned observations, the GSL biosynthesis pathway appears to be impaired in *pdr3* roots, while this defect leaves the low-Pi triggered GSL accumulation response partially unaffected. However, the question remains whether these phenotypes are root specific or if loss-of-function of HDC1 can also influence GSL abundance in the above ground tissues and their response to Pi scarcity in terms of GSL accumulation. At control conditions, our RNA-seq analysis revealed that in 6-days-old *pdr3* shoots, there was differential expression of eight GSL metabolism-related genes, compared to WT (Suppl. Table 12). Of these genes, *FMO-GS$_{OX2}$*, *MAM3*, *CYP79F1* and *MYB76* encode for enzymes catalyzing the biosynthesis or the regulation of aliphatic GSLs and were found to be downregulated in the shoots of the mutant. In contrast, two *beta*-glucosidases participating in GSL catabolism, *BGLU21* and *BGLU22*, were upregulated in the same tissue as well as one myrosinase (*TGG4, THIOGLUCOSIDE GLUCOHYDROLASE 4*); another gene participating in GSL degradation (*ESP, EPITHIOSPECIFIER PROTEIN)* had downregulated expression in *pdr3*. Subsequent qPCR-based expression analysis confirmed no statistically significant difference of the transcript levels of several GSL biosynthesis genes (including *MAM3*) between the roots of WT and *pdr3* mutants (Fig. 17A). The discrepancy between the RNA-seq and the qPCR-generated data may be attributed to technical or sampling differences. Quite interestingly, these changes do not correlate with the shoot GSL metabolic profile as expected, since *pdr3* shoots are exhibiting less abundance of five GSL compounds (6MSOH, 7MSOH, 8MSOO, 1MOI3M and 4MOI3M) even at basal +Pi conditions (Fig. 17B and detailed overview of absolute GSL content in Suppl. Table 16); the same effect is observed for the T-DNA insertion line *hdc1.* Taken together, these results indicate that the observed HDC1-dependent transcriptional regulation of GSL biosynthesis in the roots does not necessarily extend to the shoots, as only 4 genes were deregulated in *pdr3* shoots. Nevertheless, GSLs show a differential accumulation pattern in the shoots of the mutant, which could be potentially attributed to the lower abundance of the same compounds in the source root tissue.

Next, it was investigated whether shoots of *pdr3* and WT seedlings are showing the same low Pi-adjusted GSL profile as the roots. Expression analysis of 7 GSL biosynthesis genes revealed that short exposure to Pi deficiency (1 DAT to low Pi conditions) does not impact the GSL pathway on the transcriptional level in neither WT nor *pdr3* shoots (Fig. 17A).  On the metabolic level, after longer Pi limitation (4 DAT after transfer to low Pi) WT shoots showed accumulation of two long aliphatic methylsulfinyl GSLs, 6MSOH and 7MSOH, as well as 4MSOB, a short aliphatic glucosinolate that was detectable only in the shoots. Furthermore, two indolic GSLs, I3M and 1MOI3M, showed Pi-dependent accumulation and reduction respectively. Similarly, *pdr3* and *hdc1* shoots showed the same changes in the abundance of the abovementioned compounds, while four additional compounds (6MTH, 7MTH, 8MTO and 8MSOO) showed low Pi-triggered accumulation. Overexpression of HDC1 did not affect GSL profile in the shoots of OxP3, as most GSL compounds had the same abundance as WT at either Pi regime. Overall, these observations display a low Pi-induced accumulation of certain GSL species in the shoots, while impaired function of HDC1 may cause enhancement of this effect.
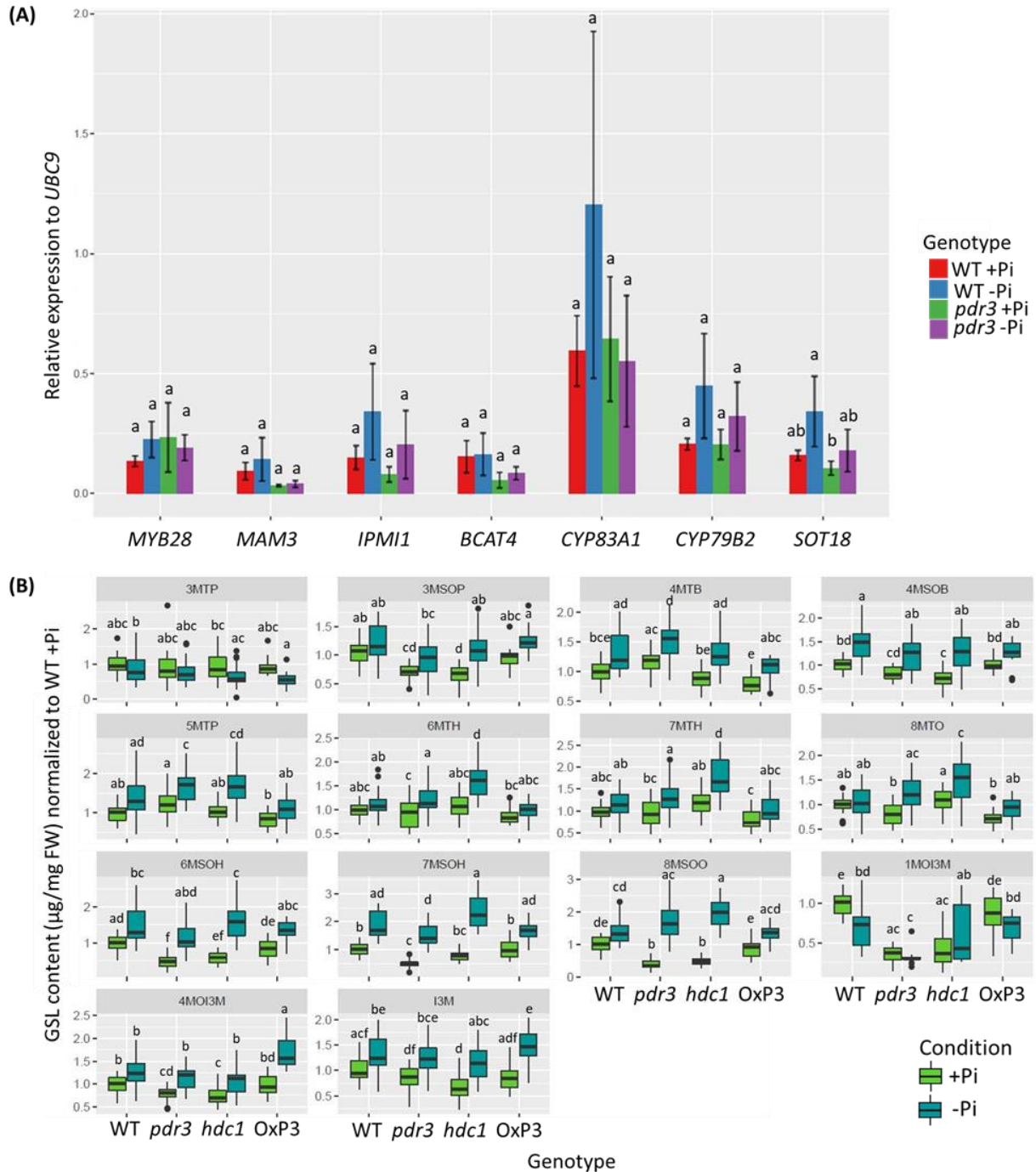
**Fig. 17 Prolonged Pi limitation induces GSL accumation in the shoots, in similar manner as in roots.**
*(A) Gene expression of selected GSL biosynthesis genes and relative in shoots of 6-days-old WT and pdr3 seedlings. 5-days-old seedlings grown at +Pi agar plates were transferred to +Pi and -Pi conditions. Shoots were excissed and harvested 1 DAT. Bars represent the means of three biological replicates (±SD), each containing a pool of ~25 shoots.*
*(B) Normalized GSL content in shoots of 9-days-old WT and pdr3 seedlings. 5-days-old seedlings were treated as described in (A) and shoots were harvested 4 DAT. The content of each analyte was normalized to fresh weight (FW) and then to the levels detected in WT. Boxplot shows medians, depicted as solid line inside the box, and interquartile ranges, from cummulative data of six biological experiments, each containing 3-4 shoots per genotype and condition. Outliers (> 1.5x interquartile range) are shown as black dots. Letters (A and B) denote statistically significant differences across genotypes and conditions, for each gene or analyte separately (depending on the distribution and homogeneity of variances in the data, two-way ANOVA, followed by Tukey's HSD post-hoc test or Kruskal-Wallis Test, followed by Dunn's post-hoc test (p < 0.05).*

47

### 2.3.4 Search for candidate suppressors of GSL biosynthesis

*2.3.4.1 Transcriptional data and bioinformatic analysis indicate WRKY46 as a candidate for negative regulation of GSL biosynthesis*

As described in the previous sections, HDC1 may act as a regulator of steady-state GSL biosynthesis in roots of young *A. thaliana* seedlings. HDC1 has been characterized as part of the HDA6 and HDA19 complexes, mediating deacetylation of lysine residues in the N-terminal tail of histones (Feng et al., 2021; Perrella et al., 2016). Histone deacetylation typically correlates with a denser chromatin state, resulting in transcriptional repression. Taken that into consideration, it would be expected that loss of HDC1 in *pdr3* mutants would lead to de-repression of its target genes and their subsequent upregulation. However, as described in the section 2.3, RNA-seq analysis of the *pdr3* root transcriptome showed that a number of genes of the GSL biosynthetic pathway were downregulated compared to WT. This fact suggests that these genes are not direct targets of HDC1-mediated transcriptional regulation, but rather that HDC1 may control a direct regulator of the GSL pathway, which probably acts as a transcriptional suppressor of basal GSL biosynthesis. In this scenario, impaired function of HDC1 would lead to aberrant transcriptional de-repression of this suppressor and subsequent downregulation of its target genes. So far, the sulfate deficiency-responsive proteins SULFUR DEFICIENCY INDUCED 1/2 (SDI1/2) have been characterized as suppressors of GSL biosynthesis, via protein-protein interaction with MYB28 and inhibition of its transcriptional activity (Aarabi et al., 2016). However, neither of these genes show transcriptional deregulation in *pdr3* roots, having comparable expression levels as in WT (Suppl. Table 17). Similarly, no transcriptional factor with binding capacity at the promoters of SDI1/2, namely SLIM1, GBF1, HYH, bZIP16 and bZIP44, showed abnormal expression in *pdr3* (Rakpenthai et al., 2022), suggesting that probably the perturbed GSL biosynthesis in this mutant is not SDI1/2-dependent. Additionally, a broader analysis was employed, searching for annotated positive or negative regulators of GSL biosynthesis, both in the literature and the TAIR database (GO:0010439). However, except for the positive regulator of indolic GSL biosynthesis, MYB51, no other transcriptional factor was found to be upregulated in *pdr3* roots (Suppl. Table 17).

To search for possible transcriptional suppressor candidates and to understand how loss-of-function of HDC1 affects the expression of transcriptional factors in roots, 52 DEGs in *pdr3* roots with an annotated function in transcription (GO:0006350) were gathered and ranked based on their expression (Suppl. Table 18). This putative suppressor can be a direct target gene of HDC1, which would mean that it would be upregulated in *pdr3*; thus, only upregulated DEGs in *pdr3* roots were taken into consideration, yielding a total of 23 DEGs with a function in transcription (Suppl. Table 18). From these, *SVP* (*SHORT VEGETATIVE PHASE*), *WRKY46* (*WRKY DNA-BINDING PROTEIN 46*) and *MEA* (*MEDEA*) have been described to have a function in gene repression. SVP is a floral suppressor, controlling the expression of *FT* (*FLOWERING LOCUS T*) and *SUPPRESSOR OF OVEREXPRESSION OF CO 1* (*SOC1*) (Li et al., 2008) while WRKY46 is transcriptional factor that, among other functions, participates in aluminum-induced root malate secretion by repressing the expression of *ALMT1* (*ALUMINUM-ACTIVATED MALATE TRANSPORTER 1*) (Ding et al., 2013). *MEDEA* encodes a methyltransferase, a member of the Polycomb Repressive Complex 2 (PRC2) (Grossniklaus et al., 1998). To extend the search for a transcriptional suppressor, genes in the GO category "negative regulation of transcription, DNA-templated" (GO:0045892) were mined (TAIR database) and were cross-checked with the dataset of DEGs in the *pdr3* roots. This approach yielded three DEGs with upregulated expression in *pdr3*, specifically SVP, MEA and an uncharacterized F-box/LRR-repeat protein (Suppl. Table 18).

To get more information about the transcriptional network governing the GSL-related DEGs in *pdr3* roots, promoter analysis of these genes was performed by investigating the co-occurrence of transcriptional factor binding sites on their respective promoters, using the online tool PlantPan 3.0 (Chow et al., 2019). Since the biosynthesis of mostly aliphatic GSLs is impaired in *pdr3* roots, the input gene list for this analysis involved only the DEGs involved in this clade of GSL biosynthesis. Among the common transcriptional factors, three were significantly deregulated in *pdr3* roots, specifically WRKY46, AGL42 (AGAMOUS-LIKE 42) and HSFA2 (HEAT SHOCK TRANSCRIPTION FACTOR A2), having binding sites on 93.8, 81.2 and 75% of the GSL biosynthesis-related genes, respectively (Fig. 18). Alternatively, this analysis was also repeated with a smaller set of input genes, for which the 5 top most downregulated GSL-related DEGs (*IPMI1, CYP83A1*, *IGMT1*, *FMO-GS_{OX2}*, *FMO-GS_{OX3}*) were selected, as well as the central regulator of aliphatic GSL biosynthesis, MYB28. However, only WRKY46 shared binding elements among the promoters of these genes, showing 100% coverage. Overall, these results indicate WRKY46 to be the most promising candidate suppressor of GSL biosynthesis, which is based on its upregulated expression in *pdr3* roots, its described function in negative regulation of transcription as a transcriptional factor, and its multiple binding sites on the promoter of each GSL biosynthesis gene.
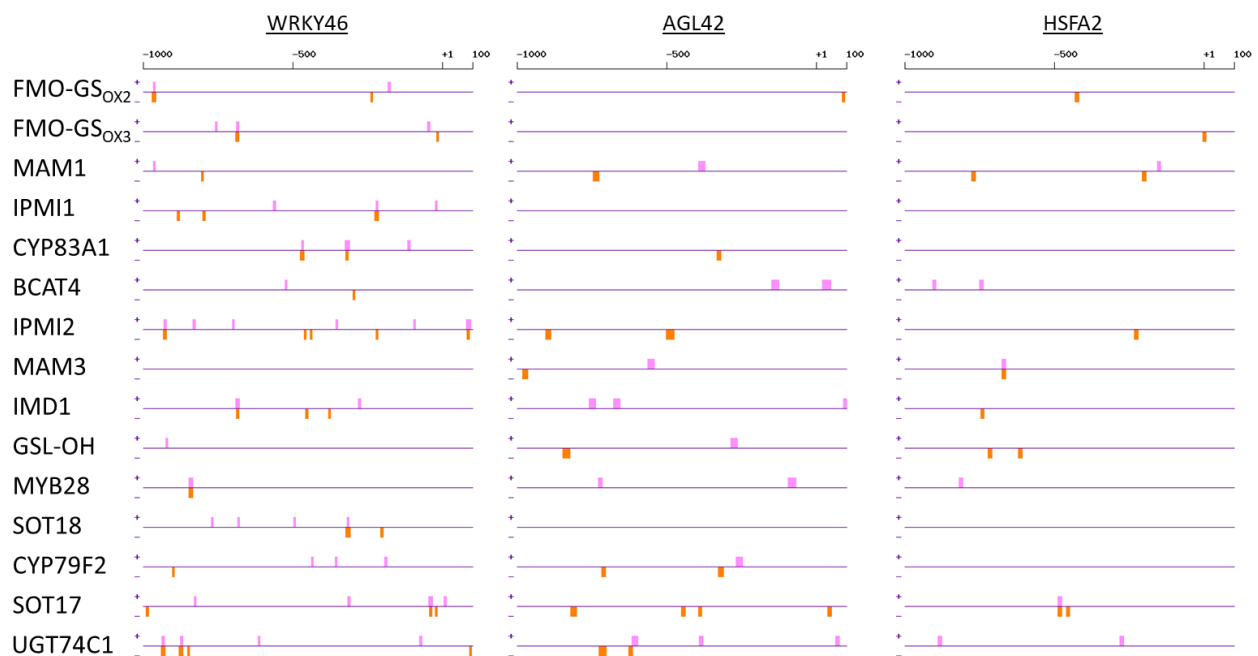


**Fig. 18 WRKY46 has multiple binding sites on the promoters of GSL biosynthesis genes.**
*Predicted binding sites of the indicated transcriptional factors on the transcriptional starting site of aliphatic GSL biosynthesis DEGs in pdr3 roots. Binding sites on the +strand (5' to 3' end) are indicated with magenta and on the -strand (3' to 5'end) with orange.*

### 2.3.4.2   Analysis of wrky46 mutants does not reveal root-specific impaired GSL biosynthesis

To test the hypothesis that WRKY46 is a transcriptional repressor of GSL biosynthesis, the activity of this pathway was assessed in a T-DNA mutant line of WRKY46 (SALK_134310C) by measuring the abundance of GSL metabolites as well as by checking the expression of genes involved in GSL biosynthesis. Assuming

that WRKY46 negatively regulates GSL abundance in the roots, it would be expected that loss of function of this protein may result in upregulated expression of the biosynthetic genes and higher GSL accumulation than WT. However, quantification of GSL in *wrky46* roots showed no significant differences to WT roots for most of the compounds tested or even lower abundance than in WT, in the cases of 5MTP, 4MOI3M and I3M (Fig. 19A). Preliminary analysis of GSL metabolites in a second, independent mutant line (SAIL_1230_H01) confirmed that loss of WRKY46 does not correlate with increased GSL abundance, but rather with decreased accumulation of most of the detected compounds (Suppl. Fig. 5). Quite interestingly, all three long methylthiolalkyl GSL (6MTH, 7MTH and 8MTO) as well as two methylsulfinylalkyl GSLs (7MSOH and 8MSOO) exhibited higher abundance than WT in shoots of *wrky46* (Fig. 19B). Nevertheless, GSL genes show root-specific transcriptional repression in *pdr3*, hence a HDC1-regulated suppressor of GSL biosynthesis would probably show a corresponding root-specific GSL profile, independent of the GSL status in the shoots. Additionally, three genes were selected for gene expression analysis based on their role in the aliphatic pathway of GSL biosynthesis or the extent of their deregulation in the *pdr3* mutant (*MYB28*, *MAM3* and *FMO-GS$_{OX3}$*). In line with the GSL metabolic analysis of *wrky46*, none of these genes showed higher expression than WT in this mutant (Fig. 19C). Overall, these results do not support a role of WRKY46 for tuning GSL biosynthesis in the roots, which likely does not participate in HDC1-mediated regulation of GSL biosynthesis.
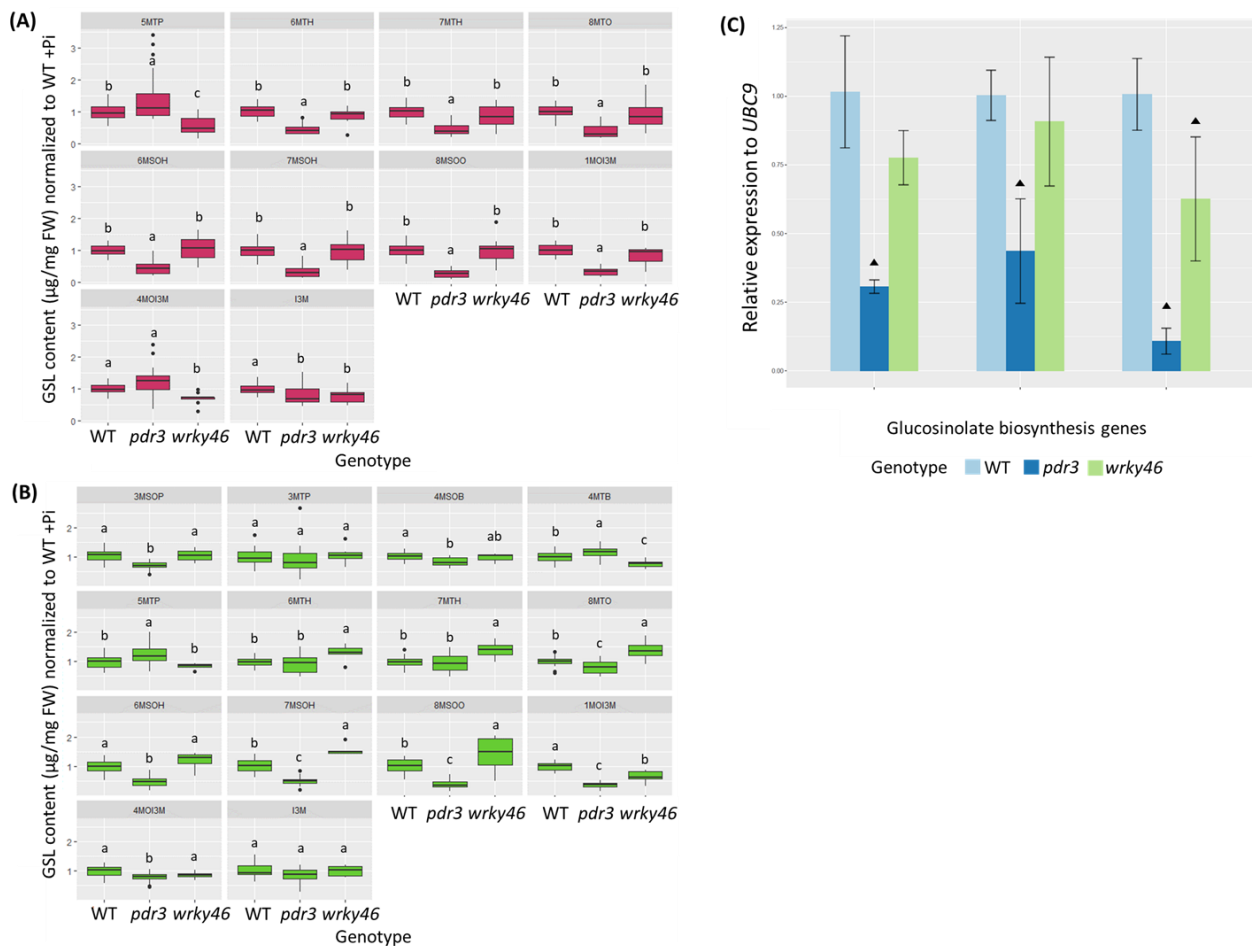


**Fig. 19 Assessment of wrky46 mutant does not infer a role of WRKY46 as negative regulator of GSL biosynthesis in the roots.**

**Fig. 19 Assessment of wrky46 mutant does not infer a role of WRKY46 as negative regulator of GSL biosynthesis in the roots. (cont.)**

*(A and B) Normalized GSL content in roots (A) and (B) shoots of 9-days-old WT, pdr3 and wrky46 seedlings. Seedlings were germinated at +Pi for 5 days and transferred to +Pi; roots and shoots were harvested 4 DAT. The content of each analyte was normalized to fresh weight (FW) and then to the levels detected in WT. Boxplot shows medians, depicted as solid line inside the box, and interquartile ranges, from cummulative data of 3 biological experiments, each containing 4 technical replicates, consisting of 7-8 roots (A) and 3-4 shoots (B) per genotype. Outliers (> 1.5 x interquartile range) are shown as black dots. Letters (A and B) denote statistically significant differences across genotypes, for each analyte separately (one-way ANOVA, followed by Tukey's HSD test ($p < 0.05$)).*

*(C) Gene expression of MYB28, MAM3 and FMO-GS$_{OX3}$ in roots of 9-days-old WT, pdr3 and wrky46 seedlings. Plant material was treated as described in (A). Bars represent the means of three biological replicates (±SD), each containing a pool of ~50 roots. Triangles denote statistically significant differences to WT for each gene respectively (Student's t-test, two-tailed, equal variances, $p<0.05$).*

### 2.3.4.3   Preliminary work for ChIP assays

This work has indicated that HDC1 may play an indirect role in preserving basal expression levels of genes participating in GSL biosynthesis in roots, presumably by controlling a negative regulator of the pathway. Although WRKY46 was a candidate for such a function, subsequent analysis showed that GSL biosynthesis is mostly unaffected in the *wrky46* mutant, suggesting that there might be another HDC1-regulated protein having a role in GSL metabolism. HDC1 has an important role in two major HDA complexes, causing accumulation of histone acetylation marks upon its loss of function (Perrella et al., 2013). Thus, it is to be expected that a putative regulator of GSL metabolism under HDC1-mediated transcriptional control would show differential histone acetylation level in the mutant. To further investigate that, a direct approach would be a chromatin immunoprecipitation (ChIP) assay coupled with next generation sequencing (ChIP-seq), which would allow the comparison of the global chromatin acetylation levels between WT and *pdr3* roots, revealing potential targets of HDC1-mediated deacetylation. Moreover, as demonstrated in section 2.2, *pdr3* mutants suffer from deregulated expression of hundreds of genes, both at standard growth conditions as well as during Pi scarcity; nevertheless, it is not clear whether these genes are direct targets of HDC1-mediated regulation or if they are affected indirectly by loss of HDC1. Comparing a ChIP-seq generated dataset with the existing RNA-seq dataset would allow more precise identification of HDC1 targets, thus rendering such an experiment central for understanding which biological pathways, including GSL biosynthesis and Pi starvation responses, are tuned by HDC1.

Since the root transcriptome of *pdr3* showed the most extensive changes in the context of GSL metabolism, it would be reasonable to seek for differentially acetylated targets of HDC1 in this tissue type. In order to perform a ChIP experiment, a first technical challenge that has to be overcome is the quantity of the starting material for the chromatin preparation. Most protocols require the use of more than 0.7 grams of fresh tissue for a successful ChIP assay (Kaufmann et al., 2010; Poza-Viejo et al., 2019; Yamaguchi et al., 2014), hence rendering the vertical plate growth system rather unpractical for harvesting such an amount of root tissue. As an alternative, a hydroponic system was employed, where seeds were directly sown on a polypropylene mesh, floating on standard liquid growth medium, inside an Erlenmeyer flask (Fig. 20A). The roots of the young seedlings were able to grow through the mesh into the media and were excised 9 days after sowing (Fig. 20B). Using this growth system, the collection of a minimum amount of 0.3 grams of root tissue per flask was possible, thus allowing fast and easy harvesting of the necessary starting material for a ChIP assay. Additionally, to confirm that roots of hydroponically grown *pdr3* seedlings exhibit the same downregulated expression of GSL-related genes as seedlings grown on vertical

square plates, the expression of *MYB28, MAM3* and *FMO-GS$_{OX3}$* was assessed by qPCR. All three genes under investigation showed similar expression profiles in the hydroponic system as in the RNA-seq analysis of plate-grown seedlings (Fig. 20C), demonstrating that this system is suitable for the investigating the transcriptional and epigenetic traits of *pdr3* mutants that lead to impaired GSL biosynthesis. As a further step for testing this system, the expression of the Pi starvation response gene *SPX1* was assessed in roots of hydroponically grown WT seedlings at Pi replete or Pi deficient conditions. Over the course of 4 days, *SPX1* was induced in Pi starved WT seedlings up to approximately 400 times in comparison to the control (Fig. 20D), further validating that a hydroponic system is applicable to this study.

Unfortunately, the pilot ChIP experiments were not successful, as it was not possible to extract sufficient chromatin from the tissues under analysis. Specifically, root tissue was harvested from hydroponically grown 9-days-old WT and *pdr3* seedlings and was used for chromatin crosslinking, extraction and fragmentation via sonication, following the manufacturer's instructions of Abcam's ChIP Kit for plants. However, monitoring of fragmented chromatin with gel electrophoresis showed no detected chromatin in samples (data not shown), indicating that further optimization of the above-mentioned processes is necessary.
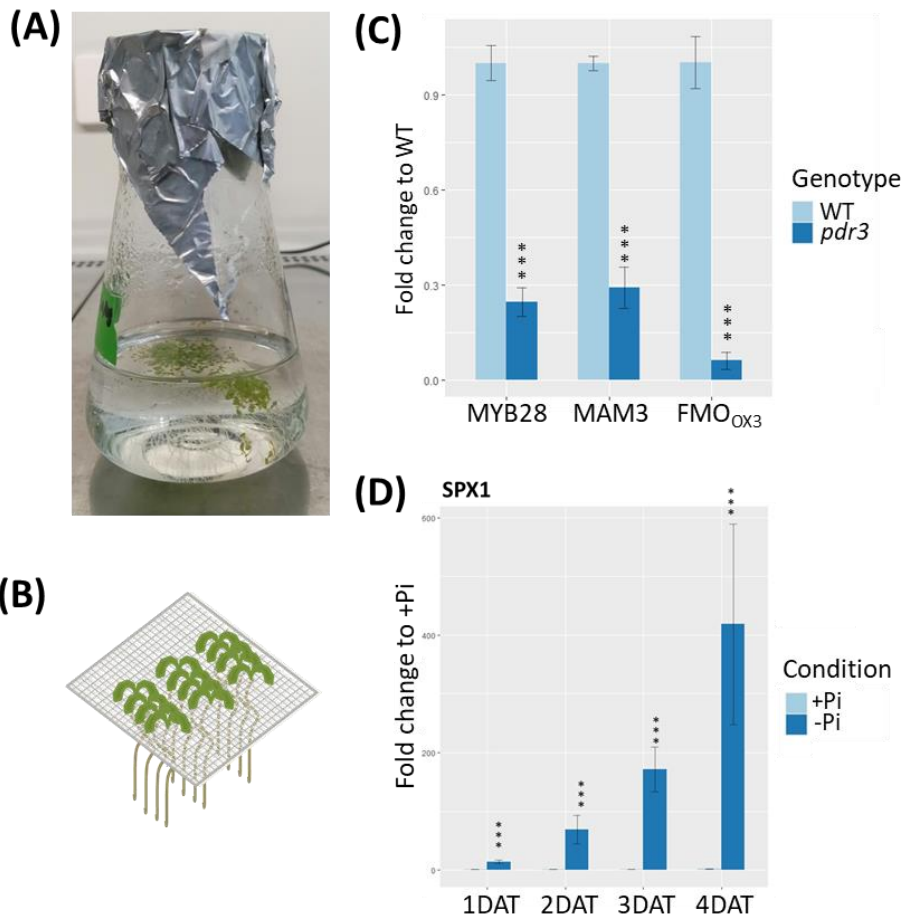


**Fig. 20 Testing of hydroponic growth system.**

**Fig. 20 Testing of hydroponic growth system. (cont.)**

*(A and B) Stratified and sterilized seedlings were sown directly on a polypropylene mesh, floating on +Pi liquid growth medium inside an 250 ml Erlenmeyer flask (A, representative image). Seedlings were grown through the mesh as shown in scheme (B) for 7 days and the mesh along with the attached seedlings was transferred to fresh flasks containing +Pi or – Pi liquid medium. Root material was typically harvested 4 DAT.*

*(C and D) Gene expression of MYB28, MAM3 and FMO-GS$_{OX3}$ in roots of 9-days-old WT and pdr3 seedlings (C) and SPX1 in roots of Pi starved WT seedlings (D). Seedlings were germinated at +Pi for 5 days and transferred to +Pi (A) or +Pi and -Pi (B) conditions. Root material was harvested at 4 DAT. Bars represent the means of three biological replicates (±SD), each containing a pool of ~50 roots. Asterisks denote statistically significant differences to WT for each gene respectively (Student's t-test, two-tailed, equal variances, \*\*\*p<0.001).*

## 2.4 Ectopic chlorophyll accumulation in *pdr3* root tips

### 2.4.1 Loss of HDC1 correlates with ectopic chlorophyll A accumulation in the cortex layer of *pdr3* root tips

As described in section 1.5, previous work in our group detected microscopically ectopic chlorophyll accumulation in root tips of young *pdr3* mutant seedlings. This was confirmed by HPLC analysis, which identified chlorophyll A (Chl A) in *pdr3* root samples. During this study, we firstly aimed to confirm these previous observations by monitoring the root tips of light-grown WT, *pdr3* and *hdc1* seedlings with confocal microscopy. Indeed, root tips of both mutant lines exhibit chlorophyll-derived auto-fluorescence, with much higher intensity in the *pdr3* roots (Fig. 21A). Strikingly, this auto-fluorescence was not emitted equally from the whole root tip, but rather followed a cell type-specific pattern of distribution. To further investigate this, confocal microscopy of *pdr3* root tips was repeated after staining with the cell wall counter-coloring dye propidium iodide (PI), aiming to clearly define the site of the chlorophyll accumulation. This approach showed that the observed chlorophyll-related auto-fluorescence was localized in the cortex cells of the meristematic zone in *pdr3* roots (Fig. 21C).

Since chlorophyll biosynthesis is usually tightly co-regulated with chloroplast differentiation and biogenesis, it was assumed that the ectopic presence of chlorophyll in *pdr3* root tips may also correspond to altered plastidial ultrastructure. To answer this, ultra-thin sections of WT and *pdr3* root tips were imaged by electron microscopy in collaboration with Dr. Gerd Hause (Biocentre, Halle, Germany), searching for the presence of differentiating chloroplasts. Plastids from the epidermis layer of both WT and *pdr3* meristems showed pro-thylakoid structures, seen as planar bilayer membranes (Fig. 21B and overview in Suppl. Fig. 6). However, when the plastids in the cortex cell layer were monitored, *pdr3* roots exhibited plastids with more structured, stacked thylakoid membranes, which were absent from WT. In parallel, to investigate the subcellular localization of the chlorophyll-derived auto-fluorescence, *pdr3* mutants were transformed with a construct expressing FNR (FERREDOXIN:NADPH OXIDOREDUCTASE), as plastidial marker (Marques et al., 2003). During the course of this work, transformed plants only from the T2 generation were monitored by confocal microscopy. In the *pdr3* background, auto-fluorescence co-localized with plastid-localized GFP signal, however only in the cortex cells, providing further evidence for the cortex specific de-repression of chlorophyll accumulation and possibly proplastid differentiation in the *pdr3* background.
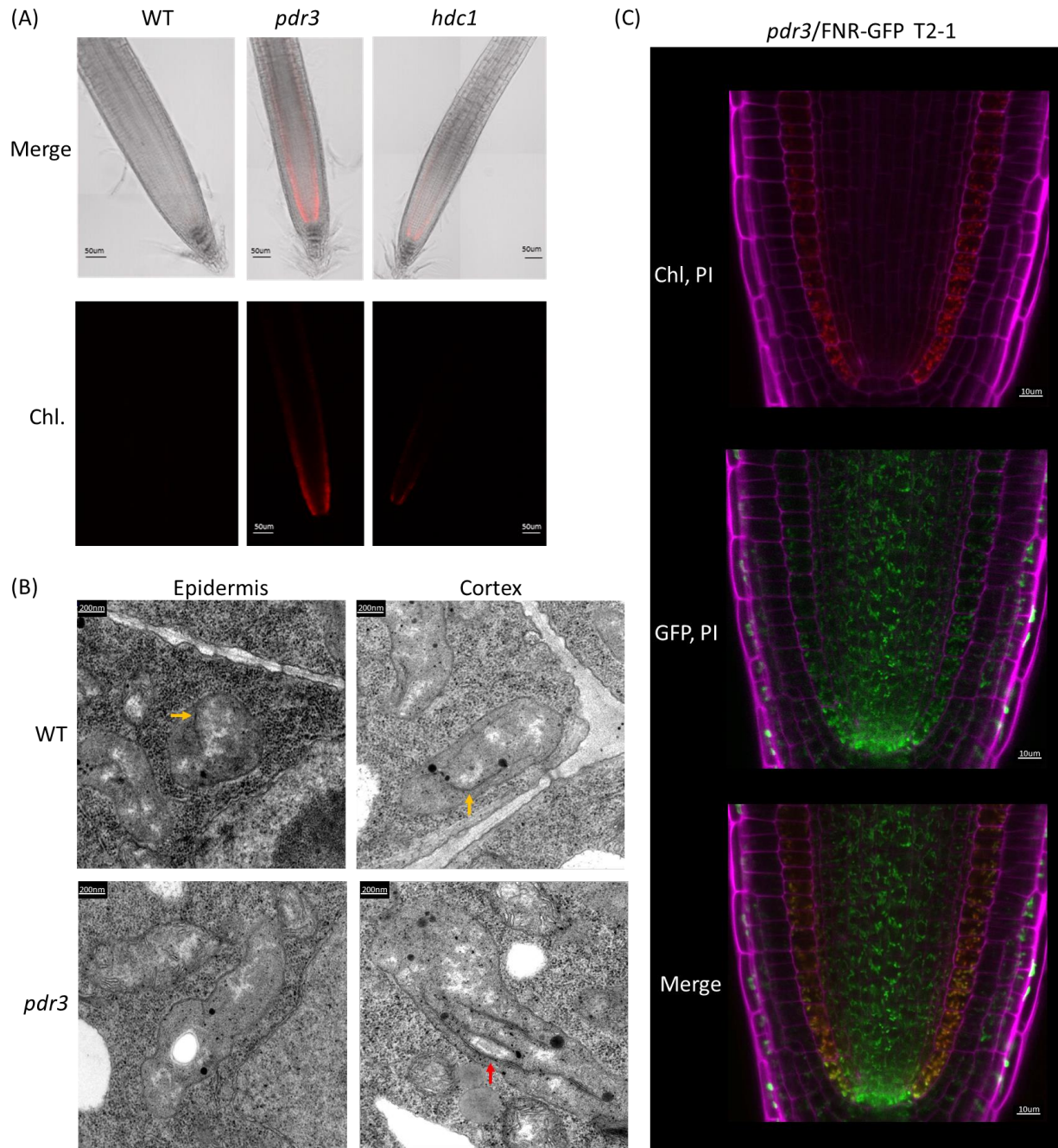
**Fig. 21 The pdr3 mutation reveals cortex-specific ectopic Chl A accumulation and partial plastid differentiation.**
*(A) Representative confocal images of WT, pdr3 and hdc1 root tips. Seedlings were germinated at standard growth conditions for 9 days and root-tip specific Chl A-derived autofluorescence was monitored with confocal microscopy (lower panels, red ). Upper panel corresponds to merged brightfield and Chl A channels.*
*(B) Representative transmission electron microscopy (TEM) images of the epidermis or cortex cells in root tips of 9-days-old WT and pdr3 seedlings, focusing on proplastids (WT, upper panel) or specialized plastids (pdr3, right lower panel). Developed thylakoid structures and pro-thylakoid formations are indicated with red or yellow arrows, respectively. This experiment was performed in collaboration with Dr. Gerd Hause (Biocentre, Halle, Germany).*
*(C) Representative confocal images of pdr3 seedlings overexpressing the FNR-GFP marker, tagging the plastids. 9-days-old seedlings germinated at standard growth conditions were stained with propidium iodine (PI) and the root tips were monitored with confocal microscopy. Cell walls are visualized with magenta (all 3 panels), GFP with green (middle and bottom panel) and Chl A-derived autofluorescence with red (upper and bottom panel). Scale bars = 0,5mm (A); 200 nm (B); 0,1 mm (C).*

54

## 2.4.2 Transcriptional analysis of *pdr3* root tips revealed de-repression of genes encoding for chlorophyll binding, photosynthetic proteins

One of the main questions that we sought to answer with the present RNA-seq approach (see section 2.2) was whether the ectopic chlorophyll accumulation in *pdr3* root tips could be attributed to derepressed chlorophyll biosynthesis genes as a result to loss of function of HDC1. To answer this question, the genes which had an annotated function in chlorophyll anabolism were retrieved from TAIR database (GO:0015995) and their expression was compared between WT and *pdr3.* To our surprise, only one gene involved in chlorophyll biosynthesis was upregulated in the mutant root tips during basal Pi replete conditions, namely *PORB* (*PROTOCHLOROPHYLLIDE REDUCTASE B*) (Suppl. Fig. 7A), which encodes a protein catalyzing the conversion of protochlorophyllide to chlorophyllide in a light-dependent manner (Franck et al., 2000). In parallel, *HEMB2* (aldolase superfamily protein) was the only gene downregulated in *pdr3* at the same conditions; both *PORB* and *HEMB2* showed the same expression trend during Pi deficient conditions.

GO enrichment analysis of the DEGs that are representing the basal transcriptional differences between WT and *pdr3* root tips revealed that the functional term of photosynthesis (GO:0015979 from TAIR database) was significantly enriched in this dataset. Most of the DEGs in this dataset encoded proteins participating in photosynthetic light reactions, including, among others, four genes of light harvesting Chl a/b-binding antennas, *LHCA2* (*PHOTOSYSTEM I LIGHT HARVESTING COMPLEX GENE 2*) and *LHCB1.3/4.3/5* (*LIGHT-HARVESTING COMPLEX II CHLOROPHYLL A/B BINDING PROTEIN 1.3/4.3/5*), as well as two genes of photosystem I and II subunits, *PSAG (PHOTOSYSTEM I REACTION CENTER SUBUNIT G)* and *PSBW* (*PHOTOSYSTEM II REACTION CENTER W*) (Fig. 22). Additionally, three genes of the Calvin cycle were found, specifically SBPASE (*SEDOHEPTULOSE-1,7-BISPHOSPHATASE*), *RBCS1A* (*RIBULOSE BISPHOSPHATE CARBOXYLASE SMALL CHAIN 1A*) and *GAPA1* (*GLYCERALDEHYDE 3-PHOSPHATE DEHYDROGENASE A SUBUNIT 1*). All of the photosynthesis-related DEGs found in this dataset are nuclear encoded and had higher expression in *pdr3* root tips; the only exception was *LFNR2* (FERREDOXIN-NADP[(+)]-OXIDOREDUCTASE 2), which was downregulated in the mutant. Overall, these findings indicate that loss of HDC1 may cause partial photosynthetic activation of *Arabidopsis* root tips, at least at the transcriptional level, which might be correlated to the accumulation of Chl A and that is observed macroscopically.
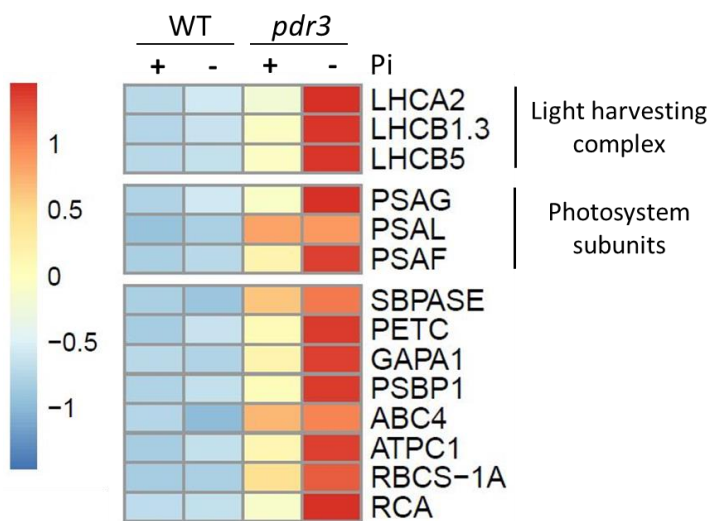


***Fig. 22 Loss of HDC1 is causing de-repression of chlorophyl binding proteins and PORB in the root tip, independing of Pi supply.***
*Heat map showing the z-scores of the mean FPKM values of selected DEGs in WT and pdr3 root tips, at +Pi or -Pi conditions. Seedlings were germinated for 5 days at +Pi media and transferred to +Pi and -Pi media; root tips were excised at 1 DAT. Genes depicted are related to the GO term "photosynthesis"; upper and middle panels, are representing genes in the protein family of light harvesting complexes and photosystem components, respectively. Lower panel shows the rest of the DEGs in this category as well as RCA (RUBISCO ACTIVASE), which has an annotated function in GO term "response to light stimulus".*

## 2.5 Investigation of HDC1 stability during Pi scarcity

As discussed in section 1.1.3.2, a recent publication suggested a model of HDC1-mediated transcriptional regulation upon Pi deficiency, in which low Pi-triggered destabilization of HDC1 results in upregulation of *ALMT1* and *LPR1* expression (Xu et al., 2020). The authors observed reduction in GFP fluorescence from roots of low Pi-grown seedlings expressing GFP-tagged HDC1, in comparison with seedlings of the same line grown at Pi replete conditions. This finding was also validated by immunodetection of HDC1-GFP in root tips of seedlings grown at different Pi regimes, using an a-GFP antibody; Western blot assays demonstrated lower HDC1-GFP levels in protein extracts of root tips from Pi starved seedlings. Additionally, the expression of *LPR1* and *ALMT1* was monitored with qPCR and showed low Pi-triggered induction both in WT as well in loss-of-function mutants of HDC1 (Xu et al., 2020). However, the RNA-seq analysis that was performed during the course of this work did not show any significant change in of LPR1 in Pi starved root tips in any genotype under investigation (Suppl. Table 20). Moreover, a recent report about *LPR1* function in Pi starved root tips showed no evidence of transcriptional regulation of *LPR1* in *Arabidopsis* roots, but rather tuning of LPR1 function in Pi deficiency responses by substrate availability (Naumann et al., 2022).

To solve the above-mentioned discrepancy, it was necessary to repeat immunodetection of the native, non-tagged HDC1 from protein extracts of seedlings grown at different Pi regimes. Since no HDC1-specific antibody is commercially available, we sought to raise an anti-HDC1 peptide antibody in rabbits. Towards that, a list of possible HDC1 peptides, which would act as immunogens, was assessed for homology with other proteins, using BlastP (Basic Local Alignment Search Tool for Proteins). Selection of the best candidates was based on least homology with other protein sequences or homology with proteins with different size than HDC1. Based on these criteria, two peptides were chosen for polyclonal antibody production. These peptides were located in positions 367-381 (C+EWGDRDKDRNDRRVS) and 685-699 (C+DYYTSKLRNNVRSRA); a dot blot assay was performed to confirm the specificity and activity of the antibodies recognizing each peptide, hereafter named a-HDC1 868 and a-HDC1 869 respectively (Fig. 23A). A-HDC1 868 successfully recognized its respective immunogen even at the lowest tested concentrations (Fig. 23A, upper panels), while a-HDC1 869 showed required higher concentration for successful detection (Fig. 23A, lower panels). Moreover, a-HDC1 868 exhibited immunogen-specific affinity, whereas a-HDC1 869 showed strong cross-reactivity against the 868 immunogenic peptide.

Subsequently, Western blot assays were performed using a-HDC1 868/869 for HDC1 detection in protein extracts from WT and *pdr3* seedlings, as well as from the overexpression line (OxP3) and a line expressing a fusion of HDC1-GFP under its native promoter in the *pdr3* background (HDC1-GFP) (Fig. 23C). For the first tests, different volumes of protein extract were loaded on an SDS-PAGE, without prior absolute quantification of protein content. Although both a-HDC1 antibodies showed clear cross-reactivity against other proteins of sizes ranging from 55-100kDa (Suppl. Fig. 8A), a band was detected at approximately around 130 kDa in WT samples, that was absent from the *pdr3* protein extracts (Fig. 23). A band of the same size was detected in OxP3 and in some cases, it had higher intensity than WT. However, since the protein abundance in the samples was not determined, it is possible that the differences in band intensity between WT and OxP3 samples are caused by different protein concentration in the material loaded on the gel and for that reason, no quantitative conclusion can be draw based on this analysis. Additionally, another band was detected at around 180kDa in the HDC1-GFP line, that could correspond to the GFP tagged HDC1. As expected from the results of the dot blot assay (Fig. 23A), a-HDC1 868 showed much higher capacity for HDC1 detection than a-HDC1 869, which showed a strong signal only in the OxP3

samples. Overall, these results show that a-HDC1 868 and at a lesser degree a-HDC1 869 can be used for HDC1 detection.

To investigate HDC1 status during Pi limitation, proteins were extracted from shoots and roots of WT, *pdr3* and OxP3 seedlings, grown at Pi replete or deficient conditions and used in Western blot assays. Preliminary results from one biological experiment demonstrated that Pi supply does not affect HDC1 content in WT shoots, as the 130 kDa band attributed to the native HDC1 was present in both WT samples (Fig. 23D, Suppl. Fig. 8C). On the contrary, in protein extracts from Pi-starved OxP3 seedlings, this band was absent. Interestingly, the same was observed for all root samples, raising the question about tissue-specific differences in HDC1 abundance. However, the samples contained very low protein concentration, which sufficed only for one SDS-PAGE that was used for the immunodetection. For that reason, it was not possible to perform Coomassie staining of the proteins as loading control. Based on that, no solid conclusion can be drawn; surprisingly, any further attempt to detect native HDC1 from samples of defined concentration was unsuccessful, as most Western blots performed later showed complete absence of any detected protein (data not shown). This inconsistency can be possibly attributed to a problematic protein extraction method, that requires further optimization, or unidentified technical factors affecting antibody sensitivity. Nevertheless, a-HDC1 868 antibodies was capable to detect GFP-tagged HDC1, after co-immunoprecipitation using a-GFP antibody covalently bound to agarose beads (GFP-trap) (Fig. 23B).
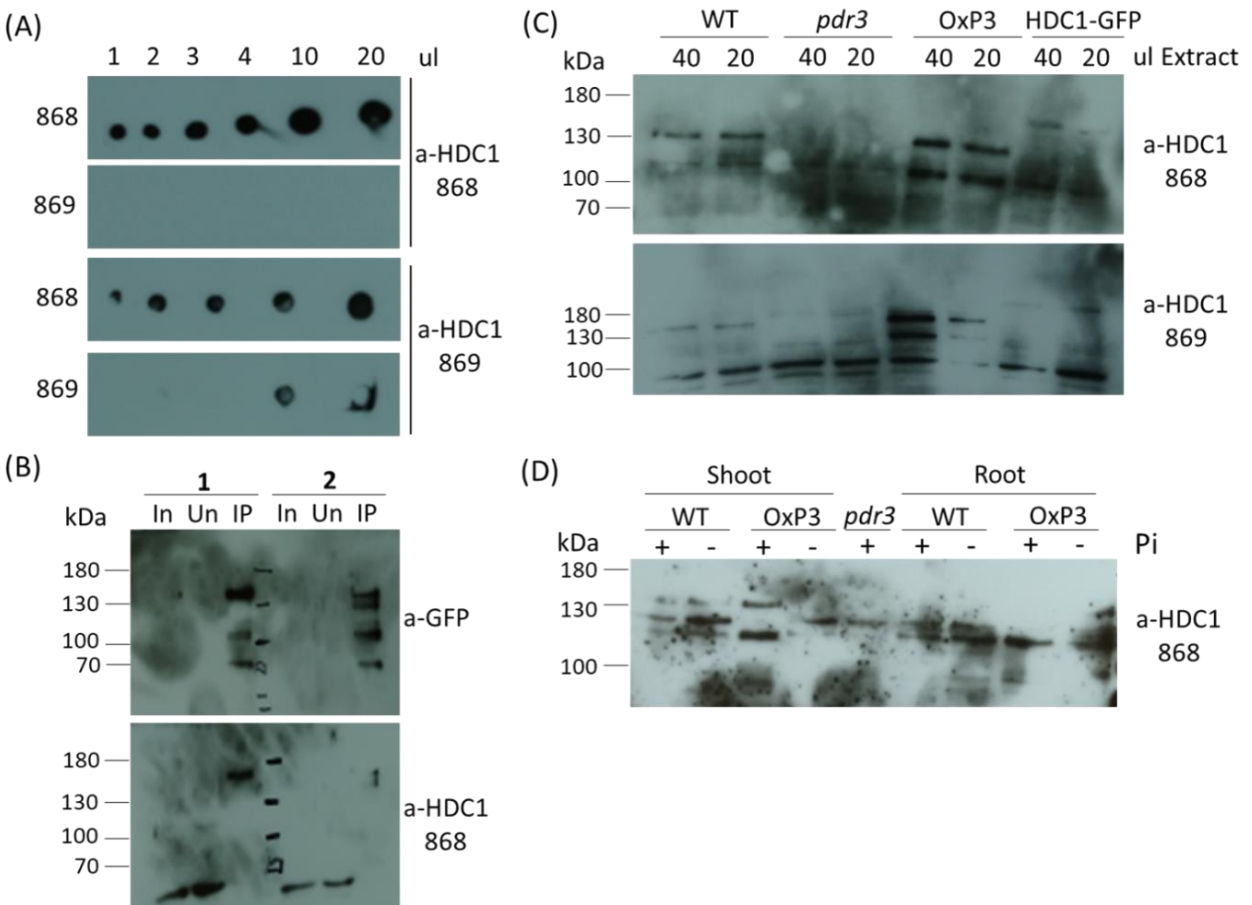


**Fig. 23 Antibody characterization and use for HDC1 detection.**

*Fig.23 Antibody characterization and use for HDC1 detection. (cont.)*

*(A) Dot blot using a-HDC1 868 and a-HDC1 869 for the detection of their respective immunogenic peptides, with amounts ranging between 1-20 µl of the original material used for the rabbit immunization.*

*(B) Western blot of immunoprecipitated HDC1-GFP, using anti-GFP antibodies bound to agarose beads (GFP trap). Immunoprecipitation was performed on total protein extracts from 6-days old seedlings, germinated on +Pi media.*

*(C-D) Western blot for HDC1 detection in protein extracts from WT, pdr3, OxP3 and HDC1-GFP seedlings (C) or shoot and root tissue (D). 5-days-old seedlings germinated on growth medium with supplemented Pi were transferred to + Pi conditions (C) or +Pi and -Pi conditions (D); tissue samples were harvested 1 DAT and protein extracts were loaded on SDS-PAGE, either at different volumes of each sample without prior protein quantification (C), or at equal protein concentrations between samples (D). The predicted molecular weight of HDC1 is 104.15kDa (TAIR).*

# 3   Discussion

## 3.1   HDC1 is a potential regulator of several metabolic pathways in *Arabidopsis*

### 3.1.1   HDC1 has a role in tuning chlorophyll biosynthesis and plastid differentiation in roots

*3.1.1.1   HDC1 participates in suppression of chlorophyll biosynthesis in the cortex of Arabidopsis root tips*
Previous work in our group demonstrated ectopic chlorophyll A (Chl A) presence in the root tips of *pdr3* mutants (section 1.5). During the course of this work, it was confirmed by confocal microscopy that loss of HDC1 causes tissue-specific accumulation of Chl A in the cortex cells of *Arabidopsis* root tips (Fig. 21C), co-localizing with plastids. Based on this observation, we propose that knockdown of HDC1 de-represses genes involved in the chlorophyll biosynthetic pathway. Surprisingly, the present root tip-specific transcriptomic analysis via RNA-seq revealed that only one gene (*PORB*) related to chlorophyll biosynthesis has enhanced expression in *pdr3* root tips. PORB participates in the conversion of PChlide to Chlide (description in section 1.4.1), a step that is light dependent. Since ectopic Chl A is present only in light-grown seedlings (Suppl. Fig. 7A), it is possible that this phenotype can be attributed to de-repression of *PORB* expression in *hdc1* loss-of-function mutants. Furthermore, this fact raises the question whether the expression of *PORB* is under direct HDC1-mediated regulation, which would result in *PORB* upregulation in the mutant. Another possibility is that loss of HDC1 influences the expression of this gene indirectly, by affecting other regulators of its expression. GOLDEN-LIKE 1/2 (GLK1/2) transcriptional factors are known positive regulators of *PORB* expression (Waters et al., 2009) and it has been shown that transgenic lines overexpressing *GLK1/2* accumulate Chl A in the root stele (Kobayashi et al., 2013), a phenotype that resembles the cortex-specific chlorophyll presence in *pdr3.* However, the present RNA-seq approach showed no proof of significant differential expression of *GLK1* or *GLK2* in *pdr3* root tips (Suppl. Table 19) and therefore it is rather unlikely that *PORB* overexpression and Chl A accumulation in *pdr3* root tips is *GLK1/2*-dependent. Nevertheless, it cannot be excluded that GLK1/2 show differential activity in *pdr3* mutants, for example due to post-translational regulation, resulting in *PORB* deregulation. Additionally, *PORB* expression follows diurnal and circadian regulation, with its expression peaking approximately 6 h after illumination, as was shown in mature plants grown in a 12-h light/12-h dark cycle (Matsumoto et al., 2004). The *pdr3* root tips showed deregulated expression of three genes involved in circadian rhythm regulation, specifically upregulation of the *FLC* and *ELF4* and strong downregulation of *LHY* (Suppl. File 5, see compact disc). ELF4 and LHY are participating in the same negative feedback loop, along with CCA1, where LHY and CCA1 are negatively regulating *ELF4* expression during the day (Li et al., 2011). Interestingly, the expression of *LHY* and *ELF4* is de-regulated only in *pdr3* root tips and not in the other tissues under investigation. *FLC* shows whole root and root-tip specific deregulation in the *pdr3* background, while it is expressed at comparable levels with WT in the shoots, which is in accordance with previous reports (Ning et al., 2019). Taken together, it is possible that in absence of functional HDC1, the circadian regulation of *PORB* is disrupted in the root tips, resulting in its uncontrolled enhanced expression and subsequent Chl A accumulation. This is corroborated by the fact that loss-of-function mutants of HDC1 are unable to retain photoperiodic regulation of flowering (Ning et al., 2019), potentially indicating an inability to translate light cues.

To further investigate how absence of HDC1 affects the regulatory network governing chlorophyll biosynthesis, the genes annotated to have a function in this process (GO:0010380) were retrieved from TAIR database and their expression was compared between WT and *pdr3* root tips. Interestingly, all genes participating in tuning of chlorophyll biosynthesis had similar transcript abundance between the two genotypes, according to the implemented thresholds of our analysis. The only two genes that showed a significant tendency (p value < 0.05) for higher expression in *pdr3*, although still below the differential fold change (FC) threshold (-1>log2FC>1), were *ELIP1/2* (*EARLY LIGHT-INDUCIBLE PROTEIN 1/2*) (Suppl. Table 19). ELIPs have chlorophyll binding capacity and they are considered to have a photoprotective role, reducing the damaging effects of high light, by preventing excess accumulation of free chlorophyll (Hayami et al., 2015; Tzvetkova-Chevolleau et al., 2007). Thus, it is rather unlikely that their slight upregulation in *pdr3* tissues has a causal effect on the observed chlorophyll accumulation there.

Additionally to *PORB*, several nuclear-encoded genes expressing proteins with a function in chlorophyll binding are upregulated in *pdr3* tips (Fig. 22), specifically one subunit of light harvesting complex I (LHCA2), two subunits of LHCII (LHCB1.3 and LHCB5) and three photosystem core proteins (PSAL, PSAG, PSAF). All of the LHCs are able to bind chlorophyll, as well as PSAG and PSAL, which additionally have a role in stabilization and docking of LHCI and LHCII, respectively (Jensen et al., 2007; Rantala et al., 2020). PSAF has also been reported to mediate binding of LHCI antenna (Rantala et al., 2020). Chlorophyll biosynthesis is tightly coordinated with its insertion in the interacting complexes as unbound chlorophyll might cause ROS generation (Wang and Grimm, 2015). Interestingly, these genes exhibit higher expression only in the root tips of *pdr3* and not in whole roots or shoots, with the exception of *LHCB1.3* that is overexpressed in the root tissue of the mutant as well, contrary to *PORB*, that was upregulated in every tissue under investigation (Fig. 22). Taken these results into consideration, it is tempting to speculate that ectopic Chl A accumulation in *pdr3* root tips is not only a result of enhanced PORB-dependent biosynthesis, but also due to enhanced stabilization of the available chlorophyll by its interacting proteins and downstream integration into the thylakoid membranes.

*3.1.1.2    Knockdown of HDC1 promotes plastidial development in pdr3 root tips*

Monitoring of plastid ultrastructure in *pdr3* root meristematic zone revealed the presence of partially differentiated plastids, with a semi-organized thylakoid structure (Fig. 21C), suggesting a role for HDC1 in repression of plastid differentiation. This fact leads also to the question whether loss of HDC1 disturbs distribution or abundance of plastids in root cell. To answer this, transgenic lines expressing a plastid marker coupled with GFP in the *pdr3* genetic background were generated (Fig. 21C). However, in the course of this work, it was not possible to compare plastid content between WT and *pdr3* seedlings as the transgenic lines *pdr3* lines were not possible to be genetically crossed with WT due to time restrictions. Moreover, the presence of the differentiated plastids was confirmed only in the cortex cells, perfectly co-localizing with the tissue that Chl. is also accumulating in *pdr3* root tips, corroborating a cortex-specific role of HDC1 in regulation of plastidial development and Chl. metabolism.

Based on the presence of necessary constituents for photosynthesis in the cortex cells of *pdr3* root tips, specifically chlorophyll and partially developed thylakoid membranes, it is intriguing to speculate on the possibility that HDC1 knockdown may lead to ectopic photosynthetic activation in this tissue. Transcript profiling of *pdr3* root tips demonstrated constitutive higher expression of genes participating in photosynthesis (Fig. 22). These include the LHC constituents and photosystem core proteins described in the previous section as well as the small chain 1A of Rubisco (RBCS-1A), a Rubisco Activase (RCA) as well

as a subunit of chloroplastic ATP synthase (ATPC1). The upregulation of these genes, along with the development of partially structured thylakoids in the root meristem of *pdr3* seedlings and the chlorophyll accumulation, could correspond to photosynthetic activity taking place in the root tips of the mutant. However, the ultrastructure of plastids in *pdr3* root tips does not resemble fully mature chloroplasts, indicating that probably they do not have the capacity for functional assembly of the photosynthetic apparatus.

### 3.1.1.3 Ectopic presence of Chl A and plastid differentiation in pdr3 root tips may affect cellular redox state

The possibility that plastids in the cortex cells of *pdr3* root tips may be photosynthetically active, along with the ectopic accumulation of chlorophyll, raises questions about the effects that this might have on cell physiology and biochemistry. Light absorption from chlorophyll pigments within PSI and PSII and electron transport chain under aerobic conditions triggers a series of redox reactions along the thylakoid membrane and resulting in reactive oxygen species (ROS) (Khorobrykh et al., 2020). Although ROS are integral components of various signaling cascades, e.g. in cell proliferation, high levels of ROS can cause oxidative damage due to high reactivity towards biomolecules, such as nucleic acids, proteins or lipids (Huang et al., 2019). ROS are produced from $O_2$ by photoreduction and include singlet oxygen ($^1O_2$), superoxide anion radical ($O2^{\bullet-}$), hydrogen peroxide ($H_2O_2$) and hydroxyl radical ($HO^{\bullet}$) (Blokhina et al., 2003). $O2^{\bullet-}$ is produced by photosynthetic electron transport chains in chloroplasts or by respiratory electron transport chains, and membrane-dependent NADPH oxidase (RESPIRATORY BURST OXIDASE HOMOLOG proteins) systems in mitochondria, through one electron reduction of $O_2$ (Pospíšil, 2016). $O^{2\bullet-}$ can also dismutate spontaneously or enzymatically to $H_2O_2$ and subsequently is reduced to $HO^{\bullet}$ via Fenton reaction (Pospíšil, 2016). Additional source of ROS is the electron transfer of the excited triplet state of chlorophyll to $^3O_2$ in the PSII when light energy absorption exceeds the capacity for $CO_2$ assimilation, resulting in $^1O_2$ formation (Laloi et al., 2004). Taking these facts into consideration, it was predicted that *pdr3* root tips suffer from oxidative stress; indeed, deep sequencing of the root tip transcriptome of these mutants revealed the upregulation of several genes annotated as responsive to oxidative stress (GO:0006979) (Fig. 9). Among them *CAT1* (*CATALASE1*) was included, a gene encoding a $H_2O_2$-metabolizing catalase, that is important for $H_2O_2$ elimination and redox maintenance (Mhamdi et al., 2012; Su et al., 2018). Additionally, four genes belonging in the class III plant peroxidase superfamily showed higher expression in *pdr3* root tips (Fig. 9). Class III peroxidases have diverse functions in plants, including cell wall lignification, auxin catabolism or defense against pathogens and have also been proposed to function in $H_2O_2$ removal (Cosio and Dunand, 2009; Shigeto and Tsutsumi, 2016). Furthermore, light-grown *pdr3* seedlings exhibit higher levels of $O^{2\bullet-}$ in the root apex, as was shown by staining with the $O^{2\bullet-}$-reacting dye NBT (Suppl. Fig. 7C). These transcriptional data support the notion that *pdr3* root tips suffer from redox imbalance, very possibly attributed to the ectopic chlorophyll presence and potential photosynthetic activity in the cortex layer. However, the accumulation of NBT staining in *pdr3* root tips was not restricted to the cortex, but rather was extended to all cell layers, suggesting that there might be additional factors contributing to enhanced ROS generation.

### 3.1.2 HDC1 participates in regulation of the glucosinolate biosynthetic pathway in the roots

*3.1.2.1 Loss of HDC1 impairs GSL biosynthesis in root tissues*

Transcriptional analysis of whole roots showed that *pdr3* mutants exhibit extensive downregulation of the pathway genes leading to glucosinolate (GSL) biosynthesis, resulting in reduced GSL content in root extracts (Fig. 14, Suppl. Table 14 and Suppl. Table 15). The transcriptional profile of the mutants shows reduced expression of genes mainly in the aliphatic branch of GSL biosynthesis, while six of them encode enzymes involved in the first step of the pathway, specifically side-chain elongation of the precursor amino acid methionine. These genes (*MAM3*, *MAM1*, *IPMI1*, *IPMI2*, *IMD1*, *BCAT4*) are positively regulated by MYB28 (Hirai et al., 2006; Sønderby et al., 2010), which is also downregulated in *pdr3* roots. Additionally, the expression of *CYP83A1* and *FMO-GS$_{OX3}$*, which encode enzymes participating in the steps of core synthesis and side-chain modification respectively, is also impaired in rosette tissue from *myb28* knockout mutants. These findings indicate that aliphatic GSL biosynthesis is transcriptionally impaired in root of *pdr3* mutants, probably as a result of basal lower expression of *MYB28*, suggesting a role for HDC1 in its regulation and as an extension, in aliphatic GSL biosynthesis. This is also corroborated by the great similarity of GSL chemotype of *pdr3* with *myb28* mutants, which show reduction of short GSLs (C3, C4 and C5) and almost total lack of long C6, C7 and C8 aliphatic GSLs (Beekwilder et al., 2008; Hirai et al., 2006). Interestingly, in the present work, indolic GSLs were also found reduced in *myb28* roots, contradicting previous findings; however, these data are preliminary, representing only one biological experiment, and therefore it is necessary to be validated through more experimental repetitions. Additionally, indolic GSL biosynthesis is affected in absence of HDC1, yet in less extend than aliphatic GSLs, as only four genes belonging in this pathway were differentially expressed in *pdr3* roots (Fig. 14A). The central indolic GSL regulator MYB51 has higher transcript abundance in the mutant, in contrast to the three downstream biosynthetic genes which are downregulated, indicating that indolic GSL content in *pdr3* roots is not necessarily dependent on the function of MYB51. This is also supported by the fact that while MYB51 has a major role in tuning indolic GSL biosynthesis in the shoots, in the roots this pathway is mainly controlled by MYB34 and secondarily, MYB122 (Frerigmann and Gigolashvili, 2014). However, no other characterized regulator of indolic GSL synthesis was abnormally expressed in *pdr3* roots, suggesting that indolic GSL content in *pdr3* roots might be dependent on other unknown factors.

The GSL-related phenotype of *pdr3* roots is rather intriguing, considering the function of HDC1 and its effect on gene expression. HDC1 is a subunit of the HDA19 and HDA6 histone deacetylase complex, which have a function generally related to gene repression (Feng et al., 2021; Perrella et al., 2016). Taken that into consideration, it can be speculated that direct targets of HDC1-mediated histone deacetylation would be upregulated in loss-of-function mutants. Since the genes encoding pathway enzymes of GSL biosynthesis are downregulated in *pdr3* mutant, it is unlikely that they are direct target genes of HDC1, but rather that a negative regulator of GSL biosynthesis is directly controlled by HDC1. In a scenario where such a suppressor is tuned transcriptionally, loss of HDC1 would de-repress its expression, causing downstream inhibition of the biosynthetic pathway. In the present study, WRKY46 was tested for having a potential negative effect on GSL accumulation or on the expression of GSL biosynthesis genes; however, the GSL-related profile of *wrky46* mutant was similar to WT in most genes and compounds under investigation (Fig. 19 and Suppl. Fig. 5) and thus, it cannot be considered as a candidate for suppressing the GSL biosynthetic pathway. More suppressor candidates can be tested in the future, following a similar approach; however, additional experiments are needed in order to narrow down the high number of candidates, generated by the RNA-seq analysis. A complementary ChIP-seq approach, as described in section 2.3.4.3, would reveal direct targets of HDC1-mediated regulation and generate a dataset that, after

overlapping with the present RNA-seq dataset, could reduce the number of candidates that would be interesting for further investigation. During the course of this work, a growth system was established, allowing fast and efficient sampling of tissue for ChIP analysis (Fig. 20); however, it was not possible to proceed to successful ChIP assays due to technical difficulties, involving chromatin extraction and fragmentation. Hence, optimization of these steps is required, focusing on sufficient DNA extraction from root tissue and setting appropriate sonication parameters for chromatin fragmentation. In parallel, it is also likely that a suppressor of GSL biosynthesis may not be regulated transcriptionally, but rather at the post-transcriptional/translational level, by an HDC1-dependent regulator. In such a case, an alternative approach would be necessary for revealing a GSL biosynthesis regulator, for example through proteomic analysis of *pdr3* roots.

### 3.1.2.2 *HDC1 affects indirectly GSL abundance in shoots of young seedlings*

Tissue specific analysis of shoot GSL content indicated that loss of HDC1 also impairs GSL accumulation in above-ground tissues (Fig. 17). Specifically, *pdr3* and *hdc1* exhibit reduced amounts of four aliphatic GSLs, three long methylsulfinylalkyl GSLs and one short C3-GSL, as well as two indolic GSLs. This finding is rather interesting, since the genes involved in the GSL biosynthesis in the shoots are not as transcriptionally perturbed as in *pdr3* roots, with only 3 biosynthesis-related genes being downregulated, namely *MAM3, FMO-GS$_{OX2}$* and *CYP79F1* (Suppl. Table 12). Moreover, *pdr3* shoots demonstrated reduced transcripts of *MYB76*, a positive regulator of aliphatic GSL biosynthesis; however, previous analyses of the transcriptome of *myb76* knockout mutants did not find evidence that this transcriptional factor controls the expression of *MAM3, FMO$_{OX2}$* and *CYP79F1* in foliar tissue, while with its knockdown mainly affected methylsulfinylated C4 aliphatic GLSs (Sønderby et al., 2010). Therefore, it is rather unlikely that the reduction of aliphatic GSL content in *pdr3* shoots is a result of MYB76-dependent deregulation. Another possibility is that the downregulation of one or all of the above-mentioned GSL biosynthetic genes is sufficient to diminish the shoot GSL content, with the most prominent candidate being *MAM3*, since knockdown of this genes results in reduced accumulation or total absence of long aliphatic GSLs, belonging in C6-C8 classes (Textor et al., 2007). However, the content of indolic GSLs and C3 GSLs in *mam3* mutants is similar to WT (Textor et al., 2007), indicating that *MAM3* downregulation is not be solely responsible for the observed phenotype in the HDC1 mutants and that there might be another factor interfering with GSL accumulation in the shoots of the mutants. Since roots are sink tissues for long aliphatic GSLs and root-to-shoot GSL transportation takes place through the phloem (Andersen et al., 2013), it is also possible that the reduced shoot GSL content in HDC1 mutants stems from the heavily diminished GSL pools in the root, rather than being attributed exclusively to transcriptional deregulation of the pathway enzymes in the shoot. This assumption is also corroborated by the fact that loss of HDC1 causes differential transcriptional deregulation in shoots and roots, by affecting different functional gene groups involved in each tissue (section 2.2.1.2). Specifically, genes encoding pathway enzymes of various metabolic processes are more primarily deregulated in the root tissue of *pdr3* mutants, while *pdr3* shoots show abnormal expression of other functional gene groups, e.g., involved in cell wall synthesis and modification (Fig. 10). Based on these facts, it is tempting to speculate that HDC1 is implicated in tuning of GSL synthesis in a tissue-specific manner; however, additional experiments, e.g., grafting of WT scions with *pdr3* roots or reversely, are necessary in order to confirm a root-exclusive role for HDC1 in GSL biosynthesis.

### 3.1.3 Loss of HDC1 impairs the expression of genes belonging in triterpenoid biosynthetic gene clusters

Analysis of root apex and whole root transcriptome revealed that further biosynthetic pathways were transcriptionally disturbed in *pdr3* root tips. Remarkably, the genes in each pathway were localized mostly in tandem on the chromosome, comprising co-expressed units called biosynthetic gene clusters (BGCs), encoding the pathway enzymes for specialized metabolites (Field and Osbourn, 2008; Huang et al., 2019; Smit and Lichman, 2022). The *pdr3* roots show differential expression of genes belonging in four triterpene BGCs, namely thalianol, marneral, tirucalladienol and arabidiol (Fig. 10), each of them exhibiting different degrees of deregulation in the mutant. The most severely affected BGCs were the ones leading to thalianol and marneral production, followed by the tirucalladienol BGC while the least affected one was the arabidiol BGC. Nevertheless, all genes shared the same expressional tendency, regardless of the BGC they were involved, demonstrating downregulated expression in the roots and root tips of *pdr3* seedlings, suggesting that HDC1 may be involved in the regulation of multiple triterpene biosynthetic pathways. A study from Nützman and Osbourn demonstrated that the thalianol and marneral BGCs might be subjected to regulation via localized chromatin remodeling, specifically via ACTIN-RELATED PROTEIN6-dependent incorporation of the H2A.Z histone variant into the nucleosomes of the pathway genes' loci (Nützmann and Osbourn, 2015). Given the genes' adjacency on the chromosome and the necessity for their coordinated expression, it is not surprising that changes in chromatin structure of their loci might serve as a regulatory mechanism for their transcriptional status. This further strengthens the notion that a histone deacetylase associated protein like HDC1 might have a role in their regulation. However, the effect of HDC1 on these triterpene BGCs is probably indirect, as a knockdown/knockout of HDC1 would abolish its repressive effect on its direct targets and result in their transcriptional upregulation. Since the genes in the above-mentioned BGCs are downregulated in the *pdr3* mutant, it is more likely that HDC1 controls their expression through another mechanism, e.g., by repressing an unknown negative regulator (suppressor), similarly to the case of GSL biosynthesis described in previous session.

Triterpenes have been suggested to play role in plant defense and signaling (Pacheco et al., 2012). Interestingly, Huang et al. demonstrated that disruption of genes located in the above mentioned BGCs, such as *THAS1, THAH1* or *THAA2,* alters triterpene composition of root extracts and exudates, interfering with attraction and establishment of a normal root microbiota community (Huang et al., 2019). The authors of this study suggested that root-derived specialized triterpenes are crucial for the assembly and maintenance of an *A. thaliana*–specific microbiota, within or around the roots. The present work showed that HDC1 seem to be involved in the tuning of two pathways leading to the biosynthesis of compounds with ecological functions, specifically GSL as well as triterpenes. Moreover, both pathways are to be positively affected by HDC1, as shown by the downregulation of the biosynthetic genes in *pdr3* mutants. Taken together, it is possible that HDC1 is positive regulator of the biosynthesis of compounds involved in defense or more general biotic interactions, by transcriptionally repressing the basal expression levels of genes encoding the pathway enzymes. Based on that, it is tempting to assume that loss-of-function mutants of HDC1 will demonstrate reduced capacity for defending against pathogens or that they will show an altered root-associated microbial community; however, this hypothesis has to be experimentally tested with insect or fungal bioassays as well as with characterization of the root-microbiota composition.

## 3.2 Transcriptional responses of *Arabidopsis* root tips to Pi deficiency and the role of HDC1

### 3.2.1 Pi scarcity reshapes the transcriptome of *Arabidopsis* root tips

#### 3.2.1.1 *Low external Pi supply enhances trehalose metabolism*

Root tips have a major role in perceiving environmental cues and decoding them to physiological and developmental adaptations that ensure plant's survival upon stress conditions. Low external Pi availability is sensed by root tips in *Arabidopsis*, leading to signaling events that cause reorganization of the root system architecture. Based on this, we sought to understand which groups of genes might be related to this adaptation as well as the general transcriptional status during early low-Pi stress. Global transcriptome analysis via RNA-seq revealed low-Pi triggered changes in the expression of a group of genes related to carbohydrate metabolism. Among those genes were *DIN10*, *MIOX2, MIOX4* and *RS2* (Fig. 11 and Suppl. Table 6), all of which have been reported to be upregulated in response to carbon depletion caused by extended darkness treatment (Gibon et al., 2006; Ma et al., 2011). This is rather interesting since this analysis was performed on light-grown seedlings, thus indicating that Pi-starved root tips may suffer from a low-carbon state. Moreover, the upregulation of the sugar transporter SUC2 is in accordance with previous reports, showing that Pi starvation-induced partitioning of photo assimilates from shoots to roots (Hammond and White, 2008).

We noticed the most significant expression changes for genes related to the metabolism of trehalose, a signaling metabolite (Fig. 11A, B). Trehalose is a non-reducing disaccharide, that is present in all major groups of organisms except vertebrates (Figueroa and Lunn, 2016). In plants, it can be detected at very low levels (micromolar concentrations) and it has been suggested to have various roles, most importantly as a signal and negative feedback regulator of intracellular sucrose levels (Figueroa and Lunn, 2016; Yadav et al., 2014). Its two step-biosynthesis starts with the generation of the intermediate trehalose 6–phosphate (Tre6P) from UDP-glucose and glucose 6–phosphate, a reaction catalyzed by Tre-6-P synthases (TPSs). The subsequent dephosphorylation by Tre6P phosphatases (TPPs) leads to the formation of trehalose. The present RNA-seq analysis indicated the induction of six trehalose synthesis-related genes in Pi-starved root tips, out of 22 genes with such an assigned function in total (Fig. 11B). Moreover, one trehalase gene (*TRE1*) was upregulated, which encodes for a protein with a function in trehalose catabolism (hydrolysis); however, the overall transcriptional tendency of this gene group points towards enhanced biosynthesis of trehalose and/or its precursor Tre6P. Although more upregulated genes encode proteins with TPS activity than with TPP activity (3 versus 2, respectively), it cannot decisively be deduced that this leads to accumulation of Tre6P or trehalose. Moreover, Yadav et al. did not observe significant changes in trehalose levels in Pi-starved seedlings; however, this study was performed using whole seedlings grown in axenic liquid cultures (Yadav et al., 2014), whereas the present study focused on excised root tips. As described above, it is possible that the changes in trehalose metabolism are specific to this organ or tissue, reflecting the local low Pi-induced metabolic changes. One of the hallmarks of local Pi deficiency is exudation of organic acids in the rhizosphere, such as malate or citrate, for the mobilization of Pi from insoluble complexes (Abel, 2017; Liang et al., 2013). Trehalose metabolism is linked with organic acid production, as accumulation of Tre6P reduced sugar levels and diverts carbon to organic acid metabolism, possibly via activation of PEP carboxylase (PEPC) and downstream anaplerotic synthesis of organic acids (Figueroa et al., 2016). Taken together, it is possible that the upregulation of genes in the trehalose metabolic pathway is part of the signaling cascade leading to rewiring of sugar metabolism in Pi starved root tips, in order to cope with the local demands for organic acid production and exudation. This hypothesis also agrees with the upregulation of low-carbon induced genes, such as *MIOX4* or *DIN10* (Suppl.

Table 6), as well as of the phosphoenolpyruvate carboxylase kinase PPCK1 (Suppl. Table 20), which is positively regulating PEPCs (Nimmo, 2003; Nimmo et al., 2001).

*3.2.1.2    Typical Pi starvation-induced phenotypes in root tips correlate with differential mRNA expression*
Previous studies have demonstrated the interplay between Pi starvation and Fe homeostasis during low Pi-induced root system re-organization. Given the Fe accumulation and downstream callose deposition in the SCN of the root meristem (Müller et al., 2015; Naumann et al., 2022), we anticipated finding differentially expressed genes regulating these processes in the transcriptome of Pi-starved root tips. However, neither functional enrichment analysis nor individual assessment of genes involved in these processes provided convincing evidence for the transcriptional representation of these processes (Suppl. Table 7). From the three genes involved in Fe homeostasis that showed differential expression during Pi scarcity, two of them, namely *FER1* and *VTL2*, are also responsive to oxidative stress. While VTL2 has been shown to transport Fe into the vacuoles (Gollhofer et al., 2014),  *FER1* has been shown to be upregulated during Pi deficiency via the central PSR (phosphate starvation responsive) transcriptional factors PHR1/PHL1 (Bournier et al., 2013), a mechanism that could be connected to its protective function against high Fe-induced oxidative stress, via excess Fe storage (Reyt et al., 2015). Overall, it is likely that Pi deficiency-triggered callose and Fe deposition in the stem cell niche are not controlled transcriptionally. This is also corroborated by the fact that the root tip-specific expression of LPR1, a multicopper ferroxidase whose loss-of-function abolishes low Pi-induced Fe or callose accumulation in the root tip, is not affected by external Pi content and its function is probably dependent on substrate availability (Suppl. Table 20 and Naumann et al., 2022; Ticconi et al., 2009). Alternatively, it is also possible that the lack of low Pi-induced genes involved in Fe or callose homeostasis may be attributed to our experimental design. Specifically, our RNA-seq analysis was conducted on seedlings exposed to Pi starvation conditions for one day; unpublished data from our group has shown that at this time point, Fe and callose depositions can already be observed in the meristematic area of the Pi-starved seedlings. Hence, it is also likely that Fe homeostasis or callose synthesis are transcriptionally regulated early during Pi deficiency responses and cannot be detected in the present analysis.

Nevertheless, the impact of the local Fe excess in the Pi-starved root tips is reflected on the upregulation of genes involved in oxidative stress responses. Apart from *FER1* and *VTL2*, two class III peroxidases, PER21 and PER54, showed upregulated expression in this gene set. As described in section 3.1.1.3, this type of peroxidases has been implicated with excess $H_2O_2$ removal (Cosio and Dunand, 2009). Although neither of these proteins has been functionally characterized, their putative role agrees with their upregulation in Pi deficient root tips, given the enhanced ROS presence during these conditions (Müller et al., 2015; Naumann et al., 2022; Shin et al., 2005). Furthermore, the histone-associated protein OXS3 was found upregulated in Pi deficient root tips (Fig. 11B). Expression of *OXS3* in yeast and rice rendered the transformants more tolerant to heavy metals or oxidizing agents, thus demonstrating its possible role in chromatin dynamics-dependent regulation against these stresses (Blanvillain et al., 2009; Wang et al., 2016). As a conclusion, low Pi-triggered Fe excess in root apex causes a ROS burst, as demonstrated in previous publications (Müller et al., 2015; Naumann et al., 2022), which results in the induction of genes responsive to oxidative stress, possibly to alleviate from the damage via scavenging or other detoxifying mechanisms.

### 3.2.2 The role of HDC1 in regulation of phosphate deficiency responses

*3.2.2.1    HDC1 is a potential regulator of PSR genes in the root tip during low Pi stress*

One of the main objectives of this study was to identify the targets of HDC1 upon Pi deficiency, thus linking low Pi-induced root responses with chromatin dynamics. Implementing a root tip-specific RNA-seq approach, we identified that WT root tips show PSR transcriptional changes mainly related to metabolism and redox balance (section 2.2.2.1). Comparison of the transcriptome of Pi-deficient *pdr3* root tips with WT demonstrated that plants of both genotypes share similar enriched GO categories and low Pi-responsive genes, indicating that *pdr3* mutants retain the capacity to induce the typical transcriptional Pi starvation response. Interestingly, *pdr3* mutants show additional quantitative changes in the expression of the PSR genes that are shared with WT, exhibiting higher induction or repression of these genes (Fig. 12B). These data suggest that HDC1 loss-of-function may not affect PSRs qualitatively, but rather intensifies the normal transcriptional PSR mechanism, which coincides with the hypersensitive response that is phenotypically observed. Since HDC1 is a subunit of the HDA6/19 histone deacetylation complexes (Feng et al., 2021; Perrella et al., 2016), its knockout could diminish the capacity of these complexes to regulate histone acetylation levels on certain loci or globally. This would result in elevated acetylation levels, which correlate with more accessible and transcriptionally active chromatin (Kumar et al., 2021). In such chromatin state, it is possible that the Pi starvation signaling pathway is transcriptionally amplified, leading to the extensively deregulated transcriptome that is observed in the Pi-starved *pdr3* mutants.

As described earlier, Pi starvation responses in the root tip include accumulation of Fe and callose, which correlate with a local ROS burst. Xu et al. provided evidence for enhanced Fe depositions in root tips of HDC1 knockdown mutants upon Pi stress (Xu et al., 2020), while preliminary data of our study showed excessive callose presence in the meristem and stele of *pdr3* root apex (Fig. 6D). Since low Pi-triggered Fe and callose accumulation in the meristematic and elongation zone of the root tip results in primary root growth inhibition (Balzergue et al., 2017; Müller et al., 2015), exaggeration of phenotype can explain the rapid root growth inhibition of *pdr3* mutants. This also reflects to the transcriptional level, as *pdr3* root tips exhibit extensive deregulation of genes involved cell wall modification (Fig. 13C), including two callose synthases and several genes encoding proteins modulating cell wall plasticity. Moreover, in accordance with WT, there was no significant transcriptional induction of Fe uptake or distribution genes in Pi starved *pdr3* root tips. This indicates that HDC1 is not involved in Pi-dependent Fe homeostatic processes in the root tip. This also agrees with the trend of root growth inhibition of the mutant in response to increasing Fe doses at Pi starvation conditions, which was similar to WT (Fig. 7). These data further support the idea that loss of HDC1 does not impair the dominant PSRs in root apex, but probably intensifies them. Moreover, since the role of the triad Fe-ROS-callose is central to local PSRs in the root tip, it would be interesting to investigate whether *pdr3* root tips suffer from ROS excess during Pi limitation, e.g., with ROS staining of Pi starved seedlings. Another low Pi hypersensitive mutant, *pdr2*, which is defective in the function of the P5-ATPase PDR2, shows similar root phenotype as *pdr3* during Pi stress, such as rapid root growth inhibition, correlated with hyperaccumulation of Fe, callose and ROS (Naumann et al., 2022). Based on that, it is quite likely that the root tips of HDC1 loss-of-function mutants also show extensive redox imbalance and oxidative stress upon Pi deficiency. This is also corroborated by the upregulation of 55 oxidative stress-responsive genes in *pdr3* tips in response to low Pi supply (section 2.2.2.3), nearly half of which belong in the peroxidase superfamily. However, *pdr3* root tips show signs of redox stress at either Pi regime, as discussed in section 3.1.1.3, which however is not sufficient to induce callose or Fe deposition during Pi replete conditions.

Xu et al. proposed that Pi limitation induces HDC1 degradation via the 26S-proteasome pathway, which results in transcriptional upregulation of *LPR1* and *ALMT1*, phenotypically leading to iron accumulation in the root tip and subsequent root growth inhibition (Xu et al., 2020). However, no evidence of low Pi-triggered upregulation of *LPR1* in the root tips was found in the present study (Suppl. Table 20), supporting the already described regulation mechanism of LPR1 during Pi deficiency responses (Müller et al., 2015; Naumann et al., 2022). Additionally, the elevated expression of *LPR1* in the root apex of *hdc1* mutants under Pi replete conditions (Xu et al. 2020 and Suppl. Table 20) does not correlate with Fe accumulation in root meristem, indicating that induction of *LPR1* expression is not sufficient to drive Fe deposition and root growth arrest and thus decoupling the shorter root phenotype of *hdc1* plants at +Pi conditions from LPR1 activity. Moreover, assuming that HDC1 suppresses transcriptionally Pi deficiency responses at growth conditions with adequate Pi supply, one could conclude that loss-of-function mutants of HDC1 would constitutively exhibit enhanced expression of low Pi-responsive genes, as absence of HDC1 would mechanistically mimic Pi starvation conditions. Mutants of suppressor components of PSR signaling, for example *spx1*/*spx2*, exhibit enhanced expression of PSR genes and increased Pi content, even at Pi replete conditions, due to uncontrolled Pi uptake (Zhou et al., 2021). Similar phenotype are observed in the *vih1*/*vih2* mutants, which are unable to synthesize InsP8, leading to SPX1/PHR1 dissociation and constitutive upregulation of PSR genes (Dong et al., 2019). However, according to the present transcriptional analysis, very few PSR genes are upregulated in *pdr3* during sufficient Pi supply in any of its tissues (Suppl. Table 20). Apart from that, *pdr3* mutants grown under +Pi conditions do not show phenotypic characteristics resembling Pi starved plants, such as anthocyanin overaccumulation in the shoots or enhanced lateral root development and root hair formation. Additionally, disruption of HDC1 function does not affect Pi content, as shown previously in our group using the *pdr3* mutants (section 1.5) and later confirmed by Xu et al. after analysis of a T-DNA insertion mutant line of *HDC1* (Xu et al., 2020). Overall, the data of the present study do not support the idea that HDC1 is a negative regulator of PSRs during Pi replete conditions, but instead suggest that HDC1 is necessary for the control of PSRs in the root tip, probably by tuning the expression levels of genes participating in these processes during Pi stress.

### 3.2.2.2  *Pi starvation differentially causes changes in glucosinolate metabolism, a process that is likely not dependent on the function of HDC1*

Total GSL analysis of Pi starved seedlings demonstrated variations in the GSL profile depending on the duration of the low Pi stress. Specifically, short exposure to low Pi conditions causes reduction of methylthioalkyl-GSLs (MT-GSLs), with few changes in the expression status of the genes participating in GSL metabolism, as *MYB28* was the only aliphatic GSL synthesis-related gene found to be differentially expressed during these conditions (Fig. 15A and Suppl. Fig. 4). In parallel, longer exposure to low Pi resulted in accumulation of methylsulfinylalkyl-GSLs (MS-GSLs) (Fig. 16B), while the low-Pi triggered increase in MS-GSLs content was accompanied with induction in the expression of the flavin-monooxygenase FMO-GS$_{OX3}$ (Fig. 16A), which catalyzes the conversion from MT-GSLs to MS-GSLs, as well as other genes encoding pathway enzymes. These data suggest that plants adapt GSL metabolism depending on the extend of the low Pi stress they are subjected to, with longer stress producing active synthesis of GSLs, while shorter stress more likely causing changes in GSL content, that most likely depend on the pre-existing cellular machinery. GSL are sulfur-rich compounds, taking up to 30% of the total sulfur content of plant organs (Falk et al., 2007). Sulfate and phosphate metabolism has been shown to be interconnected. During low Pi stress, phospholipids are replaced by galactolipids (Yu et al., 2002). The increase in sulfate shoot-to-root translocation is dependent on PHR1 (Rouached et al., 2011), demonstrating the control of sulfur

homeostasis by key players in PSRs. Based on these facts, it is possible that degradation of specific GSL compounds during short-duration Pi deficiency has a nutritional role, supplying the cells with sulfur that can be utilized for the biosynthesis of compounds that are necessary in PSRs. For instance, such a compound could be glutathione, a primary sulfur metabolite with an important antioxidant role, which could be a part of the cellular detoxification mechanism of ROS excess during Pi limitation. On the contrary, the increase of long MS-GSLs and the induction of GSL biosynthesis genes in roots of seedlings after prolonged Pi starvation may have a function unrelated to nutrition. The work of Hiruma et al. clearly showed that indolic glucosinolates are necessary for the beneficial relationship between Pi-starved *Arabidopsis* roots and a fungal endophyte, which supplied the plant with Pi (Hiruma et al., 2016). Additionally, a recent study exhibited changes in the composition of root microbiota depending on the Pi supply (Castrillo et al., 2017) as well as the simultaneous adaptation of JA-dependent defense responses. Taken together, it is possible that during longer Pi deficiency, plants prioritize Pi acquisition from biotic sources, which may result in actively modulating their GSL-related metabolism in order to accommodate these changes.

This study demonstrated that HDC1 participates in the regulation of basal GSL biosynthesis (section 2.3.1), while loss-of-function mutants are hypersensitive to external Pi supply (section 2.1). Considering these facts and the interaction between GSL metabolism and PSRs, it was tempting to speculate that HDC1 may have a role in low Pi-initiated GSL accumulation. Indeed, qPCR-based analysis of several GSL pathway genes, showed that *pdr3* mutants fail to induce *MYB28* and *FMO-GS$_{OX3}$* expression in the roots upon extended Pi limitation (Fig. 16A) in contrast to WT, while the accumulation of the metabolites is not as reactive to this stress as in WT (Fig. 16B). These data could suggest that HDC1 may be participating the transcriptional mechanism that promotes GSL production at low Pi conditions. However, it must be considered that HDC1 has a role in tuning the GSL pathway transcriptionally, irrespectively of Pi supply, potentially by controlling an unknown negative regulator of the pathway. It is possible that these two regulatory mechanisms act antagonistically and that loss of HDC1 disrupts the balance between basal repression and low Pi-triggered induction of the GSL pathway, resulting in the later to be less effective in the mutant. This could explain why induction of GSL synthesis takes place in *pdr3* and *hdc1* mutants during Pi starvation, although with less output than in WT on the transcriptional level. In conclusion, the data from this work suggest that Pi deficiency has an impact in GSL synthesis, serving different biological functions dependent on the extent of the stress, while HDC1 is a potential regulator of steady-state expression of genes involved in GSL metabolism.


### 3.2.2.3  *Does HDC1 integrate defense responses in Pi starvation signaling?*

Surprisingly, analysis of the DEGs in Pi starved *pdr3* root tips revealed the extensive deregulation of genes related to defense and biotic responses (Fig. 13, Suppl. Table 10 and Suppl. Table 11). This dataset included genes with expression responsive to one or multiple defense-related hormones, specifically JA, ethylene or SA. An explanation for the overrepresentation of genes involved in defense processes among the transcriptome of Pi deficient *pdr3* root apical tissue could potentially be that HDC1 directly controls the expression of these genes transcriptionally upon low Pi stress. However, transcriptional analysis of the *pdr2* mutant, which is also hypersensitive to Pi deficiency, also showed deregulation of many genes involved in plant immunity (unpublished data in the group, not shown). A convergence point that would result in similar phenotypical output between the *pdr3* and *pdr2* mutants could be the ROS excess, that has already been confirmed in *pdr2* root tips upon Pi limitation (Müller et al., 2015; Naumann et al., 2022).

As discussed in section 3.2.2.1, we predict that loss-of-function HDC1 also causes ROS hyperaccumulation in the root tip upon Pi deficiency. In parallel, ROS burst upon pathogen attack is an integral part of immunity signaling, initiating several processes, such as cell wall thickening in order to prevent further spread of the infection (Huang et al., 2019). Intriguingly, inducers of immunity that cause redox changes, such as SA and flg22, had been proposed to affect the function of the histone deacetylase HDA19 by causing oxidative modifications of the protein (Liu et al., 2015). HDA19-dependent chromatin remodeling is correlated with plant immunity transcriptional regulation, as HDA19 affects the expression of several activators or repressors of defense, including genes in jasmonic acid and ethylene signaling of pathogen response (Kim et al., 2008; Zhou et al., 2005). It is possible that upon Pi deficiency, ROS excess in *pdr3* root tips abolishes the normal transcriptional function of HDA19, leading to large-scale deregulation of immunity signaling. Moreover, HDC1 is a subunit of one of the HDA19-associated histone deacetylase complexes, probably contributing to the stabilization of the interacting proteins on the chromatin (Feng et al., 2021; Perrella et al., 2016). Effectively, loss-of-function of HDC1 would disrupt the normal association of the complex and as a result, the normal regulation of its targets genes; in this context, this hypothesis agrees with the abnormal expression of several immunity-related genes even in seedlings grown at Pi sufficient supply, a condition that is possibly exaggerated upon low Pi stress. In conclusion, this work provides indications that HDC1 controls directly or indirectly genes participating in pathogen defense; however, the exact mechanism has to be further investigated, focusing on the role of the HDC1-associated HDAs in this process as well as on the general cellular biochemical and physiological defects caused by HDC1 loss-of-function.

# 4 Summary

The bioavailable form of phosphorus, inorganic phosphate (Pi), has a dominant role in many biological processes, such as energy storage or signal transduction, while participating as a building component of important biomolecules. To cope with external low Pi bioavailability, sensed by root tips, plants initiate a set of adaptive responses, including root system reorganization and organic acid exudation, which result in the formation of a swallow root system with better Pi foraging capacity. However, it is still unclear how these processes are tuned transcriptionally and which genes participate in Pi status signaling in the root apex. The main focus of this work was to investigate the major transcriptional changes in the root tip upon Pi limitation and the role of HISTONE DEACETYLATION COMPLEX 1 (HDC1), a histone deacetylase-associated protein in *Arabidopsis thaliana*, in their control. In parallel, it was crucial to elucidate which processes are basally affected from loss of HDC1 on the gene expression level and understand how their transcriptional deregulation shapes plant's physiology and development.

Implementing a root-tip specific RNA-sequencing approach, we showed that Pi scarcity affects the expression of genes involved in trehalose metabolism, reflecting the changes that take place in sugar metabolism locally in the root tip, possibly to accommodate the enhanced organic acid synthesis and exudation. Moreover, certain genes with oxidative stress-responsive expression are upregulated, which is probably connected to the local Fe excess in the root tip and the consequent ROS accumulation it causes at low Pi conditions. In parallel, loss-of-function mutants of HDC1, namely *pdr3* and *hdc1*, are hypersensitive to Pi limitation, showing exaggerated root growth inhibition, while *pdr3* mutants exhibit extensive deregulation of their transcriptome at basal conditions, which is intensified during low Pi stress. Specifically, *pdr3* root tips have the capacity to transcriptionally induce phosphate deficiency responses (PSR) in similar manner as WT, however this is also accompanied with the deregulation of additional genes, which are seemingly unrelated to PSRs. Among those, a plethora of genes involved in defense were found, opening questions about the role of HDC1 in the intersection between PSRs and biotic interactions.

Our investigation of *pdr3* transcriptome also revealed the root-specific repression of two metabolic pathways, leading to the biosynthesis of the defense compounds glucosinolates or certain specialized triterpenoids, that have been shown to modulate root microbiome. While glucosinolate biosynthesis has been reported to be induced during Pi deficiency, our data did not provide strong evidence that HDC1 has a role in low Pi-triggered glucosinolate accumulation, but rather it tunes the expression of the pathway genes at basal levels, probably through regulation of an unknown suppressor of GSL biosynthesis. Nevertheless, the fact that HDC1 probably controls two biosynthetic pathways leading to formation of metabolites mediating plant-microbe interactions strengthens the notion that HDC1 may have a role in the transcriptional regulation of this process, which is not necessarily mechanistically direct.

Additionally, it was confirmed that loss-of-function of HDC1 derepresses chlorophyll accumulation in the cortex cells of the root tip. This is likely attributed to upregulation of PORB, an enzyme catalyzing a light-dependent step of the chlorophyll biosynthesis pathway, as well as of photosynthetic chlorophyll binding proteins of the light harvesting complex superfamily or photosystem component family. *PORB* is regulated by multiple pathways, one of which is dependent on the circadian clock; previous publications and data from this work demonstrated that HDC1 mutants show impaired circadian clock outputs, potentially providing a mechanistic explanation about the deregulated chlorophyll synthesis in *pdr3* root tips. Moreover, the ectopic chlorophyll accumulation coincides with partial plastid differentiation and

formation of thylakoid structures exclusively in the cortex layer, as well as widespread ROS excess, demonstrating that loss of HDC1 has a broad effect on plant physiology and development.
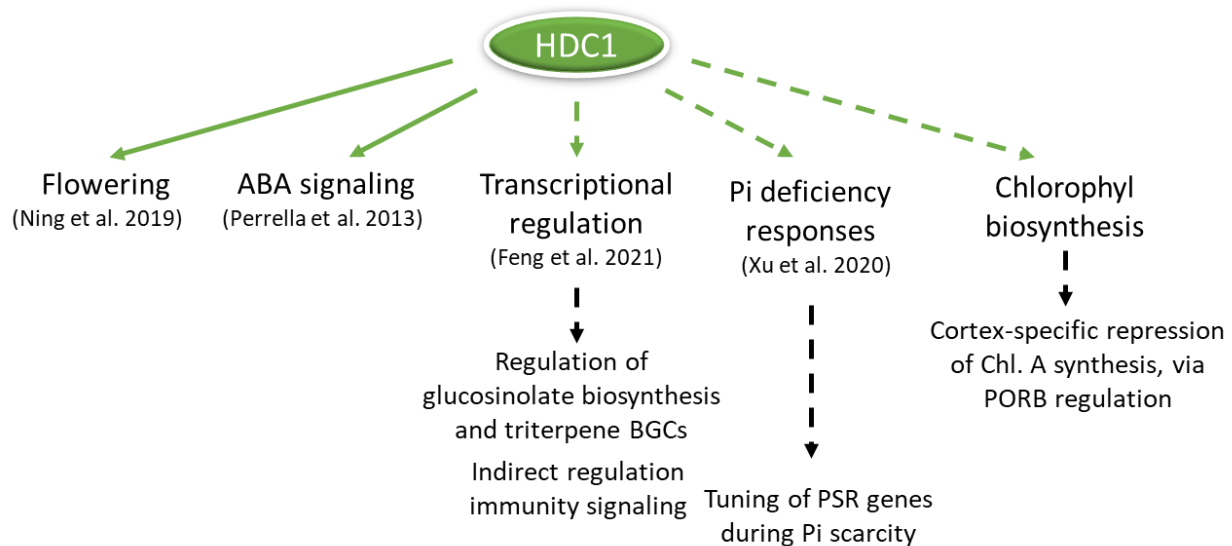


**Fig. 24 Overview of biological processes that have been shown to be affected by loss-of-function of HDC1, including new insight about the role of HDC1 in these processes.**
*Available studies demonstrating the role of HDC1 in each process are shown in parenthesis.  The pathways that were the focus of this work are highlighted with green dashed lines, while new hypotheses and data provided by this study are shown with black dashed lines.*

*HDC1 has been shown to participate in circadian control of flowering regulation (Ning et al., 2019), ABA signaling and salt tolerance (Perrella et al., 2013) as well as root reorganization during phosphate deficiency responses (Xu et al., 2020). All of these processes are affected as a result of large-scale transcriptional deregulation in loss-of-function mutants of HDC1, which is an important component of HDA19 and HDA6 histone deacetylation complexes (Feng et al., 2011). Additionally, this study focused on providing mechanistic explanation of the phenotypes in HDC1 mutants based on tissue specific transcriptomic analysis. As a result, it was shown that HDC1 contributes to the regulation of glucosinolate and specialized triterpenes, such as thalianol and marneral, in the roots; interestingly, the pathway enzymes catalyzing the synthesis of these triterpenes are encoded by genes organized in biosynthetic gene clusters (BGCs). Additionally, it was shown that loss of HDC1 derepresses chlorophyll biosynthesis in the cortex cells of the root tips, probably due to upregulation of PORB and chlorophyll binding proteins. Moreover, the transcriptome of Pi-starved pdr3 root tips was analyzed, showing extensive transcriptional deregulation, including the differential expression of many genes functionally related to defense or to biotic interactions. This could be related to regulation of immunity signaling by the HDA19-HDC1 complex, irrespective of the Pi status.*

# 5  Outlook

**To elucidate the physiological impact of the repressed metabolic pathways in *pdr3* mutants:**

- The triterpenoid content of root extracts and exudates should be measured, focusing on the compounds synthesized by the downregulated pathways in the mutant (thalianol, marneral, arabidiol and tirucalladienol).
- An unbiased untargeted metabolomic approach, aiming the complete chemical profiling of *pdr3* roots, would be important for identifying if further metabolic pathways are impaired in the mutant.
- A ChIP-seq assay and later cross-validation with the dataset from the present RNA-seq analysis is crucial for better characterization of HDC1 targets; this approach will facilitate most accurate identification of a HDC1-regulated suppressor of glucosinolate and triterpenoid biosynthesis.
- The root microbiome of *pdr3* can be compared to WT after 16S ribosomal rRNA profiling of the associated microbial community, seeking to investigate whether these mutants show an altered microbiome composition.

**To assess the effect of the ectopic Chl. A accumulation in the cortex cells of *pdr3* root tips:**

- It is important to measure photosynthetic activity of the specialized plastids in the *pdr3* root tips, for instance using pulse amplitude modulated (PAM) fluorometry.
- Transgenic lines expressing HDC1 under the control of tissue specific promoters, complementing HDC1 in cortex, endodermis and stele tissues in the *pdr3* background, are an appropriate tool in order to investigate whether HDC1 has a cortex-specific role in regulation of chlorophyll A synthesis.
- To assess if the imbalanced redox state of *pdr3* root tips is linked to chlorophyll biosynthesis or photosynthetic activity, ROS content can be measured in seedlings grown in presence of pharmacological inhibitors of these processes.
- Shoot chlorophyll concentration can be evaluated, aiming to investigate whether the detected upregulation of *PORB* in *pdr3* mutants is sufficient to significantly enrich chlorophyll content.

**To expand our understanding of the role of HDC1 in phosphate deficiency responses (PSRs):**

- It is important to conduct experiments assessing PSRs in HDC1 loss-of-function mutants using seedlings that were grown with shaded roots, in order to exclude the possibility that the hypersensitive phenotype of *pdr3* mutants is light-dependent.
- To further explore the connection between Pi deficiency-induced ROS accumulation in the root tip and the rapid root growth inhibition of the *pdr3* mutants, it would be of great interest to check ROS presence in seedlings grown at Pi deficient or Pi replete conditions. Moreover, the root growth dynamics of the mutants at low Pi conditions could be assessed after exposure to ROS scavengers. To test if a potential redox imbalance during Pi stress correlates with the deregulation of defense-related genes in *pdr3* root tips, the expression of selected genes involved in this pathway could also be measured in presence of ROS scavengers, at different Pi regimes.

# 6 Materials and methods

## 6.1 Chemicals and reagents

Unless indicated otherwise, chemicals, reagents and solvents were of reagent or HPLC grade and obtained from the following manufacturers: Carl Roth (Karlsruhe, Germany), Duchefa Biochemie (Haarlem, The Netherlands), Merck (Darmstadt, Germany), Sigma-Aldrich (St. Louis, USA), Serva (Heidelberg, Germany) and Bio-Rad (Hercules, USA). Molecular biology supplies and kits were ordered from Thermo Fischer Scientific (Massachusetts, USA), Macherey-Nagel (Düren, Germany), Abcam (Berlin, Germany) and Qiagen (Hilden, Germany). Anti-HDC1 polyclonal antibody production was carried out by Eurogentec (Seraing, Belgien). Primer synthesis was performed by Eurofins Genomics (Ebersberg, Germany).

## 6.2 Growth media

Composition of LB medium for bacterial cultures of *E.coli* and *Agrobacteria* as well as modified ATS growth medium for *A. thaliana* seedlings is listed in Table 2. All media were autoclaved to 121°C for 20 min. Filter-sterilized supplements, like antibiotics, were added to the autoclaved media.

To successfully induce low Pi stress to seedlings, residual Pi had to be removed from the agar (Haarlem, The Netherlands) supplemented into the growth media. Towards that, the agar was purified by repeated washings in Milli-Q water and subsequent dialysis using Dowex 1X8 ion-exchanger (Sigma-Aldrich, St. Luis, USA). The agar was then dried at 60° C in an oven (100% ventilation) for 2-3 days and added into liquid growth media before autoclaving.

| Medium | Composition | Reference |
|---|---|---|
| **Modified ATS medium** | 2.5 mM (+Pi) or 0 mM (-Pi) $KH_2PO_4$, 0.5% D-Sucrose, 5 mM $KNO_3$, 0.025 mM $Fe^{3+}$-EDTA, 2 mM $Ca(NO_3)_2$, 2 mM $MgSO_4$, 2.5 mM MES-KOH, 0.005 mM $CuSO_4$, 0.001 mM $ZnSO_4$, 0.07 mM $H_3BO_3$, 0.014 mM $MnCl_2$, 0.0002 mM $Na_2MoO_4$, 0.010 mM $CoCl_2$,<br><br>For solid medium, 1% Washed Agar was added. | (Wilson et al., 1990) |
| **Lysogeny broth (LB) medium** | 10 g/l tryptone; 5 g/l NaCl; 10 g/l yeast extract.<br><br>For solid medium, 15 g/l Agar was added | (Bertani, 1951) |

*Table 2 Media composition of modified ATS and LB medium for bacterial and plant cultivation, respectively.*

## 6.3 Plant material and growth conditions

### 6.3.1 Plant lines

In this study, *Arabidopsis thaliana Columbia-0* (Col-0) accession was used as wild type (WT). The *pdr3* mutant (Col-0 genetic background) was obtained through an EMS screen, as described in section 1.5. The T-DNA insertion line *hdc1* (GABI-Kat 054G03) was obtained from the group of Dr. Debora Gasperini and was previously reported as knockout mutant (Perrella et al., 2013), which was also validated by Real Time-Quantitative PCR (Suppl. Fig. 1). The following T-DNA insertion lines in Col-0 background were obtained from Nottingham Arabidopsis Stock Centre (NASC): *wkry46-1* (SALK_134310), *wkry46-2* (SAIL_1230_H01), *myb28* (SALK_136312C).

### 6.3.2 Plant cultivation

For aseptic plant cultivation, seeds were firstly sterilized as follows: Seeds were placed inside columns with silica membranes deriving from DNA extraction kit (Macheray-Nagel) and incubated for 7 min in 700 µl 70% ethanol with gentle rotation at room temperature. Ethanol solution was then removed centrifugation of the column at 10.000xg for 1 min to remove and replaced with 700 µl absolute ethanol; incubation took place for 5 min as described above. Ethanol was removed by centrifugation as before and followed by a final centrifugation to completely dry the seeds. Sterilized seeds were shown on square plates containing 50 ml of solid growth medium, supplemented with Pi as described in section 6.2 and were incubated for 2 days at 4° C in absence of light, in order to synchronize seed germination (stratification). Plates were then placed vertically in a growth chamber (Osram LumiluxDeLuxe Cool Daylight L58W/965, Osram) at 22°C under illumination at long day conditions (16 h light/8 h dark cycle, approximately 160 µmol s$^{-1}$ m$^{-2}$).

For hydroponic cultivation of *Arabidopsis* seedlings, sterilized seeds were initially stratified inside 1.5 ml Eppendorf tubes as described above. The primed seeds were then sown on a pre-autoclaved polypropylene mesh (250µm mesh opening, Sefar Propyltex, Heiden, Switzerland) which was then placed inside a 250 ml Erlenmeyer flask, containing 150 ml liquid growth medium, supplemented with Pi. The flasks were covered with autoclaved aluminum foil and were allowed to grow for 7 days inside a growth chamber, as described above, with gentle agitation.

Plants for propagation, transformation, and selection purposes were grown in the greenhouse under long-day conditions at 18-20°C and 55-65% relative humidity. The soil substrate used was "Einheitserde Typ GS 90" mixed with vermiculite (1-2 mm) in a 4:3 ratio.

### 6.3.3 Plant transformation and selection of transformed lines

Transgenic *A. thaliana* lines were generated by *A. tumefaciens* mediated transformation by floral dip (Clough and Bent, 1998). Initially, *Agrobacteria* harboring the plastidial marker FERREDOXIN-NADP[(+)]-OXIDOREDUCTASE tagged with GFP (FNR-GFP) in a binary vector (Marques et al., 2003) were acquired from Dr. Martin Schattat (Martin Luther University Halle-Wittenberg, Halle, Germany). The cells were allowed to grow for two days on LB plates containing rifampicin and spectinomycin at 28°C and then resuspended in liquid LB media, at a dilution of 2.0 (OD$_{600}$). The bacterial suspension was diluted with a 5% (w/v) sucrose solution at 4:1 ratio and supplemented with 0.03% (v/v) Silwet-L77. The inflorescences of *A. thaliana* plants (*pdr3* genetic background) at the bolting stage were dipped into the bacterial suspension and gently agitated for 10-15 sec. Transformed plants were kept in the dark for two days, lying horizontally

on a tray wrapped with aluminum foil and then, cultivated in the greenhouse as described in section 6.3.2. T1 seeds from transformed plants were harvested and sowed on growth media, supplemented with kanamycin. Antibiotic-resistant seedlings representing T1 independent lines were transferred to the soil and were grown in the greenhouse for seed setting (T2 seeds). T2 transgenic lines were selected from T2 seeds, segregating at a ratio 3:1 for kanamycin resistance. The GFP fluorescence of the transgenic lines was tested with confocal microscopy.

## 6.4    Molecular biology methods

### 6.4.1    Genotyping

For the extraction of genomic DNA, leaf plant tissue was collected into 2ml Eppendorf tubes with a 5mm stainless-steel grinding bead. Tissue was flash frozen with liquid $N_2$ and pulverized via high-speed shaking at 25 Hz for 40-60 sec, using TissueLyser II instrument (Qiagen). Then, 400 µl of DNA extraction buffer (200 mM Tris-Hcl (pH 7.5), 25 mM EDTA (pH 8), 250 mM NaCl, 0.5% w/v SDS) was added to the samples, followed by vortexing. Samples were centrifuged for 10 min at 13.000 rpm and 300 µl of the supernatant was transferred to fresh Eppendorf tube. Then, isopropanol was added at 1:1 ratio, followed by centrifugation at the same conditions. Supernatant was removed and the DNA pellets were washed with 70% ethanol. After centrifugation for 10 min at 13.000 rpm, ethanol was discarded, and the pellets were air-dried. DNA was resuspended in 50 µl Milli-Q water and if necessary, stored at -20°C.

For genotyping of T-DNA insertion lines, 20 µl PCR reactions were prepared, containing 1X Dream Taq Green buffer (Thermo Fischer Scientific), 500 µM dNTPs, 0.5 µM of gene-specific primer pair and a general T-DNA left border primer, 0.5 µl of in-house manufactured DNA polymerase and approx. 100 ng of template, diluted in Milli-Q water. PCR reactions were performed on an PCR cycler (Eppendorf), using the parameters listed in Table 3. The single nucleotide polymorphism of *pdr3* line was genotyped using derived Cleaved Amplified Polymorphic Sequence (dCAPS) assays. Briefly, PCR product of genomic DNA from *pdr3* tissue was amplified in PCR reactions as described above but without containing the general T-DNA left border primer, and then digested using the restriction enzyme *Hinf*I (Thermo Fischer Scientific). Generally, PCR products were separated on 1% agarose gels, while high percentage agarose gels (3%) were used for PCR fragments <300 bp. All primers used in this study are listed in Suppl. Table 21.

| Temperature | Duration | Amplification |
|:-:|:-:|:-:|
| **95°C** | 5 min | x 1 cycle |
| **95°C** | 30 sec | |
| **(Primer Tm-5) °C** | 30 sec | x 35 cycles |
| **72°C** | 1min/1kb of final product | |
| **72°C** | 7 min | x 1 cycle |

**Table 3 Thermal profile of PCR reactions.**

### 6.4.2    Gene expression analysis by Real-Time-Quantitative PCR

For gene expression analysis, approximately 100 µg of tissue were harvested from a pool of seedlings in biological triplicates or duplicates. RNA was extracted using peqGOLD Plant RNA kit (PEQLAB, Erlangen, Germany) according to the manufacturer's protocol. Next, genomic DNA elimination was performed with

enzymatic on-column digest, using RNase-Free DNase Set (Qiagen). RNA concentration and quality were assessed using an Infinite 200 NanoQuant (Tecan) device. Synthesis of cDNA was performed using the RevertAid Reverse Transcriptase (Thermo Fischer Scientific) system according to manufacter's protocol, with 1 µg of RNA template and oligo-dT primer. Subsequently, cDNA samples were diluted to 1:10 ratio and 3 µl were used as template in RT-qPCR (Real-Time-Quantitative PCR) reactions, containing 1X Fast SYBR Green Master Mix (Thermo Fischer Scientific) and 1 pmol of gene-specific primers. Additionally, qPCR reactions with DNase-treated RNA preparations were used as no-template controls, in order to ensure the total digestion of genomic DNA in each cDNA sample. Gene-specific primers for RT-qPCR were designed to amplify approximately 80-200 bp fragments and their specificity was tested using the Primer Blast tool of National Center for Biotechnology Information (Ye et al., 2012). Each primer pair was analyzed with a dilution series for its amplification efficiency and selected if the efficiency exceeded 90%. RT-qPCR primers used in this work are listed in Suppl. Table 21. Analysis was performed using a QuantStudio 5 Real-Time PCR system (Applied Biosystems), following the parameters described in Table 4.

| Step | Temperature | Duration | Amplification |
|---|---|---|---|
| AmpliTaq™ Fast DNA Polymerase, UP activation | 95°C | 20 sec | Hold |
| Denature | 95°C | 1 sec | x 40 cycles |
| Anneal/extend | 60 °C | 20 sec | |
| Melt curve stage | | | |
| Step 1 | 95°C | 1 sec | |
| Step 2 | 60 °C | 20 sec | |
| Step 3 | 95°C | 1 sec | |

*Table 4 Thermal profile of RT-qPCR reactions.*

### 6.4.3 Gene expression analysis by RNA-sequencing

For transcriptome profiling with RNA-sequencing (RNA-seq), WT and *pdr3* seedlings were grown in vertical plates, as described in section 6.3.2. Root tip samples were harvested 1 day after transfer (1 DAT) to +Pi or -Pi conditions, while root or shoot samples were collected 1 DAT only to +Pi conditions. Root tip samples contained generally a pool of approximately 150 root tips, after excision of the root apex between the 10th to 20th root hair of the differentiation zone. An exception to that were the samples from *pdr3* seedlings grown at -Pi conditions, which contained 200 root tips, in order to compensate for the significantly smaller size of Pi starved *pdr3* tissues. Additionally, root or shoot samples contained 50 roots or 25 scions, from seedlings dissected below the hypocotyl. All tissue samples were flash frozen in liquid $N_2$ and total RNA was extracted as in section 6.4.2. The quality of RNA samples was tested through automated electrophoresis on 2100 Bioanalyzer instrument (Agilent) and samples with RNA Integrity Number (RIN) > 6.5 were selected for RNA-seq analysis. For each genotype and condition, three biological replicates were sequenced, each corresponding to the samples harvested as described above.

Next generation sequencing was performed by Novogene (Beijing, China) according to standard protocols, briefly as follows: Firstly, RNA samples underwent quality control for the integrity and the quantity of their RNA content and then were used for library preparation, which consisted of cDNA fragments attached to sequencing adapters. Library preparations were sequenced on an Illumina platform and paired-end reads

were generated, corresponding to a collection of raw data (raw reads). Raw data were filtered by removing reads containing adapter and poly-N sequences and reads with low quality from raw data, yielding clean data that were used for all downstream analyses. Next, paired-end clean reads were mapped to the reference genome using HISAT2 software and gene expression levels was estimated based on FPKM (Fragments Per Kilobase of transcript sequence per Millions base pairs sequenced) values, which takes the effects into consideration of both sequencing depth and gene length on counting of fragments. Differential expression analysis between a pair of different groups (three biological replicates per condition/genotype) was performed using DESeq2 R package (Anders and Huber, 2010). The resulting p values were adjusted using the Benjamini and Hochberg's approach for controlling the False Discovery Rate (FDR). Genes with an adjusted p value < 0.05 found by DESeq2 were assigned as differentially expressed.

Gene Ontology (GO) enrichment analysis of differentially expressed genes was performed in-house, implementing the online tools agriGO v2.0 (Tian et al., 2017) or DAVID (Database for Annotation, Visualization and Integrated Discovery) (Huang et al., 2009), using the default parameters. Area-proportional Venn diagrams were drawn using the online tool BioVenn (Hulsen et al., 2008). Euclidean hierarchical clustering of DEGs was performed using RStudio (R versions 3.6.2 and 4.2.0).

### 6.4.4   Chromatin immunoprecipitation (ChIP)

For chromatin immunoprecipitation (ChIP) assays from the roots of young seedlings, seeds were sterilized and cultivated hydroponically on a polypropylene mesh as described in section 6.3.2. After seven days of growth, the net was removed from the culture and the roots protruding from the bottom side of the mesh were excised. Pooled root samples of hydroponically grown seedlings were used in ChIP assays, utilizing the ChIP Kit-Plants (catalog no. ab117137, Abcam) according to manufacturer's instructions. After nuclei extraction, chromatin was sheared by sonication at 4° C at medium power on a Bioruptor Pico sonication device (Diagenode, Liege, Belgium), testing sonication durations between 0 to 25 cycles, with each cycle consisting of 30 sec pulse/45 sec cooling alternations. The integrity of the sonicated chromatin was tested by electrophoresis on 1.5% (w/v) agarose gels and evaluated visually, selecting samples with chromatin sheared at a range of 200-600 bp.

### 6.5   Glucosinolate extraction and measurement

For the determination of the abundance of the different GSL compounds in shoots or roots of Arabidopsis seedlings, approximately 1-5 mg of tissue was collected in standard 2 ml Eppendorf tubes with a stainless-steel grinding bead and flash frozen with liquid $N_2$. The samples were pulverized via high-speed shaking at 20 Hz for 25-35 sec, using TissueLyser II instrument (Qiagen, Hilden, Germany). The tissue powder was subsequently mixed with 450 µl 2:1 Methanol-Chloroform extraction solution and 200 µl deionized water. As internal standard, sinigrin was used, as it is naturally absent from Col-0, by supplementation in the extraction solution at 20 µg/ml final concentration. Samples were incubated for 60 min on a rocking platform at room temperature, followed by centrifugation at 10.000xg for 20 min at the same conditions. The upper aqueous phase was then transferred to fresh tubes and used undiluted for GSL determination via Liquid Chromatography coupled with tandem Mass Spectrometry (LC-MS/MS).

The separation of the molecules was performed with a Nucleoshell RP18 column (50 × 3 mm, particle size 2.7 µm; Macherey-Nagel, Düren, Germany) at 35° C using an Agilent 1290 High Performance Liquid Chromatography (HPLC) system. As eluents A and B, water and acetonitrile each containing 0.2% acetic

acid were used respectively, with 0.5 ml/min flow rate. Initially, the separation of GSL was taking place with 0% of eluent B for the first 0.5 min, which was increased linearly to 55% over the next 4 min and then to 98% over 1 min. After washing, the column remained at 98% eluent B for 1 min. The starting conditions were restored within the next 0.5 min and the column was re-equilibrated with 0% B for 2 min. The analytes were detected by Electrospray Ionization MS/MS (ESI-MS/MS) using an API 3200 triple-quadrupole LC-MS/MS system, equipped with an ESI Turbo Ion Spray interface, operated in the negative ion mode (AB Sciex, Darmstadt, Germany). The ion source parameters were set as follows: 40 psi curtain gas, -4000 V ion spray voltage, 650°C ion source temperature, 60 psi nebulizing and drying gas. GSL-specific signals were acquired via Multiple Reaction Monitoring (MRM), with scan time of 15 msec; Q1 and Q3 masses (Q1, Q3 resolution unit) and compound specific parameters for each analyte are described in the Table 5. Peak areas were calculated automatically by IntelliQuant algorithm of the Analyst 1.6 software (AB Sciex, Darmstadt, Germany), with manual adjustment when necessary. GSL content in each sample was calculated in Microsoft Excel, after normalization to the internal standard and to fresh weight. Further normalization to WT content and statistical analysis was performed as described in section 6.9.2.

| GSL | Full name | Q1/Q3 masses (Da) | DP (V) | EP (V) | CEP (V) | CE (V) | CEX (V) | RT (min) |
|---|---|---|---|---|---|---|---|---|
| 3MSOP | 3-methylsulfinylpropyl GSL | 422.1/96.0 | -50 | -5.5 | -20 | -60 | 0 | 0.9 |
| 3MTP | 3-methylthiopentyl GSL | 406.0/96.0 | -50 | -7.5 | -28 | -64 | 0 | 2 |
| 4MSOB | 4-methylsulfinylbutyl GSL | 436.0/96.0 | -60 | -6 | -22 | -64 | 0 | 0.9 |
| 4MTB | 4-methylthiobutyl GSL | 420.0/96.0 | -50 | -7.5 | -20 | -64 | 0 | 2.4 |
| 5MTP | 5-methylthiopentyl GSL | 434.0/96.0 | -50 | -4.5 | -22 | -58 | 0 | 2.7 |
| 6MSOH | 6-methylsulfinylhexyl GSL | 464.0/96.0 | -50 | -5 | -22 | -60 | 0 | 2.1 |
| 6MTH | 6-methylthiohexyl GSL | 448.0/96.0 | -50 | -5 | -29 | -60 | 0 | 3.1 |
| 7MSOH | 7-methylsulfinylheptyl GSL | 478.0/96.0 | -50 | -6.5 | -24 | -64 | 0 | 2.3 |
| 7MTH | 7-methylthioheptyl GSL | 462.0/96.0 | -55 | -6.5 | -22 | -66 | 0 | 3.5 |
| 8MSOO | 8-methylsulfinyloctyl GSL | 492.0/96.0 | -60 | -7 | -24 | -62 | 0 | 2.5 |
| 8MTO | 8-methylthiooctyl GSL | 476.0/96.0 | -60 | -7 | -31 | -62 | 0 | 3.9 |
| I3M | indolyl-3-methyl GSL | 447.0/96.0 | -55 | -7.5 | -22 | -58 | 0 | 2.5 |
| 1MOI3M | 1-hydroxy-indolyl-3-methyl GSL | 477.0/96.0 | -50 | -4.5 | -24 | -64 | 0 | 3.1 |
| 4MOI3M | 4-hydroxy-indolyl-3-methyl GSL | 477.1/96.0 | -45 | -6.5 | -24 | -56 | 0 | 2.8 |
| Sinigrin | - | 358.0/96.0 | -40 | -6.5 | -22 | -48 | 0 | 0.9 |

**Table 5 MS parameters for the quantification of GSLs by MRM.**

*Abbr.: DP, Declustering Potential; EP, Entrance Potential; CEP, Cell Entrance Potential; CP, Collision Potential; CEX, Cell Exit Potential; RT, Retention Time*

## 6.6 Protein analysis from plant tissues

### 6.6.1 Protein extraction

For protein extraction from tissues of young Arabidopsis seedlings, an empirically determined amount of tissue (approximately 15 whole seedlings, 20 shoots or 50 roots) was harvested in an 2ml Eppendorf tube, containing a 5 mm stainless-steel grinding bead and flash frozen with liquid $N_2$. The samples were pulverized via high-speed shaking at 20 Hz for 40-60 sec, using TissueLyser II instrument (Qiagen) and total protein content was extracted with the addition of 200-400 µl RIPA extraction buffer, depending on the quantity of the starting material. The composition of RIPA extraction buffer was set as follows: Tris-Cl (50 mM, pH 7.6), NaCl (150 mM), NaF (20 mM), EGTA (1 mM), EDTA (1mM), $Na_4P_2O_7$ (10mM), nonidet P-40 (1% v/v), deoxycholate (0.5% w/v), DTT (5 mM) and PMSF (1 mM). The detergents nonidet P-40 and deoxycholate were added when necessary, while DTT and PMSF were added directly before use. The samples were mixed with the extraction buffer via vortexing and subsequently incubated at 4 °C with mild rotation for at least 30 min, followed by centrifugation at 10,000 rpm for 10 min at 4 °C. Supernatant containing protein extracts was collected in a fresh 1.5ml Eppendorf tube and protein concentration was determined by a Direct Detect® Spectrometer (Merck).

### 6.6.2 Protein electrophoresis

Protein extracts were separated with SDS-PAGE (Sodium Dodecyl Sulfate Polyacrylamide Gel Electrophoresis) according to Laemmli, 1970. The composition of SDS-PAGE is listed in Table 6. Protein samples were prepared by diluting an appropriate amount of protein extract in 5X SDS sample buffer (0.35 M Tris-HCl with pH adjusted to 6.8, 10% w/v SDS, 0.012% w/v Bromophenol blue, 30% v/v glycerol, and 0.6M DTT) and then loaded on an SDS-PAGE, consisted of a lower separating part (6% Acrylamide) and an upper stacking part (4% Acrylamide). Electrophoresis took place in SDS running buffer (25 mM Tris, 192 mM glycine and 0.1% SDS) at 60 V until the samples entered the separating fraction of the gel and then, continued at 120 V until the dye front migrated out of the gel.

| Components | Stacking gel (4%) | Separating gel (6%) |
|---|---|---|
| | Final concentration | |
| **1 M Tris pH 6.8** | 0.11 M | - |
| **1.5 M Tris pH 8.8** | - | 0.375 M |
| **10% (w/v) SDS** | 0.01 % | 0.01 % |
| **30% Acrylamide** | 4 % | 6 % |
| **10% (w/v) APS** | 0.1 % | 0.1 % |
| **TEMED** | 0.01 % | 0.01 % |

*Table 6 Composition of stacking and separating SDS-PAGE.*

### 6.6.3 Western blot

Proteins separated with SDS-PAGE as described in the previous section were immunodetected with Western blotting. Firstly, protein transfer on a PVDF membrane (Amersham Protran 0.45 µm) was performed via semi-dry electroblotting using the Power Blotter Station XL instrument (ThermoFischer Scientific). Towards that, a PVDF membrane was hydrated in absolute methanol and then equilibrated in

at 1X Power Blotter 1-Step Transfer Buffer (ThermoFischer Scientific) for 1 min, alongside with the pre-run protein gel under analysis and two pieces of Whatman filter paper. The transfer cassette was assembled by placing the protein gel on top of the activated PVDF membrane, in between of the Whatman filter papers, so that the anode is located on the bottom and the cathode on the top; the cassette was placed in the Power Blotter instrument and transfer took place at 1.3 amps for 10 min (High Molecular Weight Program).

After transfer, the membrane was blocked for 1 h in 1X TBS solution (50 mM Tris-HCl, 150 mM NaCl, pH adjusted to 7.4), supplemented with 5% Bovine Serum Albumin (BSA). Subsequently, the primed membrane was incubated with a solution of primary antibody (GFP Antibody, rat monoclonal IgG2a, ChromoTek or a-HDC1, rabbit polyclonal IG2a, Eurogentek), diluted 1:1000 times in antibody solution (1X TBS buffer, 3% BSA). Incubation took place overnight at 4°C with gentle agitation and was followed by 3 times wash with TBS-T solution (1X TBS buffer, 0.1% Tween) for 15 min. Next, the membrane was incubated with a solution of secondary antibody (Anti-rat IgG-HRP, Thermo Fischer Scientific or Anti-Rabbit IgG-HRP, Sigma Aldrich), at a 1:5000 dilution in antibody solution for 1 h at 4°C with gentle agitation and subsequently, it was rinsed with 1X TBS-T solution 3 times for 15 min. Horseradish peroxidase (HRP)-based detection of proteins was performed by exposing the membrane to Cytiva ECL Prime or ECL Select Western Blotting Detection Reagent (Thermo Fischer Scientific) and visualizing the emitted chemoluminescent with X-ray films.

### 6.6.4   Co-immunoprecipitation using the GFP-trap

Co-immunoprecipitation (Co-IP) was performed with agarose beads coupled with anti-GFP Nanobody (GFP-Trap® Agarose, ChromoTek, Planegg, Germany). Initially, tissue was harvested and pulverized as described in session 6.6.1; ground tissue was thoroughly mixed with 300-500 µl RIPA buffer, containing 1/10 of its original concentration, and incubated with mild rotation at 4 °C for 30 min. Then, cell debris was pelleted via centrifugation at 4 °C with maximum speed for 10 min and 300 µl of the supernatant were transferred into a fresh 1.5 ml Eppendorf tube, containing 500 µl RIPA buffer without detergents (session 6.6.1). A 40 µl sample was taken from the diluted protein extract, representing the input, and was used for subsequent Western blot analysis. The remaining protein extract was mixed with 15 µl GFP-trap beads, pre-equilibrated three times in 200 µl RIPA buffer without detergents and incubated with mild rotation at 4°C for 2 h. GFP-trap beads were pelleted via centrifugation at 4 °C and 2.500xg speed for 10 min and a sample was taken from the supernatant, representing the unbound fraction, for Western blot analysis. Next, the beads were washed three times by addition of 300 µl RIPA buffer without detergents, gentle inverting and centrifugation at 4°C and 2.500xg speed for 2 min. The precipitated proteins were eluted by incubation of the beads with 55 µl 2X SDS sample buffer (section 6.6.2) at 68°C for 15 min.

### 6.7   Histochemical analysis and microscopy

### 6.7.1   Histochemical staining

Callose deposition in root tips was detected after staining with a solution of 0.1% aniline blue in phosphate buffer (pH 7.2) for 2 h, followed by two times wash with phosphate buffer. Stained seedlings were imaged using a Zeiss confocal laser scanning microscope LSM780.  For cell wall staining, 9-do *Arabidopsis* seedlings were incubated in propidium iodine (PI) solution for 5-10 sec; stained seedlings were imaged immediately on a Zeiss (Jena, Germany) confocal laser scanning microscope LSM880, as described in section 6.7.2.

For superoxide visualization, 9-days-old *Arabidopsis* seedlings were stained for 15 min in a solution of 0.05% nitroblue tetrazolium (NBT) in 20 mM phosphate buffer (0.2M $Na_2HPO4$, 0.2M $NaH_2PO4$, pH 6.1) in the dark. Next, seedlings were rinsed 3 times with phosphate buffer and immediately mounted on a glass slide with chloral hydrate (1 g/ml, 15% glycerol), for imaging with Zeiss Apotome 2 microscope using a 10x/20x DIC (Differential Interference Contrast) objective. For each of the total of three independent biological experiments, 7-10 seedlings were analyzed per genotype.

## 6.7.2 Confocal microscopy

Confocal laser scanning microscopy was performed using Zeiss LSM 780 and LSM 880 instruments. Excitation/emission range parameters were set as follows: GFP: 488/493-575 nm; Chlorophyll (Autofluorescence): 639/670-754 nm; Propidium Iodine: 561/578-651 nm. Zen Software (Zeiss, Jena, Germany) was used to operate the microscope and image processing was performed in Fiji (ImageJ) or Microsoft PowerPoint. Unless stated otherwise, representative images from one biological experiment are shown, while additionally two or more biological experiments were performed, analyzing 7-10 individuals per condition or genotype.

## 6.7.3 Transmission electron microscopy

For transmission electron microscopy of plastid ultrastructure in *Arabidopsis* root tips according to Spurr, 1969, WT and *pdr3* seedlings, germinated on standard growth medium for 5 days, were transferred to fresh plates of the same medium for 4 days. Root tips from 9-do seedlings were fixed with 3% glutaraldehyde (Sigma, Taufkirchen, Germany) in 0.1 M sodium cacodylate buffer (SCP; pH 7.2) for 3 h at room temperature. After fixation, the samples were rinsed in SCP and postfixed with 1% osmium tetroxide (Roth, Karlsruhe, Germany) in SCP for 1 h at room temperature. Subsequently the segments were rinsed with water, dehydrated in a graded ethanol series (10%, 30%, 50%, and 70 % ethanol containing 1 % uranyl acetate [Chemapol, Czech Republic]), 70%, 90%, 2x100% for 30 min. each), infiltrated with epoxy resin according to Spurr (1969) and polymerized at 70°C for 18 h.

Ultrathin sections (70 nm) were made with an Ultracut R ultramicrotome (Leica, Wetzlar, Germany). Sections were transferred to Formvar-coated copper grids, post-stained with uranyl acetate and lead citrate in an EM-Stain apparatus (Leica) and subsequently observed with an EM900 transmission electron microscope (Carl Zeiss Microscopy, Jena, Germany) operating at 80 kV. The images were recorded using a Variospeed SSCCD camera SM-1k-120 (TRS, Moorenweis, Germany). The above-mentioned procedures were performed by Dr. Gerd Hause (Biocentre, Halle, Germany).

## 6.8 Assessment of primary root growth

Seedlings were germinated at solid growth media containing Pi, as described in session 6.3.2. Five days post germination, seedlings were transferred to fresh media with or without Pi supplementation. After four days of growth, images of the seedlings were taken with a Nikon camera and primary root elongation was analysed with the ImageJ software (Schneider et al., 2012), utilizing the NeuronJ plugin (Meijering et al., 2004).

## 6.9    Bioinformatic and statistical analysis

### 6.9.1    Promoter analysis with PlantPAN3.0

The co-occurrence of transcriptional factors binding sites (TFBS) on the promoter regions of gene set was predicted using the function Gene Group Analysis of online tool PlantPAN3.0 (Chow et al., 2019). The threshold for the frequency of promoters containing the TF/TFBS was set to 75%, while the upstream and downstream coordinates of the promoter were set as follows: X, 1000bp; Y, 5' UTR end; Z, 3'UTR-End. This approach generated a list of possible transcriptional factors, which was cross-checked with the RNA-seq dataset of differentially expressed genes, using Venn diagrams; common elements between these lists were considered as potential regulators of the gene set under analysis and were further studied.

### 6.9.2    Statistical analysis and data visualization

All statistical analysis in this work was performed in RStudio (R versions 3.6.2 and 4.2.0), using various packages. Barplots, boxplots and scatterplots were designed in RStudio, using the package ggplot2 (Wickham, 2016).

For estimation of the GSL content from *Arabidopsis* samples after normalization to WT, firstly the absolute content in each sample was quantified and normalized to the fresh weight, as described in section 6.5. Then, normalization to the control group (WT +Pi) was performed as follows: For each biological experiment individually, GSL content in each sample was normalized to the average value of the control group. The data from six different biological experiments were merged and further statistical analysis was performed on the cumulative subset for each analyte individually. To test if the data in each analyte subset fulfilled the assumptions for Analysis of Variance (ANOVA), Shapiro-Wilk Test and Levene's Test were performed; for normally distributed and homoscedastic data, two-way ANOVA and *post-hoc* Tukey's HSD Test were employed to identify significant differences between the groups ($p < 0.05$). If those criteria were not met, the nonparametric analog of the one-way analysis of variance Kruskal-Wallis Test was used, followed by *post-hoc* Dunn's test ($p < 0.05$).

# 7 References

Aarabi, F., Kusajima, M., Tohge, T., Konishi, T., Gigolashvili, T., Takamune, M., Sasazaki, Y., Watanabe, M., Nakashita, H., Fernie, A.R., Saito, K., Takahashi, H., Hubberten, H.-M., Hoefgen, R., Maruyama-Nakashita, A., 2016. Sulfur deficiency–induced repressor proteins optimize glucosinolate biosynthesis in plants. Sci. Adv. https://doi.org/10.1126/sciadv.1601087

Abel, S., 2017. Phosphate scouting by root tips. Curr. Opin. Plant Biol., 39 Cell signalling and gene regulation 2017 39, 168–177. https://doi.org/10.1016/j.pbi.2017.04.016

Adhikari, N.D., Froehlich, J.E., Strand, D.D., Buck, S.M., Kramer, D.M., Larkin, R.M., 2011. GUN4-Porphyrin Complexes Bind the ChlH/GUN5 Subunit of Mg-Chelatase and Promote Chlorophyll Biosynthesis in Arabidopsis. Plant Cell 23, 1449–1467. https://doi.org/10.1105/tpc.110.082503

Agrawal, A.A., Kurashige, N.S., 2003. A Role for Isothiocyanates in Plant Resistance Against the Specialist Herbivore Pieris rapae. J. Chem. Ecol. 29, 1403–1415. https://doi.org/10.1023/A:1024265420375

Anders, S., Huber, W., 2010. Differential expression analysis for sequence count data. Genome Biol. 11, 1–12. https://doi.org/10.1186/gb-2010-11-10-r106

Andersen, T.G., Nour-Eldin, H.H., Fuller, V.L., Olsen, C.E., Burow, M., Halkier, B.A., 2013. Integration of Biosynthesis and Long-Distance Transport Establish Organ-Specific Glucosinolate Profiles in Vegetative Arabidopsis. Plant Cell 25, 3133–3145. https://doi.org/10.1105/tpc.113.110890

Aung, K., Lin, S.-I., Wu, C.-C., Huang, Y.-T., Su, C., Chiou, T.-J., 2006. pho2, a Phosphate Overaccumulator, Is Caused by a Nonsense Mutation in a MicroRNA399 Target Gene. Plant Physiol. 141, 1000–1011. https://doi.org/10.1104/pp.106.078063

Bae, G., Choi, G., 2008. Decoding of Light Signals by Plant Phytochromes and Their Interacting Proteins https://doi.org/10.1146/annurev.arplant.59.032607.092859

Bak, S., Tax, F.E., Feldmann, K.A., Galbraith, D.W., Feyereisen, R., 2001. CYP83B1, a Cytochrome P450 at the Metabolic Branch Point in Auxin and Indole Glucosinolate Biosynthesis in Arabidopsis. Plant Cell 13, 101–111. https://doi.org/10.1105/tpc.13.1.101

Balzergue, C., Dartevelle, T., Godon, C., Laugier, E., Meisrimler, C., Teulon, J.-M., Creff, A., Bissler, M., Brouchoud, C., Hagège, A., Müller, J., Chiarenza, S., Javot, H., Becuwe-Linka, N., David, P., Péret, B., Delannoy, E., Thibaud, M.-C., Armengaud, J., Abel, S., Pellequer, J.-L., Nussaume, L., Desnos, T., 2017. Low phosphate activates STOP1-ALMT1 to rapidly inhibit root cell elongation. Nat. Commun. 8, 1–16. https://doi.org/10.1038/ncomms15300

Barea, J.-M., Ferrol, N., Azcón-Aguilar, C., Azcón, R., 2008. Mycorrhizal symbioses. Ecophysiol. Plant-Phosphorus Interact. 143–163. https://doi.org/10.1007/978-1-4020-8435-5_7

Barrera, L.O., Li, Z., Smith, A.D., Arden, K.C., Cavenee, W.K., Zhang, M.Q., Green, R.D., Ren, B., 2008. Genome-wide mapping and analysis of active promoters in mouse embryonic stem cells and adult organs. Genome Res. 18, 46–59. https://doi.org/10.1101/gr.6654808

Barth, C., Jander, G., 2006. Arabidopsis myrosinases TGG1 and TGG2 have redundant function in glucosinolate breakdown and insect defense. Plant J. 46, 549–562. https://doi.org/10.1111/j.1365-313X.2006.02716.x

Bauer Wr, Hayes Jj, White Jh, Wolffe Ap, 1994. Nucleosome structural changes due to acetylation. J. Mol. Biol. 236. https://doi.org/10.1006/jmbi.1994.1180

Bednarek, P., Piślewska-Bednarek, M., Svatoš, A., Schneider, B., Doubský, J., Mansurova, M., Humphry, M., Consonni, C., Panstruga, R., Sanchez-Vallet, A., Molina, A., Schulze-Lefert, P., 2009. A Glucosinolate Metabolism Pathway in Living Plant Cells Mediates Broad-Spectrum Antifungal Defense. Science 323, 101–106. https://doi.org/10.1126/science.1163732

Beekwilder, J., Leeuwen, W. van, Dam, N.M. van, Bertossi, M., Grandi, V., Mizzi, L., Soloviev, M., Szabados, L., Molthoff, J.W., Schipper, B., Verbocht, H., Vos, R.C.H. de, Morandini, P., Aarts, M.G.M., Bovy, A., 2008. The Impact of the Absence of Aliphatic Glucosinolates on Insect Herbivory in Arabidopsis. PLOS ONE 3, e2068. https://doi.org/10.1371/journal.pone.0002068

Benning, C., 1998. BIOSYNTHESIS AND FUNCTION OF THE SULFOLIPID SULFOQUINOVOSYL DIACYLGLYCEROL. Annu. Rev. Plant Physiol. Plant Mol. Biol. 49, 53–75. https://doi.org/10.1146/annurev.arplant.49.1.53

Bertani, G., 1951. STUDIES ON LYSOGENESIS I. : The Mode of Phage Liberation by Lysogenic Escherichia coli1. J. Bacteriol. 62, 293. https://doi.org/10.1128/jb.62.3.293-300.1951

Blanvillain, R., Kim, J.H., Wu, S., Lima, A., Ow, D.W., 2009. OXIDATIVE STRESS 3 is a chromatin-associated factor involved in tolerance to heavy metals and oxidative stress. Plant J. 57, 654–665. https://doi.org/10.1111/j.1365-313X.2008.03717.x

Blokhina, O., Virolainen, E., Fagerstedt, K.V., 2003. Antioxidants, Oxidative Damage and Oxygen Deprivation Stress: a Review. Ann. Bot. 91, 179–194. https://doi.org/10.1093/aob/mcf118

Bones, A.M., Rossiter, J.T., 1996. The myrosinase-glucosinolate system, its organisation and biochemistry - Bones - 1996 - Physiologia Plantarum - Wiley Online Library. https://onlinelibrary.wiley.com/doi/10.1111/j.1399-3054.1996.tb00497.x

Bournier, M., Tissot, N., Mari, S., Boucherez, J., Lacombe, E., Briat, J.-F., Gaymard, F., 2013. Arabidopsis Ferritin 1 (AtFer1) Gene Regulation by the Phosphate Starvation Response 1 (AtPHR1) Transcription Factor Reveals a Direct Molecular Link between Iron and Phosphate Homeostasis. J. Biol. Chem. 288, 22670. https://doi.org/10.1074/jbc.M113.482281

Bowler, M.W., Cliff, M.J., Waltho, J.P., Blackburn, G.M., 2010. Why did Nature select phosphate for its dominant roles in biology? New J. Chem. 34, 784–794. https://doi.org/10.1039/B9NJ00718K

Brown, P.D., Tokuhisa, J.G., Reichelt, M., Gershenzon, J., 2003. Variation of glucosinolate accumulation among different organs and developmental stages of Arabidopsis thaliana. Phytochemistry 62, 471–481. https://doi.org/10.1016/S0031-9422(02)00549-6

Brzezowski, P., S.Richter, A., Grimm, B., 2015. Regulation and function of tetrapyrrole biosynthesis in plants and algae. Biochim. Biophys. Acta BBA - Bioenerg. 1847, 968–985. https://doi.org/10.1016/j.bbabio.2015.05.007

Burow, M., Atwell, S., Francisco, M., Kerwin, R.E., Halkier, B.A., Kliebenstein, D.J., 2015. The Glucosinolate Biosynthetic Gene AOP2 Mediates Feed-back Regulation of Jasmonic Acid Signaling in Arabidopsis. Mol. Plant 8, 1201–1212. https://doi.org/10.1016/j.molp.2015.03.001

Burow, M., Müller, R., Gershenzon, J., Wittstock, U., 2006. Altered Glucosinolate Hydrolysis in Genetically Engineered Arabidopsis thaliana and its Influence on the Larval Development of Spodoptera littoralis. J. Chem. Ecol. 32, 2333–2349. https://doi.org/10.1007/s10886-006-9149-1

Carrozza, M.J., Li B, Florens L, Suganuma T, Swanson Sk, Kk, L., Wj, S., S, A., J, Y., Mp, W., Jl, W., 2005. Histone H3 methylation by Set2 directs deacetylation of coding regions by Rpd3S to suppress spurious intragenic transcription. Cell 123. https://doi.org/10.1016/j.cell.2005.10.023

Castrillo, G., Teixeira, P.J.P.L., Paredes, S.H., Law, T.F., Lorenzo, L. de, Feltcher, M.E., Finkel, O.M., Breakfield, N.W., Mieczkowski, P., Jones, C.D., Paz-Ares, J., Dangl, J.L., 2017. Root microbiota drive direct integration of phosphate stress and immunity. Nature 543, 513. https://doi.org/10.1038/nature21417

Cheminant, S., Wild, M., Bouvier, F., Pelletier, S., Renou, J.-P., Erhardt, M., Hayes, S., Terry, M.J., Genschik, P., Achard, P., 2011. DELLAs Regulate Chlorophyll and Carotenoid Biosynthesis to Prevent Photooxidative Damage during Seedling Deetiolation in Arabidopsis. Plant Cell 23, 1849–1860. https://doi.org/10.1105/tpc.111.085233

Chen, C.-Y., Wu, K., Schmidt, W., 2015. The histone deacetylase HDA19 controls root cell elongation and modulates a subset of phosphate starvation responses in Arabidopsis. Sci. Rep. 5, 1–11. https://doi.org/10.1038/srep15708

Chen Dl, Delatorre Ca, Bakker A, Abel S, 2000. Conditional identification of phosphate-starvation-response mutants in Arabidopsis thaliana. Planta 211. https://doi.org/10.1007/s004250000271

Chen, M., Chory, J., Fankhauser, C., 2004. Light Signal Transduction in Higher Plants [WWW Document]. https://doi.org/10.1146/annurev.genet.38.072902.092259

Chen, S., Glawischnig, E., Jørgensen, K., Naur, P., Jørgensen, B., Olsen, C.-E., Hansen, C.H., Rasmussen, H., Pickett, J.A., Halkier, B.A., 2003. CYP79F1 and CYP79F2 have distinct functions in the biosynthesis of aliphatic glucosinolates in Arabidopsis. Plant J. 33, 923–937. https://doi.org/10.1046/j.1365-313X.2003.01679.x

Chen, W.-Q., Drapek, C., Li, D.-X., Xu, Z.-H., Benfey, P.N., Bai, S.-N., 2019. Histone Deacetylase HDA19 Affects Root Cortical Cell Fate by Interacting with SCARECROW. Plant Physiol. 180, 276–288. https://doi.org/10.1104/pp.19.00056

Chen, X., Ding, A.B., Zhong, X., 2020. Functions and mechanisms of plant histone deacetylases. Sci. China Life Sci. 63, 206–216. https://doi.org/10.1007/s11427-019-1587-x

Chi-Nga Chow, Tzong-Yi Lee, Yu-Cheng Hung, Guan-Zhen Li, Kuan-Chieh Tseng, Ya-Hsin Liu, Po-Li Kuo, Han-Qin Zheng, and Wen-Chi Chang "PlantPAN3.0: a new and updated resource for reconstructing transcriptional regulatory networks from ChIP-seq experiments in plants" Nucleic Acids Res. 2019.

Chien, P.-S., Chiang, C.-P., Leong, S.J., Chiou, T.-J., 2018. Sensing and Signaling of Phosphate Starvation: From Local to Long Distance. Plant Cell Physiol. 59, 1714–1722. https://doi.org/10.1093/pcp/pcy148

Chow, C.-N., Lee, T.-Y., Hung, Y.-C., Li, G.-Z., Tseng, K.-C., Liu, Y.-H., Kuo, P.-L., Zheng, H.-Q., Chang, W.-C., 2019. PlantPAN3.0: a new and updated resource for reconstructing transcriptional regulatory networks from ChIP-seq experiments in plants. Nucleic Acids Res. 47, D1155. https://doi.org/10.1093/nar/gky1081

Clay, N.K., Adio, A.M., Denoux, C., Jander, G., Ausubel, F.M., 2009. Glucosinolate Metabolites Required for an Arabidopsis Innate Immune Response. Science 323, 95. https://doi.org/10.1126/science.1164627

Clough, S.J., Bent, A.F., 1998. Floral dip: a simplified method for Agrobacterium -mediated transformation of Arabidopsis thaliana. Plant J. 16, 735–743. https://doi.org/10.1046/j.1365-313x.1998.00343.x

Cosio, C., Dunand, C., 2009. Specific functions of individual class III peroxidase genes. J. Exp. Bot. 60, 391–408. https://doi.org/10.1093/jxb/ern318

Czerniawski, P., Bednarek, P., 2018. Glutathione S-Transferases in the Biosynthesis of Sulfur-Containing Secondary Metabolites in Brassicaceae Plants. Front. Plant Sci. 0. https://doi.org/10.3389/fpls.2018.01639

Danhua Jiang, Frédéric Berger, 2017. Histone variants in plant transcriptional regulation. Biochim. Biophys. Acta BBA - Gene Regul. Mech. 1860, 123–130. https://doi.org/10.1016/j.bbagrm.2016.07.002

Deckert, J., Struhl, K., 2001. Histone acetylation at promoters is differentially affected by specific activators and repressors. Mol. Cell. Biol. 21, 2726–2735. https://doi.org/10.1128/MCB.21.8.2726-2735.2001

Delaux, P.-M., Varala, K., Edger, P.P., Coruzzi, G.M., Pires, J.C., Ané, J.-M., 2014. Comparative Phylogenomics Uncovers the Impact of Symbiotic Associations on Host Genome Evolution. PLoS Genet. 10, e1004487. https://doi.org/10.1371/journal.pgen.1004487

Ding, Z.J., Yan, J.Y., Xu, X.Y., Li, G.X., Zheng, S.J., 2013. WRKY46 functions as a transcriptional repressor of ALMT1, regulating aluminum-induced malate secretion in Arabidopsis. Plant J. Cell Mol. Biol. 76. https://doi.org/10.1111/tpj.12337

Dong, J., Ma, G., Sui, L., Wei, M., Satheesh, V., Zhang, R., Ge, S., Li, J., Zhang, T.-E., Wittwer, C., J.Jessen, H., Zhang, H., An, G.-Y., Chao, D.-Y., Liu, D., Lei, M., 2019. Inositol Pyrophosphate InsP8 Acts as an Intracellular Phosphate Signal in Arabidopsis. Mol. Plant 12, 1463–1473. https://doi.org/10.1016/j.molp.2019.08.002

Duff, S.M., Moorhead, G.B., Lefebvre, D.D., Plaxton, W.C., 1989. Phosphate Starvation Inducible Bypasses' of Adenylate and Phosphate Dependent Glycolytic Enzymes in Brassica nigra Suspension Cells. Plant Physiol. 90, 1275–1278. https://doi.org/10.1104/pp.90.4.1275

Dyson, M., H., 2001. Acetyllysine-binding and function of bromodomain-containing proteins in chromatin. Front. Biosci. 6, d853. https://doi.org/10.2741/Dyson

Eklöf, J.M., Brumer, H., 2010. The XTH Gene Family: An Update on Enzyme Structure, Function, and Phylogeny in Xyloglucan Remodeling. Plant Physiol. 153, 456–466. https://doi.org/10.1104/pp.110.156844

Esfandiari, N., Sharma, R.K., Saleh, R.A., Thomas, A.J., Agarwal, A., 2003. Utility of the Nitroblue Tetrazolium Reduction Test for Assessment of Reactive Oxygen Species Production by Seminal Leukocytes and Spermatozoa. J. Androl. 24, 862–870. https://doi.org/10.1002/j.1939-4640.2003.tb03137.x

Essigmann, B., Güler, S., Narang, R.A., Linke, D., Benning, C., 1998. Phosphate availability affects the thylakoid lipid composition and the expression of SQD1, a gene required for sulfolipid biosynthesis in Arabidopsis thaliana. Proc. Natl. Acad. Sci. U. S. A. 95, 1950–1955. https://doi.org/10.1073/pnas.95.4.1950

Fahey J, Zalcmann A, Talalay P, 2001. The chemical diversity and distribution of glucosinolates and isothiocyanates among plants. Phytochemistry 56. https://doi.org/10.1016/s0031-9422(00)00316-2

Fan, J., Crooks, C., Creissen, G., Hill, L., Fairhurst, S., Doerner, P., Lamb, C., 2011. Pseudomonas sax Genes Overcome Aliphatic Isothiocyanate–Mediated Non-Host Resistance in Arabidopsis. Science. https://doi.org/10.1126/science.1199707

Feng, C., Cai, X.-W., Su, Y.-N., Li, L., Chen, S., He, X.-J., 2021. Arabidopsis RPD3-like histone deacetylases form multiple complexes involved in stress response. J. Genet. Genomics 48, 369–383. https://doi.org/10.1016/j.jgg.2021.04.004

Feng, S., Martinez, C., Gusmaroli, G., Wang, Y., Zhou, J., Wang, F., Chen, L., Yu, L., Iglesias-Pedraz, J.M., Kircher, S., Schäfer, E., Fu, X., Fan, L.-M., Deng, X.W., 2008. Coordinated regulation of Arabidopsis thaliana development by light and gibberellins. Nature 451, 475–479. https://doi.org/10.1038/nature06448

Fernández-Calvo, P., Chini, A., Fernández-Barbero, G., Chico, J.-M., Gimenez-Ibanez, S., Geerinck, J., Eeckhout, D., Schweizer, F., Godoy, M., Franco-Zorrilla, J.M., Pauwels, L., Witters, E., Puga, M.I., Paz-Ares, J., Goossens, A., Reymond, P., Jaeger, G.D., Solano, R., 2011. The Arabidopsis bHLH Transcription Factors MYC3 and MYC4 Are Targets of JAZ Repressors and Act Additively with MYC2 in the Activation of Jasmonate Responses. Plant Cell 23, 701. https://doi.org/10.1105/tpc.110.080788

Fernández-Calvo, P., Iñigo, S., Glauser, G., Vanden Bossche, R., Tang, M., Li, B., De Clercq, R., Nagels Durand, A., Eeckhout, D., Gevaert, K., De Jaeger, G., Brady, S.M., Kliebenstein, D.J., Pauwels, L., Goossens, A., Ritter, A., 2020. FRS7 and FRS12 recruit NINJA to regulate expression of glucosinolate biosynthesis genes. New Phytol. 227, 1124–1137. https://doi.org/10.1111/nph.16586

Field, B., Cardon, G., Traka, M., Botterman, J., Vancanneyt, G., Mithen, R., 2004. Glucosinolate and Amino Acid Biosynthesis in Arabidopsis. Plant Physiol. 135, 828–839. https://doi.org/10.1104/pp.104.039347

Field, B., Osbourn, A.E., 2008. Metabolic Diversification—Independent Assembly of Operon-Like Gene Clusters in Different Plants. Science 320, 543–547. https://doi.org/10.1126/science.1154990

Figueroa, C.M., Feil, R., Ishihara, H., Watanabe, M., Kölling, K., Krause, U., Höhne, M., Encke, B., Plaxton, W.C., Zeeman, S.C., Li, Z., Schulze, W.X., Hoefgen, R., Stitt, M., Lunn, J.E., 2016. Trehalose 6–phosphate coordinates organic and amino acid metabolism with carbon availability. Plant J. 85, 410–423. https://doi.org/10.1111/tpj.13114

Figueroa, C.M., Lunn, J.E., 2016. A Tale of Two Sugars: Trehalose 6-Phosphate and Sucrose. Plant Physiol. 172, 7–27. https://doi.org/10.1104/pp.16.00417

Fitter, D.W., Martin, D.J., Copley, M.J., Scotland, R.W., Langdale, J.A., 2002. GLK gene pairs regulate chloroplast development in diverse plant species. Plant J. 31, 713–727. https://doi.org/10.1046/j.1365-313X.2002.01390.x

Fong, P.M., Tian, L., Chen, Z.J., 2006. Arabidopsis thaliana histone deacetylase 1 (AtHD1) is localized in euchromatic regions and demonstrates histone deacetylase activity in vitro. Cell Res. 16, 479–488. https://doi.org/10.1038/sj.cr.7310059

Franck, F., Sperling, U., Frick, G., Pochert, B., van Cleve, B., Apel, K., Armstrong, G.A., 2000. Regulation of Etioplast Pigment-Protein Complexes, Inner Membrane Architecture, and Protochlorophyllide a Chemical Heterogeneity by Light-Dependent NADPH:Protochlorophyllide Oxidoreductases A and B. Plant Physiol. 124, 1678–1696. https://doi.org/10.1104/pp.124.4.1678

Frentzen, M., 2004. Phosphatidylglycerol and sulfoquinovosyldiacylglycerol: anionic membrane lipids and phosphate regulation. Curr. Opin. Plant Biol. 7, 270–276. https://doi.org/10.1016/j.pbi.2004.03.001

Frerigmann, H., Gigolashvili, T., 2014. MYB34, MYB51, and MYB122 Distinctly Regulate Indolic Glucosinolate Biosynthesis in Arabidopsis thaliana. Mol. Plant 7, 814–828.
 https://doi.org/10.1093/mp/ssu004

Fu, L., Wang, M., Han, B., Tan, D., Sun, X., Zhang, J., 2016. Arabidopsis Myrosinase Genes AtTGG4 and AtTGG5 Are Root-Tip Specific and Contribute to Auxin Biosynthesis and Root-Growth Regulation. Int. J. Mol. Sci. 17. https://doi.org/10.3390/ijms17060892

Fuchs, J., Demidov, D., Houben, A., Schubert, I., 2006. Chromosomal histone modification patterns--from conservation to diversity. Trends Plant Sci. 11, 199–208. https://doi.org/10.1016/j.tplants.2006.02.008

Gachon, C.M.M., Langlois-Meurinne, M., Saindrenan, P., 2005. Plant secondary metabolism glycosyltransferases: the emerging functional analysis. Trends Plant Sci. 10, 542–549. https://doi.org/10.1016/j.tplants.2005.09.007

Geu-Flores, F., Møldrup, M.E., Böttcher, C., Olsen, C.E., Scheel, D., Halkier, B.A., 2011. Cytosolic γ-Glutamyl Peptidases Process Glutathione Conjugates in the Biosynthesis of Glucosinolates and Camalexin in *Arabidopsis*. Plant Cell 23, 2456–2469. https://doi.org/10.1105/tpc.111.083998

Giamoustaris, A., Mithen, R., 1995. The effect of modifying the glucosinolate content of leaves of oilseed rape (Brassica napus ssp. oleifera) on its interaction with specialist and generalist pests. Ann. Appl. Biol. 126, 347–363. https://doi.org/10.1111/j.1744-7348.1995.tb05371.x

Gibon, Y., Usadel, B., Blaesing, O.E., Kamlage, B., Hoehne, M., Trethewey, R., Stitt, M., 2006. Integration of metabolite with transcript and enzyme activity profiling during diurnal cycles in Arabidopsisrosettes. Genome Biol. 7, 1–23. https://doi.org/10.1186/gb-2006-7-8-r76

Giehl, R.F.H., von Wirén, N., 2014. Root Nutrient Foraging. Plant Physiol. 166, 509–517. https://doi.org/10.1104/pp.114.245225

Giersch, C., Robinson, S.P., 1987. Regulation of photosynthetic carbon metabolism during phosphate limitation of photosynthesis in isolated spinach chloroplasts. Photosynth. Res. 14, 211–227. https://doi.org/10.1007/BF00032706

Gigolashvili, T., Berger, B., Mock, H.-P., Müller, C., Weisshaar, B., Flügge, U.-I., 2007a. The transcription factor HIG1/MYB51 regulates indolic glucosinolate biosynthesis in Arabidopsis thaliana. Plant J. 50, 886–901. https://doi.org/10.1111/j.1365-313X.2007.03099.x

Gigolashvili, T., Engqvist, M., Yatusevich, R., Müller, C., Flügge, U.-I., 2008. HAG2/MYB76 and HAG3/MYB29 exert a specific and coordinated control on the regulation of aliphatic glucosinolate biosynthesis in Arabidopsis thaliana. New Phytol. 177, 627–642. https://doi.org/10.1111/j.1469-8137.2007.02295.x

Gigolashvili, T., Yatusevich, R., Berger, B., Müller, C., Flügge, U.-I., 2007b. The R2R3-MYB transcription factor HAG1/MYB28 is a regulator of methionine-derived glucosinolate biosynthesis in Arabidopsis thaliana. Plant J. 51, 247–261. https://doi.org/10.1111/j.1365-313X.2007.03133.x

Gigolashvili, T., Yatusevich, R., Rollwitz, I., Humphry, M., Gershenzon, J., Flügge, U.-I., 2009. The Plastidic Bile Acid Transporter 5 Is Required for the Biosynthesis of Methionine-Derived Glucosinolates in Arabidopsis thaliana. Plant Cell 21, 1813. https://doi.org/10.1105/tpc.109.066399

Gollhofer, J., Timofeev, R., Lan, P., Schmidt, W., Buckhout, T.J., 2014. Vacuolar-Iron-Transporter1-Like Proteins Mediate Iron Homeostasis in Arabidopsis. PLOS ONE 9, e110468. https://doi.org/10.1371/journal.pone.0110468

Goodspeed, D., Chehab, E.W., Min-Venditti, A., Braam, J., Covington, M.F., 2012. *Arabidopsis* synchronizes jasmonate-mediated defense with insect circadian behavior. Proc. Natl. Acad. Sci. 109, 4674–4677. https://doi.org/10.1073/pnas.1116368109

Greenham, K., McClung, C.R., 2015. Integrating circadian dynamics with physiological processes in plants. Nat. Rev. Genet. 16, 598–610. https://doi.org/10.1038/nrg3976

Grossniklaus, U., Vielle-Calzada, J.-P., Hoeppner, M.A., Gagliano, W.B., 1998. Maternal Control of Embryogenesis by MEDEA, a Polycomb Group Gene in Arabidopsis. Science.
 https://doi.org/10.1126/science.280.5362.446

Grubb, C.D., Zipp, B.J., Kopycki, J., Schubert, M., Quint, M., Lim, E.-K., Bowles, D.J., Pedras, M.S.C., Abel, S., 2014. Comparative analysis of Arabidopsis UGT74 glucosyltransferases reveals a special role of UGT74C1 in glucosinolate biosynthesis. Plant J. 79, 92–105. https://doi.org/10.1111/tpj.12541

Grubb, C.D., Zipp, B.J., Ludwig-Müller, J., Masuno, M.N., Molinski, T.F., Abel, S., 2004. Arabidopsis glucosyltransferase UGT74B1 functions in glucosinolate biosynthesis and auxin homeostasis. Plant J. 40, 893–908. https://doi.org/10.1111/j.1365-313X.2004.02261.x

Halkier, B.A., Gershenzon, J., 2006. BIOLOGY AND BIOCHEMISTRY OF GLUCOSINOLATES. Annu. Rev. Plant Biol. 57, 303–333. https://doi.org/10.1146/annurev.arplant.57.032905.105228

Hammond, J.P., White, P.J., 2008. Sucrose transport in the phloem: integrating root responses to phosphorus starvation. J. Exp. Bot. 59, 93–109. https://doi.org/10.1093/jxb/erm221

Hansen, B.G., Kliebenstein, D.J., Halkier, B.A., 2007. Identification of a flavin-monooxygenase as the S-oxygenating enzyme in aliphatic glucosinolate biosynthesis in Arabidopsis. Plant J. 50, 902–910. https://doi.org/10.1111/j.1365-313X.2007.03101.x

Hansen, C.H., Wittstock, U., Olsen, C.E., Hick, A.J., Pickett, J.A., Halkier, B.A., 2001. Cytochrome P450 CYP79F1 from Arabidopsis Catalyzes the Conversion of Dihomomethionine and Trihomomethionine to the Corresponding Aldoximes in the Biosynthesis of Aliphatic Glucosinolates *. J. Biol. Chem. 276, 11078–11085. https://doi.org/10.1074/jbc.M010123200

Harun, S., Abdullah-Zawawi, M.-R., Goh, H.-H., Mohamed-Hussein, Z.-A., 2020. A Comprehensive Gene Inventory for Glucosinolate Biosynthetic Pathway in *Arabidopsis thaliana*. J. Agric. Food Chem. 68, 7281–7297. https://doi.org/10.1021/acs.jafc.0c01916

Hayami, N., Sakai, Y., Kimura, M., Saito, T., Tokizawa, M., Iuchi, S., Kurihara, Y., Matsui, M., Nomoto, M., Tada, Y., Yamamoto, Y.Y., 2015. The Responses of Arabidopsis Early Light-Induced Protein2 to Ultraviolet B, High Light, and Cold Stress Are Regulated by a Transcriptional Regulatory Unit Composed of Two Elements. Plant Physiol. 169, 840–855. https://doi.org/10.1104/pp.15.00398

He, Y., Galant, A., Pang, Q., Strul, J.M., Balogun, S.F., Jez, J.M., Chen, S., 2011. Structural and Functional Evolution of Isopropylmalate Dehydrogenases in the Leucine and Glucosinolate Pathways of Arabidopsis thaliana*. J. Biol. Chem. 286, 28794–28801. https://doi.org/10.1074/jbc.M111.262519

He, Y., Mawhinney, T.P., Preuss, M.L., Schroeder, A.C., Chen, B., Abraham, L., Jez, J.M., Chen, S., 2009. A redox-active isopropylmalate dehydrogenase functions in the biosynthesis of glucosinolates and leucine in Arabidopsis. Plant J. 60, 679–690. https://doi.org/10.1111/j.1365-313X.2009.03990.x

Hecht, S.S., 2000. Inhibition of carcinogenesis by isothiocyanates*. Drug Metab. Rev. https://doi.org/10.1081/DMR-100102342

Hildmann, C., Riester, D., Schwienhorst, A., 2007. Histone deacetylases--an important class of cellular regulators with a variety of functions. Appl. Microbiol. Biotechnol. 75, 487–497. https://doi.org/10.1007/s00253-007-0911-2

Hinsinger, P., 2001. Bioavailability of soil inorganic P in the rhizosphere as affected by root-induced chemical changes: a review. Plant Soil 237, 173–195. https://doi.org/10.1023/A:1013351617532

Hirai, M.Y., Sugiyama, K., Sawada, Y., Tohge, T., Obayashi, T., Suzuki, A., Araki, R., Sakurai, N., Suzuki, H., Aoki, K., Goda, H., Nishizawa, O.I., Shibata, D., Saito, K., 2006. Omics-based identification of Arabidopsis Myb transcription factors regulating aliphatic glucosinolate biosynthesis [WWW Document]. https://doi.org/10.1073/pnas.0611629104

Hiruma, K., Gerlach, N., Sacristan, S., Nakano, R.T., Hacquard, S., Kracher, B., Neumann, U., Ramırez, D., Bucher, M., O'Connell, R.J., Schulze-Lefert, P., 2016. Root Endophyte Colletotrichum tofieldiae Confers Plant Fitness Benefits that Are Phosphate Status Dependent. Cell 165, 464–474. https://doi.org/10.1016/j.cell.2016.02.028

Hoehenwarter, W., Mönchgesang, S., Neumann, S., Majovsky, P., Abel, S., Müller, J., 2016. Comparative expression profiling reveals a role of the root apoplast in local phosphate response. BMC Plant Biol. 16, 1–21. https://doi.org/10.1186/s12870-016-0790-8

Hollender, C., Liu, Z., 2008. Histone Deacetylase Genes in Arabidopsis Development. J. Integr. Plant Biol. 50, 875–885. https://doi.org/10.1111/j.1744-7909.2008.00704.x

Huang, A.C., Jiang, T., Liu, Y.-X., Bai, Y.-C., Reed, J., Qu, B., Goossens, A., Nützmann, H.-W., Bai, Y., Osbourn, A., 2019. A specialized metabolic network selectively modulates *Arabidopsis* root microbiota. Science 364, eaau6389. https://doi.org/10.1126/science.aau6389

Huang da W, Sherman Bt, Lempicki Ra, 2009. Systematic and integrative analysis of large gene lists using DAVID bioinformatics resources. Nat. Protoc. 4. https://doi.org/10.1038/nprot.2008.211

Huang, H., Ullah, F., Zhou, D.-X., Yi, M., Zhao, Y., 2019a. Mechanisms of ROS Regulation of Plant Development and Stress Responses. Front. Plant Sci. 0. https://doi.org/10.3389/fpls.2019.00800

Hull, A.K., Vij, R., Celenza, J.L., 1993. Arabidopsis cytochrome P450s that catalyze the first step of tryptophan-dependent indole-3-acetic acid biosynthesis. https://doi.org/10.1073/pnas.040569997

Hulsen, T., de Vlieg, J., Alkema, W., 2008. BioVenn – a web application for the comparison and visualization of biological lists using area-proportional Venn diagrams. BMC Genomics 9, 1–6. https://doi.org/10.1186/1471-2164-9-488

Hung, F.-Y., Chen, F.-F., Li, C., Chen, C., Chen, J.-H., Cui, Y., Wu, K., 2019. The LDL1/2-HDA6 Histone Modification Complex Interacts With TOC1 and Regulates the Core Circadian Clock Components in Arabidopsis. Front. Plant Sci. 0. https://doi.org/10.3389/fpls.2019.00233

Hung, F.-Y., Chen, F.-F., Li, C., Chen, C., Lai, Y.-C., Chen, J.-H., Cui, Y., Wu, K., 2018. The Arabidopsis LDL1/2-HDA6 histone modification complex is functionally associated with CCA1/LHY in regulation of circadian clock genes. Nucleic Acids Res. 46, 10669–10681. https://doi.org/10.1093/nar/gky749

Huq, E., Al-Sady, B., Hudson, M., Kim, C., Apel, K., Quail, P.H., 2004. PHYTOCHROME-INTERACTING FACTOR 1 Is a Critical bHLH Regulator of Chlorophyll Biosynthesis. Science.
 https://doi.org/10.1126/science.1099728

Huseby, S., Koprivova, A., Lee, B.-R., Saha, S., Mithen, R., Wold, A.-B., Bengtsson, G.B., Kopriva, S., 2013. Diurnal and light regulation of sulphur assimilation and glucosinolate biosynthesis in Arabidopsis. J. Exp. Bot. 64, 1039. https://doi.org/10.1093/jxb/ers378

Ivica Blažević, Sabine Montaut, Franko Burčul, Carl Erik Olsen, Meike Burow, Patrick Rollin, Niels Agerbirk, 2020. Glucosinolate structural diversity, identification, chemical synthesis and metabolism in plants. Phytochemistry 169, 112100. https://doi.org/10.1016/j.phytochem.2019.112100

Jensen, L.M., Kliebenstein, D.J., Burow, M., 2015. Investigation of the multifunctional gene AOP3 expands the regulatory network fine-tuning glucosinolate production in Arabidopsis. Front. Plant Sci. 0. https://doi.org/10.3389/fpls.2015.00762

Jensen, P.E., Bassi, R., Boekema, E.J., Dekker, J.P., Jansson, S., Leister, D., Robinson, C., Scheller, H.V., 2007. Structure, function and regulation of plant photosystem I. Biochim. Biophys. Acta BBA - Bioenerg. 1767, 335–352. https://doi.org/10.1016/j.bbabio.2007.03.004

Jenuwein T, Allis Cd, 2001. Translating the histone code. Science 293.
 https://doi.org/10.1126/science.1063127

Johnson, T., Dinkova-Kostova, A., Fahey, J.W. Glucosinolates from the Brassica vegetables and their health effects. In Encyclopedia of Food and Health; Elsevier Inc.: Amsterdam, The Netherlands, 2015; pp. 248–255.

Kang, M.-Y., Yoo, S.-C., Kwon, H.-Y., Lee, B.-D., Cho, J.-N., Noh, Y.-S., Paek, N.-C., 2015. Negative regulatory roles of DE-ETIOLATED1 in flowering time inArabidopsis. Sci. Rep. 5, 1–8. https://doi.org/10.1038/srep09728

Kaufmann, K., Muiño, J.M., Østerås, M., Farinelli, L., Krajewski, P., Angenent, G.C., 2010. Chromatin immunoprecipitation (ChIP) of plant transcription factors followed by sequencing (ChIP-SEQ) or

hybridization to whole genome arrays (ChIP-CHIP). Nat. Protoc. 5, 457–472. https://doi.org/10.1038/nprot.2009.244

Kawasaki, T., Yamada, K., Yoshimura, S., Yamaguchi, K., 2017. Chitin receptor-mediated activation of MAP kinases and ROS production in rice and Arabidopsis. Plant Signal. Behav. 12. https://doi.org/10.1080/15592324.2017.1361076

Khorobrykh, S., Havurinne, V., Mattila, H., Tyystjärvi, E., 2020. Oxygen and ROS in Photosynthesis. Plants 9. https://doi.org/10.3390/plants9010091

Kim, J.H., Jander, G., 2007. Myzus persicae (green peach aphid) feeding on Arabidopsis induces the formation of a deterrent indole glucosinolate. Plant J. 49, 1008–1019. https://doi.org/10.1111/j.1365-313X.2006.03019.x

Kim, J.H., Lee, B.W., Schroeder, F.C., Jander, G., 2008. Identification of indole glucosinolate breakdown products with antifeedant effects on Myzus persicae (green peach aphid). Plant J. 54, 1015–1026. https://doi.org/10.1111/j.1365-313X.2008.03476.x

Kim, K.-C., Lai, Z., Fan, B., Chen, Z., 2008. Arabidopsis WRKY38 and WRKY62 Transcription Factors Interact with Histone Deacetylase 19 in Basal Defense. Plant Cell 20, 2357–2371. https://doi.org/10.1105/tpc.107.055566

Kim, S., Piquerez, S.J.M., Ramirez-Prado, J.S., Mastorakis, E., Veluchamy, A., Latrasse, D., Manza-Mianza, D., Brik-Chaouche, R., Huang, Y., Rodriguez-Granados, N.Y., Concia, L., Blein, T., Citerne, S., Bendahmane, A., Bergounioux, C., Crespi, M., Mahfouz, M.M., Raynaud, C., Hirt, H., Ntoukakis, V., Benhamed, M., 2020. GCN5 modulates salicylic acid homeostasis by regulating H3K14ac levels at the 5' and 3' ends of its target genes. Nucleic Acids Res. 48, 5953–5966. https://doi.org/10.1093/nar/gkaa369

Kl, F., Jg, T., J, G., 2007. The effect of sulfur nutrition on plant glucosinolate content: physiology and molecular mechanisms. Plant Biol. Stuttg. Ger. 9. https://doi.org/10.1055/s-2007-965431

Klein, M., Papenbrock, J., 2009. Kinetics and substrate specificities of desulfo-glucosinolate sulfotransferases in Arabidopsis thaliana. Physiol. Plant. 135, 140–149. https://doi.org/10.1111/j.1399-3054.2008.01182.x

Kliebenstein, D.J., D'Auria, J.C., Behere, A.S., Kim, J.H., Gunderson, K.L., Breen, J.N., Lee, G., Gershenzon, J., Last, R.L., Jander, G., 2007. Characterization of seed-specific benzoyloxyglucosinolate mutations in Arabidopsis thaliana. Plant J. 51, 1062–1076. https://doi.org/10.1111/j.1365-313X.2007.03205.x

Knill, T., Reichelt, M., Paetz, C., Gershenzon, J., Binder, S., 2009. Arabidopsis thaliana encodes a bacterial-type heterodimeric isopropylmalate isomerase involved in both Leu biosynthesis and the Met chain elongation pathway of glucosinolate formation. Plant Mol. Biol. 71, 227–239. https://doi.org/10.1007/s11103-009-9519-5

Kobayashi, K., Baba, S., Obayashi, T., Sato, M., Toyooka, K., Keränen, M., Aro, E.-M., Fukaki, H., Ohta, H., Sugimoto, K., Masuda, T., 2012. Regulation of Root Greening by Light and Auxin/Cytokinin Signaling in Arabidopsis. Plant Cell 24, 1081–1095. https://doi.org/10.1105/tpc.111.092254

Kobayashi, K., Masuda, T., 2016. Transcriptional Regulation of Tetrapyrrole Biosynthesis in Arabidopsis thaliana. Front. Plant Sci. 0. https://doi.org/10.3389/fpls.2016.01811

Kobayashi, K., Sasaki, D., Noguchi, K., Fujinuma, D., Komatsu, H., Kobayashi, M., Sato, M., Toyooka, K., Sugimoto, K., Niyogi, K.K., Wada, H., Masuda, T., 2013. Photosynthesis of Root Chloroplasts Developed in Arabidopsis Lines Overexpressing GOLDEN2-LIKE Transcription Factors. Plant Cell Physiol. 54, 1365–1377. https://doi.org/10.1093/pcp/pct086

Kopečná, J., Vaca, I.C. de, Adams, N.B.P., Davison, P.A., Brindley, A.A., Hunter, C.N., Guallar, V., Sobotka, R., 2015. Porphyrin Binding to Gun4 Protein, Facilitated by a Flexible Loop, Controls Metabolite Flow through the Chlorophyll Biosynthetic Pathway *. J. Biol. Chem. 290, 28477–28488. https://doi.org/10.1074/jbc.M115.664987

Koroleva, O.A., Davies, A., Deeken, R., Thorpe, M.R., Tomos, A.D., Hedrich, R., 2000. Identification of a New Glucosinolate-Rich Cell Type in Arabidopsis Flower Stalk. Plant Physiol. 124, 599. https://doi.org/10.1104/pp.124.2.599

Kos, M., Houshyani, B., Wietsma, R., Kabouw, P., Vet, L.E.M., van Loon, J.J.A., Dicke, M., 2012. Effects of glucosinolates on a generalist and specialist leaf-chewing herbivore and an associated parasitoid. Phytochemistry 77, 162–170. https://doi.org/10.1016/j.phytochem.2012.01.005

Kroymann, J., Textor, S., Tokuhisa, J.G., Falk, K.L., Bartram, S., Gershenzon, J., Mitchell-Olds, T., 2001. A Gene Controlling Variation in Arabidopsis Glucosinolate Composition Is Part of the Methionine Chain Elongation Pathway. Plant Physiol. 127, 1077–1088. https://doi.org/10.1104/pp.010416

Kumar, V., Thakur, J.K., Prasad, M., 2021. Histone acetylation dynamics regulating plant development and stress responses. Cell. Mol. Life Sci. 78, 4467–4486. https://doi.org/10.1007/s00018-021-03794-x

Laloi, C., Apel, K., Danon, A., 2004. Reactive oxygen signalling: the latest news. Curr. Opin. Plant Biol. 7, 323–328. https://doi.org/10.1016/j.pbi.2004.03.005

Laluk, K., Prasad, K.V.S.K., Savchenko, T., Celesnik, H., Dehesh, K., Levy, M., Mitchell-Olds, T., Reddy, A.S.N., 2012. The Calmodulin-Binding Transcription Factor SIGNAL RESPONSIVE1 is a Novel Regulator of Glucosinolate Metabolism and Herbivory Tolerance in Arabidopsis. Plant Cell Physiol. 53, 2008–2015. https://doi.org/10.1093/pcp/pcs143

Lau, O.S., Deng, X.W., 2012. The photomorphogenic repressors COP1 and DET1: 20 years later. Trends Plant Sci. 17, 584–593. https://doi.org/10.1016/j.tplants.2012.05.004

Lee, J., He, K., Stolc, V., Lee, H., Figueroa, P., Gao, Y., Tongprasit, W., Zhao, H., Lee, I., Deng, X.W., 2007. Analysis of Transcription Factor HY5 Genomic Binding Sites Revealed Its Hierarchical Role in Light Regulation of Development. Plant Cell 19, 731–749. https://doi.org/10.1105/tpc.106.047688

Lee, S., Kaminaga, Y., Cooper, B., Pichersky, E., Dudareva, N., Chapple, C., 2012. Benzoylation and sinapoylation of glucosinolate R-groups in Arabidopsis. Plant J. 72, 411–422. https://doi.org/10.1111/j.1365-313X.2012.05096.x

Lei, J., Jayaprakasha, G.K., Singh, J., Uckoo, R., Borrego, E.J., Finlayson, S., Kolomiets, M., Patil, B.S., Braam, J., Zhu-Salzman, K., 2019. CIRCADIAN CLOCK-ASSOCIATED1 Controls Resistance to Aphids by Altering Indole Glucosinolate Production. Plant Physiol. 181, 1344. https://doi.org/10.1104/pp.19.00676

Leivar, P., Quail, P.H., 2011. PIFs: pivotal components in a cellular signaling hub. Trends Plant Sci. 16, 19–28. https://doi.org/10.1016/j.tplants.2010.08.003

Li, D., Liu, C., Shen, L., Wu, Y., Chen, H., Robertson, M., Helliwell, C.A., Ito, T., Meyerowitz, E., Yu, H., 2008. A Repressor Complex Governs the Integration of Flowering Signals in Arabidopsis. Dev. Cell 15, 110–120. https://doi.org/10.1016/j.devcel.2008.05.002

Li, G., Siddiqui, H., Teng, Y., Lin, R., Wan, X., Li, J., Lau, O.-S., Ouyang, X., Dai, M., Wan, J., Devlin, P.F., Deng, X.W., Wang, H., 2011. Coordinated transcriptional regulation underlying the circadian clock in Arabidopsis. Nat. Cell Biol. 13, 616–622. https://doi.org/10.1038/ncb2219

Li, J., Hansen, B.G., Ober, J.A., Kliebenstein, D.J., Halkier, B.A., 2008. Subclade of Flavin-Monooxygenases Involved in Aliphatic Glucosinolate Biosynthesis. Plant Physiol. 148, 1721–1733. https://doi.org/10.1104/pp.108.125757

Li, J., Kristiansen, K.A., Hansen, B.G., Halkier, B.A., 2011. Cellular and subcellular localization of flavin-monooxygenases involved in glucosinolate biosynthesis. J. Exp. Bot. 62, 1337–1346. https://doi.org/10.1093/jxb/erq369

Li, Y., Li, R., Sawada, Y., Boerzhijin, S., Kuwahara, A., Sato, M., Hirai, M.Y., 2021. Abscisic acid-mediated induction of FLAVIN-CONTAINING MONOOXYGENASE 2 leads to reduced accumulation of methylthioalkyl glucosinolates in Arabidopsis thaliana. Plant Sci. 303, 110764. https://doi.org/10.1016/j.plantsci.2020.110764

Liang, C., Piñeros, M.A., Tian, J., Yao, Z., Sun, L., Liu, J., Shaff, J., Coluccio, A., Kochian, L.V., Liao, H., 2013. Low pH, Aluminum, and Phosphorus Coordinately Regulate Malate Exudation through GmALMT1 to Improve Soybean Adaptation to Acid Soils. Plant Physiol. 161, 1347–1361. https://doi.org/10.1104/pp.112.208934

Liepinsh, E., Trexler, M., Kaikkonen, A., Weigelt, J., Bányai, L., Patthy, L., Otting, G., 2001. NMR structure of the LCCL domain and implications for DFNA9 deafness disorder. EMBO J. 20, 5347–5353. https://doi.org/10.1093/emboj/20.19.5347

Liu, J., Magalhaes, J.V., Shaff, J., Kochian, L.V., 2009. Aluminum-activated citrate and malate transporters from the MATE and ALMT families function independently to confer Arabidopsis aluminum tolerance. Plant J. 57, 389–399. https://doi.org/10.1111/j.1365-313X.2008.03696.x

Liu, P., Zhang, H., Yu, B., Xiong, L., Xia, Y., 2015. Proteomic identification of early salicylate- and flg22-responsive redox-sensitive proteins in Arabidopsis. Sci. Rep. 5, 1–7. https://doi.org/10.1038/srep08625

Liu, T.-Y., Huang, T.-K., Tseng, C.-Y., Lai, Y.-S., Lin, S.-I., Lin, W.-Y., Chen, J.-W., Chiou, T.-J., 2012. PHO2-Dependent Degradation of PHO1 Modulates Phosphate Homeostasis in Arabidopsis. Plant Cell 24, 2168–2183. https://doi.org/10.1105/tpc.112.096636

Liu, X., Chen, C.-Y., Wang, K.-C., Luo, M., Tai, R., Yuan, L., Zhao, M., Yang, S., Tian, G., Cui, Y., Hsieh, H.-L., Wu, K., 2013. PHYTOCHROME INTERACTING FACTOR3 Associates with the Histone Deacetylase HDA15 in Repression of Chlorophyll Biosynthesis and Photosynthesis in Etiolated Arabidopsis Seedlings. Plant Cell 25, 1258–1273. https://doi.org/10.1105/tpc.113.109710

Liu, Z., Cheema, J., Vigouroux, M., Hill, L., Reed, J., Paajanen, P., Yant, L., Osbourn, A., 2020. Formation and diversification of a paradigm biosynthetic gene cluster in plants. Nat. Commun. 11, 1–11. https://doi.org/10.1038/s41467-020-19153-6

Ma, J., Hanssen, M., Lundgren, K., Hernández, L., Delatte, T., Ehlert, A., Liu, C.-M., Schluepmann, H., Dröge-Laser, W., Moritz, T., Smeekens, S., Hanson, J., 2011. The sucrose-regulated Arabidopsis transcription factor bZIP11 reprograms metabolism and regulates trehalose metabolism. New Phytol. 191, 733–745. https://doi.org/10.1111/j.1469-8137.2011.03735.x

Ma, X., Lv, S., Zhang, C., Yang, C., 2013. Histone deacetylases and their functions in plants. Plant Cell Rep. 32, 465–478. https://doi.org/10.1007/s00299-013-1393-6

Malitsky, S., Blum, E., Less, H., Venger, I., Elbaz, M., Morin, S., Eshed, Y., Aharoni, A., 2008. The Transcript and Metabolite Networks Affected by the Two Clades of Arabidopsis Glucosinolate Biosynthesis Regulators. Plant Physiol. 148, 2021–2049. https://doi.org/10.1104/pp.108.124784

Malka, S.K., Cheng, Y., 2017. Possible Interactions between the Biosynthetic Pathways of Indole Glucosinolate and Auxin. Front. Plant Sci. 0. https://doi.org/10.3389/fpls.2017.02131

Marques, J.P., Dudeck, I., Klösgen, R.B., 2003. Targeting of EGFP chimeras within chloroplasts. Mol. Genet. Genomics 269, 381–387. https://doi.org/10.1007/s00438-003-0846-y

Martínez-Ballesta, M. del C., Moreno, D.A., Carvajal, M., 2013. The Physiological Importance of Glucosinolates on Plant Response to Abiotic Stress in Brassica. Int. J. Mol. Sci. 14, 11607. https://doi.org/10.3390/ijms140611607

Masuda, T., Fujita, Y., 2008. Regulation and evolution of chlorophyll metabolism. Photochem. Photobiol. Sci. 7, 1131–1149. https://doi.org/10.1039/b807210h

Matsumoto, F., Obayashi, T., Sasaki-Sekimoto, Y., Ohta, H., Takamiya, K., Masuda, T., 2004. Gene Expression Profiling of the Tetrapyrrole Metabolic Pathway in Arabidopsis with a Mini-Array System. Plant Physiol. 135, 2379–2391. https://doi.org/10.1104/pp.104.042408

McCormac, A.C., Terry, M.J., 2002. Light-signalling pathways leading to the co-ordinated expression of HEMA1 and Lhcb during chloroplast development in Arabidopsis thaliana. Plant J. 32, 549–559. https://doi.org/10.1046/j.1365-313X.2002.01443.x

McCully, M.E., Miller, C., Sprague, S.J., Huang, C.X., Kirkegaard, J.A., 2008. Distribution of glucosinolates and sulphur-rich cells in roots of field-grown canola (Brassica napus). New Phytol. 180, 193–205. https://doi.org/10.1111/j.1469-8137.2008.02520.x

Mehdi, S., Derkacheva, M., Ramström, M., Kralemann, L., Bergquist, J., Hennig, L., 2016. The WD40 Domain Protein MSI1 Functions in a Histone Deacetylase Complex to Fine-Tune Abscisic Acid Signaling. Plant Cell 28, 42–54. https://doi.org/10.1105/tpc.15.00763

Meijering, E., Jacob, M., Sarria, J.-C.F., Steiner, P., Hirling, H., Unser, M., 2004. Design and validation of a tool for neurite tracing and analysis in fluorescence microscopy images. Cytometry A 58A, 167–176. https://doi.org/10.1002/cyto.a.20022

Mhamdi, A., Noctor, G., Baker, A., 2012. Plant catalases: Peroxisomal redox guardians. Arch. Biochem. Biophys. 525, 181–194. https://doi.org/10.1016/j.abb.2012.04.015

Miao, H., Wei, J., Zhao, Y., Yan, H., Sun, B., Huang, J., Wang, Q., 2013. Glucose signalling positively regulates aliphatic glucosinolate biosynthesis. J. Exp. Bot. 64, 1097–1109. https://doi.org/10.1093/jxb/ers399

Mikkelsen, M.D., Naur, P., Halkier, B.A., 2004. Arabidopsis mutants in the C–S lyase of glucosinolate biosynthesis establish a critical role for indole-3-acetaldoxime in auxin homeostasis. Plant J. 37, 770–777. https://doi.org/10.1111/j.1365-313X.2004.02002.x

Mikkelsen, M.D., Petersen, B.L., Glawischnig, E., Jensen, A.B., Andreasson, E., Halkier, B.A., 2003. Modulation of CYP79 Genes and Glucosinolate Profiles in Arabidopsis by Defense Signaling Pathways. Plant Physiol. 131, 298. https://doi.org/10.1104/pp.011015

Ried, M.K., Wild, R., Zhu, J. *et al.* Inositol pyrophosphates promote the interaction of SPX domains with the coiled-coil motif of PHR transcription factors to regulate plant phosphate homeostasis. *Nat Commun* 12, 384 (2021). https://doi.org/10.1038/s41467-020-20681-4

Moon, J., Zhu, L., Shen, H., Huq, E., 2008. PIF1 directly and indirectly regulates chlorophyll biosynthesis to optimize the greening process in Arabidopsis | Proceedings of the National Academy of Sciences [WWW Document]. PNAS. URL https://www.pnas.org/doi/abs/10.1073/pnas.0803611105 (accessed 6.2.22).

Müller, J., Toev, T., Heisters, M., Teller, J., Moore, K.L., Hause, G., Dinesh, D.C., Bürstenbinder, K., Abel, S., 2015. Iron-Dependent Callose Deposition Adjusts Root Meristem Maintenance to Phosphate Availability. Dev. Cell 33, 216–230. https://doi.org/10.1016/j.devcel.2015.02.007

Müller, R., de Vos, M., Sun, J.Y., Sønderby, I.E., Halkier, B.A., Wittstock, U., Jander, G., 2010. Differential Effects of Indole and Aliphatic Glucosinolates on Lepidopteran Herbivores. J. Chem. Ecol. 36, 905–913. https://doi.org/10.1007/s10886-010-9825-z

Nakamura, H., Muramatsu, M., Hakata, M., Ueno, O., Nagamura, Y., Hirochika, H., Takano, M., Ichikawa, H., 2009. Ectopic Overexpression of The Transcription Factor OsGLK1 Induces Chloroplast Development in Non-Green Rice Cells. Plant Cell Physiol. 50, 1933–1949. https://doi.org/10.1093/pcp/pcp138

Naumann, C., Heisters, M., Brandt, W., Janitza, P., Alfs, C., Tang, N., Toto Nienguesso, A., Ziegler, J., Imre, R., Mechtler, K., Dagdas, Y., Hoehenwarter, W., Sawers, G., Quint, M., Abel, S., 2022. Bacterial-type ferroxidase tunes iron-dependent phosphate sensing during Arabidopsis root development. Curr. Biol. S0960982222005747. https://doi.org/10.1016/j.cub.2022.04.005

Naur, P., Petersen, B.L., Mikkelsen, M.D., Bak, S., Rasmussen, H., Olsen, C.E., Halkier, B.A., 2003. CYP83A1 and CYP83B1, Two Nonredundant Cytochrome P450 Enzymes Metabolizing Oximes in the Biosynthesis of Glucosinolates in Arabidopsis. Plant Physiol. 133, 63–72. https://doi.org/10.1104/pp.102.019240

Newman, R.M., Hanscom, Z., Kerfoot, W.C., 1992. The watercress glucosinolate-myrosinase system: a feeding deterrent to caddisflies, snails and amphipods. Oecologia 92, 1–7. https://doi.org/10.1007/BF00317255

Robertson NG, Lu L, Heller S, Merchant SN, Eavey RD, McKenna M, Nadol JB Jr, Miyamoto RT, Linthicum FH Jr, Lubianca Neto JF, Hudspeth AJ, Seidman CE, Morton CC, Seidman JG. Mutations in a novel cochlear gene cause DFNA9, a human nonsyndromic deafness with vestibular dysfunction. Nat Genet. 1998 Nov;20(3):299-303. doi: 10.1038/3118. PMID: 9806553.

Nimmo, H.G., 2003. Control of the phosphorylation of phosphoenolpyruvate carboxylase in higher plants. Arch. Biochem. Biophys. 414, 189–196. https://doi.org/10.1016/S0003-9861(03)00115-2

Nimmo, H.G., Fontaine, V., Hartwell, J., Jenkins, G.I., Nimmo, G.A., Wilkins, M.B., 2001. PEP carboxylase kinase is a novel protein kinase controlled at the level of expression. New Phytol. 151, 91–97. https://doi.org/10.1046/j.1469-8137.2001.00155.x

Ning, Y.-Q., Chen, Q., Lin, R.-N., Li, Y.-Q., Li, L., Chen, S., He, X.-J., 2019. The HDA19 histone deacetylase complex is involved in the regulation of flowering time in a photoperiod-dependent manner. Plant J. 98, 448–464. https://doi.org/10.1111/tpj.14229

Nintemann, S.J., Hunziker, P., Andersen, T.G., Schulz, A., Burow, M., Halkier, B.A., 2018. Localization of the glucosinolate biosynthetic enzymes reveals distinct spatial patterns for the biosynthesis of indole and aliphatic glucosinolates. Physiol. Plant. 163, 138–154. https://doi.org/10.1111/ppl.12672

Nour-Eldin Hh, Andersen Tg, Burow M, Madsen Sr, Jørgensen Me, Ce, O., I, D., R, H., D, G., Ba, H., 2012. NRT/PTR transporters are essential for translocation of glucosinolate defence compounds to seeds. Nature 488. https://doi.org/10.1038/nature11285

Nützmann, H.-W., Osbourn, A., 2015. Regulation of metabolic gene clusters in Arabidopsis thaliana. New Phytol. 205, 503. https://doi.org/10.1111/nph.13189

Nützmann, H.-W., Scazzocchio, C., Osbourn, A., 2018. Metabolic Gene Clusters in Eukaryotes. Annu. Rev. Genet. 52, 159–183. https://doi.org/10.1146/annurev-genet-120417-031237

Oborník, M., Green, B.R., 2005. Mosaic Origin of the Heme Biosynthesis Pathway in Photosynthetic Eukaryotes. Mol. Biol. Evol. 22, 2343–2353. https://doi.org/10.1093/molbev/msi230

Osterlund, M.T., Hardtke, C.S., Wei, N., Deng, X.W., 2000. Targeted destabilization of HY5 during light-regulated development of Arabidopsis. Nature 405, 462–466. https://doi.org/10.1038/35013076

Pacheco, A.G., Alcantara, A.F.C., V. G. C. Abreu, Corrêa, G.M., 2012. Relationships Between Chemical Structure and Activity of Triterpenes Against Gram-Positive and Gram-Negative Bacteria, in: A Search for Antibacterial Agents. InTech. https://doi.org/10.5772/45649

Paddock, T.N., Mason, M.E., Lima, D.F., Armstrong, G.A., 2010. Arabidopsis protochlorophyllide oxidoreductase A (PORA) restores bulk chlorophyll synthesis and normal development to a porB porC double mutant. Plant Mol. Biol. 72, 445–457. https://doi.org/10.1007/s11103-009-9582-y

Pandey, R., Müller, A., Napoli, C.A., Selinger, D.A., Pikaard, C.S., Richards, E.J., Bender, J., Mount, D.W., Jorgensen, R.A., 2002. Analysis of histone acetyltransferase and histone deacetylase families of Arabidopsis thaliana suggests functional diversification of chromatin modification among multicellular eukaryotes. Nucleic Acids Res. 30, 5036–5055. https://doi.org/10.1093/nar/gkf660

Pant, B.-D., Pant, P., Erban, A., Huhman, D., Kopka, J., Scheible, W.-R., 2015. Identification of primary and secondary metabolites with phosphorus status-dependent abundance in Arabidopsis, and of the transcription factor PHR1 as a major regulator of metabolic changes during phosphorus limitation. Plant Cell Environ. 38, 172–187. https://doi.org/10.1111/pce.12378

Papenbrock, J., Grimm, B., 2001. Regulatory network of tetrapyrrole biosynthesis – studies of intracellular signalling involved in metabolic and developmental control of plastids. Planta 213, 667–681. https://doi.org/10.1007/s004250100593

Papenbrock, J., Mock, H.-P., Kruse, E., Grimm, B., 1999. Expression studies in tetrapyrrole biosynthesis: inverse maxima of magnesium chelatase and ferrochelatase activity during cyclic photoperiods | SpringerLink [WWW Document]. URL https://link.springer.com/article/10.1007/s004250050558 (accessed 6.2.22).

Park, J., Lim, C.J., Shen, M., Park, H.J., Cha, J.Y., Iniesto, E., Rubio, V., Mengiste, T., Zhu, J.K., Bressan, R.A., et al. (2018). Epigenetic switch from repressive to permissive chromatin in response to cold stress. Proc Natl Acad Sci USA 115, E5400–E5409.

Péret, B., Desnos, T., Jost, R., Kanno, S., Berkowitz, O., Nussaume, L., 2014. Root Architecture Responses: In Search of Phosphate. Plant Physiol. 166, 1713–1723. https://doi.org/10.1104/pp.114.244541

Perrella, G., Carr, C., Asensi-Fabado, M.A., Donald, N.A., Páldi, K., Hannah, M.A., Amtmann, A., 2016. The Histone Deacetylase Complex 1 Protein of Arabidopsis Has the Capacity to Interact with Multiple Proteins Including Histone 3-Binding Proteins and Histone 1 Variants. Plant Physiol. 171, 62–70. https://doi.org/10.1104/pp.15.01760

Perrella, G., Lopez-Vernaza, M.A., Carr, C., Sani, E., Gosselé, V., Verduyn, C., Kellermeier, F., Hannah, M.A., Amtmann, A., 2013. Histone Deacetylase Complex1 Expression Level Titrates Plant Growth and Abscisic Acid Sensitivity in Arabidopsis. Plant Cell 25, 3491–3505. https://doi.org/10.1105/tpc.113.114835

Pfalz, M., Mikkelsen, M.D., Bednarek, P., Olsen, C.E., Halkier, B.A., Kroymann, J., 2011. Metabolic Engineering in Nicotiana benthamiana Reveals Key Enzyme Functions in Arabidopsis Indole Glucosinolate Modification. Plant Cell 23, 716–729. https://doi.org/10.1105/tpc.110.081711

Pfalz, M., Mukhaimar, M., Perreau, F., Kirk, J., Hansen, C.I.C., Olsen, C.E., Agerbirk, N., Kroymann, J., 2016. Methyl Transfer in Glucosinolate Biosynthesis Mediated by Indole Glucosinolate *O* -Methyltransferase 5. Plant Physiol. 172, 2190–2203. https://doi.org/10.1104/pp.16.01402

Pfalz, M., Vogel, H., Kroymann, J., 2009. The Gene Controlling the Indole Glucosinolate Modifier1 Quantitative Trait Locus Alters Indole Glucosinolate Structures and Aphid Resistance in Arabidopsis. Plant Cell 21, 985–999. https://doi.org/10.1105/tpc.108.063115

Piotrowski, M., Schemenewitz, A., Lopukhina, A., Müller, A., Janowitz, T., Weiler, E.W., Oecking, C., 2004. Desulfoglucosinolate Sulfotransferases from Arabidopsis thaliana Catalyze the Final Step in the Biosynthesis of the Glucosinolate Core Structure *. J. Biol. Chem. 279, 50717–50725. https://doi.org/10.1074/jbc.M407681200

Piślewska-Bednarek, M., Nakano, R.T., Hiruma, K., Pastorczyk, M., Sanchez-Vallet, A., Singkaravanit-Ogawa, S., Ciesiołka, D., Takano, Y., Molina, A., Schulze-Lefert, P., Bednarek, P., 2018. Glutathione Transferase U13 Functions in Pathogen-Triggered Glucosinolate Metabolism. Plant Physiol. 176, 538–551. https://doi.org/10.1104/pp.17.01455

Plaxton, W.C., Podestá, F.E., 2006. The Functional Organization and Control of Plant Respiration. Crit. Rev. Plant Sci. 25, 159–198. https://doi.org/10.1080/07352680600563876

Plaxton, W.C., Tran, H.T., 2011. Metabolic Adaptations of Phosphate-Starved Plants1. Plant Physiol. 156, 1006–1015. https://doi.org/10.1104/pp.111.175281

Porter, N.J., Christianson, D.W., 2019. Structure, Mechanism, and Inhibition of the Zinc-Dependent Histone Deacetylases. Curr. Opin. Struct. Biol. 59, 9. https://doi.org/10.1016/j.sbi.2019.01.004

Pospíšil, P., 2016. Production of Reactive Oxygen Species by Photosystem II as a Response to Light and Temperature Stress. Front. Plant Sci. 0. https://doi.org/10.3389/fpls.2016.01950

Possenti, M., Baima, S., Raffo, A., Durazzo, A., Giusti, A.M., Natella, F., 2017. Glucosinolates in Food. Glucosinolates 87–132. https://doi.org/10.1007/978-3-319-25462-3_4

Powell, A.L.T., Nguyen, C.V., Hill, T., Cheng, K.L., Figueroa-Balderas, R., Aktas, H., Ashrafi, H., Pons, C., Fernández-Muñoz, R., Vicente, A., Lopez-Baltazar, J., Barry, C.S., Liu, Y., Chetelat, R., Granell, A., Deynze, A.V., Giovannoni, J.J., Bennett, A.B., 2012. Uniform ripening Encodes a Golden 2-like Transcription Factor Regulating Tomato Fruit Chloroplast Development. Science. https://doi.org/10.1126/science.1222218

Poza-Viejo, L., Olmo, I. del, Crevillén, P., 2019. Plant Chromatin Immunoprecipitation [WWW Document]. protocols.io. URL https://www.protocols.io/view/plant-chromatin-immunoprecipitation-444gyyw (accessed 7.29.22).

Quail, P.H., 2002. Photosensory perception and signalling in plant cells: new paradigms? Curr. Opin. Cell Biol. 14, 180–188. https://doi.org/10.1016/S0955-0674(02)00309-5

Rakpenthai, A., Apodiakou, A., Whitcomb, S.J., Hoefgen, R., 2022. In silico analysis of cis-elements and identification of transcription factors putatively involved in the regulation of the OAS cluster genes SDI1 and SDI2. Plant J. 110, 1286–1304. https://doi.org/10.1111/tpj.15735

Rantala, M., Rantala, S., Aro, E.-M., 2020. Composition, phosphorylation and dynamic organization of photosynthetic protein complexes in plant thylakoid membrane. Photochem. Photobiol. Sci. 19, 604–619. https://doi.org/10.1039/D0PP00025F

Rao, I.M., Fredeen, A.L., Terry, N., 1990. Leaf Phosphate Status, Photosynthesis, and Carbon Partitioning in Sugar Beet: III. Diurnal Changes in Carbon Partitioning and Carbon Export. Plant Physiol. 92, 29–36. https://doi.org/10.1104/pp.92.1.29

Reyt, G., Boudouf, S., Boucherez, J., Gaymard, F., Briat, J.-F., 2015. Iron- and Ferritin-Dependent Reactive Oxygen Species Distribution: Impact on Arabidopsis Root System Architecture. Mol. Plant 8, 439–453. https://doi.org/10.1016/j.molp.2014.11.014

Rouached, H., Secco, D., Arpat, B., Poirier, Y., 2011. The transcription factor PHR1 plays a key role in the regulation of sulfate shoot-to-root flux upon phosphate starvation in Arabidopsis. BMC Plant Biol. 11, 19. https://doi.org/10.1186/1471-2229-11-19

Ruijter, A.J.M. de, Gennip, A.H. van, Caron, H.N., Kemp, S., Kuilenburg, A.B.P. van, 2003. Histone deacetylases (HDACs): characterization of the classical HDAC family. Biochem. J. 370, 737. https://doi.org/10.1042/BJ20021321

Ruiz-Roig, C., Viéitez, C., Posas, F., de Nadal, E., 2010. The Rpd3L HDAC complex is essential for the heat stress response in yeast. Mol. Microbiol. 76, 1049–1062. https://doi.org/10.1111/j.1365-2958.2010.07167.x

Saijo, Y., Sullivan, J.A., Wang, H., Yang, J., Shen, Y., Rubio, V., Ma, L., Hoecker, U., Deng, X.W., 2003. The COP1–SPA1 interaction defines a critical step in phytochrome A-mediated regulation of HY5 activity. Genes Dev. 17, 2642. https://doi.org/10.1101/gad.1122903

Salazar-Henao, J.E., Vélez-Bermúdez, I.C., Schmidt, W., 2016. The regulation and plasticity of root hair patterning and morphogenesis. Development 143, 1848–1858. https://doi.org/10.1242/dev.132845

Sanchez-Vallet, A., Ramos, B., Bednarek, P., López, G., Piślewska-Bednarek, M., Schulze-Lefert, P., Molina, A., 2010. Tryptophan-derived secondary metabolites in Arabidopsis thaliana confer non-host resistance to necrotrophic Plectosphaerella cucumerina fungi. Plant J. 63, 115–127. https://doi.org/10.1111/j.1365-313X.2010.04224.x

Sato, A., Miura, K., 2011. Root architecture remodeling induced by phosphate starvation. Plant Signal. Behav. https://doi.org/10.4161/psb.6.8.15752

Sawada, Y., Kuwahara, A., Nagano, M., Narisawa, T., Sakata, A., Saito, K., Yokota Hirai, M., 2009. Omics-Based Approaches to Methionine Side Chain Elongation in Arabidopsis: Characterization of the Genes Encoding Methylthioalkylmalate Isomerase and Methylthioalkylmalate Dehydrogenase. Plant Cell Physiol. 50, 1181–1190. https://doi.org/10.1093/pcp/pcp079

Schneider, C.A., Rasband, W.S., Eliceiri, K.W., 2012. NIH Image to ImageJ: 25 years of image analysis. Nat. Methods 9, 671–675. https://doi.org/10.1038/nmeth.2089

Schnepf, A., Leitner, D., Klepsch, S., Pellerin, S., Mollier, A., 2011. Modelling Phosphorus Dynamics in the Soil–Plant System. Phosphorus Action 113–133. https://doi.org/10.1007/978-3-642-15271-9_5

Schuster, J., Knill, T., Reichelt, M., Gershenzon, J., Binder, S., 2006. BRANCHED-CHAIN AMINOTRANSFERASE4 Is Part of the Chain Elongation Pathway in the Biosynthesis of Methionine-Derived Glucosinolates in Arabidopsis. Plant Cell 18, 2664–2679. https://doi.org/10.1105/tpc.105.039339

Schweizer, F., Fernández-Calvo, P., Zander, M., Diez-Diaz, M., Fonseca, S., Glauser, G., Lewsey, M.G., Ecker, J.R., Solano, R., Reymond, P., 2013. Arabidopsis Basic Helix-Loop-Helix Transcription Factors MYC2, MYC3, and MYC4 Regulate Glucosinolate Biosynthesis, Insect Performance, and Feeding Behavior. Plant Cell 25, 3117. https://doi.org/10.1105/tpc.113.115139

Sequeira-Mendes, J., Aragüez, I., Peiró, R., Mendez-Giraldez, R., Zhang, X., Jacobsen, S.E., Bastolla, U., Gutierrez, C., 2014. The Functional Topography of the *Arabidopsis* Genome Is Organized in a Reduced Number of Linear Motifs of Chromatin States. Plant Cell 26, 2351–2366.
 https://doi.org/10.1105/tpc.114.124578

Shigeto, J., Tsutsumi, Y., 2016. Diverse functions and reactions of class III peroxidases. New Phytol. 209, 1395–1402. https://doi.org/10.1111/nph.13738

Shin, R., Berg, R.H., Schachtman, D.P., 2005. Reactive Oxygen Species and Root Hairs in Arabidopsis Root Response to Nitrogen, Phosphorus and Potassium Deficiency. Plant Cell Physiol. 46, 1350–1357. https://doi.org/10.1093/pcp/pci145

Shogren-Knaak M, Ishii H, Sun Jm, Pazin Mj, Davie Jr, Peterson Cl, 2006. Histone H4-K16 acetylation controls chromatin structure and protein interactions. Science 311.
https://doi.org/10.1126/science.1124000

Shroff, R., Schramm, K., Jeschke, V., Nemes, P., Vertes, A., Gershenzon, J., Svatoš, A., 2015. Quantification of plant surface metabolites by matrix-assisted laser desorption–ionization mass spectrometry imaging: glucosinolates on Arabidopsis thaliana leaves. Plant J. 81, 961–972. https://doi.org/10.1111/tpj.12760

Shroff, R., Vergara, F., Muck, A., Svatoš, A., Gershenzon, J., 2008. Nonuniform distribution of glucosinolates in Arabidopsis thaliana leaves has important consequences for plant defense | Proceedings of the National Academy of Sciences PNAS. URL https://www.pnas.org/doi/abs/10.1073/pnas.0711730105

Smit, S.J., Lichman, B.R., 2022. Plant biosynthetic gene clusters in the context of metabolic evolution. Nat. Prod. Rep. https://doi.org/10.1039/D2NP00005A

Smith, S.E., Jakobsen, I., Grønlund, M., Smith, F.A., 2011. Focus Issue on Phosphorus Plant Physiology: Roles of Arbuscular Mycorrhizas in Plant Phosphorus Nutrition: Interactions between Pathways of Phosphorus Uptake in Arbuscular Mycorrhizal Roots Have Important Implications for Understanding and Manipulating Plant Phosphorus Acquisition. Plant Physiol. 156, 1050.
https://doi.org/10.1104/pp.111.174581

Sønderby, I.E., Burow, M., Rowe, H.C., Kliebenstein, D.J., Halkier, B.A., 2010. A Complex Interplay of Three R2R3 MYB Transcription Factors Determines the Profile of Aliphatic Glucosinolates in Arabidopsis. Plant Physiol. 153, 348–363. https://doi.org/10.1104/pp.109.149286

Sperling, U., Franck, F., van Cleve, B., Frick, G., Apel, K., Armstrong, G.A., 1998. Etioplast Differentiation in Arabidopsis: Both PORA and PORB Restore the Prolamellar Body and Photoactive Protochlorophyllide–F655 to the cop1 Photomorphogenic Mutant. Plant Cell 10, 283–296. https://doi.org/10.1105/tpc.10.2.283

Spurr, A.R., 1969. A low-viscosity epoxy resin embedding medium for electron microscopy. J. Ultrastruct. Res. 26, 31–43. https://doi.org/10.1016/S0022-5320(69)90033-1

Stephenson, P.G., Fankhauser, C., Terry, M.J., 2009. PIF3 is a repressor of chloroplast development | Proceedings of the National Academy of Sciences PNAS.
https://www.pnas.org/doi/abs/10.1073/pnas.0811684106

Sterner, D.E., Berger, S.L., 2000. Acetylation of Histones and Transcription-Related Factors. Microbiol. Mol. Biol. Rev. 64, 435–459. https://doi.org/10.1128/MMBR.64.2.435-459.2000

Stockert, J.C., Horobin, R.W., Colombo, L.L., Blázquez-Castro, A., 2018. Tetrazolium salts and formazan products in Cell Biology: Viability assessment, fluorescence imaging, and labeling perspectives. Acta Histochem. 120, 159–167. https://doi.org/10.1016/j.acthis.2018.02.005

Stratilová, B., Kozmon, S., Stratilová, E., Hrmova, M., 2020. Plant Xyloglucan Xyloglucosyl Transferases and the Cell Wall Structure: Subtle but Significant. Molecules 25. https://doi.org/10.3390/molecules25235619

Su, T., Wang, P., Li, H., Zhao, Yiwu, Lu, Y., Dai, P., Ren, T., Wang, X., Li, X., Shao, Q., Zhao, D., Zhao, Yanxiu, Ma, C., 2018. The Arabidopsis catalase triple mutant reveals important roles of catalases and peroxisome-derived signaling in plant development. J. Integr. Plant Biol. 60, 591–607. https://doi.org/10.1111/jipb.12649

Sudan, J., Raina, M., Singh, R., 2018. Plant epigenetic mechanisms: role in abiotic stress and their generational heritability. 3 Biotech 8, 172. https://doi.org/10.1007/s13205-018-1202-6

Svistoonoff, S., Creff, A., Reymond, M., Sigoillot-Claude, C., Ricaud, L., Blanchet, A., Nussaume, L., Desnos, T., 2007. Root tip contact with low-phosphate media reprograms plant root architecture. Nat. Genet. 39, 792–796. https://doi.org/10.1038/ng2041

Takahashi, A., Takeda, K., Ohnishi, T., 1991. Light-Induced Anthocyanin Reduces the Extent of Damage to DNA in UV-Irradiated Centaurea cyanus Cells in Culture. Plant Cell Physiol. 32, 541–547. https://doi.org/10.1093/oxfordjournals.pcp.a078113

Textor, S., de Kraker, J.-W., Hause, B., Gershenzon, J., Tokuhisa, J.G., 2007. MAM3 Catalyzes the Formation of All Aliphatic Glucosinolate Chain Lengths in Arabidopsis. Plant Physiol. 144, 60–71. https://doi.org/10.1104/pp.106.091579

Thangstad Op, Gilde B, Chadchawan S, Seem M, Husebye H, Bradley D, Bones Am, 2004. Cell specific, cross-species expression of myrosinases in Brassica napus, Arabidopsis thaliana and Nicotiana tabacum. Plant Mol. Biol. 54. https://doi.org/10.1023/B:PLAN.0000038272.99590.10

Thibaud, M.-C., Arrighi, J.-F., Bayle, V., Chiarenza, S., Creff, A., Bustos, R., Paz-Ares, J., Poirier, Y., Nussaume, L., 2010. Dissection of local and systemic transcriptional responses to phosphate starvation in Arabidopsis. Plant J. 64, 775–789. https://doi.org/10.1111/j.1365-313X.2010.04375.x

Tian, T., Liu, Y., Yan, H., You, Q., Yi, X., Du, Z., Xu, W., Su, Z., 2017. agriGO v2.0: a GO analysis toolkit for the agricultural community, 2017 update. Nucleic Acids Res. 45, W122. https://doi.org/10.1093/nar/gkx382

Tianyi, Z., Cooper, S., Brockdorff, N., 2015. The interplay of histone modifications – writers that read. EMBO Rep. 16, 1467–1481. https://doi.org/10.15252/embr.201540945

Ticconi, C., Abel, S., 2004. Short on phosphate: plant surveillance and countermeasures. Trends Plant Sci. 9, 548–555. https://doi.org/10.1016/j.tplants.2004.09.003

Ticconi, C.A., Lucero, R.D., Sakhonwasee, S., Adamson, A.W., Creff, A., Nussaume, L., Desnos, T., Abel, S., 2009. ER-resident proteins PDR2 and LPR1 mediate the developmental response of root meristems to phosphate availability. Proc. Natl. Acad. Sci. 106, 14174–14179.
 https://doi.org/10.1073/pnas.0901778106

Tokizawa, M., Kobayashi, Y., Saito, T., Kobayashi, M., Iuchi, S., Nomoto, M., Tada, Y., Yamamoto, Y.Y., Koyama, H., 2015. SENSITIVE TO PROTON RHIZOTOXICITY1, CALMODULIN BINDING TRANSCRIPTION ACTIVATOR2, and Other Transcription Factors Are Involved in ALUMINUM-ACTIVATED MALATE TRANSPORTER1 Expression. Plant Physiol. 167, 991–1003. https://doi.org/10.1104/pp.114.256552

Trexler, M., Bányai, L., Patthy, L., 2000. The LCCL module. Eur. J. Biochem. 267, 5751–5757. https://doi.org/10.1046/j.1432-1327.2000.01641.x

Triantaphylidès, C., Havaux, M., 2009. Singlet oxygen in plants: production, detoxification and signaling. Trends Plant Sci. 14, 219–228. https://doi.org/10.1016/j.tplants.2009.01.008

Troufflard, S., Mullen, W., Larson, T.R., Graham, I.A., Crozier, A., Amtmann, A., Armengaud, P., 2010. Potassium deficiency induces the biosynthesis of oxylipins and glucosinolates in Arabidopsis thaliana. BMC Plant Biol. 10, 1–13. https://doi.org/10.1186/1471-2229-10-172

Tzvetkova-Chevolleau, T., Franck, F., Alawady, A.E., Dall'Osto, L., Carrière, F., Bassi, R., Grimm, B., Nussaume, L., Havaux, M., 2007. The light stress-induced protein ELIP2 is a regulator of chlorophyll synthesis in Arabidopsis thaliana. Plant J. 50, 795–809. https://doi.org/10.1111/j.1365-313X.2007.03090.x

U. K. Laemmli, 1970. Cleavage of Structural Proteins during the Assembly of the Head of Bacteriophage T4 | Nature [WWW Document]. URL https://www.nature.com/articles/227680a0 (accessed 6.8.22).

Vance, C.P., Uhde-Stone, C., Allan, D.L., 2003. Phosphorus acquisition and use: critical adaptations by plants for securing a nonrenewable resource. New Phytol. 157, 423–447. https://doi.org/10.1046/j.1469-8137.2003.00695.x

Vleesschauwer, D.D., Xu, J., Höfte, M., 2014. Making sense of hormone-mediated defense networking: from rice to Arabidopsis. Front. Plant Sci. 5. https://doi.org/10.3389/fpls.2014.00611

von Arnim, A., Deng, X.-W., 2003. LIGHT CONTROL OF SEEDLING DEVELOPMENT [WWW Document]. http://dx.doi.org/10.1146/annurev.arplant.47.1.215. https://doi.org/10.1146/annurev.arplant.47.1.215

Wang, C., Guo, W., Ye, S., Wei, P., Ow, D.W., 2016. Reduction of Cd in Rice through Expression of OXS3-like Gene Fragments. Mol. Plant 9, 301–304. https://doi.org/10.1016/j.molp.2015.09.006

Wang, P., Grimm, B., 2021. Connecting Chlorophyll Metabolism with Accumulation of the Photosynthetic Apparatus. Trends Plant Sci. 26, 484–495. https://doi.org/10.1016/j.tplants.2020.12.005

Wang, P., Grimm, B., 2015. Organization of chlorophyll biosynthesis and insertion of chlorophyll into the chlorophyll-binding proteins in chloroplasts. Photosynth. Res. 126, 189–202. https://doi.org/10.1007/s11120-015-0154-5

Wang, Z.Y., Kenigsbuch, D., Sun, L., Harel, E., Ong, M.S., Tobin, E.M., 1997. A Myb-related transcription factor is involved in the phytochrome regulation of an Arabidopsis Lhcb gene. Plant Cell 9, 491–507. https://doi.org/10.1105/tpc.9.4.491

Ward, J.T., Lahner, B., Yakubova, E., Salt, D.E., Raghothama, K.G., 2008. The Effect of Iron on the Primary Root Elongation of Arabidopsis during Phosphate Deficiency. Plant Physiol. 147, 1181–1191. https://doi.org/10.1104/pp.108.118562

Wasternack, C., Hause, B., 2013. Jasmonates: biosynthesis, perception, signal transduction and action in plant stress response, growth and development. An update to the 2007 review in Annals of Botany. Ann. Bot. 111, 1021–1058. https://doi.org/10.1093/aob/mct067

Waters, M.T., Wang, P., Korkaric, M., Capper, R.G., Saunders, N.J., Langdale, J.A., 2009. GLK Transcription Factors Coordinate Expression of the Photosynthetic Apparatus in Arabidopsis. Plant Cell 21, 1109–1128. https://doi.org/10.1105/tpc.108.065250

Wentzell, A.M., Rowe, H.C., Hansen, B.G., Ticconi, C., Halkier, B.A., Kliebenstein, D.J., 2007. Linking Metabolic QTLs with Network and cis-eQTLs Controlling Biosynthetic Pathways. PLOS Genet. 3, e162. https://doi.org/10.1371/journal.pgen.0030162

Wilson Ak, Pickett Fb, Turner Jc, Estelle M, 1990. A dominant mutation in Arabidopsis confers resistance to auxin, ethylene and abscisic acid. Mol. Gen. Genet. MGG 222. https://doi.org/10.1007/BF00633843

Wittstock, U., Burow, M., 2010. Glucosinolate Breakdown in Arabidopsis: Mechanism, Regulation and Biological Significance. Arab. Book Am. Soc. Plant Biol. 8. https://doi.org/10.1199/tab.0134

Wickham, H. ggplot2: Elegant Graphics for Data Analysis. Springer-Verlag New York, 2016.

Wu, K., Tian, L., Malik, K., Brown, D., Miki, B., 2000. Functional analysis of HD2 histone deacetylase homologues in Arabidopsis thaliana. Plant J. 22, 19–27. https://doi.org/10.1046/j.1365-313x.2000.00711.x

Xu, J.M., Wang, Z.Q., Wang, J.Y., Li, P.F., Jin, J.F., Chen, W.W., Fan, W., Kochian, L.V., Zheng, S.J., Yang, J.L., 2020. Low phosphate represses histone deacetylase complex1 to regulate root system architecture remodeling in Arabidopsis. New Phytol. 225, 1732–1745. https://doi.org/10.1111/nph.16264

Xu, X., Chi, W., Sun, X., Feng, P., Guo, H., Li, J., Lin, R., Lu, C., Wang, H., Leister, D., Zhang, L., 2016. Convergence of light and chloroplast signals for de-etiolation through ABI4–HY5 and COP1. Nat. Plants 2, 1–7. https://doi.org/10.1038/nplants.2016.66

Yadav, U.P., Ivakov, A., Feil, R., Duan, G.Y., Walther, D., Giavalisco, P., Piques, M., Carillo, P., Hubberten, H.-M., Stitt, M., Lunn, J.E., 2014. The sucrose–trehalose 6-phosphate (Tre6P) nexus: specificity and mechanisms of sucrose signalling by Tre6P. J. Exp. Bot. 65, 1051. https://doi.org/10.1093/jxb/ert457

Yamaguchi, N., Winter, C.M., Wu, M.-F., Kwon, C.S., William, D.A., Wagner, D., 2014. PROTOCOL: Chromatin Immunoprecipitation from Arabidopsis Tissues. Arab. Book 2014. https://doi.org/10.1199/tab.0170

Ye, J., Coulouris, G., Zaretskaya, I., Cutcutache, I., Rozen, S., Madden, T.L., 2012. Primer-BLAST: A tool to design target-specific primers for polymerase chain reaction. BMC Bioinformatics 13, 134. https://doi.org/10.1186/1471-2105-13-134

Yu, B., Xu, C., Benning, C., 2002. *Arabidopsis* disrupted in *SQD2* encoding sulfolipid synthase is impaired in phosphate-limited growth. Proc. Natl. Acad. Sci. 99, 5732–5737. https://doi.org/10.1073/pnas.082696499

Yu, C.-W., Liu, X., Luo, M., Chen, C., Lin, X., Tian, G., Lu, Q., Cui, Y., Wu, K., 2011. HISTONE DEACETYLASE6 Interacts with FLOWERING LOCUS D and Regulates Flowering in Arabidopsis. Plant Physiol. 156, 173–184. https://doi.org/10.1104/pp.111.174417

Zeng, X.-Q., Chow, W.S., Su, L.-J., Peng, X.-X., Peng, C.-L., 2010. Protective effect of supplemental anthocyanins on Arabidopsis leaves under high light. Physiol. Plant. 138, 215–225. https://doi.org/10.1111/j.1399-3054.2009.01316.x

Zhang, Y., Li, B., Huai, D., Zhou, Y., Kliebenstein, D.J., 2015. The conserved transcription factors, MYB115 and MYB118, control expression of the newly evolved benzoyloxy glucosinolate pathway in Arabidopsis thaliana. Front. Plant Sci. 0. https://doi.org/10.3389/fpls.2015.00343

Zhong, S., Zhao, M., Shi, T., Shi, H., An, F., Zhao, Q., Guo, H., 2009. EIN3/EIL1 cooperate with PIF1 to prevent photo-oxidation and to promote greening of Arabidopsis seedlings | Proceedings of the National Academy of Sciences [WWW Document]. PNAS. URL https://www.pnas.org/doi/abs/10.1073/pnas.0907670106 (accessed 6.1.22).

Zhou, C., Zhang, L., Duan, J., Miki, B., Wu, K., 2005. HISTONE DEACETYLASE19 Is Involved in Jasmonic Acid and Ethylene Signaling of Pathogen Response in Arabidopsis. Plant Cell 17, 1196–1204. https://doi.org/10.1105/tpc.104.028514

Zhou, J., Hu, Q., Xiao, X., Yao, D., Ge, S., Ye, J., Li, H., Cai, R., Liu, R., Meng, F., Wang, C., Zhu, J.-K., Lei, M., Xing, W., 2021. Mechanism of phosphate sensing and signaling revealed by rice SPX1-PHR2 complex structure. Nat. Commun. 12, 1–10. https://doi.org/10.1038/s41467-021-27391-5

Zhu, J., Lau, K., Puschmann, R., Harmel, R.K., Zhang, Y., Pries, V., Gaugler, P., Broger, L., Dutta, A.K., Jessen, H.J., Schaaf, G., Fernie, A.R., Hothorn, L.A., Fiedler, D., Hothorn, M., 2019. Two bifunctional inositol pyrophosphate kinases/phosphatases control plant phosphate homeostasis. eLife 8. https://doi.org/10.7554/eLife.43582

# 8 Appendix

## 8.1 Supplementary figures
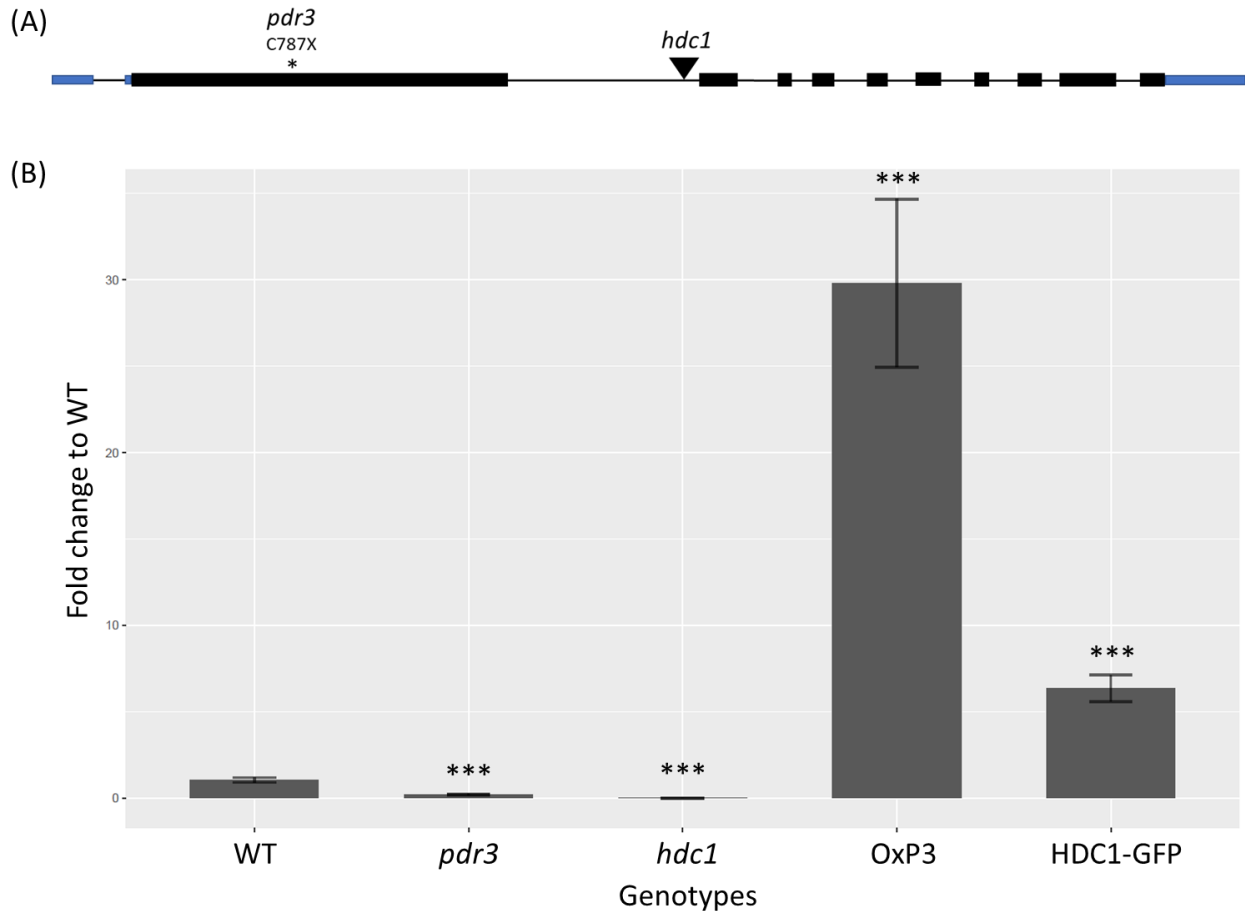


**Suppl. Fig. 1 Mutant alleles of HDC1.**

(A) Genomic map of the HDC1 (AT5G08450.1) locus. Untranslated regions and exons are indicated with blue and black boxes respectively. An asterisk indicate the position of the nonsense point mutation in the first exon of the HDC1 locus in the pdr3 mutant allele, resulting in a truncated protein. The approximate insertion site of the T-DNA in the hdc1 (GABI-Kat 054G03) knockout mutant is indicated with a triangle.

(B) Gene expression of HDC1 in seedlings of the indicated genotypes. Seedlings of WT, pdr3, hdc1 (GABI-Kat 054G03), OxP3 (pdr3/35S::HDC1) and HDC1-GFP (pdr3/HDC1p::HDC1-GFP) genetic background were germinated at +Pi condition. 9-days-old seedlings from each genotype were harvested and used for gene expression analysis with qPCR. Bars represent the means of six biological replicates per genotype from two independent experiments, each containing a pool of ~20 seedlings. Asterisks denote statistically significant differences for each genotype in comparison to WT, as shown by Student's t-test, two-tailed, equal variances (*** $p < 0.001$).
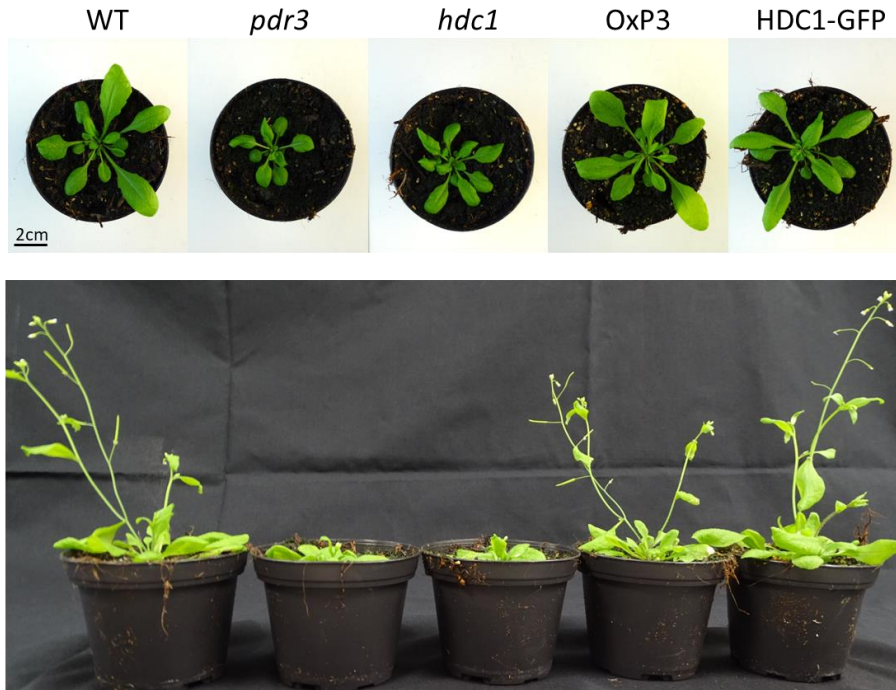
**Suppl. Fig. 2 Loss-of-function mutants of HDC1 show delayed growth and transition to flowering stage.**
*Adult plants of WT, pdr3, hdc1, OxP3 (pdr3/35S::HDC1), HDC1-GFP (pdr3/HDC1p::HDC1-GFP) backgrounds, at 3.5 weeks (upper panel) or at 5 weeks (lower panel) after transfer to soil. Scale bar: 2cm (A).*
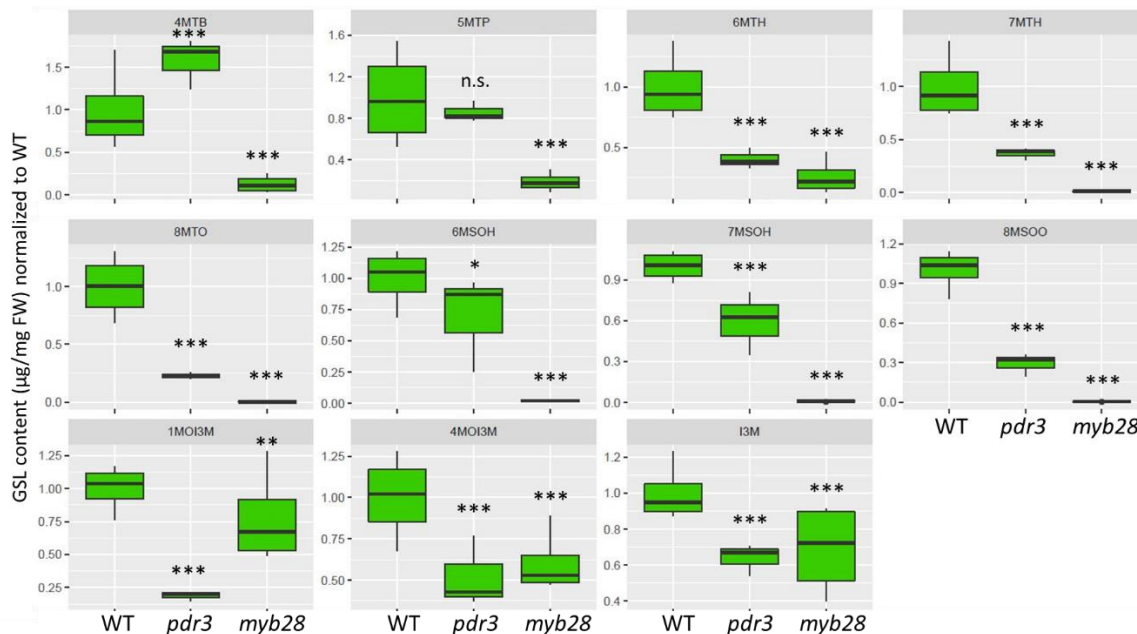


**Suppl. Fig. 3 MYB28 and HDC1 mutants share a similar glucosinolate chemotype.**
*Normalized content of indicated GSLs in roots of 9-days-old WT, pdr3 and myb28 seedlings, grown at +Pi agar plates. The content of each analyte was normalized to fresh weight (FW) and then to the levels detected in WT. Boxplot shows medians, depicted as solid line inside the box, and interquartile ranges from 1 biological experiment with 4 technical replicates, each containing 7-8 roots per genotype. Asterisks denote statistically significant shown by Student's t-test, two-tailed, equal variances (n.s., non-significant; \*\*p < 0.01;\*\*\* p < 0.001).*
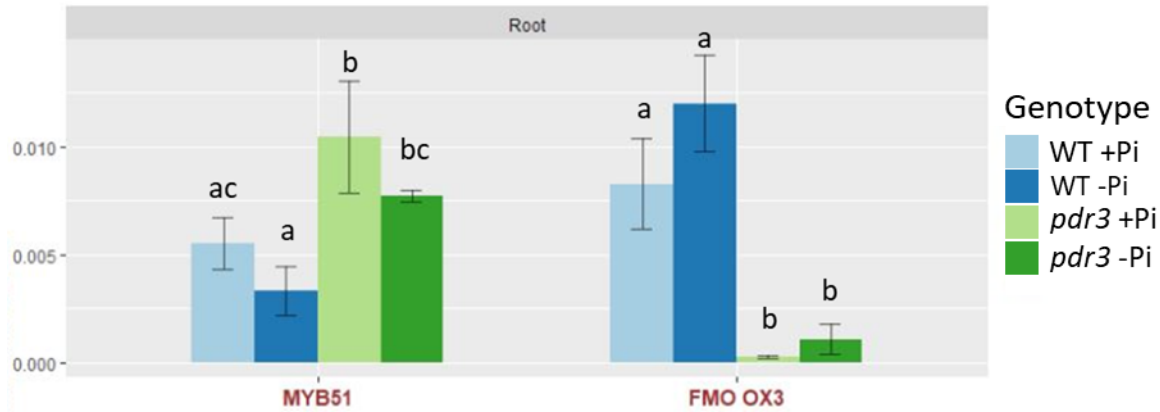
**Suppl. Fig. 4 Short Pi deficiency does not affect expression of MYB51 and FMO-GS$_{OX3}$.**
Gene expression of MYB51 and FMO-GS$_{OX3}$ in Pi starved WT and pdr3 roots. Seedlings were germinated at +Pi for 5-days-old and transferred to +Pi and -Pi conditions. Root material was harvested at 1DAT. Bars represent the means of three biological replicates (±SD), each containing a pool of ~50 roots. Letters denote statistically significant differences for each gene respectively (two-way ANOVA, followed by Tukey's HSD test, p<0.05).
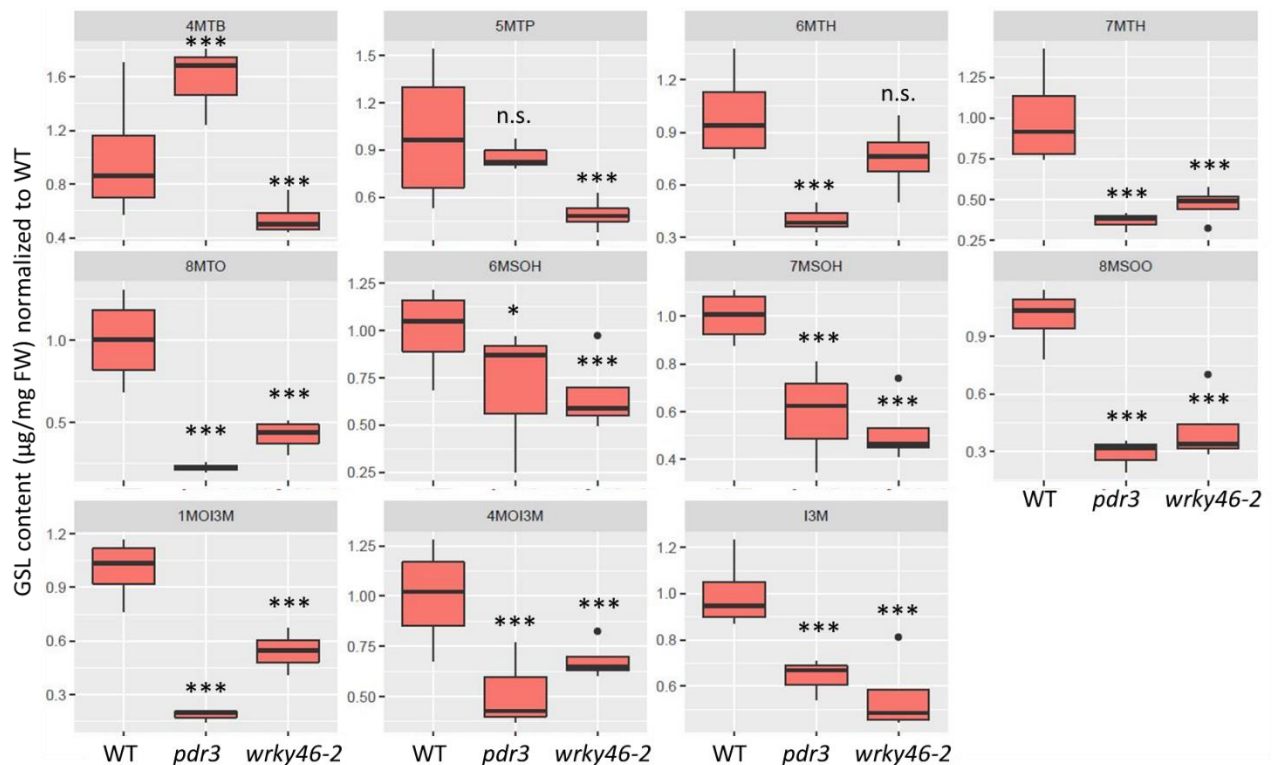


**Suppl. Fig. 5 Wrky46 and pdr3 mutants share a similar glucosinolate chemotype.**
Normalized content of indicated GSLs in roots of 9-days-old WT, pdr3 and wrky46-2 (SAIL_1230_H01) seedlings, grown at +Pi agar plates. The content of each analyte was normalized to fresh weight (FW) and then to the levels detected in WT. Boxplot shows medians, depicted as solid line inside the box, and interquartile ranges from 1 biological experiment with 4 technical replicates, each containing 7-8 roots per genotype. Outliers (> 1.5x interquartile range) are shown as a black dot. Asterisks denote statistically significant shown by Student's t-test, two-tailed, equal variances (n.s., non-significant; **p < 0.01; *** p < 0.001).
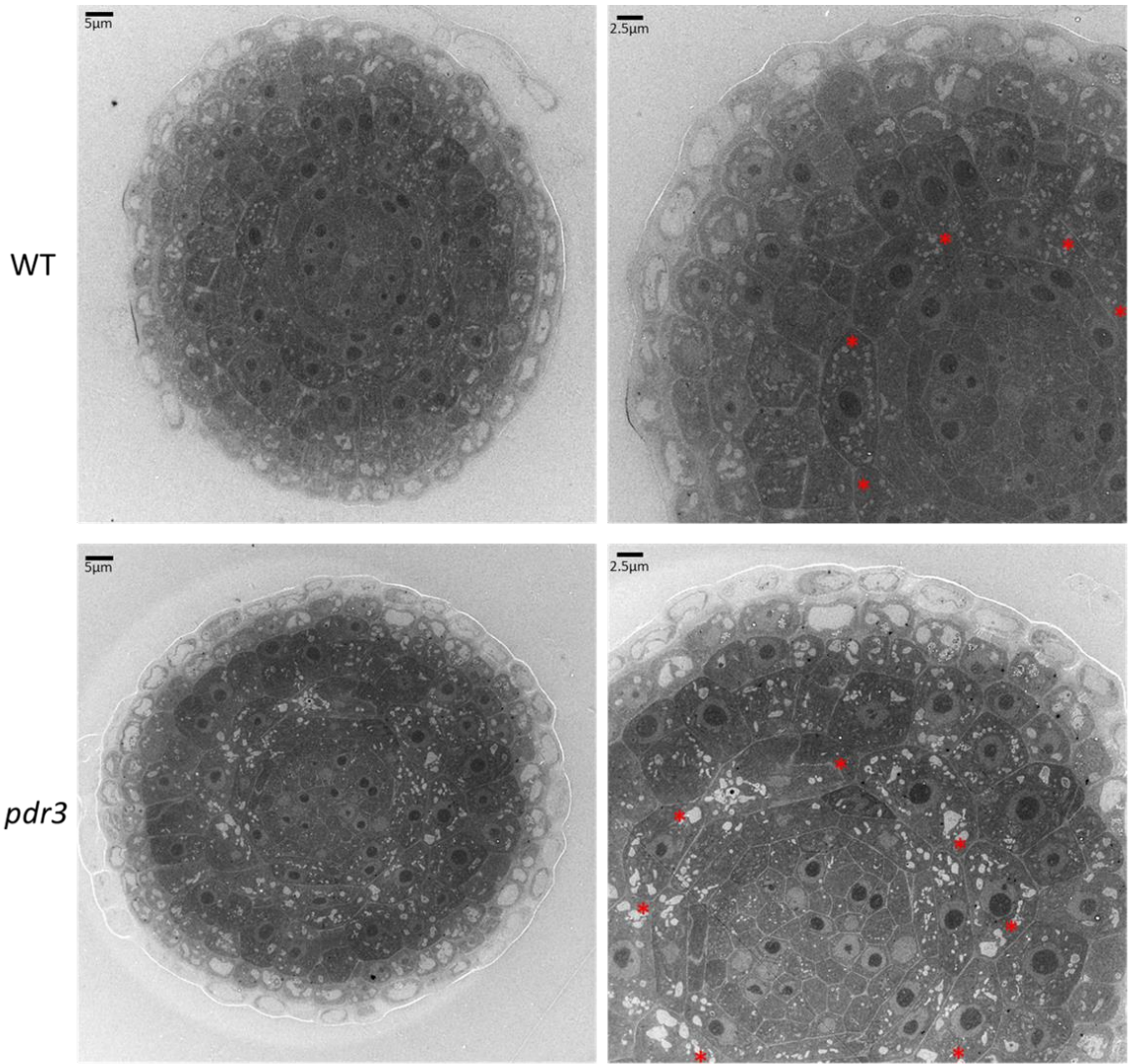
**Suppl. Fig. 6 TEM micrographs of transverse sections of WT and pdr3 apical root tips.**
*9-days-old seedlings of the indicated genotypes grown at + Pi media were used for transmission electron microscopy of plastidial ultrastructure. Red asterisks indicate the cortex layer, where the pdr3-specific specialized plastids were observed. Plastid development was also monitored in the adjacent outer layer (epidermis). Scales: 5µm (left), 2.5µm (right).*
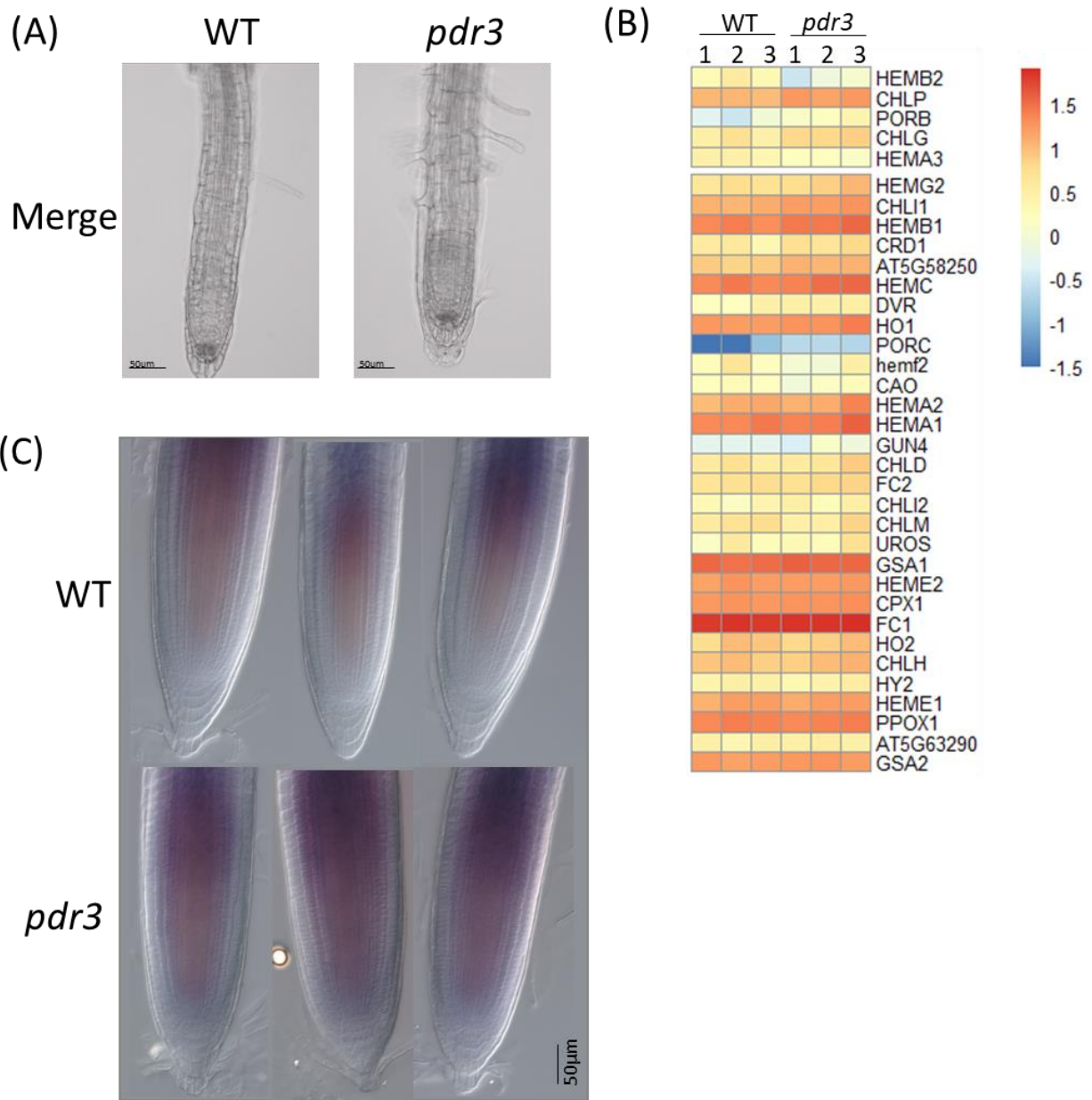
**Suppl. Fig. 7 Loss of HDC1 is interfering with chlorophyll abundance in the root tip in a light-dependent manner.**

(A) Representative confocal images of root tips from 6-days-old dark grown WT and pdr3 seedlings. Both genotypes were germinated in aluminum foil-covered plates and the Chl A-derived autofluorescence was monitored with confocal microscopy. Merged brightfield and chlorophyll channels are depicted.

 (B) Heat map showing the z-scores of the FPKM values among biological replicates (1-3) of genes with an annotated function in chlorophyll biosynthesis in 6-days-old WT and pdr3 root tips.

(C) Representative images from the detection of superoxide in WT and pdr3 root tips. 9-days-old light-grown were stained NBT and accumulation of the dye was assessed macroscopically. Scale bars= 50µm (A and C).
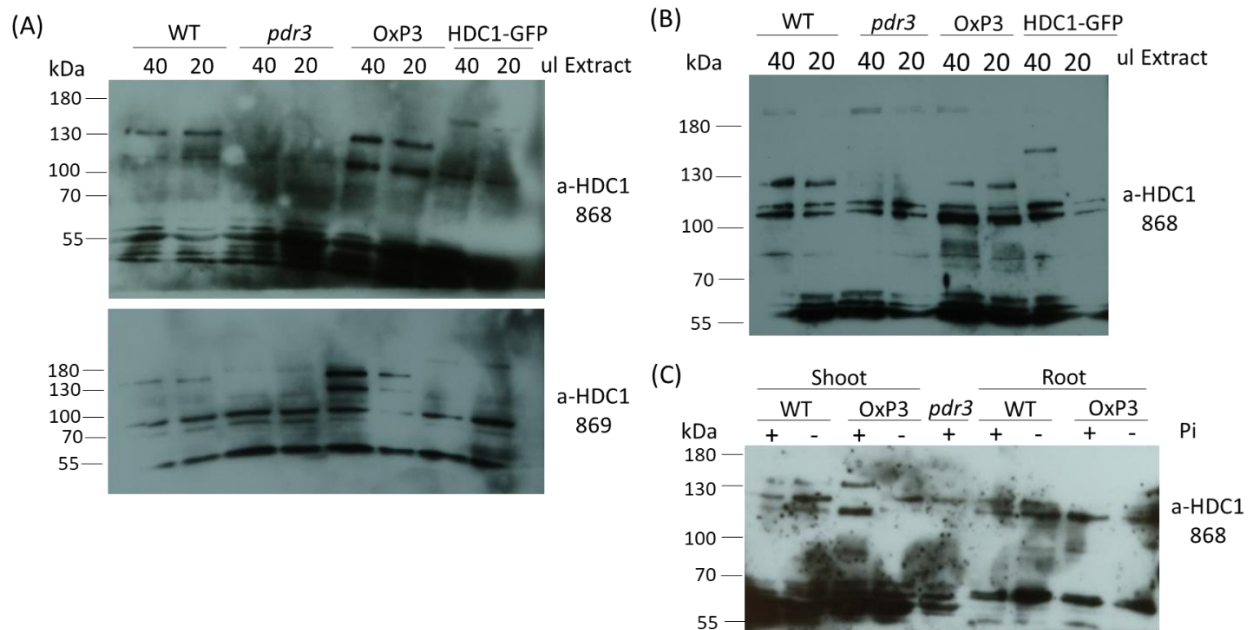
**Suppl. Fig. 8 Antibody characterization and use for HDC1 detection.**
(A) Uncropped photo of Western blot described in Fig. 23C. Ladder bands are not shown.
(B) Western blot for HDC1 detection in protein extracts from WT, pdr3, OxP3 and HDC1-GFP seedlings. 5-days-old seedlings germinated on growth medium with supplemented Pi were transferred to + Pi conditions; samples were harvested 1 DAT. Different volumes of protein extract were loaded on SDS-PAGE, as indicated for each sample, without prior quantification of protein concentration.
(C) Uncropped photo of Western blot described in Fig. 23D. Ladder bands are not shown.

## 8.2 Supplementary tables

*Suppl. Table 1 Significantly enriched GO terms of biological processes in pdr3 root tips, independently of Pi status.*

| GO ID | Term | DEGs in Term | Total mapped DEGs | Total genes in Term | FDR |
|---|---|---|---|---|---|
| GO:0050896 | response to chemical stimulus | 93 | 413 | 4057 | 5E-09 |
| GO:0042221 | photosynthesis | 57 | 413 | 2085 | 2E-07 |
| GO:0015979 | secondary metabolic process | 12 | 413 | 162 | 1E-04 |
| GO:0019748 | response to inorganic substance | 19 | 413 | 489 | 7E-04 |
| GO:0010035 | response to organic substance | 14 | 413 | 279 | 8E-04 |
| GO:0010033 | triterpenoid metabolic process | 34 | 413 | 1342 | 1E-03 |
| GO:0006722 | response to chitin | 5 | 413 | 21 | 1E-03 |
| GO:0010200 | response to abiotic stimulus | 9 | 413 | 151 | 7E-03 |
| GO:0009628 | response to carbohydrate stimulus | 33 | 413 | 1471 | 9E-03 |
| GO:0009743 | response to temperature stimulus | 11 | 413 | 240 | 9E-03 |
| GO:0009266 | response to other organism | 16 | 413 | 485 | 1E-02 |
| GO:0051707 | response to stress | 18 | 413 | 599 | 1E-02 |
| GO:0006950 | photosynthesis, light reaction | 45 | 413 | 2320 | 1E-02 |
| GO:0019684 | response to biotic stimulus | 7 | 413 | 103 | 1E-02 |
| GO:0009607 | response to cold | 18 | 413 | 638 | 2E-02 |
| GO:0009409 | response to oxidative stress | 12 | 413 | 328 | 2E-02 |
| GO:0006979 | terpenoid metabolic process | 12 | 413 | 332 | 2E-02 |
| GO:0006721 | isoprenoid metabolic process | 7 | 413 | 126 | 3E-02 |
| GO:0006720 | response to hormone stimulus | 8 | 413 | 168 | 3E-02 |
| GO:0009725 | response to endogenous stimulus | 23 | 413 | 982 | 3E-02 |
| GO:0009719 | response to metal ion | 24 | 413 | 1068 | 4E-02 |

*Suppl. Table 2 Significantly enriched GO terms of biological processes in pdr3 shoots at control conditions.*

| GO ID | Term | DEGs in Term | Total mapped DEGs | Total genes in Term | FDR |
|---|---|---|---|---|---|
| GO:0010876 | lipid localization | 11 | 675 | 24 | 7E-09 |
| GO:0009664 | plant-type cell wall organization | 16 | 675 | 79 | 7E-09 |
| GO:0050896 | response to stimulus | 127 | 675 | 4057 | 2E-07 |
| GO:0042545 | cell wall modification | 15 | 675 | 123 | 6E-06 |
| GO:0006979 | response to oxidative stress | 23 | 675 | 332 | 2E-05 |
| GO:0006950 | response to stress | 77 | 675 | 2320 | 4E-05 |
| GO:0042221 | response to chemical stimulus | 71 | 675 | 2085 | 5E-05 |
| GO:0009827 | plant-type cell wall modification | 8 | 675 | 50 | 1E-03 |
| GO:0033036 | macromolecule localization | 21 | 675 | 462 | 2E-02 |

| GO:0009828 | plant-type cell wall loosening | 6 | 675 | 40 | 2E-02 |
|---|---|---|---|---|---|
| GO:0006952 | defense response | 29 | 675 | 766 | 2E-02 |
| GO:0009831 | plant-type cell wall modification during multidimensional cell growth | 5 | 675 | 27 | 2E-02 |
| GO:0006869 | lipid transport | 11 | 675 | 163 | 2E-02 |
| GO:0042547 | cell wall modification during multidimensional cell growth | 5 | 675 | 29 | 2E-02 |
| GO:0019748 | secondary metabolic process | 21 | 675 | 489 | 2E-02 |
| GO:0009404 | toxin metabolic process | 6 | 675 | 53 | 3E-02 |
| GO:0009407 | toxin catabolic process | 6 | 675 | 53 | 3E-02 |
| GO:0051179 | localization | 55 | 675 | 1922 | 3E-02 |
| GO:0006810 | transport | 53 | 675 | 1846 | 4E-02 |
| GO:0051234 | establishment of localization | 53 | 675 | 1851 | 4E-02 |

*Suppl. Table 3 Significantly enriched GO terms of biological processes in pdr3 roots at control conditions.*

| GO ID | Term | DEGs in Term | Total mapped DEGs | Total genes in Term | FDR |
|---|---|---|---|---|---|
| GO:0019748 | secondary metabolic process | 43 | 805 | 489 | 9E-11 |
| GO:0016144 | S-glycoside biosynthetic process | 12 | 805 | 41 | 3E-07 |
| GO:0019758 | glycosinolate biosynthetic process | 12 | 805 | 41 | 3E-07 |
| GO:0019761 | glucosinolate biosynthetic process | 12 | 805 | 41 | 3E-07 |
| GO:0016138 | glycoside biosynthetic process | 15 | 805 | 79 | 3E-07 |
| GO:0016137 | glycoside metabolic process | 16 | 805 | 104 | 8E-07 |
| GO:0016143 | S-glycoside metabolic process | 13 | 805 | 62 | 8E-07 |
| GO:0019760 | glucosinolate metabolic process | 13 | 805 | 62 | 8E-07 |
| GO:0010876 | lipid localization | 9 | 805 | 24 | 3E-06 |
| GO:0050896 | response to stimulus | 135 | 805 | 4057 | 3E-05 |
| GO:0044272 | sulfur compound biosynthetic process | 14 | 805 | 115 | 7E-05 |
| GO:0034637 | cellular carbohydrate biosynthetic process | 17 | 805 | 177 | 9E-05 |
| GO:0016051 | carbohydrate biosynthetic process | 20 | 805 | 277 | 6E-04 |
| GO:0009607 | response to biotic stimulus | 32 | 805 | 638 | 2E-03 |
| GO:0006722 | triterpenoid metabolic process | 6 | 805 | 21 | 2E-03 |
| GO:0006629 | lipid metabolic process | 38 | 805 | 841 | 2E-03 |
| GO:0044262 | cellular carbohydrate metabolic process | 24 | 805 | 417 | 2E-03 |
| GO:0009404 | toxin metabolic process | 8 | 805 | 53 | 3E-03 |
| GO:0009407 | toxin catabolic process | 8 | 805 | 53 | 3E-03 |
| GO:0006790 | sulfur metabolic process | 16 | 805 | 220 | 3E-03 |
| GO:0051179 | localization | 65 | 805 | 1922 | 2E-02 |
| GO:0051234 | establishment of localization | 63 | 805 | 1851 | 2E-02 |
| GO:0051707 | response to other organism | 27 | 805 | 599 | 2E-02 |
| GO:0006810 | transport | 62 | 805 | 1846 | 2E-02 |

| GO:0006720 | isoprenoid metabolic process | 12 | 805 | 168 | 2E-02 |
| GO:0006721 | terpenoid metabolic process | 10 | 805 | 126 | 3E-02 |
| GO:0009628 | response to abiotic stimulus | 51 | 805 | 1471 | 4E-02 |
| GO:0006950 | response to stress | 73 | 805 | 2320 | 4E-02 |
| GO:0042221 | response to chemical stimulus | 67 | 805 | 2085 | 4E-02 |
| GO:0008610 | lipid biosynthetic process | 21 | 805 | 439 | 4E-02 |
| GO:0008299 | isoprenoid biosynthetic process | 10 | 805 | 135 | 4E-02 |
| GO:0015833 | peptide transport | 7 | 805 | 68 | 4E-02 |
| GO:0006857 | oligopeptide transport | 7 | 805 | 68 | 4E-02 |

*Suppl. Table 4 Overview of the expression of genes participating in triterpenoid biosynthetic gene clusters in pdr3 tissues.*

| BGC | Gene ID | Gene name | Root tips +Pi | | Root tips -Pi | | Roots +Pi | |
|---|---|---|---|---|---|---|---|---|
| | | | $log_2FC$ | padj | log2FC | padj | $log_2FC$ | padj |
| Thalianol | AT5G47980 | BAHD1 | -2.01 | 1E-07 | -0.72 | 3E-01 | -2.01 | 3E-03 |
| | AT5G47990 | CYP705A5 | -2.62 | 9E-27 | -1.93 | 2E-08 | -2.21 | 1E-06 |
| | AT5G48000 | CYP708A2 | -4.66 | 3E-19 | -2.83 | 2E-22 | -2.18 | 1E-05 |
| | AT5G48010 | THAS1 | -4.98 | 3E-72 | -2.89 | 3E-31 | -2.17 | 3E-07 |
| | AT5G47950 | THAA2 | -0.29 | 5E-01 | -0.43 | 2E-01 | -0.80 | 2E-04 |
| | AT3G29250 | SDR4 | -0.31 | 4E-01 | -0.71 | 5E-03 | -1.24 | 4E-16 |
| | AT1G66800 | AT1G66800 | -0.87 | 4E-02 | -1.54 | 2E-03 | -1.92 | 1E-02 |
| | | | | | | | | |
| Marneral | AT5G42600 | MRN1 | -2.23 | 3E-02 | -5.60 | 2E-07 | -3.67 | 6E-04 |
| | AT5G42590 | CYP71A16 | -0.99 | 1E-07 | -1.20 | 3E-09 | -2.03 | 8E-19 |
| | AT5G42580 | CYP705A12 | -1.05 | 5E-02 | -0.29 | 6E-01 | -3.47 | 6E-37 |
| | | | | | | | | |
| Tirucalladienol | AT5G36150 | PEN3 | NA | NA | NA | NA | -2.17 | 2E-02 |
| | AT5G36140 | CYP716A2 | -4.54 | 5E-02 | -3.34 | 3E-01 | -2.33 | 2E-02 |
| | AT5G36130 | AT5G36130 | -5.43 | 5E-01 | -0.29 | 9E-01 | -2.44 | 3E-04 |
| | AT5G36120 | CCB3 | NA | NA | NA | NA | -1.11 | 5E-01 |
| | AT5G36110 | CYP716A1 | NA | NA | NA | NA | 0.18 | 5E-01 |
| | | | | | | | | |
| Arabidiol | AT4G15400 | BIA1 | -1.64 | 3E-04 | -0.90 | 8E-02 | -1.38 | 2E-07 |
| | AT4G15390 | AT4G15390 | -0.34 | 5E-01 | 1.07 | 1E-02 | -0.56 | 2E-03 |
| | AT4G15380 | CYP705A4 | -1.78 | 6E-02 | -1.46 | 5E-02 | -0.93 | 1E-05 |
| | AT4G15370 | BARS1 | -2.21 | 2E-01 | -0.13 | 9E-01 | -0.74 | 6E-01 |
| | AT4G15360 | CYP705A3 | -2.99 | 3E-03 | -3.31 | 8E-05 | -3.83 | 1E-04 |
| | AT4G15350 | CYP705A2 | -0.26 | 7E-01 | -0.35 | 4E-01 | -0.32 | 4E-01 |
| | AT4G15340 | PEN1 | 0.05 | 1E+00 | 2.82 | 3E-04 | 0.50 | 1E-01 |
| | AT4G15330 | CYP705A1 | -0.10 | 9E-01 | 1.86 | 9E-04 | -0.73 | 6E-02 |

*WT and pdr3 seedlings were germinated on +Pi media and transferred to +Pi and -Pi media; root material was collected 1DAT only from +Pi conditions, while root tips were harvested 1DAT from +Pi or -Pi conditions. Transcriptional analysis was performed with RNA-seq. Logarithmic fold change ($log_2FC$) values indicate differences in mean expression of the genes between pdr3 and WT roots across 3 biological replicates, each containing a pool of 50 roots or 150-200 root tips, with negative values signifying lower transcript levels in the mutant at each condition. Adjusted p-values (padj) signify statistically significant changes after adjustment for multiple testing using FDR. NA values signify absence of detected transcripts.*

*Suppl. Table 5 Significantly enriched GO terms of biological processes in Pi-starved WT root tips.*

| GO ID | Term | DEGs in Term | Total mapped DEGs | Total genes in Term | FDR |
|---|---|---|---|---|---|
| GO:0050896 | response to stimulus | 123 | 361 | 6250 | 2E-04 |
| GO:0005991 | trehalose metabolic process | 7 | 361 | 24 | 2E-04 |
| GO:0055062 | phosphate ion homeostasis | 6 | 361 | 23 | 9E-04 |
| GO:0005992 | trehalose biosynthetic process | 6 | 361 | 22 | 9E-04 |
| GO:0072506 | trivalent inorganic anion homeostasis | 6 | 361 | 23 | 9E-04 |
| GO:0055082 | cellular chemical homeostasis | 12 | 361 | 163 | 1E-03 |
| GO:0006811 | ion transport | 24 | 361 | 645 | 2E-03 |
| GO:0005984 | disaccharide metabolic process | 8 | 361 | 66 | 2E-03 |
| GO:0048878 | chemical homeostasis | 17 | 361 | 352 | 2E-03 |
| GO:0055081 | anion homeostasis | 6 | 361 | 30 | 2E-03 |
| GO:0050801 | ion homeostasis | 13 | 361 | 229 | 4E-03 |
| GO:0006873 | cellular ion homeostasis | 10 | 361 | 138 | 5E-03 |
| GO:0009311 | oligosaccharide metabolic process | 9 | 361 | 108 | 5E-03 |
| GO:0098771 | inorganic ion homeostasis | 12 | 361 | 215 | 6E-03 |
| GO:0006979 | response to oxidative stress | 18 | 361 | 453 | 6E-03 |
| GO:0046351 | disaccharide biosynthetic process | 6 | 361 | 42 | 6E-03 |
| GO:0044262 | cellular carbohydrate metabolic process | 17 | 361 | 407 | 6E-03 |
| GO:0019725 | cellular homeostasis | 14 | 361 | 314 | 1E-02 |
| GO:0042221 | response to chemical | 60 | 361 | 2853 | 1E-02 |
| GO:0005975 | carbohydrate metabolic process | 31 | 361 | 1144 | 1E-02 |
| GO:0042592 | homeostatic process | 19 | 361 | 542 | 2E-02 |
| GO:0006949 | syncytium formation | 4 | 361 | 16 | 2E-02 |
| GO:0009642 | response to light intensity | 9 | 361 | 144 | 2E-02 |
| GO:0009646 | response to absence of light | 5 | 361 | 35 | 2E-02 |
| GO:0044699 | single-organism process | 154 | 361 | 9448 | 2E-02 |
| GO:0000160 | phosphorelay signal transduction system | 11 | 361 | 225 | 3E-02 |
| GO:0030001 | metal ion transport | 12 | 361 | 263 | 3E-02 |
| GO:0010033 | response to organic substance | 45 | 361 | 2023 | 3E-02 |
| GO:0006820 | anion transport | 11 | 361 | 227 | 3E-02 |
| GO:0009312 | oligosaccharide biosynthetic process | 6 | 361 | 65 | 3E-02 |
| GO:0015698 | inorganic anion transport | 7 | 361 | 95 | 3E-02 |
| GO:0072502 | cellular trivalent inorganic anion homeostasis | 3 | 361 | 9 | 4E-02 |
| GO:0030643 | cellular phosphate ion homeostasis | 3 | 361 | 9 | 4E-02 |
| GO:0009743 | response to carbohydrate | 8 | 361 | 133 | 4E-02 |
| GO:0031669 | cellular response to nutrient levels | 9 | 361 | 170 | 4E-02 |
| GO:0071484 | cellular response to light intensity | 3 | 361 | 10 | 4E-02 |
| GO:0006950 | response to stress | 67 | 361 | 3506 | 4E-02 |
| GO:0030002 | cellular anion homeostasis | 3 | 361 | 10 | 4E-02 |
| GO:0055085 | transmembrane transport | 20 | 361 | 667 | 4E-02 |
| GO:0070413 | trehalose metabolism in response to stress | 3 | 361 | 11 | 5E-02 |

*Suppl. Table 6 Overview of the expression of phosphate starvation responsive genes, participating in trehalose metabolism and carbohydrate metabolism, in WT root tips.*

### Trehalose metabolic process (GO:0005991)

| Locus | Gene name | log$_2$FC | padj |
|---|---|---|---|
| AT5G65140 | TPPJ | 1.21 | 2E-04 |
| AT4G22590 | TPPG | 1.10 | 2E-05 |
| AT5G10100 | TPPI | -1.07 | 5E-03 |
| AT1G70290 | TPS8 | 1.66 | 2E-10 |
| AT1G23870 | TPS9 | 1.41 | 8E-08 |
| AT2G18700 | TPS11 | 1.56 | 4E-07 |
| AT4G24040 | TRE1 | 1.30 | 7E-04 |

### Cellular carbohydrate metabolic process (GO:0044262)

| Locus | Gene name | log$_2$FC | padj |
|---|---|---|---|
| AT4G26260 | MIOX4 | 4.95 | 8E-06 |
| AT2G43620 | - | 3.15 | 1E-08 |
| AT5G20250 | DIN10 | 3.13 | 7E-05 |
| AT1G80160 | - | 2.78 | 5E-02 |
| AT2G19800 | MIOX2 | 2.50 | 5E-05 |
| AT5G14470 | GLCAK2 | 2.43 | 2E-02 |
| AT5G65690 | PCK2 | 2.42 | 4E-06 |
| AT5G18670 | BAM9 | 2.38 | 3E-03 |
| AT3G02040 | GDPD1 | 1.97 | 4E-21 |
| AT1G10640 | - | 1.74 | 3E-03 |
| AT5G41080 | GDPD2 | 1.63 | 1E-03 |
| AT1G22710 | SUC2 | 1.54 | 7E-06 |
| AT5G42720 | - | 1.42 | 4E-11 |
| AT3G57520 | RFS2 | 1.40 | 2E-09 |
| AT4G18340 | - | 1.37 | 2E-07 |
| AT4G28850 | XTH26 | 1.20 | 8E-06 |
| AT5G57560 | XTH22 | 1.16 | 3E-02 |
| AT3G43270 | PME32 | 1.11 | 2E-07 |
| AT1G13250 | GATL3 | 1.05 | 4E-03 |
| AT5G57540 | XTH13 | 1.05 | 5E-13 |
| AT4G37950 | - | -1.22 | 8E-03 |
| AT3G44990 | XTH31 | -1.38 | 1E-02 |
| AT1G70500 | - | -1.41 | 2E-02 |
| AT1G48300 | - | -2.49 | 1E-13 |

*WT seedlings were germinated on +Pi media and transferred to +Pi and -Pi media; root tip material was collected 1DAT and was used for transcriptional analysis with RNA-seq. Logarithmic fold change (log$_2$FC) values indicate differences in mean expression of the genes between -Pi WT and +Pi WT across 3 biological replicates, each containing a pool of 150-200 root tips, with negative values signifying lower transcript levels in -Pi WT. Adjusted p-values (padj) signify statistically significant changes after adjustment for multiple testing using FDR. Significantly differentially expressed genes according to cutoff thresholds (1< log2FC< -1, padj< 0.05) are marked with bold.*

*Suppl. Table 7 Overview of the expression of phosphate starvation responsive genes, participating in callose synthesis, callose deposition on the cell wall and iron homeostasis, in WT root tips.*

| Biosynthesis of (1->3)-beta-D-glucans (GO:0006075) | | | | Iron homeostasis (GO:0055072) | | | |
|---|---|---|---|---|---|---|---|
| Gene ID | Gene name | log$_2$FC | padj | Gene ID | Gene name | log$_2$FC | padj |
| AT1G05570 | CALS1 | -0.60 | 0.05 | AT3G19860 | BHLH121 | 0.35 | 0.52 |
| AT1G06490 | CALS7 | -0.27 | 0.81 | AT3G08040 | DTX43 | -0.39 | 0.89 |
| AT2G31960 | CALS2 | -0.34 | 0.25 | AT3G56980 | ORG3 | NA | NA |
| AT2G36850 | CALS10 | -0.28 | 0.41 | AT1G18910 | - | -0.28 | 0.59 |
| AT3G07160 | GSL10 | -0.31 | 0.34 | AT3G56970 | ORG2 | NA | NA |
| AT3G14570 | CALS8 | -0.51 | 0.23 | AT4G22220 | ISU1 | 0.04 | 0.96 |
| AT3G59100 | CALS6 | -0.32 | 0.61 | AT4G04770 | ABCI8 | 0.03 | 0.98 |
| AT4G03550 | CALS12 | -0.09 | 0.85 | AT4G28630 | ABCB23 | 0.03 | 0.97 |
| AT4G04970 | CALS11 | -0.10 | 0.86 | AT3G11050 | FER2 | 0.33 | 0.23 |
| AT5G13000 | CALS3 | -0.17 | 0.64 | AT5G58270 | ABCB25 | -0.21 | 0.60 |
| AT5G36870 | CALS4 | -1.02 | 0.74 | AT5G24290 | MEB2 | -0.11 | 0.92 |
| | | | | AT3G58060 | MTPC3 | NA | NA |
| **Callose deposition to cell wall (GO:0052543)** | | | | AT5G03570 | IREG2 | -0.53 | 0.85 |
| Gene ID | Gene name | log$_2$FC | padj | AT3G18290 | BTS | -0.23 | 0.54 |
| AT5G46330 | FLS2 | -2.01 | 0.27 | AT4G19690 | IRT1 | NA | NA |
| AT4G39950 | CYP79B2 | 0.10 | 0.92 | AT4G27870 | - | 0.19 | 0.54 |
| AT3G54640 | TSA1 | 0.03 | 0.97 | AT5G26820 | IREG3 | -0.69 | 0.05 |
| AT4G23100 | GSH1 | 0.10 | 0.79 | AT1G01580 | FRO2 | 0.16 | 0.88 |
| AT4G26850 | VTC2 | 0.09 | 0.89 | AT4G27850 | - | 0.47 | 0.63 |
| AT1G24100 | UGT74B1 | 0.02 | 0.98 | AT3G56090 | FER3 | 0.51 | 0.00 |
| AT5G57220 | CYP81F2 | 0.41 | 0.79 | AT4G27860 | - | -0.04 | 0.96 |
| AT1G59870 | ABCG36 | 0.13 | 0.89 | AT3G47640 | BHLH47 | 0.33 | 0.42 |
| AT5G03280 | EIN2 | -0.08 | 0.84 | **AT3G61010** | **-** | **-1.07** | **0.01** |
| AT1G66340 | ETR1 | -0.06 | 0.93 | AT2G41240 | BHLH100 | NA | NA |
| AT5G44070 | PCS1 | 0.03 | 0.97 | **AT1G76800** | **VTL2** | **1.10** | **0.01** |
| AT2G22330 | CYP79B3 | -0.96 | 0.23 | AT5G67330 | NRAMP4 | 0.08 | 0.95 |
| AT4G03550 | CALS12 | -0.09 | 0.85 | **AT5G01600** | **FER1** | **1.65** | **0.00** |
| AT4G31500 | CYP83B1 | 0.19 | 0.68 | AT3G25190 | - | 0.30 | 0.96 |
| AT1G18570 | MYB51 | 0.22 | 0.89 | AT1G21140 | - | 0.75 | 0.46 |
| AT2G44490 | BGLU26 | 0.22 | 0.50 | AT1G74770 | - | 0.14 | 0.90 |
| AT3G07160 | ATGSL10 | -0.31 | 0.34 | AT4G04950 | GRXS17 | -0.05 | 0.96 |
| AT1G34350 | - | 0.10 | 0.85 | AT4G03240 | FH | 0.04 | 0.96 |
| AT5G11630 | - | 0.01 | 0.99 | AT5G04150 | BHLH101 | -0.65 | 0.86 |
| AT5G17310 | UGP1 | -0.05 | 0.95 | AT2G01770 | VIT1 | -1.23 | 0.70 |
| AT1G06170 | BHLH89 | NA | NA | AT2G40300 | FER4 | 0.36 | 0.12 |
| AT2G31220 | BHLH10 | 0.03 | 0.99 | AT5G09830 | BOLA2 | 0.16 | 0.79 |
| AT3G03250 | UGP | 0.15 | 0.57 | AT3G07700 | - | -0.49 | 0.45 |
| AT5G61130 | PDCB1 | 0.16 | 0.75 | AT2G23150 | NRAMP3 | 0.23 | 0.65 |
| AT1G77850 | ARF17 | 0.11 | 0.96 | AT4G34600 | CIF2 | -0.42 | 0.67 |
| AT5G50800 | SWEET13 | -2.21 | 0.28 | AT1G66590 | ATCOX19-1 | -0.12 | 0.90 |

| | AT5G64940 | ATATH13 | -0.71 | 0.00 |
| --- | --- | --- | --- | --- |
| | AT1G51070 | bHLH115 | 0.12 | 0.77 |
| | AT4G16370 | ATOPT3 | 0.32 | 0.73 |
| | AT3G13440 | - | -0.04 | 0.96 |
| | AT2G16385 | CIF1 | -1.15 | 0.51 |
| | AT1G07030 | - | -0.02 | 0.98 |
| | AT1G58340 | DTX48 | -0.39 | 0.79 |
| | AT1G20110 | FREE1 | -0.12 | 0.77 |
| | AT2G30160 | - | 0.05 | 0.96 |
| | AT4G37650 | SHR | 0.32 | 0.37 |
| | AT5G51720 | NEET | NA | NA |
| | AT5G06410 | - | -0.10 | 0.89 |

*WT seedlings were germinated on +Pi media and transferred to +Pi and -Pi media; root tip material was collected 1DAT and was used for transcriptional analysis with RNA-seq. Logarithmic fold change (log$_2$FC) values indicate differences in mean expression of the genes between -Pi WT and +Pi WT across 3 biological replicates, each containing a pool of 150-200 root tips, with negative values signifying lower transcript levels in -Pi WT. Adjusted p-values (padj) signify statistically significant changes after adjustment for multiple testing using FDR. Significantly differentially expressed genes according to cutoff thresholds (1< log$_2$FC <-1, padj< 0.05) are marked with bold. NA values signify absence of detected transcripts.*

*Suppl. Table 8 Significantly enriched GO terms of biological processes, common in Pi starved WT and pdr3 root tips (common phosphate starvation responsive DEGs).*

| GO ID | Term | DEGs in Term | Total mapped DEGs | Total genes in Term | FDR |
| --- | --- | --- | --- | --- | --- |
| GO:0009642 | response to light intensity | 9 | 219 | 144 | 3E-03 |
| GO:0006979 | response to oxidative stress | 15 | 219 | 453 | 3E-03 |
| GO:0005991 | trehalose metabolic process | 5 | 219 | 24 | 3E-03 |
| GO:0055082 | cellular chemical homeostasis | 9 | 219 | 163 | 4E-03 |
| GO:0009646 | response to absence of light | 5 | 219 | 35 | 6E-03 |
| GO:0005984 | disaccharide metabolic process | 6 | 219 | 66 | 7E-03 |
| GO:0009311 | oligosaccharide metabolic process | 7 | 219 | 108 | 9E-03 |
| GO:0048878 | chemical homeostasis | 12 | 219 | 352 | 9E-03 |
| GO:0055062 | phosphate ion homeostasis | 4 | 219 | 23 | 1E-02 |
| GO:0005992 | trehalose biosynthetic process | 4 | 219 | 22 | 1E-02 |
| GO:0072506 | trivalent inorganic anion homeostasis | 4 | 219 | 23 | 1E-02 |
| GO:0050896 | response to stimulus | 73 | 219 | 6250 | 2E-02 |
| GO:0005975 | carbohydrate metabolic process | 22 | 219 | 1144 | 2E-02 |
| GO:0009743 | response to carbohydrate | 7 | 219 | 133 | 2E-02 |
| GO:0050801 | ion homeostasis | 9 | 219 | 229 | 2E-02 |
| GO:0044262 | cellular carbohydrate metabolic process | 12 | 219 | 407 | 2E-02 |
| GO:0006873 | cellular ion homeostasis | 7 | 219 | 138 | 2E-02 |
| GO:0071484 | cellular response to light intensity | 3 | 219 | 10 | 2E-02 |
| GO:0055081 | anion homeostasis | 4 | 219 | 30 | 2E-02 |
| GO:0070413 | trehalose metabolism in response to stress | 3 | 219 | 11 | 2E-02 |

| GO:0019725 | cellular homeostasis | 10 | 219 | 314 | 2E-02 |
| GO:0098771 | inorganic ion homeostasis | 8 | 219 | 215 | 4E-02 |
| GO:0042592 | homeostatic process | 13 | 219 | 542 | 4E-02 |
| GO:0046351 | disaccharide biosynthetic process | 4 | 219 | 42 | 4E-02 |

*Suppl. Table 9 Significantly enriched GO terms of biological processes exclusively in Pi-starved pdr3 root tips.*

| GO ID | Term | DEGs in Term | Total mapped DEGs | Total genes in Term | FDR |
|---|---|---|---|---|---|
| GO:0050896 | response to stimulus | 471 | 1379 | 6250 | 4E-20 |
| GO:0042221 | response to chemical | 262 | 1379 | 2853 | 6E-19 |
| GO:0010033 | response to organic substance | 192 | 1379 | 2023 | 2E-14 |
| GO:0009719 | response to endogenous stimulus | 169 | 1379 | 1732 | 2E-13 |
| GO:0009725 | response to hormone | 150 | 1379 | 1631 | 7E-10 |
| GO:1901700 | response to oxygen-containing compound | 144 | 1379 | 1557 | 1E-09 |
| GO:0006950 | response to stress | 263 | 1379 | 3506 | 2E-09 |
| GO:0010200 | response to chitin | 31 | 1379 | 134 | 2E-08 |
| GO:0010243 | response to organonitrogen compound | 33 | 1379 | 166 | 1E-07 |
| GO:0009723 | response to ethylene | 45 | 1379 | 307 | 4E-07 |
| GO:0042744 | hydrogen peroxide catabolic process | 22 | 1379 | 83 | 1E-06 |
| GO:1901698 | response to nitrogen compound | 40 | 1379 | 264 | 1E-06 |
| GO:0009628 | response to abiotic stimulus | 160 | 1379 | 2022 | 2E-06 |
| GO:0006979 | response to oxidative stress | 55 | 1379 | 453 | 2E-06 |
| GO:0009607 | response to biotic stimulus | 110 | 1379 | 1253 | 4E-06 |
| GO:0044699 | single-organism process | 561 | 1379 | 9448 | 4E-06 |
| GO:0006952 | defense response | 129 | 1379 | 1566 | 5E-06 |
| GO:0042743 | hydrogen peroxide metabolic process | 23 | 1379 | 104 | 5E-06 |
| GO:0071369 | cellular response to ethylene stimulus | 33 | 1379 | 206 | 6E-06 |
| GO:0043207 | response to external biotic stimulus | 105 | 1379 | 1212 | 1E-05 |
| GO:0051707 | response to other organism | 105 | 1379 | 1210 | 1E-05 |
| GO:0001101 | response to acid chemical | 103 | 1379 | 1181 | 1E-05 |
| GO:0009605 | response to external stimulus | 128 | 1379 | 1582 | 1E-05 |
| GO:0070887 | cellular response to chemical stimulus | 98 | 1379 | 1176 | 1E-04 |
| GO:0051704 | multi-organism process | 125 | 1379 | 1631 | 2E-04 |

| GO:0072593 | reactive oxygen species metabolic process | 26 | 1379 | 169 | 2E-04 |
|---|---|---|---|---|---|
| GO:0009768 | photosynthesis, light harvesting in photosystem I | 10 | 1379 | 23 | 3E-04 |
| GO:0010035 | response to inorganic substance | 80 | 1379 | 926 | 3E-04 |
| GO:0032870 | cellular response to hormone stimulus | 77 | 1379 | 879 | 3E-04 |
| GO:0009617 | response to bacterium | 47 | 1379 | 441 | 3E-04 |
| GO:0009873 | ethylene-activated signaling pathway | 27 | 1379 | 185 | 3E-04 |
| GO:0045229 | external encapsulating structure organization | 55 | 1379 | 551 | 3E-04 |
| GO:0000160 | phosphorelay signal transduction system | 30 | 1379 | 225 | 4E-04 |
| GO:0071495 | cellular response to endogenous stimulus | 77 | 1379 | 890 | 4E-04 |
| GO:0071555 | cell wall organization | 52 | 1379 | 518 | 4E-04 |
| GO:0072358 | cardiovascular system development | 10 | 1379 | 26 | 5E-04 |
| GO:0001944 | vasculature development | 10 | 1379 | 26 | 5E-04 |
| GO:0072359 | circulatory system development | 10 | 1379 | 26 | 5E-04 |
| GO:0009404 | toxin metabolic process | 14 | 1379 | 60 | 8E-04 |
| GO:0071310 | cellular response to organic substance | 84 | 1379 | 1023 | 8E-04 |
| GO:0044710 | single-organism metabolic process | 252 | 1379 | 3970 | 1E-03 |
| GO:0010411 | xyloglucan metabolic process | 13 | 1379 | 57 | 2E-03 |
| GO:0007154 | cell communication | 152 | 1379 | 2223 | 3E-03 |
| GO:0042742 | defense response to bacterium | 37 | 1379 | 354 | 4E-03 |
| GO:0009765 | photosynthesis, light harvesting | 11 | 1379 | 44 | 4E-03 |
| GO:0009266 | response to temperature stimulus | 51 | 1379 | 559 | 4E-03 |
| GO:0098542 | defense response to other organism | 75 | 1379 | 936 | 5E-03 |
| GO:0009737 | response to abscisic acid | 52 | 1379 | 578 | 5E-03 |
| GO:0097305 | response to alcohol | 52 | 1379 | 583 | 6E-03 |
| GO:0033993 | response to lipid | 63 | 1379 | 772 | 1E-02 |
| GO:0009636 | response to toxic substance | 16 | 1379 | 102 | 1E-02 |
| GO:0046351 | disaccharide biosynthetic process | 10 | 1379 | 42 | 1E-02 |
| GO:0009755 | hormone-mediated signaling pathway | 66 | 1379 | 821 | 1E-02 |
| GO:0009753 | response to jasmonic acid | 26 | 1379 | 225 | 1E-02 |

| GO:1990267 | response to transition metal nanoparticle | 17 | 1379 | 119 | 2E-02 |
| GO:0019748 | secondary metabolic process | 44 | 1379 | 492 | 2E-02 |
| GO:0010337 | regulation of salicylic acid metabolic process | 6 | 1379 | 14 | 2E-02 |
| GO:0009644 | response to high light intensity | 13 | 1379 | 76 | 2E-02 |
| GO:0051716 | cellular response to stimulus | 181 | 1379 | 2856 | 2E-02 |
| GO:0005984 | disaccharide metabolic process | 12 | 1379 | 66 | 2E-02 |
| GO:0055114 | oxidation-reduction process | 108 | 1379 | 1566 | 3E-02 |
| GO:0005975 | carbohydrate metabolic process | 83 | 1379 | 1144 | 3E-02 |
| GO:0009620 | response to fungus | 48 | 1379 | 573 | 3E-02 |
| GO:0000302 | response to reactive oxygen species | 20 | 1379 | 166 | 3E-02 |
| GO:0009733 | response to auxin | 37 | 1379 | 407 | 3E-02 |
| GO:0010039 | response to iron ion | 10 | 1379 | 51 | 3E-02 |
| GO:0044262 | cellular carbohydrate metabolic process | 37 | 1379 | 407 | 3E-02 |
| GO:0044700 | single organism signaling | 131 | 1379 | 1995 | 4E-02 |
| GO:0023052 | signaling | 131 | 1379 | 1997 | 4E-02 |
| GO:0035556 | intracellular signal transduction | 53 | 1379 | 660 | 4E-02 |
| GO:0009642 | response to light intensity | 18 | 1379 | 144 | 4E-02 |
| GO:0010410 | hemicellulose metabolic process | 14 | 1379 | 96 | 4E-02 |
| GO:0007165 | signal transduction | 129 | 1379 | 1965 | 4E-02 |
| GO:0032101 | regulation of response to external stimulus | 12 | 1379 | 74 | 4E-02 |
| GO:0071281 | cellular response to iron ion | 8 | 1379 | 35 | 5E-02 |
| GO:0009312 | oligosaccharide biosynthetic process | 11 | 1379 | 65 | 5E-02 |
| GO:0071554 | cell wall organization or biogenesis | 55 | 1379 | 704 | 5E-02 |

*Suppl. Table 10 Overview of PSR DEGs in pdr3 root tips, with an annotated function in defense.*

| Gene ID | Gene name | log$_2$FC | padj | Hormone pathway | Gene ID | Gene name | log$_2$FC | padj | Hormone pathway |
|---|---|---|---|---|---|---|---|---|---|
| AT4G11393 | - | 9.38 | 8E-11 | | AT1G12200 | - | 1.52 | 2E-03 | |
| AT3G23120 | AtRLP38 | 7.28 | 3E-06 | | AT3G10190 | CML36 | 1.51 | 1E-03 | |
| AT4G29305 | LCR25 | 6.75 | 4E-05 | | AT3G15356 | LEC | 1.50 | 3E-03 | JA, SA, ET |
| AT3G23240 | ERF1B | 5.97 | 5E-03 | JA, ET | AT2G43610 | - | 1.50 | 5E-04 | |
| AT5G61890 | ERF114 | 5.87 | 3E-07 | ET | AT3G23110 | AtRLP37 | 1.44 | 5E-02 | |
| AT2G02120 | PDF2.1 | 5.61 | 5E-03 | | AT5G63020 | - | 1.44 | 4E-03 | |

| | | | | | | | | | |
|---|---|---|---|---|---|---|---|---|---|
| AT3G06490 | MYB108 | 5.15 | 2E-02 | JA, ET | AT4G24180 | TLP1 | 1.43 | 5E-05 | ET |
| AT5G06720 | PER53 | 5.12 | 4E-20 | | AT4G04220 | AtRLP46 | 1.41 | 4E-02 | |
| AT5G10380 | ATL55 | 5.05 | 2E-03 | | AT3G26830 | CYP71B15 | 1.40 | 3E-03 | |
| AT1G53940 | GLIP2 | 4.82 | 3E-02 | JA, SA, ET | AT3G50970 | XERO2 | 1.38 | 6E-07 | |
| AT5G26920 | CBP60G | 3.99 | 3E-17 | | AT1G33590 | - | 1.36 | 1E-03 | |
| AT1G74930 | ERF018 | 3.72 | 5E-03 | ET | AT1G33560 | ADR1 | 1.34 | 1E-14 | |
| AT1G31290 | AGO3 | 3.71 | 6E-03 | | AT2G39730 | RCA | 1.33 | 2E-03 | JA |
| AT1G59620 | CW9 | 3.62 | 2E-02 | | AT5G36925 | - | 1.32 | 2E-02 | |
| AT5G47220 | ERF2 | 3.61 | 3E-06 | JA, ET | AT3G52430 | PAD4 | 1.31 | 4E-06 | JA, SA, ET |
| AT3G26450 | - | 3.38 | 1E-03 | | AT2G39660 | BIK1 | 1.28 | 1E-08 | SA |
| AT3G14210 | ESM1 | 3.12 | 3E-04 | | AT4G19700 | BOI | 1.27 | 3E-08 | |
| AT1G63750 | - | 2.99 | 1E-09 | | AT2G31865 | PARG2 | 1.25 | 5E-02 | |
| AT1G66090 | - | 2.98 | 4E-05 | | AT5G46050 | NPF5.2 | 1.23 | 5E-08 | JA, SA |
| AT1G20160 | CRSP | 2.84 | 5E-04 | | AT2G40880 | CYS3 | 1.22 | 2E-02 | |
| AT2G44840 | ERF13 | 2.81 | 1E-08 | ET | AT4G12720 | AtNUDT7 | 1.21 | 6E-09 | |
| AT1G72930 | TIR | 2.78 | 4E-08 | | AT3G50260 | ERF011 | 1.21 | 4E-06 | ET |
| AT3G04220 | - | 2.72 | 1E-05 | | AT1G07570 | APK1A | 1.19 | 9E-06 | |
| AT1G02920 | GSTF7 | 2.71 | 2E-07 | | AT4G01250 | WRKY22 | 1.18 | 2E-03 | |
| AT1G23120 | - | 2.63 | 9E-06 | | AT5G61420 | MYB28 | 1.18 | 1E-02 | JA, SA |
| AT1G05760 | RTM1 | 2.59 | 3E-09 | | AT5G47550 | CYS5 | 1.17 | 2E-02 | |
| AT3G25510 | - | 2.56 | 1E-02 | | AT2G22300 | CAMTA3 | 1.16 | 2E-03 | |
| AT2G02100 | PDF2.2 | 2.49 | 4E-09 | | AT3G09260 | BGLU23 | 1.16 | 2E-04 | |
| AT3G58350 | RTM3 | 2.36 | 8E-08 | | AT4G39950 | CYP79B2 | 1.16 | 7E-04 | |
| AT5G04890 | RTM2 | 2.27 | 5E-09 | | AT2G02130 | PDF2.3 | 1.14 | 7E-06 | |
| AT1G72900 | - | 2.20 | 7E-07 | | AT3G18490 | ASPG1 | 1.12 | 2E-04 | |
| AT3G49120 | PER34 | 2.20 | 7E-04 | | AT1G09090 | RBOHB | 1.11 | 6E-03 | |
| AT4G24250 | MLO13 | 2.19 | 1E-06 | | AT1G35260 | MLP165 | 1.11 | 1E-03 | |
| AT1G73805 | SARD1 | 2.17 | 1E-03 | | AT3G29160 | KIN11 | 1.09 | 1E-03 | |
| AT4G35480 | ATL45 | 2.14 | 5E-05 | | AT1G72850 | - | 1.08 | 5E-03 | |
| AT3G07040 | RPM1 | 2.10 | 5E-04 | | AT3G45640 | MPK3 | 1.07 | 1E-03 | |
| AT5G46350 | WRKY8 | 2.08 | 1E-03 | | AT3G28740 | CYP81D11 | 1.07 | 4E-05 | |
| AT3G50930 | HSR4 | 2.07 | 3E-13 | SA | AT5G09440 | EXL4 | 1.06 | 1E-02 | |
| AT3G59930 | - | 2.07 | 1E-04 | | AT1G58410 | RXW24L | 1.06 | 2E-04 | |
| AT5G38350 | - | 2.03 | 2E-03 | | AT2G40140 | CZF1 | 1.06 | 2E-03 | |
| AT2G32140 | - | 2.02 | 4E-02 | | AT5G06320 | NHL3 | 1.05 | 1E-03 | SA |
| AT3G56400 | WRKY70 | 1.98 | 2E-04 | JA, SA | AT1G28380 | NSL1 | 1.05 | 3E-02 | SA |
| AT3G02150 | TCP13 | 1.97 | 1E-03 | | AT5G04720 | ADR1-L2 | 1.03 | 2E-04 | |
| AT4G02520 | GSTF2 | 1.90 | 3E-03 | | AT5G44510 | TAO1 | 1.01 | 3E-05 | |
| AT2G05940 | RIPK | 1.83 | 5E-05 | | AT3G48990 | AAE3 | 1.01 | 4E-05 | |
| AT3G44630 | - | 1.81 | 4E-04 | | AT4G38540 | MO2 | 1.00 | 2E-05 | |
| AT4G17490 | ERF6 | 1.74 | 1E-05 | ET | AT2G22000 | PEP6 | -1.00 | 3E-02 | |
| AT5G60270 | LECRK17 | 1.72 | 3E-03 | | AT2G33210 | HSP60-2 | -1.15 | 2E-05 | |
| AT5G64810 | WRKY51 | 1.66 | 1E-12 | JA | AT2G25620 | AtDBP1 | -1.16 | 7E-03 | |
| AT4G37410 | CYP81F4 | 1.66 | 2E-14 | | AT4G00360 | CYP86A2 | -1.19 | 2E-03 | |
| AT1G15010 | - | 1.65 | 4E-02 | | AT1G58170 | DIR19 | -1.27 | 4E-02 | |

| AT5G61600 | ERF104 | 1.64 | 5E-05 | ET | AT4G20260 | PCAP1 | -1.27 | 5E-08 | |
|---|---|---|---|---|---|---|---|---|---|
| AT4G31800 | WRKY18 | 1.61 | 3E-03 | SA | AT4G18760 | RLP51 | -1.34 | 3E-07 | |
| AT4G17500 | ERF1A | 1.60 | 4E-04 | ET | AT5G52640 | HSP90-1 | -1.35 | 3E-04 | |
| AT4G11170 | - | 1.59 | 6E-03 | | AT2G26330 | ERECTA | -1.45 | 2E-02 | |
| AT1G72920 | - | 1.59 | 1E-04 | | AT1G61560 | MLO6 | -1.75 | 5E-03 | |
| AT1G30990 | - | 1.59 | 3E-09 | | AT1G27950 | LTPG1 | -1.84 | 1E-08 | |
| AT5G13220 | JAZ10 | 1.59 | 6E-03 | JA | AT4G23670 | - | -1.85 | 3E-02 | |
| AT5G20230 | BCB | 1.56 | 3E-03 | | AT2G19190 | SIRK | -1.86 | 3E-02 | |
| AT1G12010 | - | 1.56 | 3E-04 | | AT4G33220 | PME44 | -1.98 | 1E-03 | |
| AT1G75380 | BBD1 | 1.55 | 9E-04 | | AT1G02205 | CER1 | -2.13 | 1E-06 | |
| AT3G01080 | WRKY58 | 1.54 | 7E-04 | | AT1G53130 | GRI | -2.30 | 8E-06 | JA, SA |
| AT1G14370 | PBL2 | 1.53 | 1E-07 | | AT1G64670 | BDG1 | -2.37 | 2E-02 | |
| AT5G41750 | - | 1.53 | 8E-03 | | AT4G11210 | DIR14 | -2.43 | 3E-07 | |

*Pdr3 seedlings were germinated on +Pi media and transferred to +Pi and -Pi conditions; root tip material was collected 1DAT and transcriptional analysis was performed with RNA-seq. Logarithmic fold change (log$_2$FC) values indicate differences in mean expression of the genes between pdr3 -Pi and pdr3 +Pi across 3 biological replicates, each containing a pool of 150-200 root tips, with negative values signifying lower transcript levels in pdr3 +Pi. Adjusted p-values (padj) signify statistically significant changes after adjustment for multiple testing using FDR.*

**Suppl. Table 11 Overview of PSR DEGs in pdr3 root tips, with an annotated function in the indicated GO terms.**

| Response to bacterium (GO:0009617) | | | Response to fungus (GO:0009620) | | | Response to chitin (GO:0010200) | | |
|---|---|---|---|---|---|---|---|---|
| Gene ID | Gene name | log$_2$FC | Gene ID | Gene name | log$_2$FC | Gene ID | Gene name | log$_2$FC |
| AT5G10380 | ATL55 | 5.05 | AT4G11393 | - | 9.38 | AT3G44350 | anac061 | 6.15 |
| AT1G53940 | GLIP2 | 4.82 | AT4G29305 | LCR25 | 6.75 | AT2G17040 | anac036 | 5.10 |
| AT5G26920 | CBP60G | 3.99 | AT1G17420 | LOX3 | 5.90 | AT5G10380 | ATL55 | 5.05 |
| AT5G47220 | ERF2 | 3.61 | AT5G61890 | ERF114 | 5.87 | AT2G46400 | WRKY46 | 3.66 |
| AT3G14210 | ESM1 | 3.12 | AT2G02120 | PDF2.1 | 5.61 | AT5G47220 | ERF2 | 3.61 |
| AT1G20160 | CRSP | 2.84 | AT3G06490 | MYB108 | 5.15 | AT1G51700 | DOF1.7 | 3.52 |
| AT1G02920 | GSTF7 | 2.71 | AT5G10380 | ATL55 | 5.05 | AT2G44840 | ERF13 | 2.81 |
| AT3G49120 | PER34 | 2.20 | AT5G26920 | CBP60G | 3.99 | AT1G34180 | anac016 | 2.43 |
| AT1G73805 | SARD1 | 2.17 | AT1G02920 | GSTF7 | 2.71 | AT4G35480 | ATL45 | 2.14 |
| AT5G46350 | WRKY8 | 2.08 | AT2G02100 | PDF2.2 | 2.49 | AT3G56400 | WRKY70 | 1.98 |
| AT3G50930 | HSR4 | 2.07 | AT3G49120 | PER34 | 2.20 | AT3G23250 | MYB15 | 1.95 |
| AT3G56400 | WRKY70 | 1.98 | AT5G46350 | WRKY8 | 2.08 | AT1G27730 | ZAT10 | 1.80 |
| AT4G02520 | GSTF2 | 1.90 | AT3G59930 | - | 2.07 | AT4G17490 | ERF6 | 1.74 |
| AT4G09950 | IAN13 | 1.84 | AT3G56400 | WRKY70 | 1.98 | AT4G18880 | HSFA4A | 1.67 |
| AT2G05940 | RIPK | 1.83 | AT4G02520 | GSTF2 | 1.90 | AT4G31800 | WRKY18 | 1.61 |
| AT1G61340 | - | 1.76 | AT2G35940 | BLH1 | 1.80 | AT4G33050 | EDA39 | 1.60 |
| AT3G44300 | NIT2 | 1.73 | AT5G38280 | PR5K | 1.72 | AT4G17500 | ERF1A | 1.60 |
| AT5G64810 | WRKY51 | 1.66 | AT5G64810 | WRKY51 | 1.66 | AT5G51190 | ERF105 | 1.59 |
| AT4G31800 | WRKY18 | 1.61 | AT1G15010 | - | 1.65 | AT5G03720 | HSFA3 | 1.57 |

| Locus | Gene | log₂FC | Locus | Gene | log₂FC | Locus | Gene | log₂FC |
|---|---|---|---|---|---|---|---|---|
| AT4G24180 | TLP1 | 1.43 | AT5G61600 | ERF104 | 1.64 | AT3G55980 | SZF1 | 1.57 |
| AT1G33970 | IAN9 | 1.43 | AT4G31800 | WRKY18 | 1.61 | AT3G15356 | LEC | 1.50 |
| AT3G26830 | CYP71B15 | 1.40 | AT5G20230 | BCB | 1.56 | AT3G56770 | BHLH107 | 1.25 |
| AT1G33560 | ADR1 | 1.34 | AT1G75380 | BBD1 | 1.55 | AT3G50260 | ERF011 | 1.21 |
| AT2G39730 | RCA | 1.33 | AT1G12200 | - | 1.52 | AT2G23320 | WRKY15 | 1.19 |
| AT3G52430 | PAD4 | 1.31 | AT3G10190 | CML36 | 1.51 | AT4G01250 | WRKY22 | 1.18 |
| AT4G19700 | BOI | 1.27 | AT3G15356 | LEC | 1.50 | AT4G33940 | - | 1.17 |
| AT5G46050 | NPF5.2 | 1.23 | AT3G26830 | CYP71B15 | 1.40 | AT4G26400 | - | 1.09 |
| AT4G12720 | AtNUDT7 | 1.21 | AT3G50970 | XERO2 | 1.38 | AT4G37260 | MYB73 | 1.09 |
| AT3G50260 | ERF011 | 1.21 | AT3G10985 | SAG20 | 1.30 | AT3G45640 | MPK3 | 1.07 |
| AT5G61420 | MYB28 | 1.18 | AT2G39660 | BIK1 | 1.28 | AT2G40140 | CZF1 | 1.06 |
| AT2G22300 | CAMTA3 | 1.16 | AT4G19700 | BOI | 1.27 | AT2G26150 | HSFA2 | -1.25 |
| AT4G39950 | CYP79B2 | 1.16 | AT2G31865 | PARG2 | 1.25 | | | |
| AT3G45640 | MPK3 | 1.07 | AT5G61420 | MYB28 | 1.18 | | | |
| AT3G53180 | - | 1.06 | AT2G22300 | CAMTA3 | 1.16 | | | |
| AT5G06320 | NHL3 | 1.05 | AT3G09260 | BGLU23 | 1.16 | | | |
| AT5G04720 | ADR1-L2 | 1.03 | AT2G02130 | PDF2.3 | 1.14 | | | |
| AT5G44510 | TAO1 | 1.01 | AT1G37130 | NIA2 | 1.14 | | | |
| AT4G20260 | PCAP1 | -1.27 | AT5G09440 | EXL4 | 1.06 | | | |
| AT4G18760 | RLP51 | -1.34 | AT2G40140 | CZF1 | 1.06 | | | |
| AT5G52640 | HSP90-1 | -1.35 | AT3G25780 | AOC3 | 1.05 | | | |
| AT2G26330 | ERECTA | -1.45 | AT3G48990 | AAE3 | 1.01 | | | |
| AT5G03760 | CSLA9 | -1.65 | AT4G38540 | MO2 | 1.00 | | | |
| AT4G23670 | - | -1.85 | AT5G16590 | LRR1 | -1.23 | | | |
| AT2G19190 | SIRK | -1.86 | AT2G26330 | ERECTA | -1.45 | | | |
| AT4G33220 | PME44 | -1.98 | AT1G61560 | MLO6 | -1.75 | | | |
| AT1G02205 | CER1 | -2.13 | AT1G27950 | LTPG1 | -1.84 | | | |
| AT1G53130 | GRI | -2.30 | AT1G02205 | CER1 | -2.13 | | | |
| | | | AT1G64670 | BDG1 | -2.37 | | | |

*Pdr3 seedlings were germinated on +Pi media and transferred to +Pi and -Pi conditions; root tip material was collected 1DAT and transcriptional analysis was performed with RNA-seq. Logarithmic fold change (log₂FC) values indicate differences in mean expression of the genes between pdr3 -Pi and pdr3 +Pi across 3 biological replicates, each containing a pool of 150-200 root tips, with negative values signifying lower transcript levels in pdr3 +Pi. All of the above-mentioned genes showed statistically significant adjusted p-values (padj<0.05), after adjustment for multiple testing using FDR.*

**Suppl. Table 12 List of GSL-related DEGs in pdr3 shoots at control conditions.**

| Locus | Gene name | Full name | log₂FC | padj | Function | Pathway |
|---|---|---|---|---|---|---|
| **AT1G62540** | *FMO-GS$_{OX2}$* | *FLAVIN-MONOOXYGENASE GLUCOSINOLATE S-OXYGENASE 2* | -2.20 | 2E-07 | Biosynthesis | Aliphatic GSL |
| **AT5G23020** | *MAM3* | *METHYLTHIOALKYMALATE SYNTHASE-LIKE 3* | -2.03 | 2E-14 | Biosynthesis | Aliphatic GSL |

| | | | | | | |
|---|---|---|---|---|---|---|
| AT1G54040 | *ESP* | *EPITHIOSPECIFIER PROTEIN* | -1.77 | 2E-05 | Catabolism | |
| AT5G07700 | *MYB76* | *MYB DOMAIN PROTEIN 76* | -1.34 | 5E-03 | Regulation | Aliphatic GSL |
| AT1G16410 | *CYP79F1* | *CYTOCHROME P450, FAMILY 79, SUBFAMILY F, POLYPEPTIDE 1* | -1.14 | 2E-04 | Biosynthesis | Aliphatic GSL |
| AT1G66280 | *BGLU22* | *BETA-GLUCOSIDASE 22* | 1.84 | 7E-06 | Catabolism | |
| AT1G66270 | *BGLU21* | *BETA-GLUCOSIDASE 21* | 3.16 | 7E-06 | Catabolism | |
| AT1G47600 | *TGG4* | *MYROSINASE 4* | 4.73 | 5E-05 | Catabolism | |

*WT and pdr3 seedlings were germinated on +Pi media and transferred to +Pi media; root material was collected 1DAT and transcriptional analysis was performed with RNA-seq. Logarithmic fold change (log$_2$FC) values indicate differences in mean expression of the genes between pdr3 and WT roots across 3 biological replicates, each containing a pool of 25 shoots, with negative values signifying lower transcript levels in the mutant. Adjusted p-values (padj) signify statistically significant changes after adjustment for multiple testing using FDR.*

**Suppl. Table 13. Overview of DEGs in pdr3 root tissue, related to GSL metabolism and regulation.**

| Gene ID | Gene name | log$_2$FC | padj | Function | Pathway |
|---|---|---|---|---|---|
| AT5G61420 | *MYB28* | -1.18 | 4.41E-15 | Biosynthesis | Aliphatic GSL |
| AT5G14200 | *IMD1* | -1.36 | 2.06E-14 | Biosynthesis | Aliphatic GSL |
| AT2G25450 | *GSL-OH* | -1.39 | 5.19E-13 | Biosynthesis | Aliphatic GSL |
| AT4G12030 | *BAT5* | -1.5 | 2.27E-14 | Biosynthesis | Aliphatic GSL |
| AT5G23020 | *MAM3* | -1.55 | 9.10E-15 | Biosynthesis | Aliphatic GSL |
| AT2G43100 | *IPMI2* | -1.62 | 1.58E-04 | Biosynthesis | Aliphatic GSL |
| AT1G74090 | *SOT18* | -1.64 | 1.06E-13 | Biosynthesis | Aliphatic GSL |
| AT1G16400 | *CYP79F2* | -1.64 | 1.82E-04 | Biosynthesis | Aliphatic GSL |
| AT1G18590 | *SOT17* | -1.66 | 1.28E-15 | Biosynthesis | Aliphatic GSL |
| AT3G19710 | *BCAT4* | -1.81 | 2.80E-05 | Biosynthesis | Aliphatic GSL |
| AT2G31790 | *UGT74C1* | -1.89 | 1.46E-17 | Biosynthesis | Aliphatic GSL |
| AT5G23010 | *MAM1* | -1.99 | 1.15E-04 | Biosynthesis | Aliphatic GSL |
| AT3G58990 | *IPMI1* | -2.02 | 1.22E-05 | Biosynthesis | Aliphatic GSL |
| AT4G13770 | *CYP83A1* | -2.41 | 4.68E-12 | Biosynthesis | Aliphatic GSL |
| AT1G62540 | *FMO-GS$_{OX2}$* | -2.95 | 7.94E-03 | Biosynthesis | Aliphatic GSL |
| AT1G62560 | *FMO-GS$_{OX3}$* | -4.32 | 3.82E-23 | Biosynthesis | Aliphatic GSL |
| AT4G39950 | *CYP79B2* | -1.04 | 2.51E-06 | Biosynthesis | Indolic GSL |
| AT4G37410 | *CYP81F4* | -1.33 | 6.03E-13 | Biosynthesis | Indolic GSL |
| AT1G21100 | *IGMT1* | -2.66 | 6.80E-11 | Biosynthesis | Indolic GSL |
| AT1G27130 | *GSTU13* | -1.03 | 4.62E-12 | Catabolism | Aliphatic GSL |
| AT3G16390 | *NSP3* | -1.57 | 1.69E-03 | Catabolism | Aliphatic GSL |
| AT5G28510 | *BGLU24* | -1.52 | 3.25E-02 | Catabolism | Unknown |
| AT1G18570 | *MYB51* | 1.38 | 2.53E-04 | Regulation | Indolic GSL |

*5-days-old seedlings germinated on +Pi growth medium were transferred to fresh +Pi media. Root tips were harvested 1DAT and were used for RNA extraction and transcriptional analysis via RNA-seq. Logarithmic fold change (log$_2$FC) values indicate differences in mean expression of the genes between pdr3 and WT roots across 3 biological replicates, each containing a pool of 50 roots, with negative values signifying lower transcript levels in the mutant. Adjusted p-values (padj) signify statistically significant changes after adjustment for multiple testing using FDR.*

*Suppl. Table 14 Overview of absolute GSL content in roots of 6-days-old Arabidopsis seedlings.*

| 1 DAT | | WT | | | pdr3 | | |
|---|---|---|---|---|---|---|---|
| Analyte | Pi | Mean Abs. Conc. | SD Abs. Conc. | n | Mean Abs. Conc. | SD Abs. Conc. | n |
| 4MTB | +Pi | 0.03 | 0.01 | 4 | 0.13 | 0.06 | 4 |
| | -Pi | 0.06 | 0.04 | 4 | 0.08 | 0.03 | 4 |
| 5MTP | +Pi | 0.01 | 0.00 | 8 | 0.02 | 0.00 | 7 |
| | -Pi | 0.01 | 0.01 | 8 | 0.02 | 0.00 | 7 |
| 6MSOH | +Pi | 0.03 | 0.01 | 8 | 0.02 | 0.01 | 8 |
| | -Pi | 0.04 | 0.02 | 7 | 0.02 | 0.01 | 8 |
| 6MTH | +Pi | 0.06 | 0.01 | 7 | 0.04 | 0.01 | 7 |
| | -Pi | 0.04 | 0.01 | 7 | 0.03 | 0.01 | 8 |
| 7MSOH | +Pi | 0.18 | 0.04 | 7 | 0.12 | 0.03 | 8 |
| | -Pi | 0.19 | 0.06 | 8 | 0.12 | 0.01 | 8 |
| 7MTH | +Pi | 0.39 | 0.11 | 7 | 0.28 | 0.07 | 8 |
| | -Pi | 0.20 | 0.07 | 7 | 0.19 | 0.05 | 7 |
| 8MSOO | +Pi | 1.30 | 0.39 | 8 | 0.80 | 0.10 | 7 |
| | -Pi | 1.36 | 0.40 | 7 | 0.70 | 0.17 | 8 |
| 8MTO | +Pi | 1.31 | 0.28 | 8 | 0.84 | 0.21 | 7 |
| | -Pi | 1.12 | 0.33 | 8 | 0.52 | 0.11 | 8 |
| I3M | +Pi | 0.24 | 0.07 | 8 | 0.25 | 0.06 | 8 |
| | -Pi | 0.23 | 0.09 | 8 | 0.20 | 0.04 | 8 |
| 1MOI3M | +Pi | 0.96 | 0.20 | 8 | 0.47 | 0.15 | 8 |
| | -Pi | 0.72 | 0.25 | 7 | 0.35 | 0.11 | 8 |
| 4MOI3M | +Pi | 0.05 | 0.02 | 8 | 0.05 | 0.02 | 8 |
| | -Pi | 0.04 | 0.01 | 7 | 0.06 | 0.02 | 8 |

| | | | | | | | |
|---|---|---|---|---|---|---|---|
| Total SA | +Pi | 0.04 | | | 0.15 | | |
| | -Pi | 0.07 | | | 0.10 | | |
| Total LA (MTH) | +Pi | 1.75 | | | 1.16 | | |
| | -Pi | 1.35 | | | 0.74 | | |
| Total LA (MS) | +Pi | 1.52 | | | 0.94 | | |
| | -Pi | 1.59 | | | 0.84 | | |
| Total Indolic | +Pi | 1.25 | | | 0.77 | | |
| | -Pi | 0.98 | | | 0.60 | | |

*5-days-old seedlings germinated on +Pi growth medium were transferred to +Pi or -Pi conditions; root tissue was harvested 1 DAT and was used for GSL extraction and HPLC-MS analysis. For each sample, the absolute GSL concentration was normalized to the fresh weight (µg/mg). The mean content of each GSL compound from two independent experiments (±SD) is presented here, consisting of 3-4 technical replicates, each containing a pool of ~8 roots. Abbreviations: Abs. Conc., Absolute Concentration; SD, Standard Deviation; n, number of samples; SA: Short Aliphatic GSLs; LA (MTH), Long Aliphatic methylthiolalkyl GSLs; LA (MS), Long Aliphatic methylsulfinyllalkyl GSLs.*

*Suppl. Table 15 Overview of absolute GSL content in roots of 9-days-old Arabidopsis seedlings.*

| 4 DAT | | WT | | | pdr3 | | | hdc1 | | | OxP3 | | |
|---|---|---|---|---|---|---|---|---|---|---|---|---|---|
| Analyte | Pi | Mean Abs. Conc. | SD Abs. Conc. | n | Mean Abs. Conc. | SD Abs. Conc. | n | Mean Abs. Conc. | SD Abs. Conc. | n | Mean Abs. Conc. | SD Abs. Conc. | n |
| 4MTB | +Pi | 0.01 | 0.00 | 20 | 0.04 | 0.02 | 20 | 0.02 | 0.00 | 20 | 0.01 | 0.01 | 16 |
| | -Pi | 0.01 | 0.01 | 20 | 0.07 | 0.05 | 20 | 0.26 | 1.07 | 20 | 0.01 | 0.01 | 16 |
| 5MTP | +Pi | 0.01 | 0.00 | 24 | 0.01 | 0.01 | 24 | 0.01 | 0.00 | 24 | 0.00 | 0.00 | 16 |
| | -Pi | 0.01 | 0.00 | 24 | 0.01 | 0.01 | 24 | 0.05 | 0.20 | 23 | 0.01 | 0.00 | 16 |
| 6MSOH | +Pi | 0.03 | 0.01 | 24 | 0.01 | 0.00 | 24 | 0.02 | 0.01 | 24 | 0.03 | 0.01 | 16 |
| | -Pi | 0.06 | 0.02 | 23 | 0.03 | 0.01 | 24 | 0.05 | 0.04 | 23 | 0.05 | 0.02 | 16 |
| 6MTH | +Pi | 0.06 | 0.01 | 24 | 0.03 | 0.01 | 24 | 0.05 | 0.02 | 24 | 0.06 | 0.02 | 16 |
| | -Pi | 0.06 | 0.03 | 24 | 0.04 | 0.01 | 24 | 0.07 | 0.09 | 23 | 0.06 | 0.02 | 16 |
| 7MSOH | +Pi | 0.19 | 0.06 | 24 | 0.05 | 0.03 | 23 | 0.09 | 0.04 | 24 | 0.16 | 0.06 | 16 |
| | -Pi | 0.47 | 0.16 | 23 | 0.17 | 0.06 | 24 | 0.36 | 0.24 | 23 | 0.42 | 0.14 | 16 |
| 7MTH | +Pi | 0.40 | 0.10 | 24 | 0.17 | 0.08 | 23 | 0.31 | 0.13 | 24 | 0.38 | 0.12 | 16 |
| | -Pi | 0.37 | 0.19 | 24 | 0.17 | 0.08 | 24 | 0.38 | 0.38 | 23 | 0.39 | 0.14 | 16 |
| 8MSOO | +Pi | 1.20 | 0.34 | 24 | 0.31 | 0.17 | 24 | 0.51 | 0.16 | 24 | 1.13 | 0.44 | 16 |
| | -Pi | 2.53 | 1.02 | 24 | 0.92 | 0.35 | 24 | 2.07 | 1.39 | 23 | 2.66 | 1.41 | 16 |
| 8MTO | +Pi | 1.73 | 0.46 | 24 | 0.71 | 0.39 | 24 | 1.29 | 0.28 | 24 | 1.71 | 0.68 | 16 |
| | -Pi | 1.20 | 0.48 | 24 | 0.59 | 0.27 | 23 | 1.18 | 0.68 | 23 | 1.35 | 0.47 | 16 |
| 1MOI3M | +Pi | 1.01 | 0.30 | 24 | 0.36 | 0.11 | 24 | 0.47 | 0.14 | 24 | 0.89 | 0.23 | 16 |
| | -Pi | 0.98 | 0.53 | 24 | 0.72 | 0.18 | 23 | 0.78 | 0.37 | 23 | 0.91 | 0.26 | 16 |
| 4MOI3M | +Pi | 0.06 | 0.02 | 24 | 0.10 | 0.04 | 24 | 0.10 | 0.05 | 24 | 0.13 | 0.08 | 16 |
| | -Pi | 0.07 | 0.03 | 24 | 0.09 | 0.07 | 24 | 0.12 | 0.13 | 23 | 0.30 | 0.74 | 16 |
| I3M | +Pi | 0.22 | 0.07 | 24 | 0.19 | 0.09 | 24 | 0.17 | 0.05 | 24 | 0.18 | 0.06 | 16 |
| | -Pi | 0.46 | 0.25 | 24 | 0.54 | 0.16 | 24 | 0.39 | 0.11 | 23 | 0.39 | 0.09 | 16 |

| | | WT | pdr3 | hdc1 | OxP3 |
|---|---|---|---|---|---|
| Total SA | +Pi | 0.02 | 0.05 | 0.03 | 0.01 |
| | -Pi | 0.02 | 0.09 | 0.32 | 0.02 |
| Total LA (MTH) | +Pi | 2.19 | 0.91 | 1.64 | 2.14 |
| | -Pi | 1.63 | 0.80 | 1.64 | 1.80 |
| Total LA (MS) | +Pi | 1.42 | 0.37 | 0.62 | 1.32 |
| | -Pi | 3.06 | 1.11 | 2.48 | 3.14 |
| Total Indolic | +Pi | 1.30 | 0.64 | 0.74 | 1.19 |
| | -Pi | 1.50 | 1.34 | 1.30 | 1.60 |

*5-days-old seedlings germinated on +Pi growth medium were transferred to +Pi or -Pi conditions; root tissue was harvested 4 DAT and was used for GSL extraction and HPLC-MS analysis. For each sample, the absolute GSL concentration was normalized to the fresh weight (µg/mg). The mean content of each GSL compound from four-six independent experiment (±SD) is presented here, each consisting of 3-4 technical replicates, containing a pool of ~8 roots. Abbreviations: Abs. Conc., Absolute Concentration; SD, Standard Deviation; n, number of samples; SA: Short Aliphatic GSLs; LA (MTH), Long Aliphatic methylthiolalkyl GSLs; LA (MS), Long Aliphatic methylsulfinyllalkyl GSLs; DAT, day after transfer.*

*Suppl. Table 16 Overview of absolute GSL content in shoots of 9-days-old Arabidopsis seedlings.*

| 4 DAT | | WT | | | pdr3 | | | hdc1 | | | OxP3 | | |
|---|---|---|---|---|---|---|---|---|---|---|---|---|---|
| Analyte | Pi | Mean Abs. Conc. | SD Abs. Conc. | n | Mean Abs. Conc. | SD Abs. Conc. | n | Mean Abs. Conc. | SD Abs. Conc. | n | Mean Abs. Conc. | SD Abs. Conc. | n |
| 3MSOP | +Pi | 0.04 | 0.01 | 20 | 0.02 | 0.01 | 20 | 0.02 | 0.01 | 20 | 0.03 | 0.01 | 16 |
| | -Pi | 0.04 | 0.01 | 20 | 0.03 | 0.01 | 20 | 0.04 | 0.02 | 20 | 0.04 | 0.01 | 16 |
| 3MTP | +Pi | 0.01 | 0.00 | 24 | 0.01 | 0.00 | 24 | 0.01 | 0.00 | 24 | 0.01 | 0.00 | 16 |
| | -Pi | 0.01 | 0.00 | 24 | 0.01 | 0.00 | 24 | 0.01 | 0.00 | 24 | 0.01 | 0.00 | 16 |
| 4MSOB | +Pi | 0.60 | 0.17 | 24 | 0.45 | 0.20 | 24 | 0.41 | 0.15 | 24 | 0.56 | 0.18 | 16 |
| | -Pi | 0.83 | 0.30 | 24 | 0.72 | 0.31 | 24 | 0.71 | 0.28 | 24 | 0.77 | 0.36 | 16 |
| 4MTB | +Pi | 1.46 | 0.26 | 24 | 1.67 | 0.28 | 24 | 1.24 | 0.28 | 24 | 1.20 | 0.30 | 16 |
| | -Pi | 1.75 | 0.52 | 24 | 2.20 | 0.48 | 24 | 1.59 | 0.68 | 24 | 1.49 | 0.42 | 16 |
| 5MTP | +Pi | 0.23 | 0.06 | 24 | 0.26 | 0.06 | 24 | 0.22 | 0.05 | 24 | 0.20 | 0.06 | 16 |
| | -Pi | 0.28 | 0.09 | 24 | 0.36 | 0.08 | 24 | 0.32 | 0.14 | 24 | 0.26 | 0.08 | 16 |
| 6MSOH | +Pi | 0.01 | 0.00 | 24 | 0.01 | 0.00 | 24 | 0.01 | 0.00 | 24 | 0.01 | 0.01 | 16 |
| | -Pi | 0.02 | 0.01 | 24 | 0.01 | 0.00 | 24 | 0.02 | 0.01 | 24 | 0.02 | 0.01 | 16 |
| 6MTH | +Pi | 0.11 | 0.03 | 24 | 0.10 | 0.03 | 24 | 0.12 | 0.03 | 24 | 0.11 | 0.03 | 16 |
| | -Pi | 0.12 | 0.04 | 24 | 0.13 | 0.04 | 24 | 0.16 | 0.06 | 24 | 0.12 | 0.03 | 16 |
| 7MSOH | +Pi | 0.03 | 0.01 | 24 | 0.02 | 0.01 | 24 | 0.03 | 0.01 | 24 | 0.03 | 0.01 | 16 |
| | -Pi | 0.07 | 0.02 | 24 | 0.05 | 0.01 | 24 | 0.09 | 0.04 | 24 | 0.06 | 0.01 | 16 |
| 7MTH | +Pi | 0.40 | 0.12 | 24 | 0.38 | 0.11 | 24 | 0.48 | 0.12 | 24 | 0.37 | 0.15 | 16 |
| | -Pi | 0.47 | 0.14 | 24 | 0.53 | 0.16 | 24 | 0.66 | 0.24 | 24 | 0.44 | 0.14 | 16 |
| 8MSOO | +Pi | 0.15 | 0.05 | 24 | 0.06 | 0.03 | 24 | 0.08 | 0.03 | 24 | 0.14 | 0.06 | 16 |
| | -Pi | 0.22 | 0.07 | 24 | 0.24 | 0.07 | 24 | 0.36 | 0.23 | 24 | 0.20 | 0.05 | 16 |
| 8MTO | +Pi | 0.58 | 0.16 | 24 | 0.47 | 0.14 | 24 | 0.63 | 0.16 | 24 | 0.54 | 0.23 | 16 |
| | -Pi | 0.59 | 0.18 | 24 | 0.71 | 0.22 | 24 | 0.91 | 0.32 | 24 | 0.57 | 0.18 | 16 |
| 1MOI3M | +Pi | 0.38 | 0.14 | 20 | 0.15 | 0.05 | 20 | 0.15 | 0.06 | 20 | 0.38 | 0.12 | 16 |
| | -Pi | 0.28 | 0.09 | 20 | 0.18 | 0.12 | 20 | 0.23 | 0.13 | 20 | 0.29 | 0.07 | 16 |
| 4MOI3M | +Pi | 0.22 | 0.07 | 24 | 0.17 | 0.05 | 24 | 0.17 | 0.05 | 24 | 0.31 | 0.16 | 16 |
| | -Pi | 0.27 | 0.07 | 24 | 0.26 | 0.11 | 24 | 0.22 | 0.06 | 24 | 0.45 | 0.11 | 16 |
| I3M | +Pi | 0.83 | 0.15 | 24 | 0.71 | 0.22 | 24 | 0.54 | 0.15 | 24 | 0.78 | 0.21 | 16 |
| | -Pi | 1.15 | 0.33 | 24 | 1.08 | 0.28 | 24 | 0.90 | 0.35 | 24 | 1.30 | 0.29 | 16 |

| | | WT | | | pdr3 | | | hdc1 | | | OxP3 | | |
|---|---|---|---|---|---|---|---|---|---|---|---|---|---|
| Total SA | +Pi | 2.32 | | | 2.41 | | | 1.90 | | | 2.00 | | |
| | -Pi | 2.91 | | | 3.32 | | | 2.66 | | | 2.56 | | |
| Total LA (MTH) | +Pi | 1.09 | | | 0.95 | | | 1.23 | | | 1.01 | | |
| | -Pi | 1.18 | | | 1.38 | | | 1.73 | | | 1.13 | | |
| Total LA (MS) | +Pi | 0.20 | | | 0.08 | | | 0.11 | | | 0.19 | | |
| | -Pi | 0.31 | | | 0.31 | | | 0.47 | | | 0.28 | | |
| Total Indolic | +Pi | 1.43 | | | 1.03 | | | 0.85 | | | 1.47 | | |
| | -Pi | 1.69 | | | 1.52 | | | 1.35 | | | 2.04 | | |

*5-days-old seedlings germinated on +Pi growth medium were transferred to +Pi or -Pi conditions; shoot tissue was harvested 4 DAT and was used for GSL extraction and HPLC-MS analysis. For each sample, the absolute GSL concentration was normalized to the fresh weight (µg/mg). The mean content of each GSL compound from four-six independent experiment (±SD) is presented here, each consisting of 3-4 technical replicates, containing a pool of 3-4 shoots. Abbreviations: Abs. Conc., Absolute Concentration; SD, Standard Deviation; n, number of samples; SA: Short Aliphatic GSLs; LA (MTH), Long Aliphatic methylthiolalkyl GSLs; LA (MS), Long Aliphatic methylsulfinyllalkyl GSLs; DAT, day after transfer.*

*Suppl. Table 17 Overview of the expression of genes participating in regulation of glucosinolate biosynthesis in pdr3 roots.*

| Locus | Gene name | $log_2FC$ | padj |
|---|---|---|---|
| AT3G09710 | IQD1 | 0.88 | 2E-11 |
| AT1G32640 | MYC2 | -0.83 | 2E-07 |
| AT5G60890 | MYB34 | -0.57 | 7E-06 |
| AT1G18570 | **MYB51** | **1.38** | **3E-04** |
| AT5G46760 | MYC3 | -0.42 | 2E-03 |
| AT2G46830 | CCA1 | 0.31 | 1E-01 |
| AT3G06250 | FRS7 | 0.24 | 1E-01 |
| AT1G07640 | OBP2 | -0.36 | 1E-01 |
| AT3G23590 | MED33A | 0.20 | 2E-01 |
| AT4G17880 | MYC4 | -0.21 | 2E-01 |
| AT5G11260 | HY5 | 0.20 | 2E-01 |
| AT5G48850 | SDI1 | 0.41 | 3E-01 |
| AT1G25540 | MED25 | 0.14 | 4E-01 |
| AT2G22300 | CAMTA3 | -0.16 | 4E-01 |
| AT5G18960 | FRS12 | 0.12 | 5E-01 |
| AT1G73730 | EIL3 | 0.13 | 5E-01 |
| AT1G74080 | MYB122 | -0.17 | 8E-01 |
| AT1G04770 | SDI2 | 0.10 | 9E-01 |
| AT5G07690 | MYB29 | NA | NA |
| AT5G07700 | MYB76 | NA | NA |
| | | | |
| AT1G73730 | EIL3 | 0.13 | 0.51 |
| AT4G36730 | GBF1 | -0.44 | 0.01 |
| AT3G17609 | HYH | 0.20 | 0.40 |
| AT2G35530 | BZIP16 | 0.20 | 0.30 |
| AT1G75390 | BZIP44 | 0.15 | 0.37 |

*5-days-old seedlings germinated on +Pi growth medium were transferred to fresh +Pi media. Root tissue was harvested 1DAT and was used for RNA extraction and transcriptional analysis via RNA-seq. Logarithmic fold change ($log_2FC$) values indicate differences in mean expression of the genes between pdr3 and WT roots across 3 biological replicates, each containing a pool of 50 roots, with negative values signifying lower transcript levels in the mutant. Adjusted p-values (padj) signify statistically significant changes after adjustment for multiple testing using FDR. Significantly differentially expressed genes according to cutoff thresholds (1< log2FC< -1, padj< 0.05) are marked with bold. NA values signify absence of detected transcripts. List of genes participating in this GO term were obtained from TAIR, while the 5 genes at the bottom of the table are participating in SDI1/2 regulation as described in Rakpenthai et al., 2022.*

*Suppl. Table 18 Overview of the expression of DEGs in pdr3 roots, with a function in transcription (GO:0006350).*

| Locus | Gene name | log$_2$FC | padj | Locus | Gene name | log$_2$FC | padj |
|---|---|---|---|---|---|---|---|
| AT5G25470 | - | 2.36 | 3E-02 | AT4G25400 | - | -1.01 | 4E-05 |
| AT3G02150 | TCP13 | 2.18 | 4E-03 | AT4G18130 | PHYE | -1.05 | 6E-08 |
| AT1G75250 | ATRL6 | 2.04 | 3E-03 | AT4G21750 | ATML1 | -1.10 | 4E-04 |
| AT3G16980 | NRPB9A | 2.01 | 2E-07 | AT5G10970 | - | -1.11 | 2E-05 |
| AT4G33280 | - | 2.00 | 4E-02 | AT5G03680 | PTL | -1.11 | 4E-04 |
| AT2G46400 | WRKY46 | 1.99 | 1E-02 | AT1G62975 | BHLH125 | -1.11 | 2E-06 |
| AT5G58610 | - | 1.79 | 1E-09 | AT4G05100 | AtMYB74 | -1.15 | 2E-03 |
| AT1G05230 | HDG2 | 1.55 | 1E-04 | AT3G50410 | DOF3.4 | -1.18 | 1E-02 |
| AT2G36270 | ABI5 | 1.49 | 3E-04 | AT5G61420 | MYB28 | -1.18 | 4E-15 |
| AT4G38340 | NLP3 | 1.43 | 2E-10 | AT5G23000 | RAX1 | -1.18 | 4E-02 |
| AT5G65330 | AGL78 | 1.41 | 7E-03 | AT2G20180 | PIF1 | -1.21 | 5E-02 |
| AT1G18570 | MYB51 | 1.38 | 3E-04 | AT1G30210 | TCP24 | -1.30 | 7E-04 |
| AT2G22540 | SVP | 1.36 | 6E-09 | AT2G46680 | ATHB-7 | -1.36 | 1E-13 |
| AT5G62165 | AGL42 | 1.36 | 4E-07 | AT5G57980 | NRPB5L1 | -1.37 | 1E-11 |
| AT1G70920 | ATHB-X | 1.33 | 1E-03 | AT5G53980 | ATHB-52 | -1.40 | 3E-03 |
| AT1G22490 | - | 1.30 | 3E-04 | AT2G39250 | SNZ | -1.43 | 7E-05 |
| AT5G64810 | WRKY51 | 1.23 | 1E-05 | AT1G48000 | MYB112 | -1.45 | 6E-03 |
| AT1G26680 | - | 1.20 | 4E-06 | AT3G25990 | GT-4 | -1.46 | 5E-02 |
| AT3G02790 | MBS1 | 1.16 | 9E-16 | AT3G61890 | ATHB-12 | -1.51 | 9E-04 |
| AT1G02580 | MEA | 1.12 | 7E-03 | AT1G46768 | RAP2-1 | -1.58 | 2E-04 |
| AT5G65320 | BHLH99 | 1.11 | 2E-08 | AT5G51190 | ERF105 | -1.69 | 2E-02 |
| AT1G06170 | BHLH89 | 1.10 | 2E-03 | AT4G25410 | BHLH126 | -1.73 | 8E-11 |
| AT2G40340 | DREB2C | 1.09 | 6E-03 | AT4G04450 | WRKY42 | -1.78 | 1E-04 |
| | | | | AT5G67180 | TOE3 | -1.79 | 5E-02 |
| | | | | AT5G52260 | AtMYB19 | -1.87 | 3E-03 |
| | | | | AT5G51790 | - | -1.91 | 2E-06 |
| | | | | AT4G00050 | UNE10 | -2.18 | 1E-03 |
| | | | | AT4G25480 | DREB1A | -2.29 | 5E-02 |
| | | | | AT4G16610 | - | -4.44 | 2E-15 |

*5-days-old seedlings germinated on +Pi growth medium were transferred to fresh +Pi media. Root tissue was harvested 1DAT and was used for RNA extraction and transcriptional analysis via RNA-seq. Logarithmic fold change (log$_2$FC) values indicate differences in mean expression of the genes between pdr3 and WT roots across 3 biological replicates, each containing a pool of 50 roots, with negative values signifying lower transcript levels in the mutant (columns on the right of the table). Adjusted p-values (padj) signify statistically significant changes after adjustment for multiple testing using FDR.*

*Suppl. Table 19 Overview of the expression of genes participating in regulation of chlorophyll biosynthesis (left) or photosynthesis (right) in pdr3 root tips.*

| Regulation of chlorophyll metabolic process | | | | Regulation of photosynthesis | | | |
|---|---|---|---|---|---|---|---|
| Locus | Gene name | Log$_2$FC | padj | Locus | Gene name | Log$_2$FC | padj |
| AT4G14690 | ELIP2 | 0.98 | 0 | AT2G47400 | CP12-1 | 0.96 | 0 |
| AT3G22840 | ELIP1 | 0.74 | 0.01 | **AT2G30570** | **PSBW** | **1.92** | **0** |
| AT5G40850 | UPM1 | 0.45 | 0.01 | **AT1G55670** | **PSAG** | **1.36** | **0.01** |
| AT2G20570 | GLK1 | -2.8 | 0.1 | AT1G71500 | - | 0.67 | 0.07 |
| AT5G56860 | GATA21 | -2.12 | 0.12 | AT1G67740 | PSBY | 0.87 | 0.12 |
| AT1G27320 | AHK3 | 0.39 | 0.29 | AT3G03380 | DEGP7 | -0.36 | 0.16 |
| AT5G35750 | AHK2 | -0.44 | 0.35 | AT4G00630 | KEA2 | -0.38 | 0.2 |
| AT3G04060 | anac046 | 0.36 | 0.4 | AT1G61800 | GPT2 | 1.69 | 0.25 |
| AT5G58270 | ABCB25 | -0.27 | 0.5 | AT1G68890 | PHYLLO | -0.77 | 0.3 |
| AT1G20780 | PUB44 | 0.19 | 0.54 | AT1G32070 | NSI | 0.35 | 0.32 |
| AT2G42810 | PAPP5 | -0.17 | 0.57 | AT3G15850 | ADS3 | 0.31 | 0.39 |
| AT1G69935 | SHW1 | -0.5 | 0.57 | AT1G77510 | PDIL1-2 | 0.27 | 0.45 |
| AT4G31920 | ARR10 | 0.16 | 0.62 | AT4G04020 | PAP1 | -0.38 | 0.45 |
| AT3G22690 | - | -0.28 | 0.63 | AT5G01920 | STN8 | 0.32 | 0.47 |
| AT5G50920 | CLPC1 | 0.16 | 0.64 | AT1G76560 | CP12-3 | 0.35 | 0.49 |
| AT4G11910 | SGR2 | -0.94 | 0.69 | AT5G65810 | CGR3 | -0.22 | 0.51 |
| AT4G26150 | GATA22 | 1.48 | 0.71 | AT3G61320 | - | 0.32 | 0.53 |
| AT2G35260 | - | 0.38 | 0.71 | AT5G52520 | OVA6 | -0.15 | 0.66 |
| AT2G25180 | ARR12 | -0.13 | 0.79 | AT5G66570 | PSBO1 | 0.28 | 0.66 |
| AT2G41680 | NTRC | 0.09 | 0.89 | AT1G75540 | BBX21 | -0.16 | 0.67 |
| AT3G16857 | ARR1 | 0.07 | 0.91 | AT1G01790 | KEA1 | -0.24 | 0.7 |
| AT3G57180 | BPG2 | -0.06 | 0.95 | AT1G67840 | CSK | -0.26 | 0.73 |
| AT5G44190 | GLK2 | 0.06 | 0.95 | AT1G64860 | SIGA | 0.19 | 0.75 |
| AT5G47110 | LIL3.2 | 0.01 | 0.98 | AT5G57050 | ABI2 | -0.16 | 0.82 |
| AT4G31390 | ABC1K1 | 0.02 | 0.99 | AT4G26160 | ACHT1 | 0.17 | 0.83 |
| AT3G19290 | ABF4 | -0.01 | 0.99 | AT1G68830 | STN7 | 0.18 | 0.84 |
| AT4G17600 | LIL3.1 | -0.01 | 1 | AT3G49720 | CGR2 | -0.1 | 0.85 |
| AT1G56200 | NA | NA | NA | AT3G11670 | DGD1 | -0.12 | 0.85 |
| | | | | AT4G27800 | PPH1 | -0.19 | 0.87 |
| | | | | AT4G04850 | KEA3 | -0.08 | 0.91 |
| | | | | AT5G50950 | FUM2 | -0.17 | 0.91 |
| | | | | AT2G30950 | VAR2 | 0.04 | 0.93 |
| | | | | AT5G42270 | FTSH5 | 0.04 | 0.93 |
| | | | | AT4G30950 | FAD6 | -0.04 | 0.94 |
| | | | | AT4G01800 | AGY1 | -0.06 | 0.95 |
| | | | | AT3G50820 | PSBO2 | -0.05 | 0.98 |
| | | | | AT4G31390 | ABC1K1 | 0.02 | 0.99 |
| | | | | AT3G62410 | CP12-2 | -0.04 | 1 |

| | AT2G45870 | - | 0 | 1 |
|---|---|---|---|---|
| | AT4G37230 | - | NA | NA |
| | ATCG00300 | PSBZ | NA | NA |

*5-days-old seedlings germinated on +Pi growth medium were transferred to fresh +Pi media. Root tips were harvested 1DAT and were used for RNA extraction and transcriptional analysis via RNA-seq. Logarithmic fold change (log$_2$FC) values indicate differences in mean expression of the genes between pdr3 and WT roots across 3 biological replicates, each containing a pool of 150 root tips, with negative values signifying lower transcript levels in the mutant. Adjusted p-values (padj) signify statistically significant changes after adjustment for multiple testing using FDR. Significantly differentially expressed genes according to cutoff thresholds (1<log2FC<-1, padj< 0.05) are marked with bold. NA values signify absence of detected transcripts. List of genes participating in each process were obtained from TAIR.*

**Suppl. Table 20** *Overview of the expression of genes participating in cellular response to phosphate starvation (GO:0016036) among different tissues and Pi regimes.*

| | | Log$_2$FC | | | | | |
|---|---|---|---|---|---|---|---|
| Locus | Gene name | *pdr3*_RT +Pi vs WT_RT +Pi | *pdr3*_RT -Pi vs WT_RT -Pi | *pdr3*_S +Pi vs WT_S +Pi | *pdr3*_R +Pi vs WT_R +Pi | WT_RT -Pi vs WT_RT +Pi | *pdr3*_RT -Pi vs *pdr3*_RT +Pi |
| AT1G27320 | AHK3 | X | 0.84 | X | X | X | X |
| AT2G01830 | AHK4 | X | X | 0.55 | X | -0.54 | X |
| AT2G02470 | AL6 | X | X | X | X | X | X |
| AT1G18420 | ALMT3 | X | X | X | X | X | X |
| AT5G03545 | AT4 | X | X | X | **-1.59** | **4.09** | **4.04** |
| AT1G66270 | BGLU21 | X | X | **3.16** | X | 0.47 | X |
| AT3G25710 | BHLH32 | X | 0.76 | X | X | X | X |
| AT3G27740 | CARA | X | X | X | X | X | X |
| AT1G29900 | CARB | X | -0.57 | X | -0.26 | X | X |
| AT1G20630 | CAT1 | **1.28** | **1.85** | X | 0.62 | X | 0.93 |
| AT4G35090 | CAT2 | 0.47 | 0.76 | -0.56 | X | X | X |
| AT1G20620 | CAT3 | X | **1.35** | 0.62 | X | X | 0.97 |
| AT4G00550 | DGD2 | X | X | X | X | X | X |
| AT3G08040 | DTX43 | **1.36** | **3.25** | X | X | X | **1.46** |
| AT3G51770 | ETO1 | X | X | X | X | X | X |
| AT5G21040 | FBX2 | X | X | X | X | X | X |
| AT5G38480 | GRF3 | X | X | X | X | X | X |
| AT3G25790 | HHO1 | X | 0.56 | X | X | X | X |
| AT1G25550 | HHO3 | X | X | X | X | 0.84 | X |
| AT1G13300 | HRS1 | X | X | X | X | X | X |
| AT3G09922 | IPS1 | X | X | X | X | X | X |
| AT2G22240 | IPS2 | X | X | X | -0.53 | X | X |
| AT1G23010 | **LPR1** | **1.18** | **1.94** | X | X | X | X |
| AT1G71040 | LPR2 | X | 0.86 | 0.52 | X | X | **1.03** |
| AT5G20410 | MGD2 | X | **-2.21** | -0.93 | X | X | **-2.19** |
| AT2G11810 | MGD3 | X | X | X | X | X | X |
| AT2G25095 | MIR156A | X | X | X | X | X | X |
| AT4G31877 | MIR156C | X | X | X | X | X | X |

| | | | | | | | |
|---|---|---|---|---|---|---|---|
| AT5G10945 | MIR156D | X | X | X | X | X | X |
| AT3G13405 | MIR169A | X | X | X | X | X | X |
| AT5G24825 | MIR169B | X | X | X | X | X | X |
| AT1G19371 | MIR169H | X | X | X | X | X | X |
| AT3G26815 | MIR169K | X | X | **-3.30** | X | X | X |
| AT2G03445 | MIR398A | X | X | X | X | X | X |
| AT5G14545 | MIR398B | X | X | X | X | X | X |
| AT5G14565 | MIR398C | X | X | X | X | X | X |
| AT1G77235 | MIR402 | X | X | X | X | X | X |
| AT4G27765 | MIR828A | X | X | X | X | X | X |
| AT2G47190 | MYB2 | X | X | X | X | X | X |
| AT3G03520 | NPC3 | X | X | X | X | X | X |
| AT3G09560 | PAH1 | X | X | X | X | X | X |
| AT5G42870 | PAH2 | X | X | X | X | X | X |
| AT2G16430 | PAP10 | 0.96 | 0.86 | X | 0.55 | X | X |
| AT2G27190 | PAP12 | X | -0.40 | X | X | 0.50 | X |
| AT4G37870 | PCKA | X | 0.98 | X | X | X | 0.70 |
| AT5G23630 | PDR2 | X | X | X | X | X | X |
| AT3G52190 | PHF1 | X | X | X | X | X | X |
| AT3G24120 | PHL2 | X | 0.67 | X | 0.49 | X | 0.66 |
| AT3G23430 | PHO1 | X | **1.25** | X | -0.34 | X | 0.96 |
| AT1G14040 | PHO1;H3 | X | X | X | 0.41 | X | X |
| AT1G68740 | PHO1-H1 | X | **2.53** | X | X | X | **2.77** |
| AT1G69480 | PHO1-H10 | X | X | X | **1.05** | X | X |
| AT2G03260 | PHO1-H2 | X | X | X | X | X | X |
| AT4G25350 | PHO1-H4 | X | X | X | 0.79 | X | X |
| AT2G03240 | PHO1-H5 | X | **1.27** | X | X | X | **1.43** |
| AT1G26730 | PHO1-H7 | X | **2.95** | X | X | X | **2.18** |
| AT1G35350 | PHO1-H8 | X | X | X | X | X | X |
| AT4G28610 | PHR1 | X | X | X | X | X | X |
| AT5G43350 | PHT1-1 | X | X | **1.30** | X | 0.95 | X |
| AT5G43370 | PHT1-2 | X | X | X | X | **3.47** | X |
| AT1G55180 | PLDALPHA4 | X | X | X | -0.54 | X | X |
| AT3G16785 | PLDP1 | X | X | X | X | X | X |
| AT3G05630 | PLPZETA2 | X | X | X | 0.56 | X | X |
| AT3G03710 | PNP1 | X | X | X | X | X | X |
| AT1G53310 | PPC1 | X | X | X | X | X | X |
| AT3G04530 | PPCK2 | X | X | X | X | X | X |
| AT3G20330 | PYRB | X | X | X | 0.36 | X | X |
| AT3G54470 | PYRE-F | X | -0.94 | X | X | X | X |
| AT5G60810 | RGF1 | X | **2.93** | X | X | X | X |
| AT1G13620 | RGF2 | 0.93 | 0.94 | X | **1.12** | X | X |
| AT4G02270 | RHS13 | X | **1.28** | 3.02 | X | X | **1.17** |
| AT2G02990 | RNS1 | **1.21** | 0.77 | **1.62** | **1.12** | **1.87** | **1.40** |
| AT1G58250 | SAB | X | X | X | X | X | X |

| AT5G60410 | SIZ1 | X | X | X | X | X | X |
|---|---|---|---|---|---|---|---|
| AT5G20150 | SPX1 | X | **-1.38** | X | X | **3.09** | **1.33** |
| AT2G26660 | SPX2 | X | X | X | X | 0.73 | X |
| AT2G45130 | SPX3 | X | X | X | X | X | **5.22** |
| AT5G15330 | SPX4 | X | X | X | X | X | X |
| AT4G33030 | SQD1 | 0.65 | X | X | 0.50 | 0.99 | X |
| AT5G01220 | SQD2 | X | X | X | X | X | X |
| AT3G25795 | TAS4 | X | **3.63** | X | **1.13** | X | **3.07** |
| AT3G62980 | TIR1 | X | X | X | X | X | X |
| AT2G33770 | UBC24 | X | 0.82 | X | X | **-1.03** | X |
| AT3G03250 | UGP | X | X | X | -0.25 | X | X |
| AT3G53900 | UPP | 0.56 | X | 0.41 | 0.60 | X | X |
| AT1G62300 | WRKY6 | X | X | X | X | 0.57 | X |
| | | | | | | | |
| AT1G08430 | ALMT1 | **3.38** | **3.51** | **5.52** | X | X | **1.49** |
| AT1G08650 | PPCK1 | X | **-1.38** | X | -0.45 | **1.02** | X |
| AT2G42600 | PPC2 | -0.64056 | -0.74 | X | -0.45 | X | X |
| AT3G14940 | PPC3 | X | X | 0.997342 | X | X | X |

*5-days-old seedlings germinated on +Pi growth medium were transferred to fresh +Pi media or to -Pi media. Root tips were harvested 1DAT from seedlings grown at +Pi or -Pi conditions; shoots and roots were harvested only from +Pi media. Tissue samples were used for RNA extraction and transcriptional analysis via RNA-seq. Logarithmic fold change (log2FC) values indicate differences in mean expression of the genes between pdr3 and WT roots across 3 biological replicates, each containing a pool of 150-200 root tips or 25 shoots or 50 roots. Adjusted p-values (padj) were calculated after adjustment for multiple testing using FDR; in the table, genes marked with X did not show statistically significant difference in their expression within the indicated comparison (genotype and/or condition). Significantly differentially expressed genes according to cutoff thresholds (1< log2FC< -1, padj< 0.05) are marked with bold. The genes at the bottom of the table (ALMT1, PPCK1, PPC2, PPC3) do not belong in the indicated GO term but have important functions in phosphate starvation responses.*
*Abbr.: RT, root tips; S, shoot; R, root.*

**Suppl. Table 21. List of oligonucleotides used in genotyping and in qPCR reactions.**

| Name | 5'->3' Sequence | Purpose |
|---|---|---|
| **Primers for genotyping** | | |
| **pdr3 Fw** | GCGCAGAGAGATCTTTAGGC | genotyping of *pdr3*, after digest with HinfI: |
| **pdr3 Rev** | TCAGGGTCCTAAGAGTGACAGG | WT=199bp + 108bp/*pdr3*=307bp |
| **hdc1 LP** | CAAGGACTGGTGCTGAGAAAG | genotyping of GABI_054G03 |
| **hdc1 RP** | GCAGCCAAAATCTCAAGTAGC | |
| **wrky46-1 LP** | GAGTCTCTTCTCGAAGCTGGG | genotyping of SALK_134310 |
| **wrky46-1 RP** | GATCCTTCCCTTTTCGAAGTG | |
| **wrky46-2 LP** | GAGTCTCTTCTCGAAGCTGGG | genotyping of SAIL_1230_H01 |
| **wrky46-2 RP** | GATCCTTCCCTTTTCGAAGTG | |
| **myb28-1 LP** | TTTTTCATTATGCGTTTGCAG | genotyping of SALK_136312C |
| **myb28-1 RP** | CTCTTTCCACACCGTTTCAAC | |
| **GFP Fw** | TTCTTCAAGGACGACGGCAA | genotyping of pdr3/PDR3p::PDR3-GFP |
| **GFP Rev** | TCGATGTTGTGGCGGATCTT | |

| | | |
|---|---|---|
| **LBb1.3** | ATTTTGCCGATTTCGGAAC | genotyping of SALK lines (left border primer) |
| **LB1** | GCCTTTTCAGAAATGGATAAATAGCCTTGCTTCC | genotyping of SAIL lines (left border primer) |
| **Primers for qPCR** | | |
| **HDC1 qRT F** | GAAGGAGCTACCGAGAGGGA | *HDC1* (AT5G08450) |
| **HDC1 qRT R** | GACACCTCTGACTTGCCTTG | |
| **MYB28 qRT F** | AGGAAACTTCGAGGGATGGTC | *MYB28* (AT5G61420) |
| **MYB28 qRT R** | GCGAGTCTGAGTCGGTGTC | |
| **MYB51 qRT F** | CCCTTCACGGCAACAAATGG | *MYB51* (AT1G18570) |
| **MYB51qRT R** | GTCGGTACCGGAGGTTATGC | |
| **MAM1 qRT F** | GGCAGGTCGGACAAGGATTT | *MAM1* (AT5G23010) |
| **MAM1 qRT R** | TGGCATGTTGATCCCTACCG | |
| **MAM3 qRT F** | AGAGGCCGAGGGTAATGCTA | *MAM3* (AT5G23020) |
| **MAM3 qRT R** | CACGGCCATCTCGATCACTT | |
| **CYP79B2 qRT F** | CCGCCGATGAAATCAAACCC | *CYP79B2* (AT4G39950) |
| **CYP79B2 qRT R** | CGAGTCTCTCTTTCCCGACG | |
| **CYP83A1 qRT F** | AGAGAGTCAAGCCCGAAACC | *CYP83A1* (AT4G13770) |
| **CYP83A1 qRT R** | CCCGCCACTACAATATCCAAGA | |
| **BCAT4 qRT F** | CCTCTTCCTGTGAGTGTTTCG | *BCAT4* (AT3G19710) |
| **BCAT4 qRT R** | CTCCATGATTGCACTTCGCA | |
| **IPMI1 qRT F** | GAGAGACTTTCCACGGCCTC | *IPMI1* (AT3G58990) |
| **IPMI1 qRT R** | CGTACTCGGCGGGGATTATT | |
| **SOT18 qRT F** | GCCCCTGATCGAGTATGGTG | *SOT18* (AT1G74090) |
| **SOT18 qRT R** | GAGGAAGTCACTGGGTCGTG | |
| **FMO-GS$_{OX3}$ qRT F** | GGCGGGTTCTTGGAAGATGA | *FMO$_{GS-OX3}$* (AT1G62560) |
| **FMO-GS$_{OX3}$ qRT R** | ATATCGGCACCACTCGCAAA | |
| **GSL-OH qRT F** | ATTGGCGTGAAAGGACTCGT | *GSL-OH* (AT2G25450) |
| **GSL-OH qRT R** | TGCTACGTTAACATGCGGGT | |

*Abbr.: Fw, forward; Rev, reverse*

# Acknowledgements

The great Greek poet C. Cavafy once wrote "As you set out for Ithaka, hope your road is a long one, full of adventure, full of discovery", emphasizing the importance of the journey towards reaching an important goal, rather than the actual goal itself. Likewise, this doctorate work has been a long road that gifted me with experiences and knowledge, equally important with the academic title that comes at the end of it. And alongside each step, I had many companions, towards whom I would like to express my deepest gratitude.

First and foremost, I would like to thank my supervisor Prof. Dr. Steffen Abel for giving me the opportunity to work in his group. Without his trust, this wonderful journey would not have even begun. Under his supervision, I realized what kind of scientist I would like to be and for that, I thank him sincerely.

A big thanks belongs to all members of Nutrient Sensing group, past and present, for being my work family the last three years. Specifically, I would like to acknowledge Dr. Jörg Ziegler for his immense support, throughout my entire stay in this group. His knowledge and advice helped me to achieve significant advances in my work, while the interest he showed in my project inspired me at times that I needed it the most. Moreover, I would like to thank Dr. Christin Nauman for helping me to find my place in the group during my first months in the lab and for always been available when I needed assistance. I cannot help but express my sincerest gratitude towards our amazing technicians Kathrin, Birgit and Nancy, for their willingness to provide help in every way possible. Their calm energy and constant reassurance were a grounding force for me, when things were getting particularly tough. A warm thanks to Willi for all the great discussions we shared and his overall presence in our group. Of course, this acknowledgement section would be incomplete if I didn't refer to my "partners-in-crime", Caro, Mingdan and Samuel, my fellow PhD students of the group. I cannot even begin to thank them for the support, team spirit and kindness they showed all this time.

I would like to thank the entire MSV department for the great working atmosphere and excellent cooperation in all aspects of our everyday lab life. Moreover, I would like to thank Hagen Stellmach for patiently helping me with my microscopy experiments. Also, a big thanks to Dr. Khabat Vahabi for his assistance with the RNA-seq analysis and to Dr. Gerd Hause for performing the TEM-based analysis that was included in this work.

As a part of RTG2498, I had the pleasure to meet and work with a group of very talented people, who continuously provided help and assistance with my project. Firstly, I would like to express how grateful I am towards Prof. Dr. Kristina Kühn and Dr. Mareike Heilman, for their contribution in my work as my mentors. Their valuable feedback and guidance greatly helped me to navigate this project. Of course, my gratitude extends to all PhD students and PIs of the group. In particular, I would like to thank Dr. Debora Gasperini, Prof. Dr. Bettina Hause and Dr. Martin Schattat for all the fruitful discussions we had and for the resources that they eagerly shared with me. Special thanks to Dr. Julia Grimmer for her excellent work in coordinating the group and assisting all of us.

# Curriculum Vitae

| | |
|---|---|
| Name: | Pinelopi Moutesidi |
| Nationality: | Greek |

**Education**

| | |
|---|---|
| *07/2019-present* | **Doctorate**<br>Faculty of Natural Sciences 1 - Biosciences, Martin Luther University Halle-Wittenberg<br>Research Graduate School 2498 (RTG2498)<br>Dissertation: Investigation of Arabidopsis HDC1-mediated histone deacetylation and its role in phosphate deficiency response<br>Supervisor: Prof. Dr. Steffen Abel<br>Leibniz Institute of Plant Biochemistry, Halle (Saale), Germany |
| *01/2018-02/2018* | **Research internship**<br>Supervisor: Dr. Franziska Turck<br>Max Planck Institute for Plant Breeding Research, Cologne, Germany |
| *09/2017-12/2017* | **Scientific student assistant**<br>Laboratory of Prof. Dr. Dorothea Bartels<br>Institute for Molecular Physiology and Biotechnology of plants, Bonn, Germany |
| *02/2017-04/2017* | **Research internship**<br>Supervisor: Prof. Dr. Dorothea Bartels<br>Institute for Molecular Physiology and Biotechnology of plants, Bonn, Germany |
| *10/2016-10/2018* | **Master of Science**<br>Rhenish Friedrich Wilhelm University of Bonn<br>Plant Sciences Master program<br>Final mark: 1.6 (Good)<br>Master thesis: Developing enChIP as a method to measure long-range chromatin interactions in plants<br>Supervisor: Dr. Franziska Turck<br>Max Planck Institute for Plant Breeding Research, Cologne, Germany |

| | |
|---|---|
| *03/2016-05/2016* | **Erasmus Traineeship** |
| | University of Potsdam, Golm, Germany |
| | Project: Molecular basis of heat stress memory in plants |
| | Supervisor: Prof. Isabel Bäurle |
| | Institute for Biochemistry and Biology, Golm, Germany |
| | |
| *06/2011-07/2016* | **Bachelor of Science** |
| | Department of Biology, University of Crete, Heraklion, Greece |
| | Final mark: 7.21/10 (Very Good) |
| | Bachelor thesis: Investigation of the effect of Prune Dward Virus and Prune Necrotic Ringspot Virus on RNA silencing mechanism of *N. benthamiana* |
| | Supervisor: Assoc. Prof. Kriton Kalantidis |
| | Institute of Molecular Biology and Biotechnology University of Crete, Heraklion, Greece |
| | |
| *09/2008-06/2011* | **High School education (Lyceum)** |
| | General High School of Batheos Aylidos, Aylida, Greece |
| | Final mark: 18.9/20 (Excellent) |

**Conference and workshop attendances**

Molecular responses of plants facing climate change-EMBO Workshop, 13-17 June 2022, Montpellier, France

Plant Cell Compartments: Stay Connected, 17-18 March 2022, Online format

## Statutory declaration

Hiermit erkläre ich an Eides statt, dass ich mich mit der vorliegenden wissenschaftlichen Arbeit erstmals um die Erlangung des Doktorgrades bewerbe, die Arbeit selbstständig und ohne fremde Hilfe verfasst, nur die angegebenen Quellen und Hilfsmittel genutzt und die den benutzten Werken wörtlich oder inhaltlich entnommenen Stellen als solche kenntlich gemacht habe.


Halle (Saale), den ___20.02.2024___                                        Pinelopi Moutesidi